

Investigating the impact of aeolian deposition to the Southern Ocean using dissolved aluminium concentrations

Tomas Andrew Remenyi

BSc, BComm, BAntStud (Hons)

Submitted in fulfilment of the requirements for the Degree of

Doctor of Philosophy in Quantitative Marine Science

(A joint CSIRO and UTAS PhD program in quantitative marine science)

University of Tasmania

June 18, 2013



Statement of Declaration

I declare that this thesis contains no material which has been accepted for a degree or diploma by the University or any other institution, except by way of background information and duly acknowledged in the thesis, and to the best of my knowledge and belief no material previously published or written by another person except where due acknowledgement is made in the text of the thesis, nor does the thesis contain any material that infringes copyright.

This thesis may be reproduced, archived, and communicated in any material form in whole or in part by the University of Tasmania or its agents. The publishers of the papers [Remenyi et al. \(2011\)](#) and [Remenyi et al. \(2012\)](#), included as Chapters 2 and 3, hold the copyright for that content, and access to the material should be sought from the respective journals. The remaining non published content of the thesis may be made available for loan and limited copying in accordance with the Copyright Act 1968.

Tomas Andrew Remenyi

Statement of Co-Authorship

The following people and Institutions contributed to the publication of work undertaken as part of this thesis:

Tomas Andrew Remenyl, QMS, ACECRC, IMAS, ACROSS	Primary author (Candidate)
Prof. Pavel Nesterenko, ACROSS	Author 1
Dr. Andrew Bowie, ACECRC	Author 2
Dr. Ed Butler, ACECRC, CSIRO	Author 3
Prof. Paul Haddad, ACROSS	Author 4

Author details and their roles:

(Example)

Paper 1: Fast and sensitive determination of aluminium with Reversed Phase – High Performance Liquid Chromatography using an ultra-short monolithic column

Located in chapter 2

Candidate was the primary author (85%) and with Authors 1 (10%), 2 (2%), 3 (2%) and 4 (1%) contributing to the idea, its formalisation, development, refinement and presentation.

Paper 2: Reversed Phase – High Performance Liquid Chromatographic determination of dissolved aluminium in open ocean seawater

Located in chapter 3

Candidate was the primary author (85%) and with Authors 1 (5%), 2 (5%), 3 (4%) and 4 (1%) contributing to the idea, its formalisation, development, refinement and presentation.

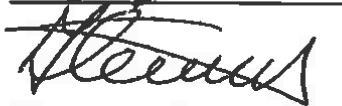
We the undersigned agree with the above stated “proportion of work undertaken” for each of the above published (or submitted) peer-reviewed manuscripts contributing to this thesis:

Signed:

Candidate



Author 1



Author 2



Author 3



Author 4



Date: _____

Statement of Co-Authorship

The following people and institutions contributed to the publication of work undertaken as part of this thesis:

Tomas Andrew Remenyi, QMS, ACECRC, ACROSS, IMAS	Primary author (Candidate)
Prof. Pavel Nesterenko, ACROSS	Author 1
Dr. Andrew Bowie, ACECRC	Author 2
Dr. Ed Butler, ACECRC, CSIRO	Author 3
Prof. Paul Haddad, ACROSS	Author 4

Author details and their roles:

(Example)

Paper 1: Fast and sensitive determination of aluminium with Reversed Phase – High Performance Liquid Chromatography using an ultra-short monolithic column

Located in chapter 2

Candidate was the primary author (85%) and with Authors 1 (10%), 2 (2%), 3 (2%) and 4 (1%) contributing to the idea, its formalisation, development, refinement and presentation.

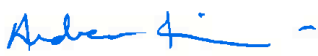
Paper 2: Reversed Phase – High Performance Liquid Chromatographic determination of dissolved aluminium in open ocean seawater

Located in chapter 3


Candidate was the primary author (85%) and with Authors 1 (5%), 2 (5%), 3 (4%) and 4 (1%) contributing to the idea, its formalisation, development, refinement and presentation.

We the undersigned agree with the above stated “proportion of work undertaken” for each of the above published (or submitted) peer-reviewed manuscripts contributing to this thesis:

Signed: _____



Dr. Andrew Bowie
Supervisor
Institute of Marine and Antarctic Studies
University of Tasmania



Prof. Thomas Trull
Director
Quantitative Marine Science Program
University of Tasmania

Date: _____

4 / 12 / 12

Abstract

Atmospheric dust deposition (aeolian deposition) is thought to be an important source of bio-limiting trace elements to the Southern Ocean (SO). Aluminium (Al) has been established as a proxy for dust deposition due to its limited role biologically, short residence times in the surface ocean and supply mechanisms to the open ocean that are typically dominated by atmospheric delivery of dust. Prior to this study, Al distributions within Australian sector of the SO had not been investigated thoroughly and atmospheric dust deposition was poorly constrained by field observations. This PhD project presents the first dissolved Al (dAl) observations in the Australian sector of the SO. These were used: to improve the understanding of Al biogeochemical cycling in the SO; as inputs to the model for the Measurement of Aluminium for Dust Calculation in Oceanic Waters (MADCOW) (Measures and Brown, 1996) to estimate aeolian deposition; to compare and assess the performance of model estimates of surface ocean dAl concentrations in the SO by Han et al. (2008) and van Hulst et al. (2012) to *in situ* observations; and to compare estimates of dust deposition from this study to those from published atmospheric models.

To achieve this, a novel method for the determination of sub-nM dAl in seawater was developed (RP-HPLC with fluorescence detection of the Al–lumogallion complex (Remenyi et al., 2011, 2012)). Total required sample volume (including rinses) was 1.5 mL. Analysis time was 2.7 min per injection. Limit of detection was 0.13 ± 0.05 nM, with precision of 2.7% at 1.06 nM. Agreement with SAFe reference samples was within $4.6 \pm 4.6\%$ ($n = 13$). It provides improvements in sample efficiency, operational robustness and analysis times relative to popular shipboard techniques, especially when applied to samples where dAl approaches the limit of detection.

More than 440 samples were then analysed from two voyages (GIPY2, SAZ-Sense and GIPY6, SR3 repeat transect). dAl was depleted throughout the region from 0.05 to 7.5 nM, with most values < 1 nM. This places it at the low end of the global range (0.1–180 nM). Maximum dAl values were within the proximity of the East Australia Current (EAC). Minimum dAl values were in the Subantarctic Zone (SAZ), coinciding with the region with a very deep winter mixed layer (ML). Trends were latitudinal rather than following watermasses, probably due to the distance from landmasses coupled with the strong eastward flow of the Antarctic Circumpolar Current. Aeolian deposition of soluble Al was low and as such lateral advection of waters that are relatively enriched in dAl appear to dominate the biogeochemistry of the region. Evidence of sedimentary entrainment from the Australian continental shelf and the Kerguelen Plateau was observed. Satellite observations indicate bushfire (wild fire) ash/smoke may be an important source of dAl East of Tasmania, but appropriate field observations were not available (eg. black carbon).

Modelling by Han et al. (2008) (DEAD-MADCOW) overestimated surface dAl concentrations in the SO. This was probably because it overestimated the solubility of Al delivered in dust and

underestimated dilution (MLD) and scavenging rates. Modelling by [van Hulten et al. \(2012\)](#) (NEMO-PISCES) was much more sophisticated and consequently had much better agreement with observations. Agreement between the NEMO-PISCES model and the observed data is excellent south of the Polar Front, where the model assumptions and mechanisms are appropriate (where [van Hulten et al. \(2012\)](#) use biogenic silica concentrations to estimate scavenging). However, differences between observations and model estimates are much greater in the SAZ and surrounding Tasmania. In the EMLDZ of the SAZ, the NEMO-PISCES model overestimated dAl, probably because the dilution factor applied in their model is too low. However around Tasmania, the model substantially underestimates dAl. This could be due to either an underestimate of sources, or an overestimate of sinks. The biogenic silica field used to estimate scavenging in the NEMO-PISCES model is ~ 5 -fold greater than observations in the SAZ and the STZ ([Rosenberg, 2007, 2008](#)). The associated scavenging rate will also be too large (interestingly this does not correct the overestimated values observed in the EMLDZ of the SAZ). It is likely that the source mechanisms in the NEMO-PISCES model underestimate entrainment within the EAC, and almost certainly do not account for supply from bushfires.

Dust deposition rate estimates using the MADCOW model ([Measures and Brown, 1996](#)) without adjusting the original parameters (intended for use in the mid-Atlantic) were reasonable, and in relatively good agreement with both DEAD ([Zender et al., 2003](#)) and INCA ([Seze et al., 1991](#); [Whitehead et al., 1998](#); [Schulz et al., 2009](#)) model estimates. However, application of the model with mixed layer depths (M), scavenging rates (Sc) and solubility rates (S) that were more appropriate for the SO resulted in extremely high dust deposition rate estimates and these were considered unreasonable. Investigation revealed the lack of variance of dAl observations with depth and latitude along the SR3 transect, coupled with the physical oceanographic conditions in the Australia sector of the SO invalidate many of the assumptions required by the MADCOW model. Therefore, dAl concentrations in the SO cannot be used as inputs to the MADCOW model to quantify dust deposition rates into the SO.

Given the lack of quality satellite observation of dust deposition over the SO and the infrequent collection of aerosol concentrations in the SO, there are currently no reliable methods for estimating dust deposition to the SO. The best estimates of trace element availability in the SO is from direct measurement of water samples.

The key finding from this thesis is: aeolian deposition of dust to the open ocean in the Australian sector of the SO is very limited, so sources of bio-limiting trace elements to surface waters are likely to be from lateral advection or from upwelling depending on the region.

Acknowledgements

I dedicate this thesis to Caroline, my beautiful wife. This thesis would not have been completed without her continuing support and constant reminder that it is just science. I thank her for keeping me grounded, reminding me to laugh and above all, for loving me, especially during the “last three weeks”. Thank you to my wonderful children, Hugh and Sebastian. Their carefree attitude to life has taught me a lot and provided me with a fantastic distraction from work at the times I have needed it most. Without their help, this thesis would not be what it is.

To all the Remenyis and the Lapworths, their constant support throughout these difficult 4 years of our lives has been invaluable and always appeared when it was most needed. Thank you. To all those at ACECRC, IASOS, IMAS, ACROSS and QMS, thank you for providing a wonderful working environment that made coming to work a joy. Special thanks to James Culverhouse, Alex Fraser, Ben Galton-Fenzi, Paul Harvey, Robert Johnson, Ben Joseph, Delphine Lannuzel, Jan Lieser, Pier van der Merwe for their technical assistance over the past 4 years. To Kate Maloney, Wenneke ten Hout, Denbeigh Armstrong and Heidi Arman, a special thank you for their assistance navigating the administrative pathways of finance, governance and reporting during this project and for providing additional financial support when personal circumstances were difficult.

This study was supported by the Australian Centre for Research on Separation Science; Australian Governments Cooperative Research Centre program through the Antarctic Climate & Ecosystems Co-operative Research Centre; the Institute for Marine and Antarctic Studies; IRGS 100097 grant of the University of Tasmania; a joint CSIRO-UTAS PhD scholarship in Quantitative Marine Science (QMS) and a top-up CSIRO PhD stipend (through the Marine and Atmospheric Research division). During the SAZ-Sense and CASO-SR3 voyages, we would like to thank the captain, officers, and crew of the RSV Aurora Australis for all their support; we are grateful to Mark Rosenberg, Sergei Sokolov and the hydrography team (from both ACECRC and/or CSIRO) for provision of CTD data ([Rosenberg, 2007, 2008](#); [Rosenberg et al., 2010](#)) and ADCP data ([Sokolov and Rintoul, 2007a,b, 2009a,b](#)). Neil Johnson and Alicia Navidad for nutrients analysis, Alan Poole and Aaron Spurr for technical support. The authors would like to thank the developers of L^AT_EX, R ([R-Development-Core-Team, 2010](#)), JabRef ([Team, 2013](#)), Ocean Data View ([Schlitzer, 2002, 2012](#)) and HYSPLIT ([Draxler and Rolph, 2012](#)).

Last, but by no means least, I have been very fortunate to have had a dedicated, generous and wise team of supervisors. To Andrew Bowie, Pavel Nesternenko, Ed Butler, Paul Haddad, thank you all for your guidance, encouragement and constant support during this challenging project.

Contents

Statement of Declaration	i
Abstract	iv
Acknowledgements	vi
Contents	vii
List of Figures	xiv
List of Tables	xviii
List of Acronyms	xx
1 Introduction and literature review	2
1.1 The GEOTRACES program	2
1.2 Characteristics of Aluminium	2
1.3 Aluminium as a biogeochemical tracer	5
1.4 The importance of Fe as a micronutrient	8
1.5 Estimating dust deposition to the ocean	9
1.6 Dissolved Al concentrations as a proxy for dust deposition	13
1.7 The distribution of dAl in the global oceans	14
1.8 Previous work that guided the practical direction of this project	19
1.9 The aims of this project	23

2	Fast and sensitive determination of Al with RP-HPLC using an ultra-short monolithic column	24
2.1	Introduction	24
2.2	Experimental	29
2.2.1	Apparatus	29
2.2.2	Reagents	30
2.2.3	Sample types	30
2.2.4	Reversed phase HPLC	31
2.2.5	Flame Atomic Absorption Spectroscopy (FAAS)	33
2.3	Results and discussion	33
2.3.1	Optimisation of separation conditions	33
2.3.2	Column temperature and flow rate selection	40
2.3.3	Pre-column-reaction chemistry	41
2.3.4	Comparison between RP-HPLC and FAAS for analysis of Al ³⁺ in a tea-infusion	41
2.4	Conclusions	43
3	RP-HPLC determination of dAl in open ocean seawater	45
3.1	Introduction	45
3.2	Methods and Procedures	46
3.2.1	Apparatus	46

3.2.2	Reagents	47
3.2.3	Sample collection and analysis protocols	47
3.2.4	Sample analysis	48
3.3	Assessment	49
3.3.1	Blank estimation	49
3.3.2	Calibration and limit of detection	51
3.3.3	Accuracy and precision	52
3.3.4	Synthesis of the lumogallion-Al complex	54
3.4	Discussion	54
3.4.1	Robustness and automation	57
3.4.2	Required sample volume	58
3.5	Conclusions	58
4	Using dissolved aluminium concentrations to constrain trace element supply to the subantarctic SO south of Australia	61
4.1	Introduction	61
4.2	Methods	63
4.2.1	Voyage track and strategy	63
4.2.2	Oceanographic Setting	65
4.2.3	Sampling and processing	68
4.2.4	Analysis	69

4.2.5	Air mass trajectory analysis	69
4.2.6	Model for estimating annual aeolian deposition rates	70
4.3	Results and Discussion	71
4.3.1	Summary of all results	71
4.3.2	Subantarctic Zone – West (SAZ–W): Process station 1 (P1)	79
4.3.3	Polar Front Zone (PFZ): Process station 2 (P2)	80
4.3.4	Subantarctic Zone–East (SAZ–E): Process station 3 (P3)	82
4.3.5	Process Station Comparisons	88
4.4	Conclusions	89
5	The distribution and biogeochemistry of Al along the WOCE SR3 repeat transect (GEOTRACES voyage GIPY6)	91
5.1	Introduction	91
5.1.1	Source regions of dust to the SO	92
5.1.2	Oceanographic setting	95
5.2	Methods	102
5.2.1	Voyage track and strategy	102
5.2.2	Sampling and processing	102
5.2.3	Model for estimating annual aeolian deposition rates	103
5.3	Results	103
5.3.1	Quality assessment	103

5.3.2	Summary of dAl concentrations within each watermass	110
5.3.3	Summary of dAl concentrations within deep, intermediate and surface waters	111
5.3.4	Summary of dAl concentrations within each major ocean zone	111
5.3.5	Summary of dAl concentrations within each sub-zone	112
5.4	Aeolian deposition estimates using MADCOW	114
5.5	Discussion	114
5.5.1	The nature of the overall trends in dAl	114
5.5.2	Comparison to previous observations in the SO	115
5.5.3	Why was dAl relatively enriched in the IPFZ?	116
5.5.4	Why was dAl relatively enriched in the STZ?	119
5.5.5	Why was dAl relatively depleted within the SZ-S (the surface of which was defined as AASW)?	119
5.5.6	Why was dAl relatively depleted within the EMLDZ?	120
5.5.7	The relationship of Al with other parameters along SR3	121
5.5.8	Aeolian deposition rates	125
5.6	Conclusions	125
6	Comparison of different model estimates of aeolian deposition to the SO	126
6.1	Introduction	126
6.1.1	Aims of this chapter	126

6.1.2	Background	126
6.1.3	Estimates of aeolian deposition to the SO	127
6.1.4	Estimates of dAl concentrations in the SO	130
6.1.5	Measurement of Aluminium for Dust Calculation in Oceanic Waters: MADCOW	130
6.2	Methods	131
6.2.1	Comparing surface dAl concentrations from observations and model outputs	131
6.2.2	Comparison of dust deposition estimates along the SR3 transect	131
6.2.3	Estimating summer MLD (M)	132
6.2.4	Estimating scavenging rates (Sc)	132
6.2.5	Estimating solubility rates (S)	133
6.2.6	Estimating stock dAl concentration	133
6.3	Results and Discussion	134
6.3.1	Surface dAl concentrations: Comparison of observations to model output.	134
6.3.2	Application of reasonable values for M , Sc and S per station using the MADCOW model	137
6.3.3	DEAD and INCA vs. MADCOW	138
6.4	Conclusion	143
7	Conclusion and Future Work	144
7.1	Key goals and tasks	144

7.1.1	To overcome the shortcomings of existing methods used for the determination of dAl in open ocean seawater samples	144
7.1.2	To investigate the distribution of dAl in the Australian sector of the SO . .	147
7.1.3	To conduct biogeochemical oceanographic interpretation of these dAl concentrations to elucidate the relative contribution of various supply mechanisms to the waters sampled	149
7.1.4	To compare dAl observations in the SO to model estimates	151
7.1.5	To estimate aeolian deposition of dust to the SO using dAl concentrations as a proxy (using MADCOW, or if necessary develop an alternative model) and subsequently compare these estimates to those from atmospheric models	152
A Dissolved Aluminium Data collected during this project		154
References		169

List of Figures

1.1	Planned voyage tracks of the GEOTRACES program	3
1.2	Speciation characteristics of Al seawater	4
1.3	Relative kinetics of a range of metals	5
1.4	Simplified conceptual model of the biogeochemical processing of Al in the ocean.	7
1.5	Schematic of global overturning circulation	8
1.6	Comparison of nitrate and chlorophyll-a concentrations in the surface ocean	10
1.7	Schematic describing the ‘biological pump’ and the ‘solubility pump’	11
1.8	Mean retrieval rate of AOD measured from satellites	12
1.9	Recent modelling of annual aeolian deposition to the ocean surface ($g\ m^{-2}\ yr^{-1}$) .	15
1.10	Summary of all dAl observations prior to 2007	16
1.11	Estimates of dAl in the surface ocean from previous modelling studies	17
1.12	Geographic range of existing dAl measurements	18
1.13	Schematics of the FIA method presented by Brown and Bruland (2008)	20
1.14	Schematics of the HPCIC method presented by Tria et al. (2008b)	21
1.15	Schematics of the RP-HPLC method presented by Lee et al. (1996)	21
2.1	Simplified version of Van Deemter plot.	28

2.2	A comparison of the structure and performance of monolithic vs. packed bed columns	29
2.3	Response of the RP-HPLC system to lumogallion concentration	32
2.4	Effect of the type of analytical column on the shape of the Al peak observed	35
2.5	Effect of isocratic and gradient elution programs when determining dAl in seawater	36
2.6	Effect of MeOH concentration during matrix elimination and analyte elution . . .	38
2.7	Effect of reduced column length and increased methanol concentration in the eluent on peak shape and analysis time.	40
2.8	Example calibration curve; and example chromatogram	44
3.1	RP-HPLC with fluorescence detection system schematic	48
3.2	Chromatograms of 0.1–100 nM standards made up in SAFe–D2	50
3.3	Representative 16-point calibration curve	52
3.4	Example depth profile of dissolved Al	59
4.1	MODIS image: 8-day composite chlorophyll-a	62
4.2	SAZ-Sense voyage station locations relative to the relevant oceanographic features	64
4.3	Estimate of the SE atmospheric pathway	66
4.4	AeroSAZ sample collection transits presented with airmass back trajectories from each oceanographic station location during the SAZ-Sense voyage	71
4.5	Depth profiles for dAl from each process station	72
4.6	Major parameters of the hydrographic section along P2–P3–Tasmania in late summer	75
4.7	Supplementary parameters of the hydrographic section along P2–P3–Tasmania in late summer	76

4.8	Dissolved Al of the hydrographic section along P2–P3–Tasmania in late summer	77
4.9	Aeolian deposition rates at each station during the SAZ-Sense voyage.	78
4.10	Potential density isosurface and TS profiles around P3	82
4.11	Comparison of dAl depth profiles at stations around P3	83
4.12	Comparison of dAl and dFe profiles at 17b and 17j	85
4.13	Active fires in Tasmania on the 18 February 2007	87
4.14	HYSPLIT dispersion density modelling of smoke plumes on 18-Feb-2007	88
5.1	Global model estimates of dust deposition (Jickells et al., 2005) and the expected source regions for this dust (Mahowald et al., 2006)	93
5.2	ADCP data superimposed over SSHA contours during the SR3 voyage	97
5.3	Oceanographic TS plot overlain with neutral density contours	98
5.4	Depth vs. latitude sections of physical (Rosenberg, 2008) and nutrient parameters (CSIRO) along the SR3 transect.	99
5.5	Estimates of MLD in the SO	100
5.6	Depth vs. latitude section plot of other trace elements along the SR3 transect.	101
5.7	Depth vs. latitude section of dAl concentrations along the SR3 transect	104
5.8	Depth profiles of dAl within each major zone.	105
5.9	Section plot of dAl along SR3, with latitude vs. neutral density	106
5.10	Visualisation of the spread of dAl data and associated quality assurance comparisons	107
5.11	The dAl data set subset by watermass, ocean zone and frontal zone.	108
5.12	MADCOW estimates of aeolian deposition of dust along the SR3 transect	109

5.13	Comparison of dissolved Si and Al along the SR3 transect.	123
5.14	Comparison of Si and Al separated by watermass along the SR3 transect.	124
6.1	Recent modelling of annual aeolian deposition to the ocean surface ($g\ m^{-2}\ yr^{-1}$) .	128
6.2	Estimates of aeolian deposition along SR3 transect from DEAD and INCA.	129
6.3	Comparison of dAl observations along SR3 to previous model estimates	136
6.4	(a) Percentage change of M , Sc and S at each station relative to the original settings of the MADCOW model. (b) Individual impact of adjusting either M , Sc or S per station on the dust deposition rate estimates provided by the MADCOW model. (c) Combined impact of adjusting either M , Sc or S per station on the dust deposition rate estimates provided by the MADCOW model. The potential influence of underlying waters during winter is also compared (i.e. A vs. A').	139
6.5	Comparison of aeolian deposition rate estimates from DEAD, INCA and MADCOW models	140

List of Tables

1.1	Molar concentrations of the major elements in seawater relative to Al. Adapted from Dickson and Goyet (1994)	4
1.2	An overview of methods used for determination of dAl in natural waters	22
2.1	Performance comparison of FIA, ICP-MS and RP-HPLC for the determination of dAl	34
3.1	Blank values as concentrations used to calculate the LOD of the RP-HPLC system	53
3.2	Analysis of the various SAFe sub-samples using the RP-HPLC method	54
3.3	Performance parameters comparison: RP-HPLC, FIA and ICP-MS	55
4.1	Aeolian deposition rates at each station during the SAZ-Sense voyage.	78
4.2	Aerosol fluxes from at sea measurements during the SAZ-Sense voyage.	80
4.3	Aerosol concentrations collected at sea during the SAZ-Sense voyage.	81
5.1	Observed dAl concentrations (nM) in the ocean south of 40°S.	92
5.2	Definitions of ocean fronts, zones and sub-zones along the SR3 transect.	94
5.3	Definitions of watermasses during the April 2008 SR3 repeat	98
5.4	Description of dAl values determined in each watermass.	110
5.5	t-test p-values comparing watermasses along SR3	110
5.6	Description of dAl values determined in each depth class.	111
5.7	t-test p-values comparing dAl in each depth class along SR3	111

5.8	Description of dAl values determined in each major ocean zone.	112
5.9	t-test p-values comparing dAl in major ocean zones along SR3	112
5.10	Description of dAl values determined in each sub-zone. Each region was defined by the front on its southern boundary.	113
5.11	t-test p-values comparing dAl in minor ocean zones along SR3	113
5.12	Description of aeolian deposition estimates (g/m ² /yr) values determined in each major ocean zone using MADCOW (solubility = 1.5%).	114
5.13	t-test p-values comparing aeolian deposition in major ocean zones along SR3 . . .	115
6.1	Parameter descriptions and assigned values in the MADCOW model as described in Measures and Brown (1996)	131
6.2	MADCOW input parameter values per station and the associated dust deposition estimates along the SR3 transect. M_s =summer MLD; M_w =winter MLD; Sc =scavenging rate; S =solubility; A =dAl in the summer ML; G_A =dust estimate given A ; A' =dAl in the summer ML additional to that supplied from underlying waters; $G_{A'}$ =dust estimate given A' , G_o =dust estimate given original parameter settings (A ; $M=30m$; $Sc=0.2$; $S=0.015$).	137
A.1	Dissolved aluminium data collected during the SAZSense voyage (GEOTRACES voyage GIPY2)	154
A.2	Dissolved aluminium data collected during the WOCE SR3 repeat transect voyage (GEOTRACES voyage GIPY6).	159

List of Acronyms

8-HQ	8-hydroxyquinoline
8-HQS	8-hydroxyquinoline-5-sulfonic acid
γ	Neutral Density ($kg.m^{-3}$)
Θ	Absolute Salinity ($g.kg^{-1}$)
σ	Standard deviation
AABW	Antarctic Bottom Water
AAIW	Antarctic Intermediate Water
AASW	Antarctic Surface Water
ACC	Antarctic Circumpolar Current
AcN	Acetonitrile
ADCP	Acoustic Doppler Current Profiler
AeroSAZ	An aerosol sample collected on the SAZ-Sense voyage
AES	Atomic Emission Spectroscopy
AI	Aerosol Index
AOD	Aerosol Optical Depth
AOT	Aerosol Optical Thickness
AZ	Antarctic Zone
BEC	Biogeochemical Elemental Cycling
BSW	Bass Strait Waters
C ₁₈	Octadecylsilane
CMORPH	global precipitation analyses at very high spatial and temporal resolution
CRM	Certified Reference Material
CSV	Cathode Stripping Voltammetry
CSG	Chromazurol S immobilised silica gel
CTD	Conductivity, Temperature and Depth instrument package
dAl	dissolved aluminium
DASA	1,2-dihydroxyanthraquinone-3-sulphonic acid
DEAD	Dust Entrainment And Deposition model
DMADCOW	The attempt within this project at reconstructing the underlying equation of the MADCOW model
DIW	Deionised Water

EAC	East Australia Current
ECD	Electron Capture Detection
ECD-GC	Electron Capture Detection Gas Chromatography
EDTA	Ethylenediaminetetraacetic acid
EMLDZ	Extreme Mixed Layer Depth Zone
FAAS	Flame Atomic Absorption Spectroscopy
FIA	Flow Injection Analysis
GC	Gas Chromatography
GC-GF-AAS	Gas Chromatography Graphite Furnace Flame Atomic Absorption Spectroscopy
GCM	General Circulation Model
GEOTRACES	Collaborative international program to investigate the biogeochemical cycling of trace elements in the ocean
GF	Graphite Furnace
GF-AAS	Graphite Furnace Flame Atomic Absorption Spectroscopy
HEPA	High-Efficiency Particulate Air
HNLC	High-Nutrient Low-Chlorophyll
HPCIC	High-performance Chelation-Ion-Chromatography
HPLC	High-Performance Liquid-Chromatography
HPLC-MS/MS	High-Performance Liquid-Chromatography Mass Spectrometry - Mass Spectrometry
HTFA	1,1,1-trifluoro-2,4-pentanedione
HYSPLIT	Hybrid Single Particle Lagrangian Integrated Trajectory model
ICP	Inductively Coupled Plasma
ICP-MS	Inductively Coupled Plasma Mass Spectrometry
IDA	Iminodiacetic acid (2,2'-azanediylidiacetic acid)
IDAS	Iminodiacetic acid functionalised silica
IE	Ion-Exchange liquid-chromatography
INAA	Instrumental Neutron Activation Analysis
IPFZ	Inter Polar Frontal Zone
INCA	Interaction of Chemistry and Aerosol module
K_{sp}	Solubility coefficient
KHP	Potassium hydrogen phthalate buffer
LCDW	Lower Circumpolar Deep Water
LDPE	Low-Density Polyethylene
LMDzT	Laboratoire de Météorologie Dynamique (LMD) General Circulation Model
LMDzT-INCA	Interaction of chemistry and aerosol module of the Laboratoire de Météorologie Dynamique (LMD) General Circulation Model
LOD	Limit Of Detection
LOQ	Limit Of Quantification

MADCOW	The model for the Measurement of Aluminium for Dust Calculation in Oceanic Waters
MeOH	Methanol
MES	2-(N-morpholino)ethanesulfonic acid
ML	Mixed Layer
MLD	Mixed Layer Depth
MODIS	Moderate-resolution Imaging Spectroradiometer
MPF	Middle Polar Front
MS	Mass Spectrometry
MSAF	Middle Subantarctic Front
NEMO	Nucleus of European Modelling of the Ocean
NPF	Northern Polar Front
NPZD	Nutrient, Phytoplankton, Zooplankton, Depth model
NSACCF	Northern Southern Antarctic Circumpolar Front
NSAF	Northern Subantarctic Front
ODS	Octadecylsilane
OMI	Ozone Monitoring Instrument
P1	Process Station 1
P2	Process Station 2
P3	Process Station 3
PAR	Photosynthetically Available Radiation
PF	Polar Front
PFZ	Polar Frontal Zone
PFZ-N	Polar Frontal Zone - North
PFZ-S	Polar Frontal Zone - South
PISCES	A biogeochemical model which simulates the marine biological productivity and that describes the biogeochemical cycles of carbon and of the main nutrients (P, N, Si, Fe).
PTFE	Polytetra Fluoroethylene
PP	Polypropylene
RP	Reversed Phase
RP-18	C ₁₈ functionalised Reversed-Phase column
RP-18e	RP-18 with endcapped silanol groups not bound to C ₁₈
RP-HPLC	Reversed Phase High-Performance Liquid-Chromatography
SAPH	Salicylaldehyde Picolinoylhydrazone
SAF	Subantarctic Front
SAFZ	Subantarctic Frontal Zone
SAFZ-N	Subantarctic Frontal Zone North
SAFZ-S	Subantarctic Frontal Zone South
SAFe	An international collaborative project to standardise sampling and analysis techniques for trace elements in the ocean called Sampling and Analysis of Iron. This project produced quasi-certified reference materials called SAFe reference standards

SAFe-D1	A bulk sample from the SAFe project, collected from deep water
SAFe-D2	A bulk sample from the SAFe project, collected from deep water
SAFe-S	A bulk sample from the SAFe project, collected surface water
SAMW	Subantarctic Mode Water
SAZ	Subantarctic Zone
SAZ-N	Subantarctic Zone - North
SAZ-S	Subantarctic Zone - South
SAZ-Sense	A biogeochemical process study in the SO surrounding Tasmania
SDME	Single Drop Microextraction
SeaWiFS	Sea-viewing Wide Field-of-view Sensor
SEC	Size Exclusion Chromatography
SHW	Shelf Water
SIA	Sequential Injection Analysis
SO	Southern Ocean
SPF	Southern Polar Front
SR3	A WOCE repeat transect
SSACCF	Southern Southern Antarctic Circumpolar Front
SSAF	Southern Subantarctic Front
SSH	Sea Surface Height
SSHA	Sea Surface Height Anomaly
STF	Subtropical Front
STZW	Subtropical Zone Water
Sv	Sverdrup ($10^6 \text{ m}^3 \text{ s}^{-1}$)
SZ	Southern Zone
SZ-M	Southern Zone - Middle
SZ-N	Southern Zone - North
SZ-S	Southern Zone - South
TMR	Trace Metal Rosette
TS	Temperature vs. Salinity
UCDW	Upper Circumpolar Deep Water
UV-Vis	Ultra Violet – Visible light spectrum
WOCE	World Ocean Circulation Experiment
WW	Winter Water
ZC	Zeehan Current
ZOMBIEDMADCOW	the ZOnally Mutable BasIc Equation for the Deconstructed MADCOW model

Chapter

1

Introduction and literature review

1.1 The GEOTRACES program

The first reliable measurements of trace metals in the environment occurred after 1965, when [Patterson \(1965\)](#) described the importance of limiting sample contamination by following trace element clean protocols. Since then there has been slow progress achieving global coverage of trace element distributions in the global ocean. This slow progress is due to the difficulty of obtaining uncontaminated samples, the extremely low concentrations of these analytes, the high ionic-strength matrix of seawater and the general emphasis over the past few decades to focus on the physical and biological aspects of oceanography.

The international GEOTRACES program was developed as a cooperative solution to this problem of data scarcity. This program has brought together independent researchers who now collaborate with regards to resources and knowledge.

The goal is to develop a global database of key trace elements and their isotopes which will be used to develop an understanding of the biogeochemical cycles of each parameter. Figure 1.1 presents the proposed transects where samples will be analysed for all GEOTRACES key parameters (Fe, Al, Mn, Zn, Cd, Cu, $\delta^{15}\text{N}$, $\delta^{13}\text{C}$, $\delta^{230}\text{Th}$, $\delta^{231}\text{Pa}$ and isotopes of Pb and Nd) ([SCOR Working Group, 2012](#)). Al was selected as a key parameter because of its ability to be used as a biogeochemical tracer.

1.2 Characteristics of Aluminium

Aluminium (Al) is $\sim 8\%$ of the Earth's crust ([Taylor, 1964](#); [Wedepohl, 1995](#); [Yaroshevsky, 2006](#)). Despite this abundance in rocks, sediments and soils, dissolved Al (dAl) is of relatively low concentration in natural waters, ranging from μM in rivers and lakes ([Anders et al., 2003](#)), nM in the coastal ocean ([Hydes and Liss, 1977b,a](#); [Hydes et al., 1988](#); [Upadhyay and Sen Gupta, 1995](#); [Brown et al., 2010](#)) and pM in remote regions of the open ocean ([Orians and Bruland,](#)

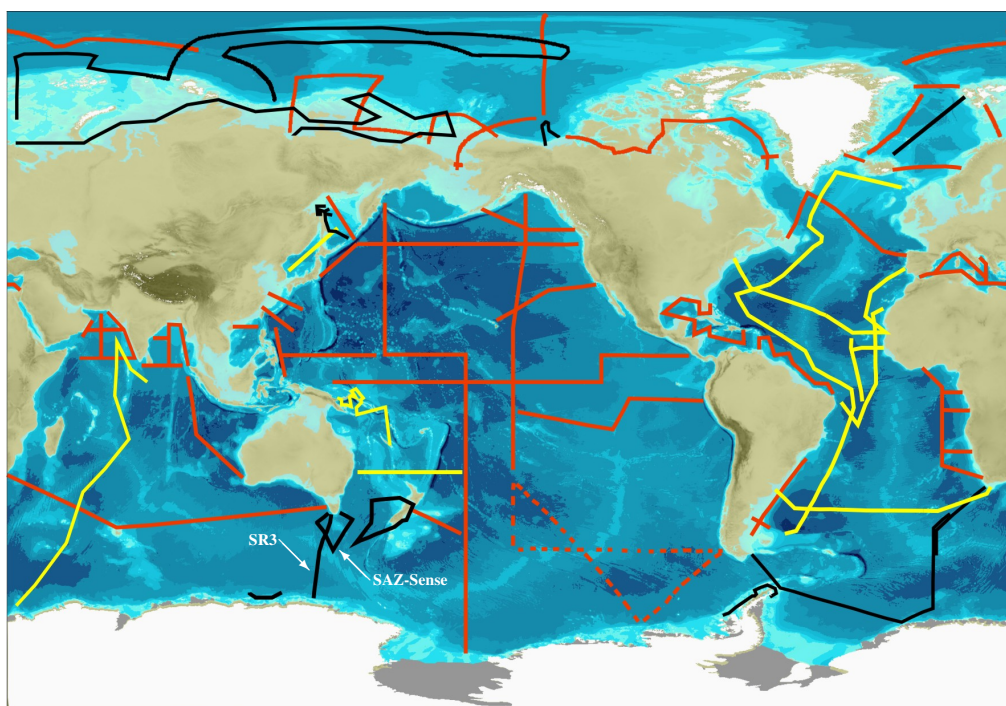


Figure 1.1: Voyage tracks part of the GEOTRACES program. In red: Planned Sections. In yellow: Completed Sections. In black: Sections completed as GEOTRACES contribution to the IPY. Reproduced with permissions from [SCOR Working Group \(2012\)](#)

1985, 1986; Vanbennekom et al., 1991; Hydes and Kremling, 1993; VanBeusekom et al., 1997; Measures, 2002; Middag et al., 2011c). This is due to its propensity to rapidly react with H_2O to form $Al(OH)_3^0$, a highly insoluble compound ($K_{sp} = 10^{-32.65}$) (Roberson and Hem, 1969). Al is less soluble in seawater relative to freshwater due to additional matrix constituents that also form insoluble complexes with Al^{3+} and $Al(OH)_4^-$ (eg. $AlCl_3$, $AlPO_4$, $2Al_2O_3 \cdot B_2O_3$, $3Al_2O_3 \cdot 2SiO_2$) and has a preference to adsorb to particles, especially those high in silicon (Si) (Mackin and Aller, 1984c; Moran and Moore, 1988; Erofeeva et al., 1989; Lydersen, 1990; Ščančar and Milačič, 2006; Savenko and Savenko, 2011). Fluvial sources of Al to the coastal ocean significantly influence local dAl concentrations (Hydes and Liss, 1977b; Mackin and Aller, 1984b; Upadhyay and Sen Gupta, 1995; Brown et al., 2010; Middag et al., 2012a). However, this influence is typically localised due to dilution, the reduced solubility of Al in seawater and the high particulate concentrations typical of regions where rivers enter the ocean (Mackin and Aller, 1984c; Stoffyn and Mackenzie, 1982; Mackin and Aller, 1984a,b, 1986; Upadhyay and Sen Gupta, 1995). Table 1.1 presents the average composition of seawater. Note the concentration of Al relative to top 12 constituents by magnitude.

Figure 1.2, originally presented by Tria (2009) (and is very similar to those presented by Gabelich et al. (2005); Moller et al. (2006); Ščančar and Milačič (2006); Savenko and Savenko (2011)), is

Table 1.1: Molar concentrations of the major elements in seawater relative to Al. Adapted from [Dickson and Goyet \(1994\)](#)

Component	Concentration (mol/kg)
H ₂ O	53.6
Cl ⁻	0.55
Na ⁺	0.47
Mg ²⁺	0.05
SO ₄ ²⁻	0.03
Ca ²⁺	0.01
K ⁺	0.01
C	0.002
Br ⁻	0.0008
B	0.0004
Sr ²⁺	0.00009
F ⁻	0.00007
Al ³⁺	0.000000001

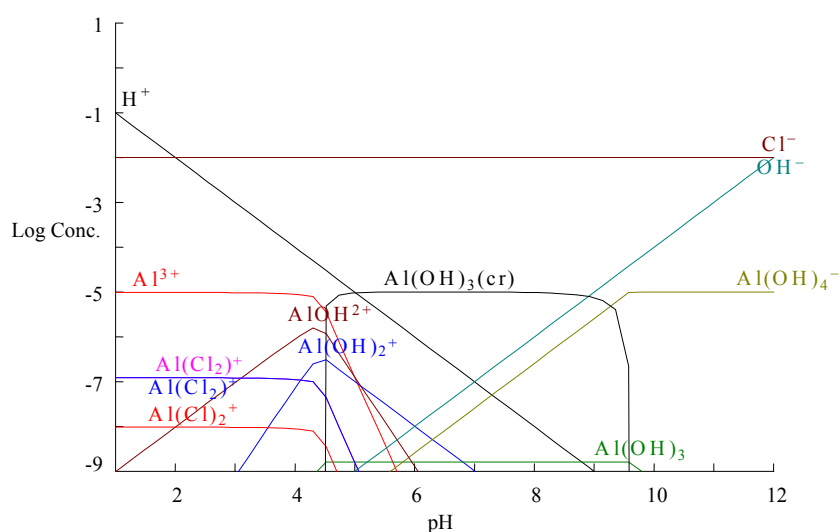


Figure 1.2: Diagram of Al speciation in 0.6 M NaCl solution (i.e. simplified seawater). Reproduced with permissions from [Tria \(2009\)](#)

a diagram of Al speciation in simplified seawater (i.e. ~ 0.6 M NaCl in H₂O). Seawater typically ranges from pH 7.5–8.5, where Al(OH)₃ dominates ([Roberson and Hem, 1969](#); [Lydersen, 1990](#); [Kumar, 1999](#); [Saukkoriipi, 2010](#); [Savenko and Savenko, 2011](#)). The dissolved phase is complex, where labile (or reactive) Al is primarily Al(OH)₄⁻ at pH >8.1, and Al(OH)₂⁺ at pH <8.1 ([Savenko and Savenko, 2011](#)). However, trace element samples are typically acidified on collection to pH

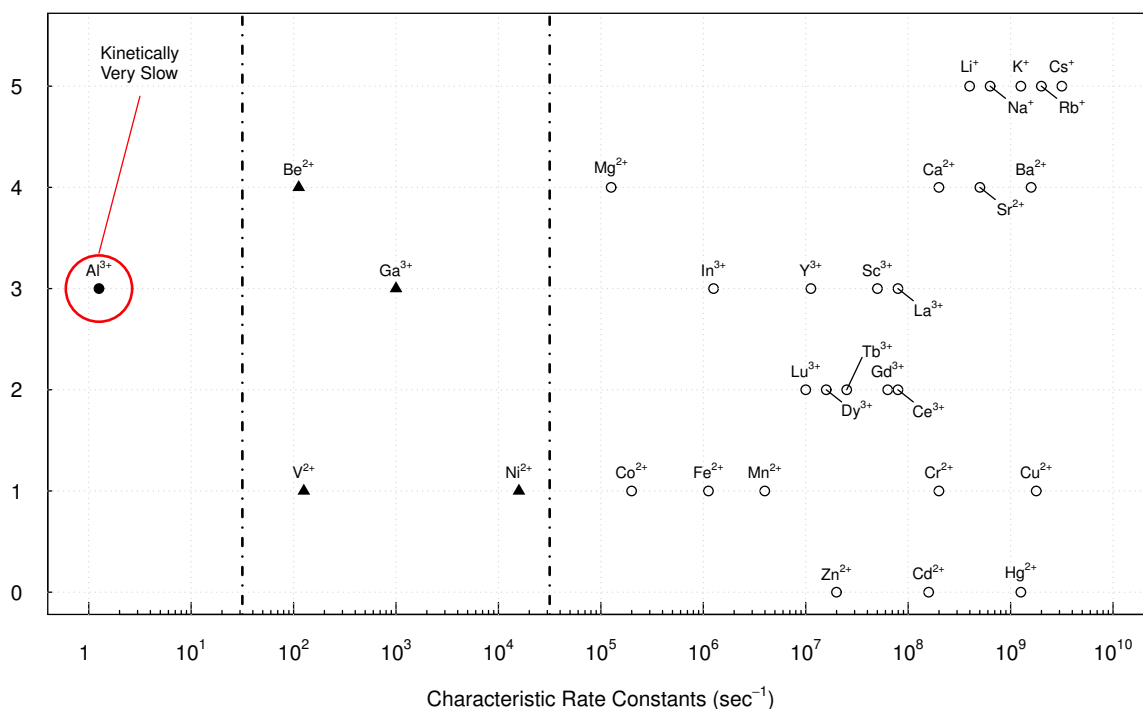


Figure 1.3: Characteristic rate constants for various metals. Al is kinetically very slow compared to most metals. Adapted from Eigen (1963); Bennetto and Caldin (1971a,b,c)

1.8, where Al^{3+} is the dominant species (Roberson and Hem, 1969; Lydersen, 1990; Kumar, 1999; Saukkoriipi, 2010; Savenko and Savenko, 2011). As such, labile Al for analytical purposes is almost always referred to as Al^{3+} regardless of the pH at sampling and this convention is maintained for simplicity throughout this thesis.

Relative to other metals Al's chemistry is characterised as kinetically slow (Eigen, 1963; Bennetto and Caldin, 1971a,b,c). Figure 1.3 is an adaptation from (Eigen, 1963) that compares the kinetics of various metals, highlighting Al as a lone outlier with a rate constant six orders of magnitude slower than almost all other metals. Slow kinetics makes it more difficult to analyse and has implications when attempting to develop analytical methods.

1.3 Aluminium as a biogeochemical tracer

The biogeochemical cycling of Al in the ocean was first comprehensively described by Stoffyn and Mackenzie (1982) and a simplified conceptual model is presented in Figure 1.4. Aluminium is not readily delivered to the open ocean by rivers due to the relatively low concentrations in

natural freshwater (μM) and the precipitation of Al species once in the presence of complexing agents typical of the seawater matrix (Mackin and Aller, 1984c,a, 1986; Erofeeva et al., 1989; Lydersen, 1990; Ščančar and Milačič, 2006; Savenko and Savenko, 2011). To date, limited convincing evidence has been found to suggest hydrothermal activity to be an important source of Al to the ocean (unlike Mn and Fe) (Stoffyn and Mackenzie, 1982; Middag et al., 2011b). This leaves two potential mechanisms of delivery: atmospheric transport of terrestrial dust with subsequent deposition in the surface ocean (herein referred to as aeolian deposition); and dissolution of sediments and the subsequent upward (or lateral) transport into the overlying waters. Once dissolved in the ocean, there are three dominant mechanisms that convert dAl into Al in sediments: adsorption onto sinking particles that reach the ocean floor (incorporating spontaneous precipitation); consumption by phytoplankton that on senescence themselves become sediment; and the consumption by zooplankton with subsequent excretion as faecal pellets that become sediments (Paces, 1978; Stoffyn, 1979; Mackin and Aller, 1984c; Walker et al., 1988; Moran and Moore, 1988, 1992). VanBeusekom et al. (1997) discuss the potential for biogenic silica in sediments to act as a cap, limiting remineralisation of Al from the sediments into the overlying waters. However, limited supporting evidence or investigations are available apart from this study. In almost every paper about Al in the ocean published since 1960, its biogeochemical behaviour as either a nutrient, a scavenged element or both has been discussed. Although it does not appear to be a limiting nutrient, it does appear to have at least a catalytic function, promoting growth to some extent (Stoffyn, 1979). However, the nutrient-like profiles in some parts of the ocean (usually where dAl concentrations are quite high, $>30\text{ nM}$) (Stoffyn and Mackenzie, 1982; Hydes et al., 1988) could be due to scavenging rather than biological uptake (Hydes, 1979; Measures et al., 1986; Moran and Moore, 1988). This differentiation has yet to be established one way or the other. As such, for the purposes of this thesis, it is assumed scavenging dominates biological uptake (Mackin and Aller, 1984c; Moran and Moore, 1988; Erofeeva et al., 1989; Lydersen, 1990; Ščančar and Milačič, 2006; Savenko and Savenko, 2011; Vanbennekomp et al., 1991; VanBeusekom et al., 1997; Paces, 1978; Stoffyn, 1979; Mackin and Aller, 1984c; Walker et al., 1988; Moran and Moore, 1988, 1992).

The residence time of Al has been estimated to range from about 1 month to 4 years in the surface ocean (the euphotic zone in Figure 1.4) (Orlans and Bruland, 1986; Moran and Moore, 1988; Jickells et al., 1994) and 50–200 years in the deep ocean (Orlans and Bruland, 1985, 1986). These time-frames are both considered relatively short residence times, especially relative to global overturning circulation of the ocean which is ~ 1000 years (see Figure 1.5) (Schmitz, 1996, and references therein). The short residence time makes Al useful as a tracer of recent aeolian deposition events (Measures and Edmond, 1989; Resing and Measures, 1994; Measures et al., 2008c; Han et al., 2008, and references therein).

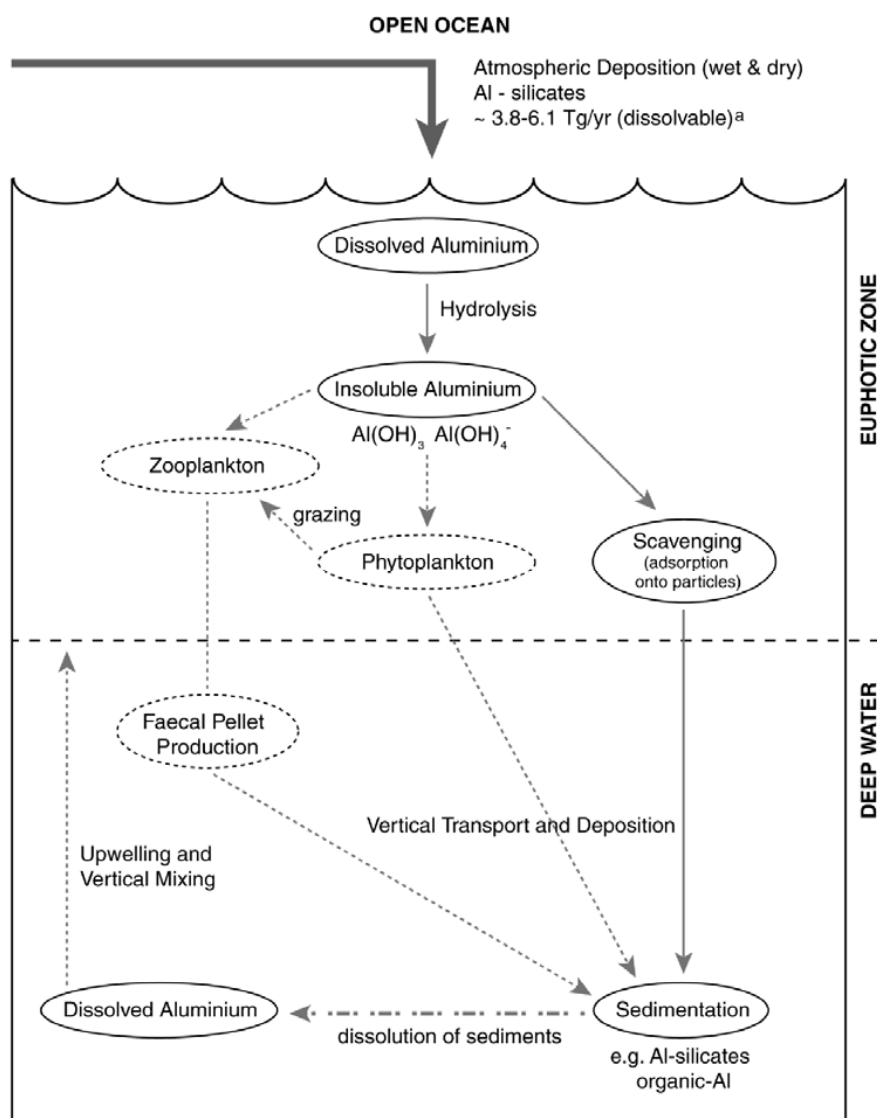


Figure 1.4: Simplified conceptual model of the biogeochemical processing of Al in the ocean. Reproduced with permissions from [Tria \(2009\)](#)

The magnitude of aeolian deposition to the open ocean has become of increased interest to the biogeochemical community over the last decade as it is considered to be an important source of micronutrients, such as Fe, to open ocean ecosystems ([Martin, 1990](#); [Duce and Tindale, 1991](#); [Boyd et al., 1998](#)). Recent studies investigating the effect of Fe fertilisation on ocean productivity have estimated Fe to be bio-limiting in ~40% of the global ocean, most of which is in the high-nutrient low-chlorophyll (HNLC) region of the SO ([Martin, 1990](#); [de Baar et al., 2005](#); [Bowie et al., 2011a](#), and references therein). Figure 1.6 contrasts global distribution of annual mean chlorophyll against *in situ* nitrate concentrations, where the HNLC character of the SO can be observed in locations

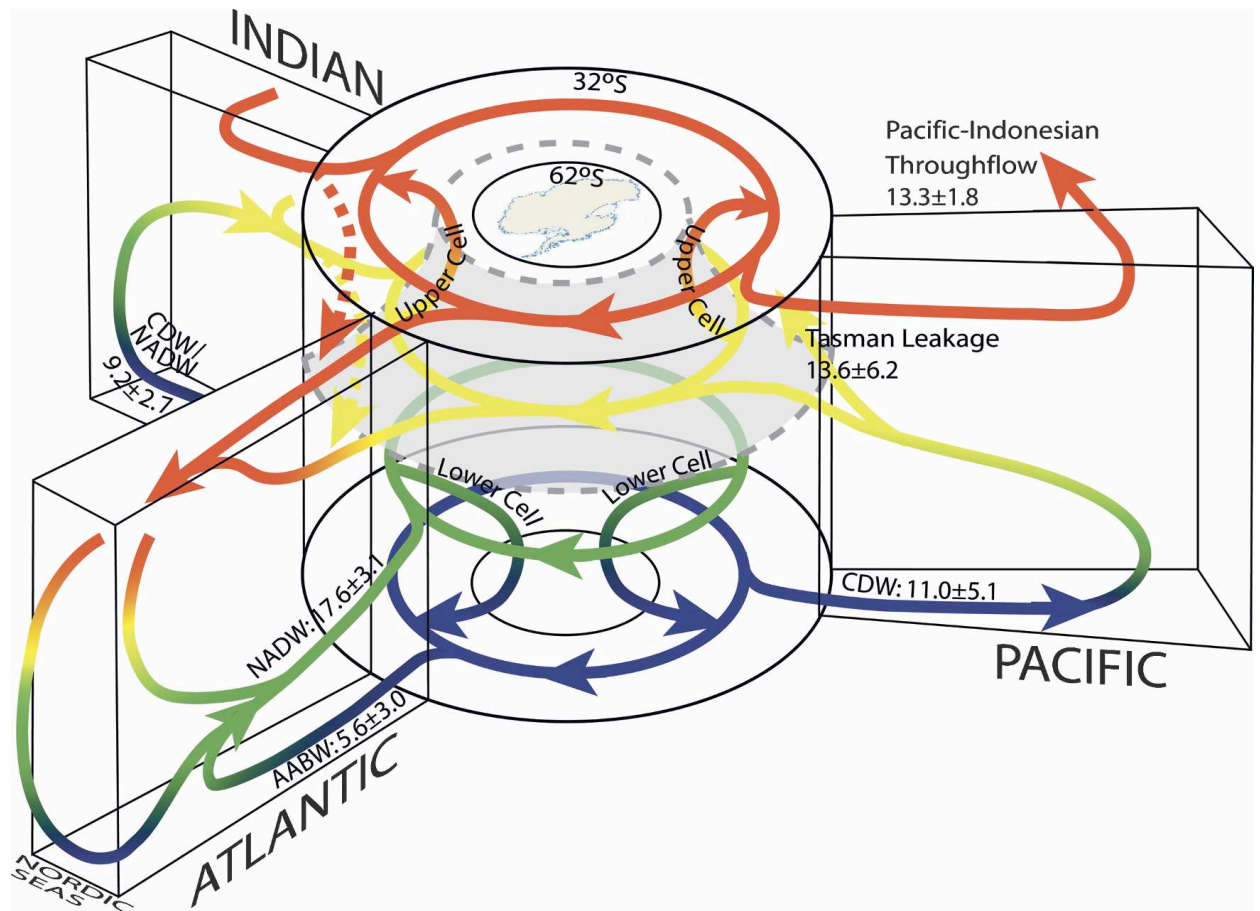


Figure 1.5: Schematic of global overturning circulation Reproduced with permissions from Lumpkin and Speer (2007) (which was adapted from Schmitz (1996)). Colour indicates approximate density ranges. Red: upper, $\gamma^n < 27.0$; yellow: intermediate, $\gamma^n \approx 27.0$ to 27.6 ; green: deep, $\gamma^n \approx 27.6$ to 28.15 ; blue: bottom, $\gamma^n > 28.15$. Gray surface with dashed edges is $\gamma^n = 27.6$ at 32°S , separating upper and lower cell transformation in the SO. Dashed arrows indicate Indian-to-Atlantic westward exchange between Africa and the ACC. Shallow subtropical cells not included.

where productivity is limited despite high concentrations of bioavailable macronutrients.

1.4 The importance of Fe as a micronutrient

Fe is an essential nutrient to many marine phytoplankton that form the basis of the food chain in the open ocean (Brand, 1991; Sunda et al., 1991; Sunda and Huntsman, 1995). Marine phytoplankton are a major component of the global carbon cycle as they are an important pathway to transfer gaseous CO_2 from the atmosphere into deep ocean and sediments where it will remain for hundreds or millions of years (Broecker et al., 1979; Broecker, 1984; Libes, 1992). This is referred to as the biological pump, visualised and described in Figure 1.7. Although the vast majority of the CO_2

taken up by phytoplankton is returned to the atmosphere through the respiration of their predators, the proportion that is transported to depth is substantial when aggregated globally. Therefore, the influence of CO₂ on global climate both now and into the future, is directly related to the magnitude of carbon sequestration performed by marine phytoplankton.

Estimates of biomass, productivity and carbon cycling are least constrained within the HNLC regions of the open ocean and these are the very regions where Fe fertilisation from aeolian deposition is most likely to have a significant impact (Martin, 1990; Duce and Tindale, 1991; Chisholm, 2000; Ussher et al., 2004; de Baar et al., 2005; Ito et al., 2012). As Fe is an essential nutrient, where it is bio-limiting it has a residence time in the surface ocean of days to weeks (Turner and Hunter, 2001), so determination of *in situ* dFe does not reflect the relative supply mechanisms. This makes elucidating the biogeochemical cycling of Fe difficult. Methods are required to evaluate the magnitude of aeolian deposition as a supply of Fe to these HNLC regions relative to other sources, such as lateral advection or upwelling.

1.5 Estimating dust deposition to the ocean

Aeolian deposition events are episodic and vary substantially in their magnitude per event. This impacts on the variability at any one site annually. Estimates of annual aeolian deposition to the surface ocean can be made using a variety of techniques, such as collection of aerosol samples at sea, remote sensing with optical instruments onboard satellites, and analysis of chemical proxies (eg. dAl) within the surface ocean.

Aerosol sampling in the open ocean is extremely difficult. Permanent research stations (either occupied or automated on moorings) within regions of interest are not feasible in most cases either due to financial or technological constraints. Deployment of personnel once an event is identified is also not possible due to logistical constraints (the time-frames of events are much shorter than those of personnel deployment systems). The coincidence of appropriate resources being deployed, ready, operational and in the correct region during a dust event has and will be fortuitous rather than planned in most cases.

Once in the field, contamination from research platforms (i.e. exhaust particles) can be a problem (even with the implementation of sector control during aerosol sampling), as rarely is a voyage dedicated solely to research of aeolian deposition. This makes aeolian deposition events difficult to study by direct measurement and has led to the development of indirect methods using satellites and chemical proxies.

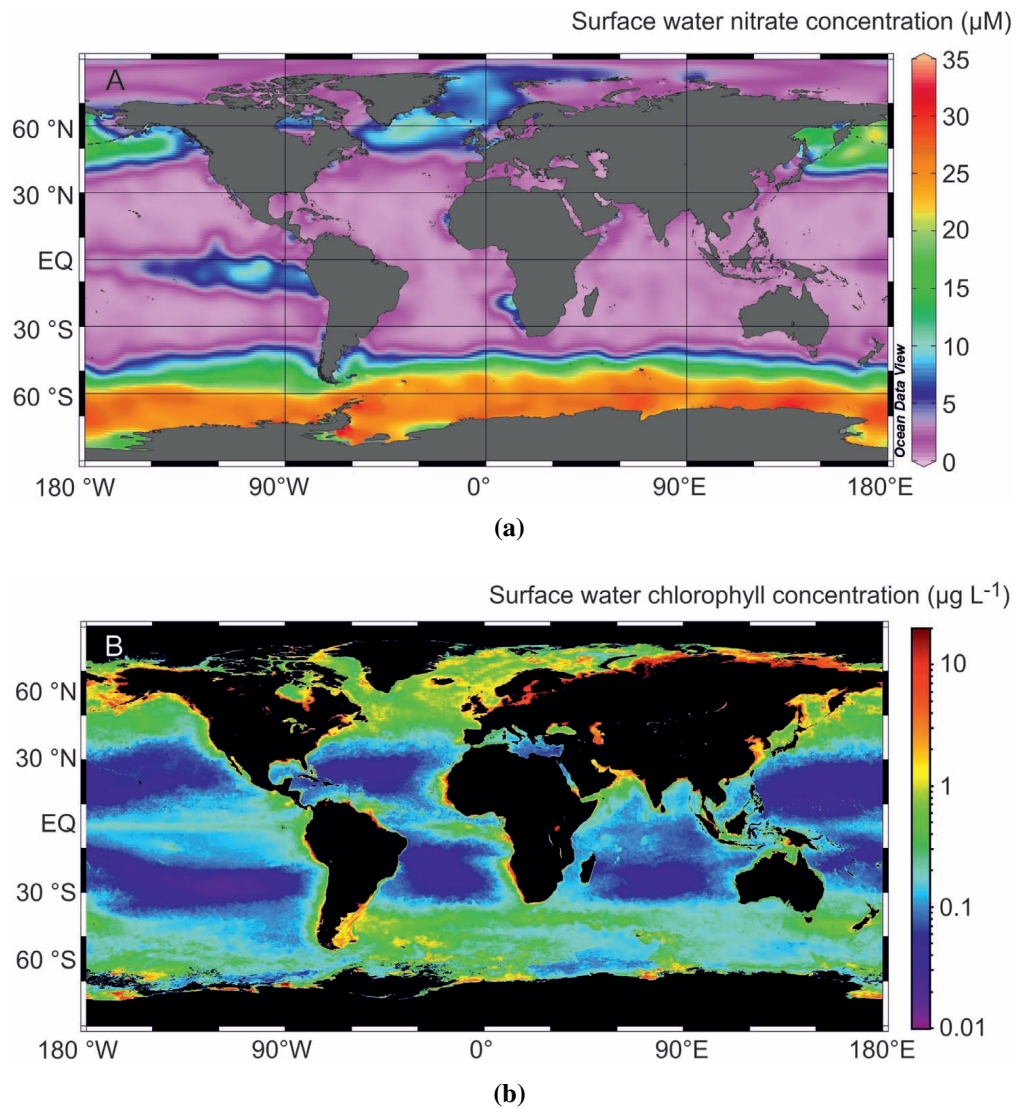


Figure 1.6: (a) Annualized average nitrate (μM) obtained using data from the World Ocean Atlas 2009 (http://www.nodc.noaa.gov/OC5/WOA09/pr_woa09.html) (b) Composite chlorophyll a (mg L^{-1}) distributions observed in surface waters in the global ocean. Produced from 2009 Aqua MODIS chlorophyll composite data (<http://oceancolor.gsfc.nasa.gov/cgi/l3>). Both (a) and (b) are Reproduced with permissions from Gledhill and Buck (2012).

Aeolian deposition can be estimated using wavelength-based measurements from satellite instruments. Aerosol optical depth (AOD) (also termed aerosol optical thickness, AOT) is the parameter targeting aerosols, of which dust is one component (Hastings and Emery, 1992; Tsai et al., 1999; Hooker and McClain, 2000). Major events in Australia have been reliably tracked using AOD imagery for some time (McTainsh, 1985; McTainsh and Strong, 2007; Mackie et al., 2008, and references therein). However, this has not been the case for smaller events. This is because dust particles can act as cloud condensation nuclei and are typically the same size as cloud droplets,

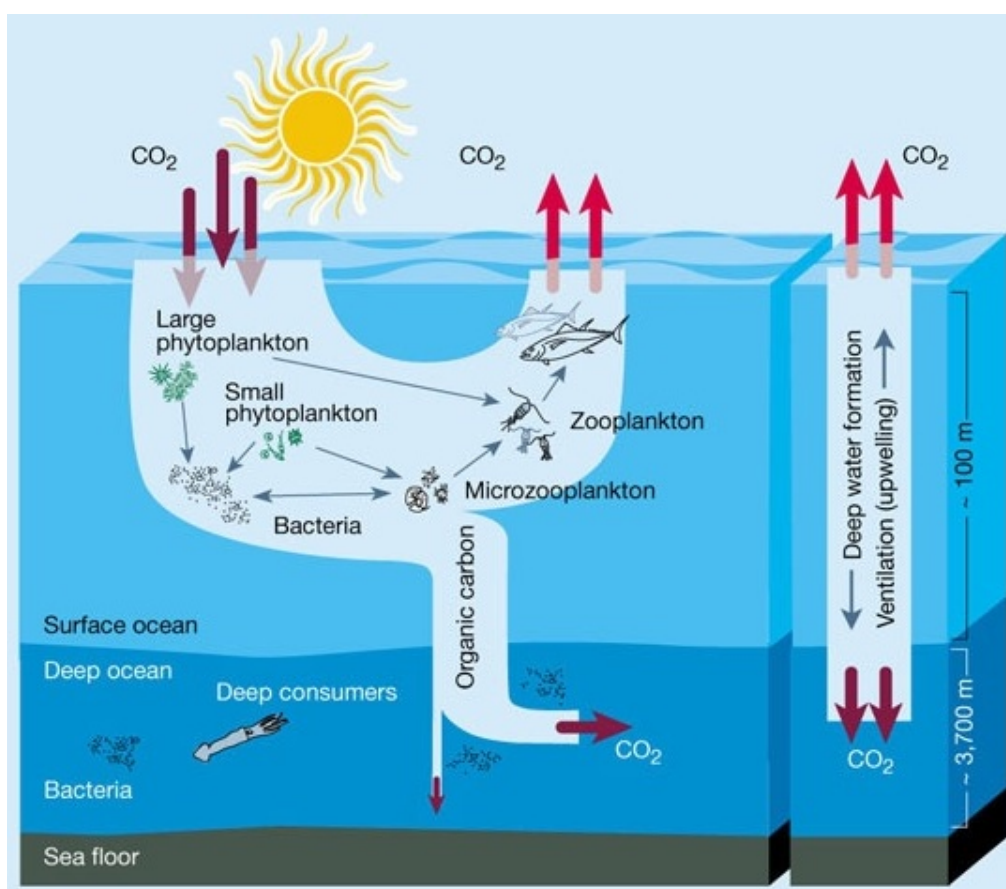


Figure 1.7: The ‘biological pump’ is a collective property of a complex phytoplankton-based food web. Together with the ‘solubility pump’ (right), which is driven by chemical and physical processes, it maintains a sharp gradient of CO₂ between the atmosphere and the deep oceans where 38×10^{18} g of carbon is stored. Using sunlight for energy and dissolved inorganic nutrients, phytoplankton convert CO₂ to organic carbon, which forms the base of the marine food web. As the carbon passes through consumers in surface waters, most of it is converted back to CO₂ and released to the atmosphere. But some finds its way to the deep ocean where it is remineralised back to CO₂ by bacteria. The net result is transport of CO₂ from the atmosphere to the deep ocean, where it stays, on average, for ~1,000 years. The food web’s structure and the relative abundance of species influences how much CO₂ will be pumped to the deep ocean. This structure is dictated largely by the availability of inorganic nutrients such as nitrate, phosphate, silicic acid and iron. Iron is the main limiting nutrient in the SO, which is why many Fe fertilisation experiments conducted there (e.g. [Boyd et al. \(2000\)](#)). Figure and caption Reproduced with permissions from [Chisholm \(2000\)](#).

so differentiating between clouds and dust using wavelength-based techniques has mostly proved unreliable ([Gordon, 1997](#); [Gordon et al., 1997](#); [Moulin et al., 2001](#); [Smirnov et al., 2002](#)). Remote sensing is limited by its dependence on various target parameters returning a different spectral signature. Recent work investigating the dust-chlorophyll correlation has postulated that dust and chlorophyll in the ocean are sometimes indistinguishable by satellite sensors as dust changes the optical properties of seawater towards green ([Moulin et al., 2001](#); [Smirnov et al., 2002](#); [Claustre](#)

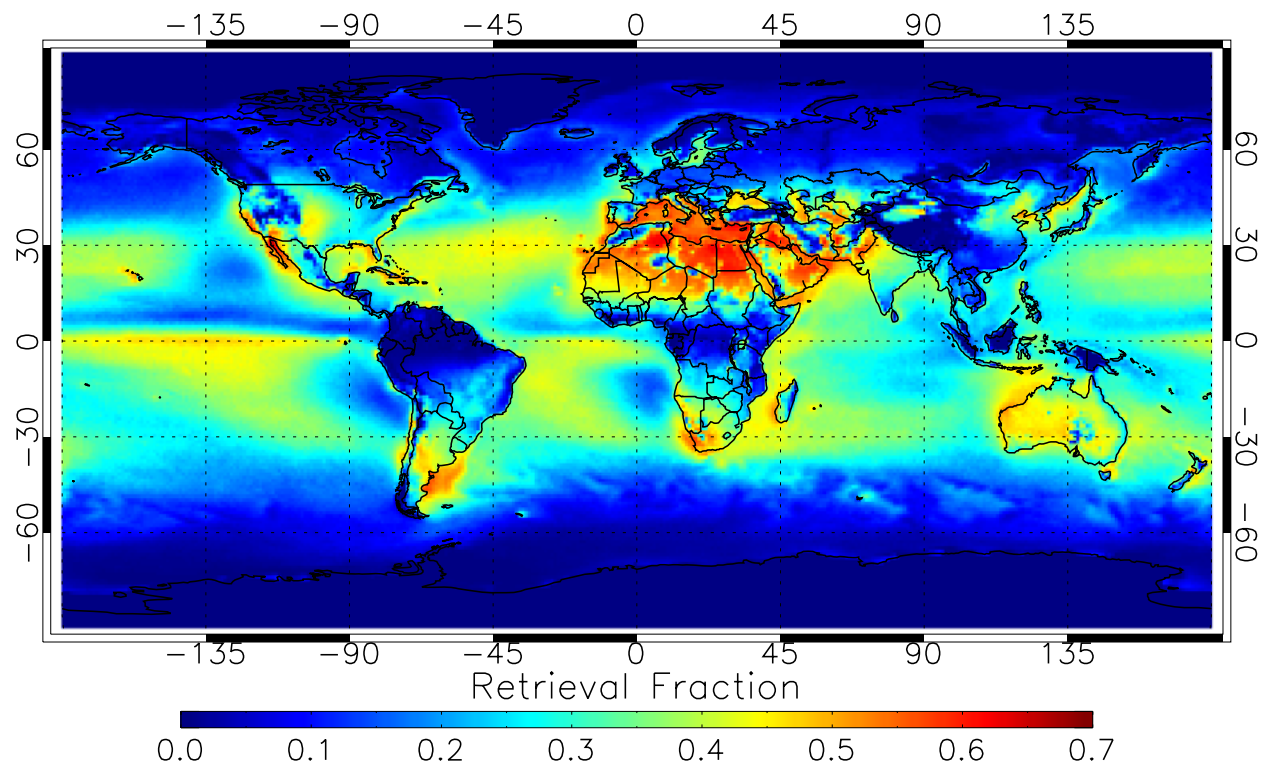


Figure 1.8: Mean retrieval rate of AOD wavelengths from SeaWiFS, Terra/MODIS and Aqua/MODIS. Low values (blue) represent poor signal quality due to darkness, cloud or snow. Polar regions exhibited much poorer coverage than mid-latitudes. Reproduced with permissions from [Hsu et al. \(2012\)](#).

[et al., 2002](#); [Volpe et al., 2009](#)). That is, on the delivery of dust, the seawater becomes greener, regardless of chlorophyll response. Therefore, dust-chlorophyll correlation studies should exclude short time-lag comparisons (0–2 days) ([Claustre et al., 2002](#); [Volpe et al., 2009](#)). To date, there has been limited evidence globally correlating aeolian deposition with increased primary productivity over longer times-lags ([Gabric et al., 2010](#); [Boyd et al., 2010](#)), although this could be because the satellite methods used have been inappropriate. Satellites are also subject to more general interference. Mean AOD retrieval rates (which is the number of days per year that data were obtained) for the period 1997–2010 from MODIS (Terra and Aqua) and SeaWiFS satellites are presented in Figure 1.8. Low retrieval rates are characteristic of regions with persistent darkness, cloud or snow ([Hsu et al., 2012](#)). AOD retrieval rates were much lower in the polar regions, reducing the opportunity for their use in applied studies.

Through a combination of meteorological data, land-based aerosol measurements and computer modelling, estimates of global annual aeolian deposition have been achieved by [Seze et al. \(1991\)](#); [Whitehead et al. \(1998\)](#); [Zender et al. \(2003\)](#); [Jickells et al. \(2005\)](#); [Schulz et al. \(2009\)](#). The most recent studies have produced very similar estimates (see Figure 1.9), with variability attributed to

different assumptions concerning up-lift thresholds of dust and characteristics of defined source regions. These estimates match well with much of the ground-truthing methods available, but data are limited, even from terrestrial sources (Textor et al., 2006). Once an estimate of aeolian deposition is obtained (either through direct measurement, interpretation of satellite measurements or modelling), conversion to dissolved values (of any element) that are relevant to biological systems is not straightforward. This conversion is dependent on parameters such as the solubility of the element of interest, the particle size of dust delivered, mode of delivery (wet vs. dry) and geographical provenance (recently reviewed by Sholkovitz et al. (2012)). Therefore, *in situ* measurement can provide insight into the relative influence of dust on the biology of a region in a way which complements satellite and modelling-based estimates.

1.6 Dissolved Al concentrations as a proxy for dust deposition

Aluminium is delivered to the open ocean chiefly by aeolian processes and once dissolved has a short residence time due to its particle-active nature. Solubility of delivered dust ranges from 0.1–20% of the total mass, with the higher values usually the result of wet deposition of young soils and low values the result of dry deposition of old soils (Mackie et al., 2008; Sholkovitz et al., 2009; Buck et al., 2010; Ito, 2011; Sholkovitz et al., 2012, and references therein). It is thought to be biologically inert, primarily removed from the dissolved pool by adsorbing onto suspended particulate matter. However, Al is known to be incorporated into the silica frustules of siliceous organisms (e.g. diatoms) (Mackenzie et al., 1978; Stoffyn, 1979; Gehlen et al., 2002). Whether this action is active or passive is not yet known and at present it is assumed to be passive. Measures and Edmond (1989) proposed the use of Al as a proxy of aeolian deposition due to its unique biogeochemical properties and despite potential problems, *in situ* measurements of dAl in seawater have been established as a quasi-reliable method for estimating annual aeolian deposition rates (Measures and Edmond, 1989; Measures and Brown, 1996; Measures and Vink, 2000).

Measures and Brown (1996) were the first to present a dAl-to-dust conversion model (called the model for the Measurement of Aluminium for Dust Calculation in Oceanic Waters, MADCOW), developed by comparing aerosol samples and surface ocean dAl concentrations from the mid-Atlantic. MADCOW has since been utilised in multiple studies, most recently in work by Han et al. (2008). They combined MADCOW with the aeolian deposition model described by (Zender et al., 2003) (Dust Entrainment And Deposition, DEAD) to provide the first global estimates dAl distributions in the surface ocean.

1.7 The distribution of dAl in the global oceans

[Hydes and Liss \(1976\)](#) described the first analytical method capable of determining Al in seawater at trace levels. Since then there have been a limited number of studies investigating the distributions of dAl in the major ocean basins, the vast majority of which have been in the Atlantic (see [Figure 1.12](#)). [Han et al. \(2008\)](#) is the most complete study to have aggregated all published dAl data into a single database. A summary of the global distribution of dAl concentrations is presented in [Figure 1.10](#).

Globally, open ocean dAl concentrations range by more than 3 orders of magnitude from ~ 0.1 to 180 nM (see [Figure 1.10a](#)). Within any ocean basin, the range remains at least 2 orders of magnitude and a characteristic profile can be associated with each ocean basin (evident in [Figure 1.10b](#)). This Al signature is due to the short residence time of dAl, where Al is removed from the watermass at a rate faster than it travels between ocean basins. More recently, [van Hulst et al. \(2012\)](#) presented the first four-dimensional (space and time) investigation of the biogeochemical cycling of Al in the ocean. Their estimate of global surface ocean dAl is presented in [Figure 1.11](#) and agrees broadly with existing observations.

As can be seen in [Figure 1.12](#), there is an obvious paucity of dAl observations in the Australian sector of the SO. One of the key goals of the present project was to constrain relative mechanisms contributing to the biogeochemical cycling of Al in the Australian sector of the SO through the interpretation of two new data sets. The voyage tracks where these samples were collected are the black lines surrounding Tasmania in [Figure 1.1](#): SAZ-Sense (GIPY2); and the SR3 repeat transect (GIPY6).

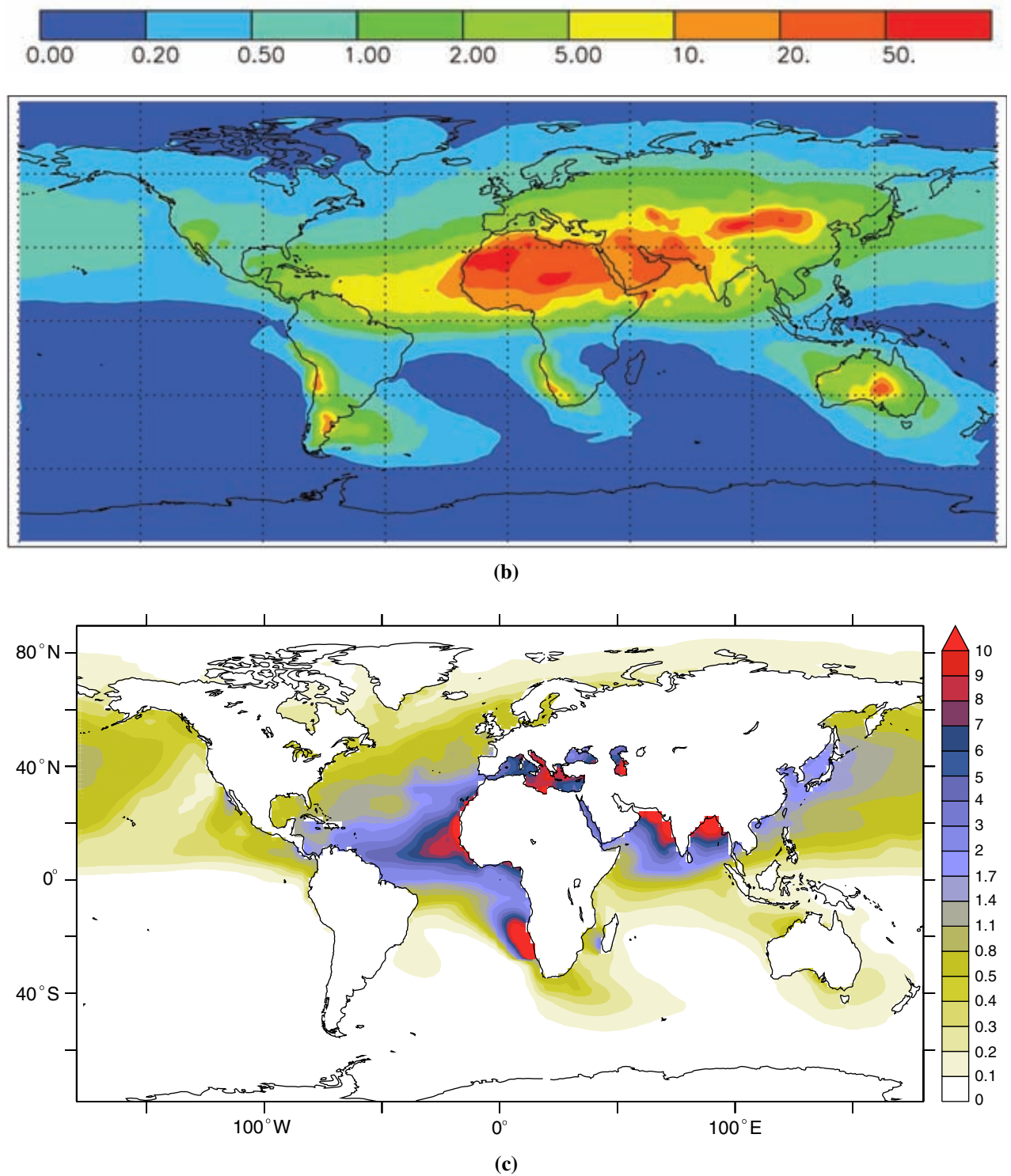
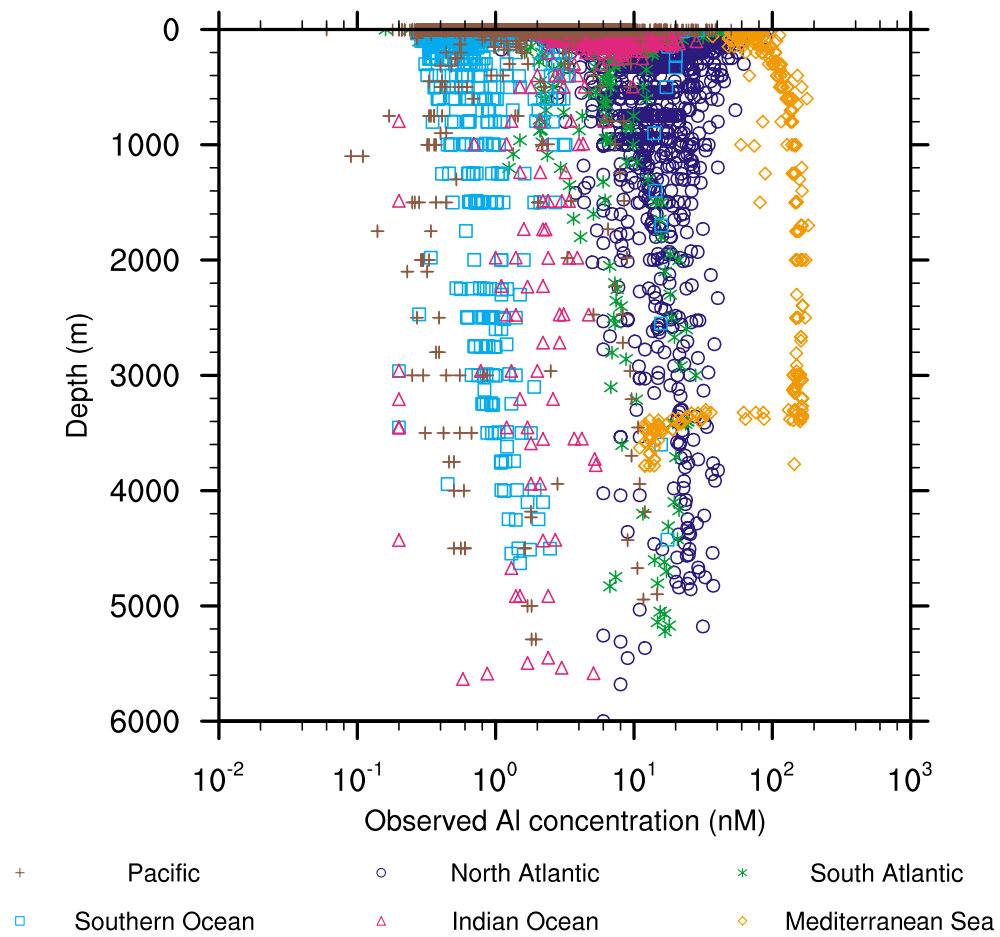


Figure 1.9: Recent modelling of annual aeolian deposition to the ocean surface ($g\ m^{-2}\ yr^{-1}$): (a) predicted by the Dust Entrainment And Deposition model (DEAD) described by Zender et al. (2003). Figure from Jickells et al. (2005) is a composite of outputs from three modelling studies (Duce, 1991; Ginoux et al., 2001; Hand et al., 2004) with output extremely similar to that from DEAD. (b) predicted by the Interaction of Chemistry and Aerosol module (INCA) of the Laboratoire de Météorologie Dynamique General Circulation model (LMDzT) described by Seze et al. (1991); Whitehead et al. (1998); Schulz et al. (2009). Figure from van Hulst et al. (2012).

Ocean Basin	Approximate range of observed values (nM)			
	Mean 0–50 m	Mean 150–500 m	Min.	Max.
Mediterranean Sea	65	97	10	180
North Atlantic	24	15	1	100
South Atlantic	16	7	0.2	50
Indian	15	7.5	0.2	30
Pacific	3	3	0.1	40
Southern	2	2.5	0.1	10
Arctic	1	3	0.1	25

(a)



(b)

Figure 1.10: (a) Observed range of dAl in different ocean basins. Data taken from a summary of 40 voyages presented by Han et al. (2008). (b) Depth profiles of dAl concentrations in different ocean basins. Figure Reproduced with permissions from Han et al. (2008).

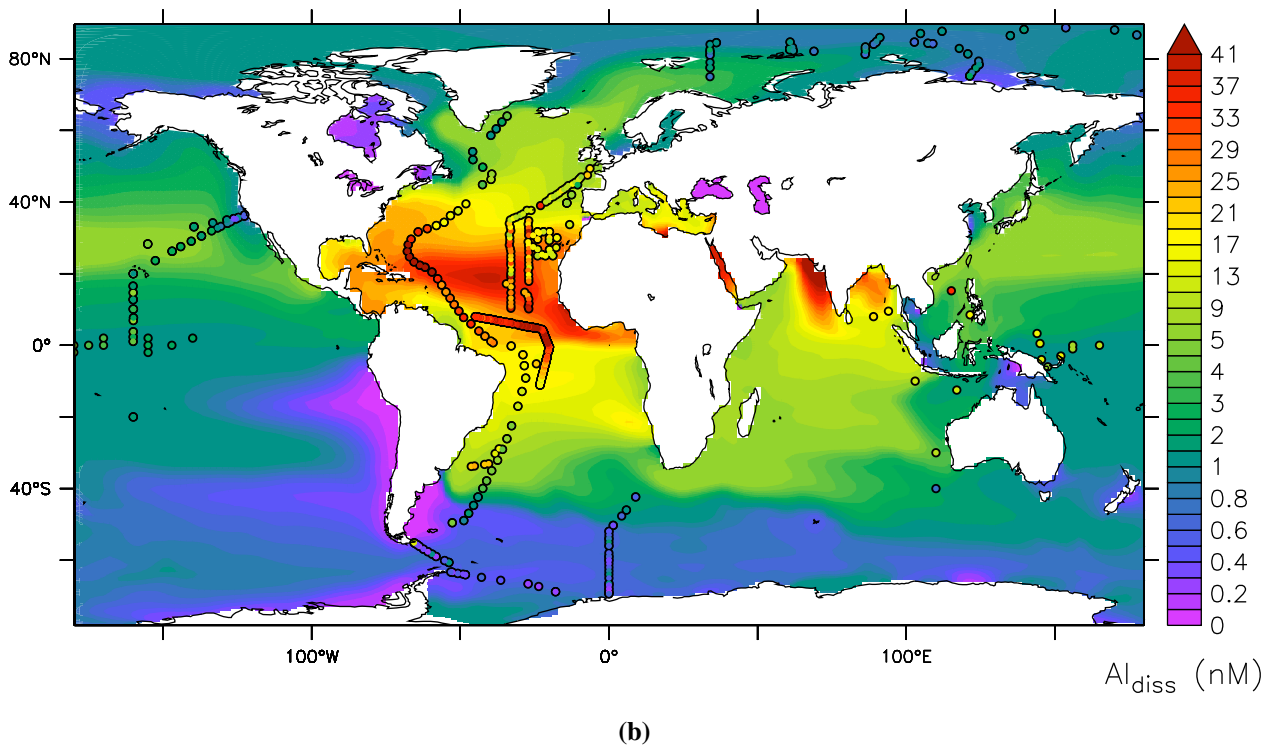
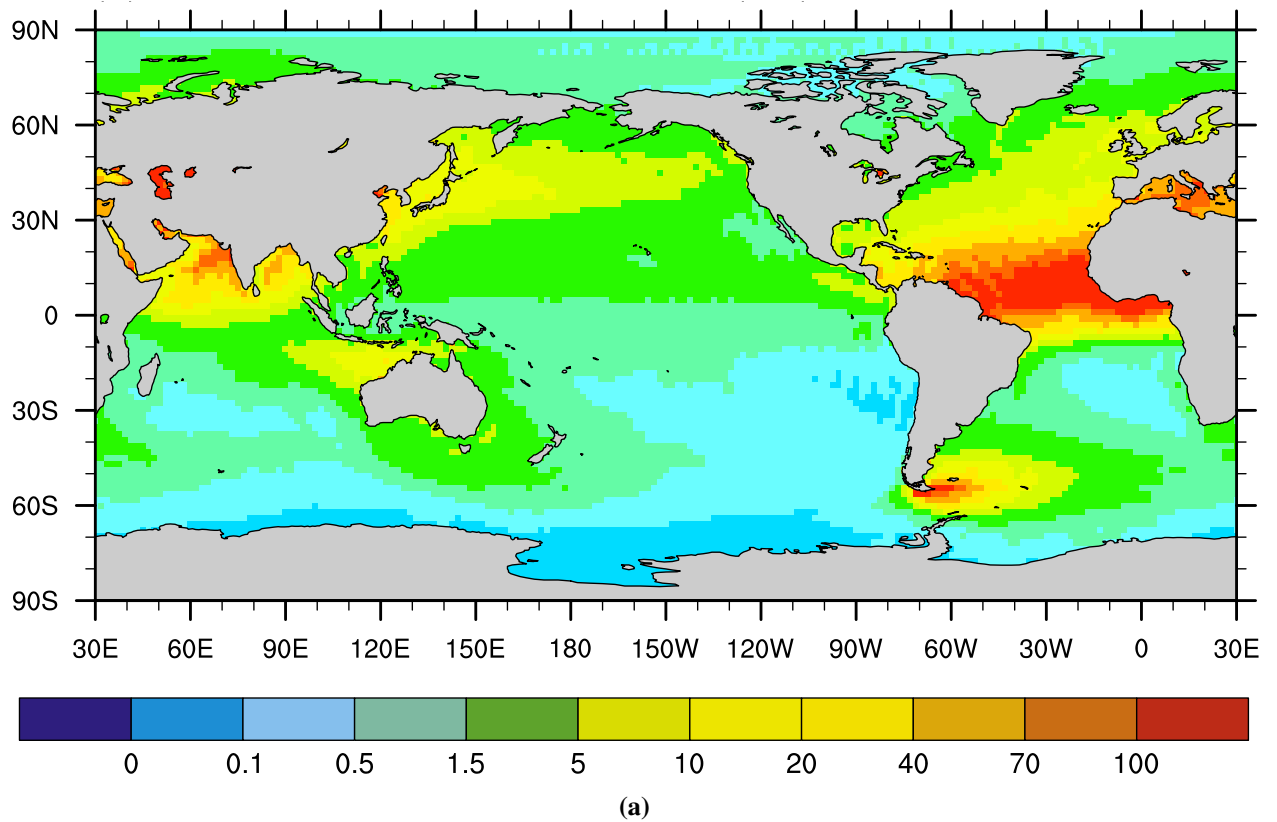


Figure 1.11: Estimates of dAl (nM) in the surface ocean from two models: (a) The DEAD-MADCOW model (reproduced with permissions from [Han et al. \(2008\)](#)) (b) The NEMO-PISCES model (reproduced with permissions from [van Hulten et al. \(2012\)](#), which has the available insitu dAl observations plotted on top of it). Note that the scales are expanded for low concentrations.

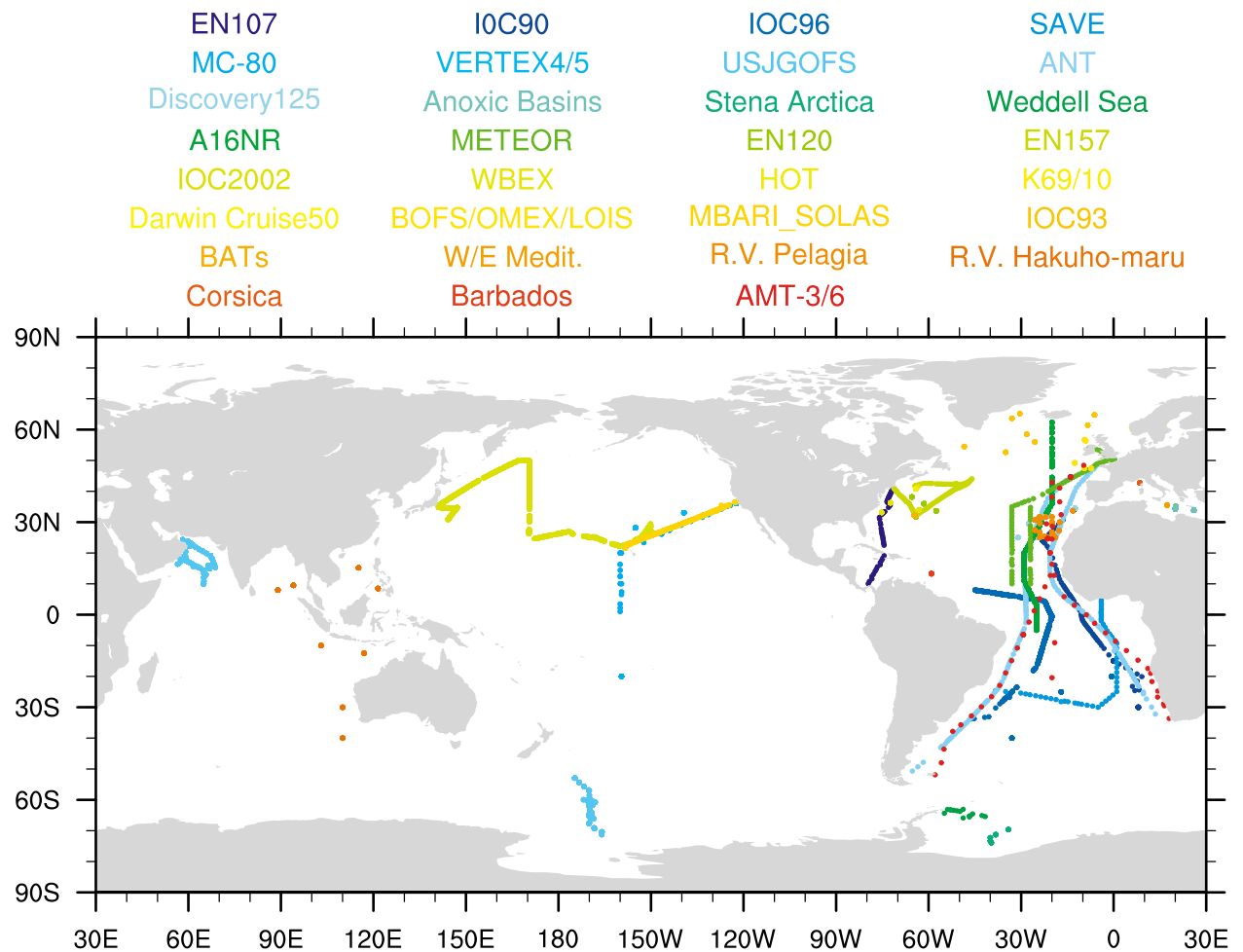


Figure 1.12: Locations of all dAl values published before 2007. Reproduced with permissions from Han et al. (2008).

1.8 Previous work that guided the practical direction of this project

The goal of this project was to investigate the impact of aeolian deposition to the Australian Sector of the SO using dAl concentrations. All previous estimates suggested dAl concentrations to be very low (~ 1 nM). Methods for determining ultra-trace levels of dAl in complex samples are limited. The most common method used for oceanographic analyses was the FIA technique first described by [Resing and Measures \(1994\)](#) and modified by [Brown and Bruland \(2008\)](#).

The initial goal of the overall project (which began in 2003 as the PhD project of Dr Juliette Tria, ([Tria, 2009](#))) was to apply the method of [Resing and Measures \(1994\)](#) to SO samples to obtain the first high resolution data set of dAl in the Australian sector. However, Dr Tria encountered significant technical difficulties during implementation of this FIA technique. After direct input from Prof. Measures, it became obvious the apparatus as utilised lacked robustness. Accuracy and precision (compared to SAFe reference materials) were not achieved. Dr Tria identified some of the limitations of the FIA system and addressed many through the development of a high-performance chelation-ion-chromatography (HPCIC) method ([Tria et al., 2008b](#)). During the final stages of Dr. Tria's PhD thesis the work presented in this dissertation then commenced.

The initial plan of this PhD project was to apply the method of [Tria et al. \(2008b\)](#) to seawater samples. As this was a new method, it required validation against an appropriate certified reference material (CRM). Unfortunately, Al is rarely certified in natural waters. The National Research Council of Canada has a river water CRM (SLRS) certified for Al ($\sim 50 \mu\text{g.kg}^{-1}$). Although the HPCIC method did show good agreement with the certified values for Al in SLRS, it was not reasonable to extend this agreement to sub-nM levels in seawater. The trace element biogeochemical community (pre-GEOTRACES) had recently developed the SAFe reference standards, although these had only been analysed for dAl by three groups at that time. These quasi-certified SAFe values were used to assess the performance of the HPCIC method. Al in the SAFe values using the HPCIC method were found to be ~ 5.0 nM, ~ 5 -fold higher than those previously reported (although precision was maintained at $< 5\%$). This apparent inaccuracy at low concentrations of dAl coupled with analysis times ~ 3 -fold greater than those using FIA prompted a departure from the HPCIC approach. It was decided to revisit FIA, applying the (then recent) modifications of [Brown and Bruland \(2008\)](#). Using the [Brown and Bruland \(2008\)](#) approach, a marginal improvement was observed in system performance from previous attempts in our lab, with a system appropriate for samples > 5 nM. However this particular system was still temperamental and exhibited most of the same limitations identified by Dr. Tria. These limitations deemed the FIA (as constructed and implemented in Hobart) inappropriate for the SO samples of interest.

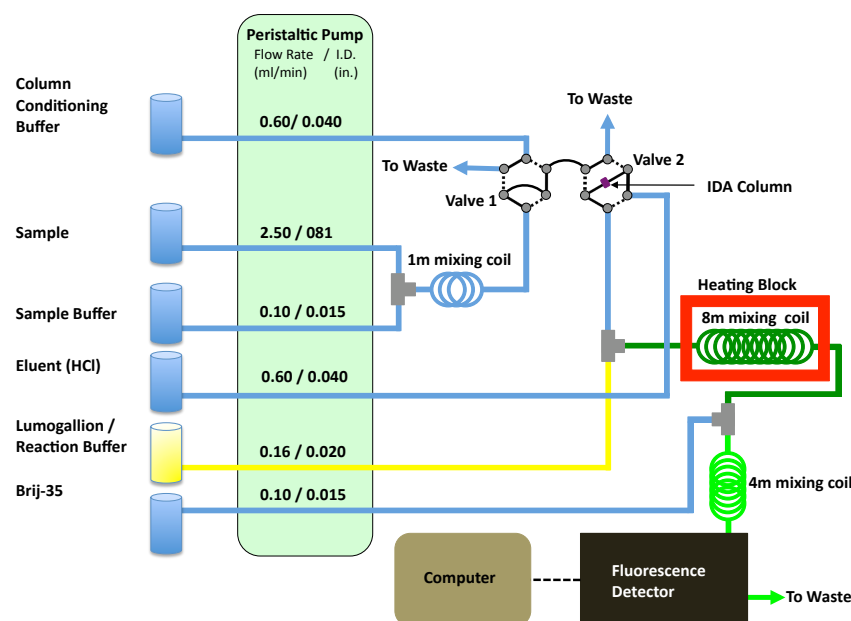


Figure 1.13: Schematics of the FIA method presented by Brown and Bruland (2008)

The performance of a range of alternative methods from the literature were reassessed. During this assessment of previous methods, particular attention was taken to determine the extent of trace-clean protocols applied and how advances in analytical technology could be applied to improve current methodologies. A summary of the methods considered is presented in Table 1.2. Of these, the RP-HPLC method presented by Wu et al. (1995); Zhou et al. (1995) appeared to have the greatest potential for improvement. This is discussed in Chapter 2. Schematics of the FIA, HPCIC and RP-HPLC methods are presented for comparison in Figures 1.13, 1.14 and 1.15.

It has been recognised recently by the oceanographic community that the technological advances within the field of analytical chemistry over the past 40 years have not yet been applied fully to oceanographic analyses. There is significant interest in the advancement and standardisation of analytical methods currently being applied for oceanographic studies, with a workshop titled the Collaborative on Oceanographic Chemical Analysis (COCA), held in March 2013 (http://www.soest.hawaii.edu/oceanography/faculty/chris/COCA/What_is_COCA.html).

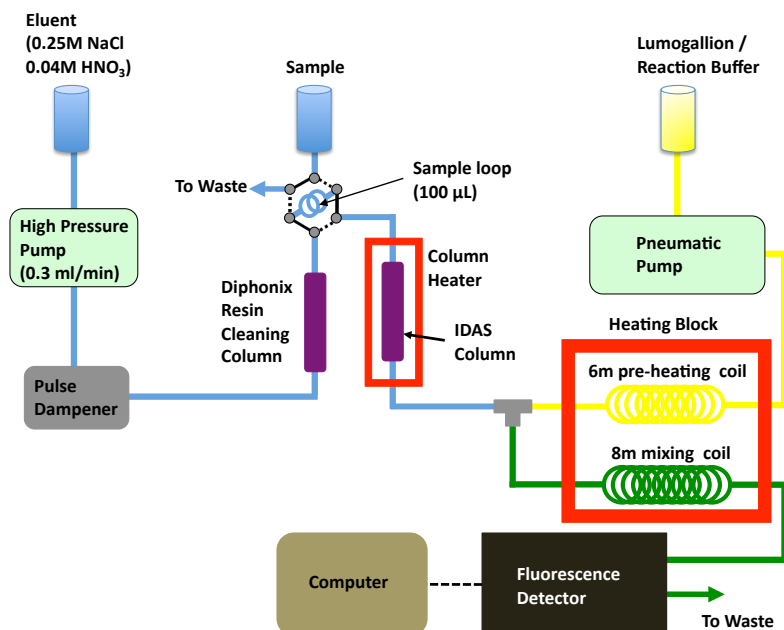


Figure 1.14: Schematics of the HPCIC method presented by [Tria et al. \(2008b\)](#)

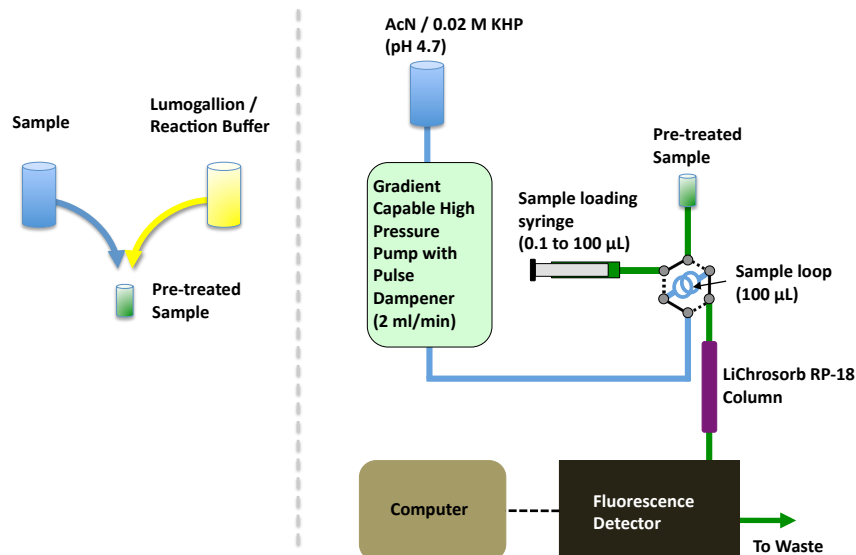


Figure 1.15: Schematics of the RP-HPLC method presented by [Lee et al. \(1996\)](#)

Table 1.2: An overview of analytical methods used for the determination of Al in natural water matrices (concentrations reported in the original articles have been converted to M or nM here for comparison purposes). Reproduced and updated from [Tria \(2009\)](#).
Atomic Emission Spectroscopy (AES); Cathode Stripping Voltammetry (CSV); Chromazuril S immobilised silica gel (CSG); Electron Capture Detection (ECD); Ethylenediaminetetraacetic acid (EDTA); Gas Chromatography (GC); Graphite Furnace (GF); High-performance Chelation-Ion-Chromatography (HPCIC); High-Performance liquid-chromatography (HPLC); Inductively Coupled Plasma (ICP); Ion-Exchange liquid-chromatography (IE); Limit Of Detection (LOD); Mass Spectrometry (MS); octadecylsilane (ODS and C₁₈); salicylaldehyde picolinylhydrazine (SAPH); Single drop microextraction (SDME); C₁₈ functionalised Reversed-Phase column (RP-18); Ultra Violet – Visible light spectrum (UV-Vis); 1,1,1-trifluoro-2,4-pentanedione (HTFA); 1,2-dihydroxyanthraquinone-3-sulphonic acid (DASA); 8-hydroxyquinoline (8-HQ); 8-hydroxyquinoline-5-sulfonic acid (8-HQS)

Method type	Pre-concentration	Sample matrix	LOD	Precision	Ref.
GF-AAS	Solvent extraction (8-HQ)	Sea water	0.1 nM	5% at 1.0 nM	Orians and Bruland (1986)
ICP-AES	HPLC (CSG)	Sea and river water	10.4 nM	Not reported	Hirayama et al. (1994)
ICP-MS	SDME	Lake and synthetic water	0.12 nM (synthetic)	10% at 37 nM	Xia et al. (2005)
ICP-MS	Solid phase extraction (EDTA)	Sea, river and lake water	0.27 nM	<9% at 1 nM	Sohrin et al. (2008)
CSV	Hg drop electrode using DASA	Sea water	1.0 nM	2% at 15 nM	van den Berg et al. (1986) ; Hernandez-Brito et al. (1994)
ECD-GC	Solvent extraction (HTFA)	Seawater	0.6 nM	3.8% at 19 nM	Measures and Edmond (1989)
HPLC-UV-Vis	Kromasil C ₁₈ , Spherisorb ODS-2, LiChrosorb RP-18, Nova-Pak C ₁₈	River water	51.9 nM	1% at 5.2 M	Lian et al. (2004b)
Fluorometry					
RP-HPLC-	LiChrosorb RP-18	Sea and tap water	1.85 nM	2.4% at 1.9 μ M	Wu et al. (1995) ; Zhou et al. (1995)
Lumogallion		Lake and river water	1.85 nM	1.8% at 1.0 μ M	Lian et al. (2004a)
RP-HPLC-Morin	Spherisorb ODS	ter			
HPCIC-	IDAS	Sea, river, tap and waste water	0.39 nM		Tria et al. (2008b)
Lumogallion					
FIA-	Solid phase extraction (8-HQ)	Sea water	0.15 nM	1.7% at 2.6 nM	Resing and Measures (1994) ; Brown and Bruland (2008)
Lumogallion					Giesbrecht (2007)
SIA-	None	Sea and Fresh water	24 nM	2.0% at 75 nM	
Lumogallion		ter			
IE-8-HQS	Amberlite IR-120	Salt and fresh water	3.7 nM	2% at 0.37 μ M	Alonso et al. (1989)
8-HQ	Solvent extraction (chloroform)	River, drinking and waste water	7.4 nM	4.9% at 1.9 μ M	Alonso et al. (2001)
SAPH	None	Sea water	11.1 nM	1.9% at 7.4 nM	Manuel-Vez et al. (1997)

1.9 The aims of this project

The major aims of this project were:

- (i) To improve existing methods used for the determination of dAl in open ocean seawater samples.
- (ii) To investigate the distribution of dAl in the Australian sector of the SO.
- (iii) To conduct biogeochemical and oceanographic interpretation of these dAl concentrations to elucidate the relative contribution of various supply mechanisms to the waters sampled.
- (iv) To compare dAl observations in the SO to model estimates.
- (v) To estimate aeolian deposition of dust to the SO using dAl concentrations as a proxy (using MADCOW, or if necessary develop an alternative model) and subsequently compare these estimates to those from atmospheric models.

Chapter

2

Fast and sensitive determination of Al with RP-HPLC using an ultra-short monolithic column

[This is a complete type script of [Remenyi et al. \(2011\)](#)]

2.1 Introduction

Aluminium is a known toxicant for biological organisms and it is regularly monitored in many different kinds of samples including lake, river and drinking waters ([Zhou et al., 1995](#); [Bi et al., 2003](#); [Ščančar and Milačič, 2006](#)), fish ([Rietz et al., 1997](#)), human serum ([Wu et al., 1995](#)) and human urine ([Lee et al., 1996](#)). In environmental chemistry, Al is also used as a tracer of aeolian deposition events and the movement of water bodies in the ocean ([Measures and Edmond, 1990](#); [Johnson et al., 2003](#); [Han et al., 2008](#); [Tria et al., 2008a,b](#); [Middag et al., 2009](#)).

Determination of total Al in this wide range of samples has been achieved using a number of methods, mainly spectroscopic, including graphite furnace atomic absorption spectroscopy (GF-AAS) ([Ranau et al., 1999](#)), flame atomic absorption spectroscopy (FAAS) ([Liu et al., 2005](#)), ultraviolet - visible spectrophotometry (UV-VIS) ([Erdemoğlu and Güçer, 2005](#)), instrumental neutron activation analysis (INAA) ([Rietz et al., 1997](#)), electron capture detection gas chromatography ([Measures and Edmond, 1989](#)), and inductively coupled plasma mass spectrometry (ICP-MS) ([Rietz et al., 1997](#); [Nagae and Sato, 2005](#)). However, as these methods only determine total Al, different methods are required to analyse the various species of Al in a sample, such as differentiating between reactive and non-reactive forms ([Tria et al., 2007](#)).

Chromatographic techniques are an effective option and have advantages over other techniques. They can remove analytes from their sample matrix while simultaneously separating different chemical species of an element from each other. They typically have lower detection limits, require smaller sample volumes and can be used to improve performance of existing techniques. Some examples where chromatography is utilised to improve the performance of existing techniques are: GC-GF-AAS ([Measures and Edmond, 1990](#)); both sequential injection analysis (SIA) ([Šatinský et al., 2003, 2004](#)) and flow injection analysis (FIA) ([Resing and Measures, 1994](#); [Brown and](#)

Bruland, 2008) with in-line concentration columns; high performance chelation ion chromatography (HPCIC) (Tria et al., 2008a,b); and HPLC-MS/MS (Gao et al., 2010).

It should be noted that SIA and FIA techniques that use in-line pre-concentration onto mini-columns (both conventional and monolithic) with an elution program, may be considered as a sort of low-pressure liquid-chromatography techniques, such as Victory et al. (2004) and Pelletier and Lucy (2006). Many of the technical disadvantages of these low-pressure systems (e.g. relatively large dead-volumes, a requirement for larger sample volumes, backpressure difficulties, relatively high baseline noise due to pump pulsation) can be avoided if they are modified into high-pressure systems. Further advantages of high pressure systems include improving the in-line column's efficiency by allowing it to be longer, more tightly packed, with smaller particle sizes, as well as increasing flow-rate, since backpressure is less of an issue.

Determination of Al using chromatography has been achieved using ion chromatography (Chaudry et al., 1988), high performance chelation ion chromatography (HPCIC) (Tria et al., 2008a,b), size exclusion chromatography (SEC) (Flaten and Lund, 1997) and reversed-phase high-pressure liquid-chromatography (RP-HPLC) of metal chelates (Zhou et al., 1995; Wu et al., 1995; Lee et al., 1996; Nagae and Sato, 2005) (schematics of methods relevant to this thesis are compared in Figures 1.13, 1.14 and 1.15). RP-HPLC of metal chelates was selected as it is one of the most sensitive, accurate and efficient methods for determination of Al (Nagae and Sato, 2005). This method detects Al in the form of a hydrophobic chelate, and can do so in samples with a complicated matrix (e.g. human urine, digested fish flesh, seawater) and is easily deployed into remote locations (e.g. instrumentation used on oceanographic voyages).

Usually, methods that employ RP-HPLC of metal chelates have two major steps. The first step is the formation of an Al-ligand complex by adding an organic ligand to the sample. The second step is injection of the pre-treated sample onto an analytical column. The ligands preferred for RP-HPLC determination of complexed Al are 8-hydroxyquinoline (Hambali and Haddad, 1980), morin (Lian et al., 2003) and lumogallion (Wu et al., 1995). Lumogallion (2,2',4'-trihydroxy-5-chloroazobenzene-3-sulfonic acid) was selected for this study as it is highly selective for Al complexation over other metals (with the exception of gallium, which is normally in extremely low concentrations), forming a highly fluorescent, very stable Al-lumogallion complex allowing for extremely sensitive detection (Hydes and Liss, 1976; Nagae and Sato, 2005). For these reasons RP-HPLC with fluorescence detection of the Al-lumogallion complex has been found to be the second most sensitive method for determination of Al in aqueous samples (Nagae and Sato, 2005).

Our aim was to develop a method that could determine the Al concentration in an aqueous sample faster than existing methods using RP-HPLC with an ultra-short monolithic column. This paper

demonstrates this technique is simpler, faster and cheaper than previous methods while maintaining sensitivity, accuracy and precision and is suitable for use in existing applications. This is vital for the analysis of large sample arrays such as those in environmental monitoring or oceanographic investigations.

Detection of Al in seawater at sub-nM concentrations is difficult. ICP-MS cannot be used for direct determination of seawater due to interference from the saline matrix. Therefore other approaches are required. AAS techniques cannot achieve the detection limits necessary in open ocean seawater without preconcentration, and the sample volumes required for this preconcentration are prohibitive. Al is invisible to UV-Vis or fluorescence techniques, however, Al can create stable complexes with compounds that contain chromophores and can be detected using these techniques. Fluorescence is at least 10-fold more sensitive than UV-Vis, so only fluorometric approaches are discussed here.

Fluorescence is a remarkably sensitive technique. The analyte is bombarded with photons at a specific wavelength, where electrons are temporarily excited and on relaxation, emit photons of a corresponding longer wavelength. This emission of light is then detected. It is highly sensitive because potential for interference is low. The derivatives that have been successfully applied for direct determination of Al in seawater include lumogallion, 8-HQ, 8-HQS, SAPH and morin. Of these, lumogallion provides the best performance. Lumogallion is highly selective for Al and very stable at room temperature. It has greater fluorescence yield than alternatives due to this selectivity and so can provide greater sensitivity. However, even the highly sensitive fluorometry technique cannot achieve detection limits suitable for application in open ocean seawater samples ([Giesbrecht, 2007](#)). Therefore, some form of preconcentration is required before detection using any method.

Preconcentration can be achieved through solid phase extraction where Al is adsorbed onto an adsorbent while unretained components are eluted (limiting potential inference later on). The Al is then eluted into the detection system as a much smaller volume than the sample injected. This is the mechanism used in the methods by [Resing and Measures \(1994\)](#); [Brown and Bruland \(2008\)](#); [Tria et al. \(2008b\)](#) where 8-HQ or IDA functionalised columns retain Al^{3+} through chelation. 8-HQ has maximum retention of Al at pH 5.5, this is unfortunate, as it is also the pH of minimum Al solubility (the dominant form is $\text{Al}(\text{OH})_3^0$). IDA has the advantage that it can retain Al even at low pH, and so can minimise pH manipulations, and thus reduce loss of analyte from the dissolved phase. However, both IDA and 8-HQ (and other chelating functional groups) also retain other metals that can interfere with Al determination with lumogallion (like Fe).

Another approach is to complex the Al^{3+} in seawater with compounds that have non-polar components (such as lumogallion) and then preconcentrate the Al-complex from the seawater

matrix using non-polar separation mechanisms. Here, the non-polar portion of the complex is adsorbed, whilst the polar components of the matrix are eluted, and then the complex is eluted to the detection system. This approach has been applied in RP-HPLC using both Al–lumogallion and Al–morin derivatives and has the advantage of selectively excluding non-target analytes during the preconcentration step, whilst also preconcentrating the derivative for highly sensitive fluorescence detection. The determination of Al–lumogallion by RP-HPLC was described by Wu et al. (1995); Zhou et al. (1995); Lee et al. (1996). The figures of merit presented by Wu et al. (1995); Zhou et al. (1995) and Lee et al. (1996) appeared promising, given that none of the previous authors had applied trace element clean protocols. It was further believed that further improvements could be achieved by applying new monolithic column technology. To understand how monolithic technology can achieve gains in performance, it is necessary to present some fundamentals of chromatography.

The capacity of a HPLC system to separate different target analytes within a sample mixture is termed separation efficiency. Good separation efficiency is when multiple analytes are separated into narrow discrete bands within a short time period. Separation efficiency can be optimised by altering: the affinity of analytes to the stationary phase relative to the mobile phase (i.e. changing the functional groups on the column, or in the eluent); the flow rate of the mobile phase past the stationary phase; the ratio of sample to column surface area (i.e. the sample volume, column length or the particle size of the stationary phase); and the kinetics of the system (i.e. heat and pressure).

Stationary and mobile phase components (the column and eluent respectively) of a separation system are selected for their capacity to adsorb and desorb target analytes within a sample mixture, while allowing non-target analytes to be unretained. Different target analytes have different affinities and therefore travel through the column at different rates, eventually separating into discrete bands. The time where the maximum peak height of an unretained component is observed is called the breakthrough time (t_0). The time where the maximum peak height of an analyte is observed is its retention time (t_R). The retention factor of an analyte in a system is k , where $k = \frac{t_R - t_0}{t_0}$. Ensuring different analytes have different values for k results in separation. The resolution of a chromatographic system (R_s) is defined by the distance between two peak maxima and the arithmetic mean of the peak widths. It reflects if peaks are co-eluted or baseline resolved. Optimal value is $R_s = 1.5$ – 2.0 . Larger values reflect analysis time could have been shorter, smaller values indicate analyte co-elution. For multiple analytes, the optimum value for each adjacent pair must be selected.

Columns with a greater number of binding sites (i.e. surface area) have greater capacity to separate analytes. Therefore, columns tightly packed with smaller size particles, used with eluent forced through at high pressure can achieve many orders of magnitude greater separation efficiency than

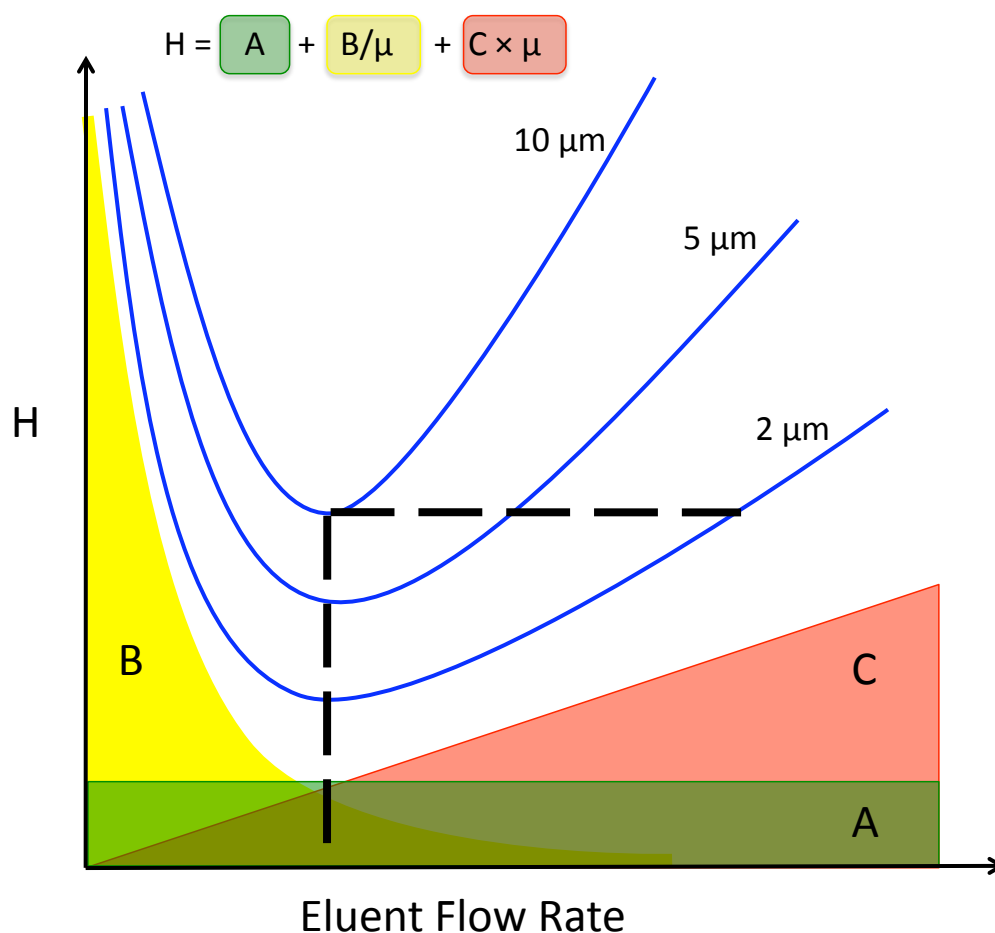


Figure 2.1: Simplified version of Van Deemter plot. The effect of each term is the shaded area of matching colour. A = Eddy-diffusion term, proportional to the linearity and uniformity of the flow through the column of similar sized particles; B = diffusion coefficient of the eluting particles in the longitudinal direction; C = Resistance to mass transfer coefficient of the analyte between mobile and stationary phase; μ = linear velocity; H = Theoretical plate number.

low-pressure systems using loosely packed columns (such as the solid-phase extraction columns used in FIA). The Van Deemter Equation describes the effect of physical parameters (column length, particle size, flow rate, on separation efficiency. A simplified model description is presented in Figure 2.1. Using this equation, lower values represent improved efficiency. The optimal flow rate is defined as the minimum of each blue curve. Each column has its own particular shaped curve. The different curves represent how columns of the same length packed with smaller particles either have improved efficiency at the same flow rate, or equal efficiency at faster flow rates. In this theoretical example, decreasing the particle size from 10- μm to 2- μm , particles would allow flow rates to more than double (and analysis times to be reduced by more than half) with no loss of analytical performance.

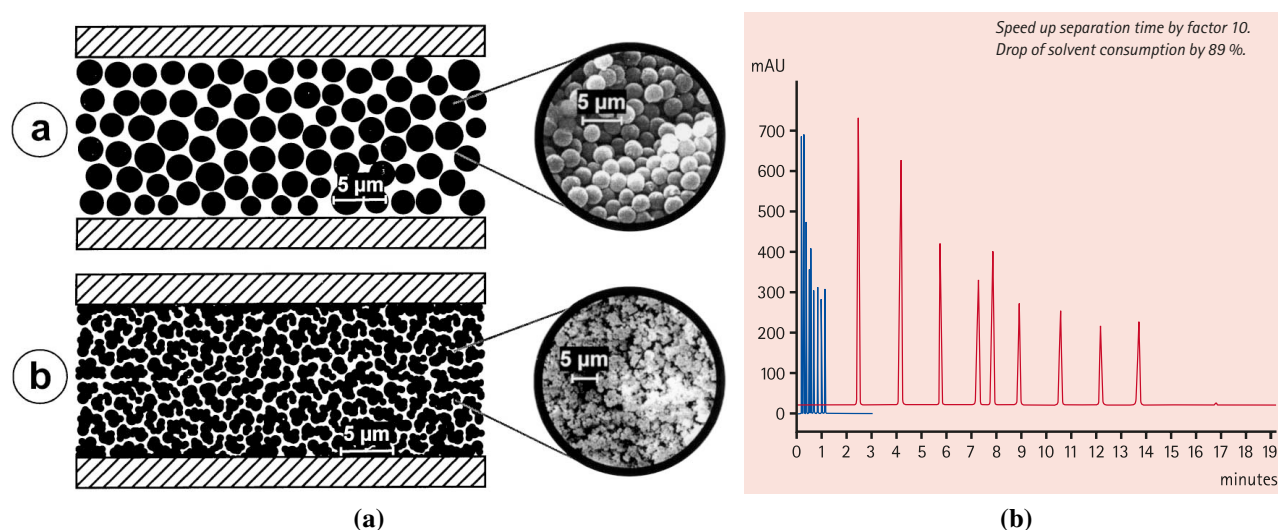


Figure 2.2: (a) Schematic of the internal structure of monolithic vs. packed bed columns. Reproduced with permission from [Oberacher and Huber \(2002\)](#). (b) Comparison of separation performance of monolithic column (in blue) vs. packed bed columns (in red) under identical separation conditions. The monolithic columns achieve the separation 10-fold faster, with improved signal-to-noise. Figure provided by Merck Millipore.

A limitation of tightly packed columns within HPLC systems, is that the decreased interstitial volume results in increased backpressure, requiring expensive pumping systems, or limiting flow-rates. A recent advance in chromatographic column technology has resulted in the development of monolithic columns. These, unlike packed columns, are a single piece of porous stationary phase that achieves high surface area, without associated high backpressure. A comparison to packed particle columns is presented in Figure 2.2. These have been demonstrated to improve overall system performance and flexibility when used in both low-pressure and high pressure systems ([Victory et al., 2004](#); [Remenyi et al., 2011](#)). Improvements include reduced analysis times, improved separation efficiency and capacity to take greater sample volumes (improving signal to noise ratios). A less obvious advantage is improved versatility. Given the reduced backpressure, eluents of high viscosity, previously discounted, can be utilised, offering the potential for improved chemistry ([Remenyi et al., 2011](#)).

2.2 Experimental

2.2.1 Apparatus

Samples and pre-column reagent were stirred using a Fisher Brand Whirlimixer®. pH was measured with a labCHEM-pH meter (TPS Pty Ltd, Brisbane, Australia). Sample management was done

using an Alliance 2690 HPLC system (Waters, Milford, USA), dwell volume = 1.2 mL. Analyte concentration and separation was achieved on a Chromolith® RP-18e Guard (10 × 4.6 mm) column (Merck KGaA, Darmstadt, Germany). Note that initial studies were conducted using a Chromolith® RP-18e Performance (100 × 4.6 mm) column (Merck KGaA, Darmstadt, Germany). Analytes were detected using a scanning fluorescence detector Waters model 474, gain = 1, λ_{ex} = 505 nm bandwidth = 18 nm, λ_{em} = 574 nm bandwidth = 18 nm, with control and signal processing achieved using Empower® software (Waters, Milford, USA).

Samples were also analysed with a SpectrAA-800 FAAS using an Al hollow cathode neon-filled lamp, lamp current = 10 mA, fuel = acetylene, support = nitrous oxide, flame stoichiometry = reducing; red cone 1-2 cm high, wavelength = 309.3 nm, slit width = 0.5 nm, with system control and signal processing done using SpectrAA software (Varian, Palo Alto, USA).

Sample bottles were made of low-density polyethylene (LDPE) and reagent flasks were made of polypropylene (PP).

2.2.2 Reagents

All deionised water was from a Milli-Q® Elix® and Gradient® coupled system (Millipore, Billerica, USA). The eluent was deionised water and Supragradient® HPLC grade methanol (Scharlau Chemie S.A., Sentmenat, Spain). Lumogallion (97%, powdered, Pfaltz & Bauer Inc. Waterbury, USA) was made up to 5 mM in deionised water (0.0517 g / 30 mL). 2-(N-morpholino)ethanesulfonic acid, also known as solid MES hydrate 99.5% (Sigma-Aldrich, St Louis, USA), was made up to 1 M in deionised water (19.523 g / 100 mL, this solution has a pH < 3), it was then purified with respect to transition elements by passing it through a 200×4.6 mm I.D. column packed with Diphonix® resin, particle size 75-150 μ m (Eichrom Technologies Inc., Lisle, USA) at 0.2 mL min⁻¹ (Tria et al., 2008b). MES solutions at higher concentrations than 1 M created precipitates when stored below 4 °C. pH adjustment was done using 16 M Seastar Chemicals Inc. (British Columbia, Canada) SEASTAR™Baseline® nitric acid and 5 M sodium hydroxide solution, made up from pelletised AnalR® sodium hydroxide (BDH, Dorset, UK) in deionised water (20.00 g / 100 mL). All standards were made up using 1000 mg.L⁻¹ (0.371 M) Al³⁺ in 0.5 M nitric acid (Merck KGaA, Darmstadt, Germany). All stock solutions were stored in the dark at < 4 °C. Samples and standards were diluted in deionised water acidified to pH 1.8.

2.2.3 Sample types

Preliminary method development used deionised water spiked with Al³⁺, selected because it was free from interferences.

Matrix interference studies used open-ocean seawater collected and stored using GEOTRACES protocols (Cutter et al., 2010) and spiked with Al^{3+} . Seawater was selected because the eventual aim was to use this method to analyse samples collected from the open ocean.

Linearity, recovery and method comparison (to FAAS) studies used a tea-infusion made from a commercially branded black tea in boiled water. It was selected because it has a relatively simple matrix, is commonly used as a test solution in method development and its Al concentration is known to be within the working range of many methods (ranging from 0.4 to 4000 μM) (Erdemoğlu and Güçer, 2005).

2.2.4 Reversed phase HPLC

Sample preparation

Deionised water, seawater and tea-infusions were prepared in the same way. A 10-mL aliquot was collected in a clean syringe, passed through a 30-mm 0.45- μm PES Plus® syringe filter (Micro Sciences, Redondo Beach, USA) filtered into a 10-mL Sarstedt polypropylene tube and then acidified to pH 1.8 (if necessary) with 9.9 μL of 16 M nitric acid (to ensure dAl remained in solution (Cutter et al., 2010)).

Development of the pre-column reagent

The purpose of the pre-column reagent mixture is to allow and promote the formation of the fluorescent Al–lumogallion complex.

Optimum yield is achieved at pH 5.0–5.5 (Resing and Measures, 1994; Wu et al., 1995; Lee et al., 1996; Brown and Bruland, 2008), therefore, the pre-column reagent pH must be adjusted to account for the pH of the sample of interest. In this study, all samples were collected and stored at pH 1.8. The pre-column reagent mixture needed to be adjusted to pH 6.1 to bring the combined mixture to the correct reaction pH.

The speed of the reaction increases from 0–70°C (Tria et al., 2008b), >70°C, the fluorescence decreases rapidly towards zero probably as the complex decomposes.

As can be seen in Figure 2.3, lumogallion was required to be greater than 5.0 μM in order to successfully complex all contaminant Al in the pre-column reagent. To ensure the excess of lumogallion was much greater than Al in the sample, the pre-column reagent was made so it contained 0.18 mM lumogallion.

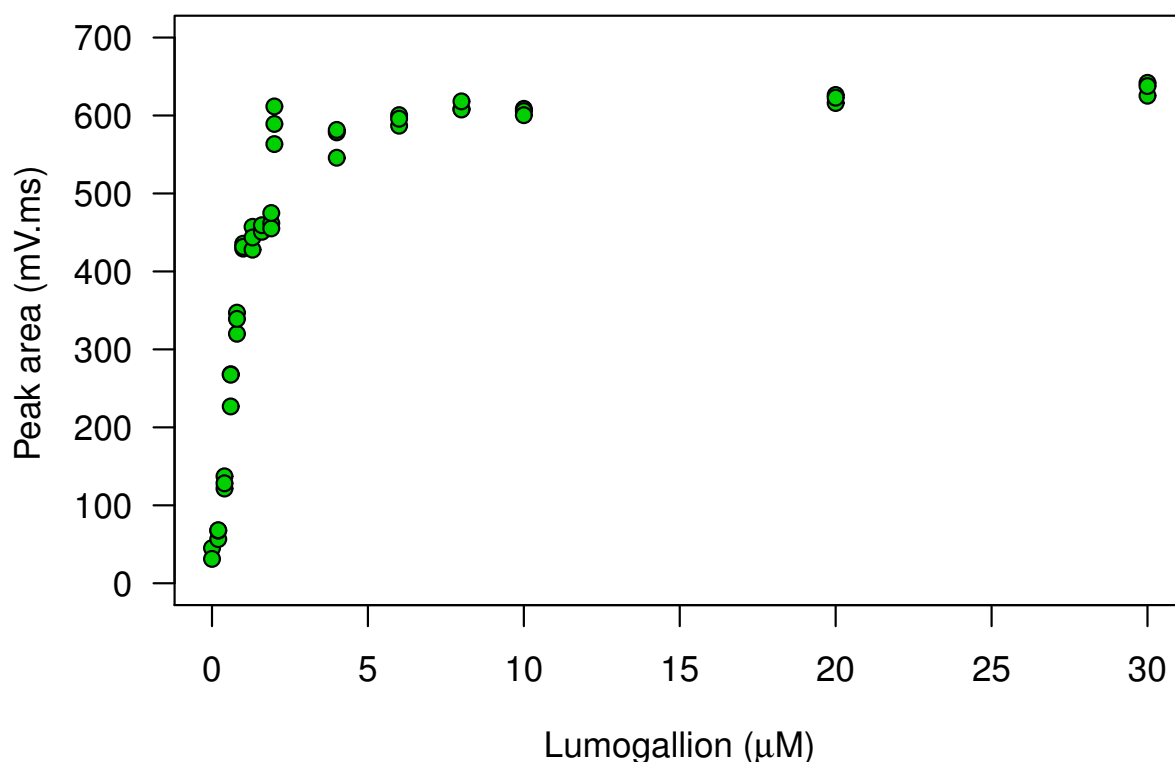


Figure 2.3: The effect of lumogallion concentration in the pre-column reagent on peak area (fluorescence response). Only the pre-column reagent was injected (no sample). The concentration of dAl in the pre-column reagent was unknown, so the level of lumogallion required in the pre-column reagent was also unknown. Below 5 μM lumogallion, contaminant Al in the pre-column reagent was in excess. Above 5 μM lumogallion, lumogallion was in excess of contaminant Al. Peak area is not significantly affected by excess lumogallion, suggesting lumogallion does not contribute substantially to Al contamination.

Synthesis of the lumogallion-Al complex

Pre-column reagent was 0.18 mM lumogallion – 0.9 M MES at $\text{pH } 6.1 \pm 0.1$. A 125- μL aliquot of pre-column reagent, followed by 375- μL aliquot of sample/standard, were added to a 600- μL polypropylene vial, stirred using a Fisher Brand Whirlimixer® for 60 s and then loaded into the auto-sampler. The solutions were then left for > 10 h at room temperature, after which time the derivative concentration stabilised, and remained stable for at least 3 days. This time could be reduced if both the samples and the pre-column reagent were heated before being combined (similar to the approach used by [Resing and Measures \(1994\)](#) and ([Brown and Bruland, 2008](#))).

Sample analysis

After complex formation was complete, samples were analysed. 10 μL of sample was injected onto the column. At a constant flow rate of 2 mL min^{-1} , a stepped-gradient elution program was applied, with a matrix elimination step of 5/95 (v/v) methanol/water for 60 s, followed by an isocratic elution step of 90/10 (v/v) methanol/water for 60 s, followed by 5/95 methanol/water for 30 s in preparation for the next injection. Each vial was analysed in triplicate. The blank was quantified by using deionised water as a sample in the methods described above without any standard addition of Al^{3+} and were made up in quintuplets (5 vials). Recovery was assessed by spiking a sample with known concentration of Al^{3+} with a standard addition of 1.484 mM Al^{3+} and analysed as above.

2.2.5 Flame Atomic Absorption Spectroscopy (FAAS)

Sample and standard addition preparation

Seven aliquots (10.00, 9.99, 9.98, 9.96, 9.92, 9.90, 9.80 mL) of the sample/standard to be analysed were collected in a clean syringe, filtered during transfer into 10 mL Sarstedt polypropylene tubes and then acidified with 9.9 μL of 16 M nitric acid to pH 1.8 (to ensure dAl remained in solution (Cutter et al., 2010)). Each solution was then spiked with a volume (0, 10, 20, 40, 80, 100, 200 μL) of 37.1 mM Al standard in 0.5 M nitric acid to make up standard additions of 0, 0.037, 0.074, 0.148, 0.296, 0.371, 0.741 mM Al^{3+} .

2.3 Results and discussion

2.3.1 Optimisation of separation conditions

Column selection

Previous authors (Wu et al., 1995; Zhou et al., 1995; Lee et al., 1996) that have successfully used RP-HPLC for analysis of the Al–lumogallion complex did so with a range of columns of variable performance. These are compared in Table 2.1.

Of the columns presented in Table 2.1, only the Nova-Pak® C₁₈ 4- μm 150×3.9 mm I.D. (Waters, Milford, USA) was available to our laboratory (due to limited resources). The major drawback of the Nova-Pak® column was high backpressure caused by the relatively high viscosity of the

Table 2.1: A comparison of performance characteristics of previously published methods for determination of Al³⁺ using RP-HPLC of metal chelates. (LOD = limit of detection, LOQ = limit of quantification)

Column Type	Eluent Composition	Run time (min)	LOD (nM)	LOQ (nM)	No. peaks
LiChrosorb RP-18e 10- μ m 250 \times 4.6 mm I.D. (Merck KGaA, Darmstadt, Germany) ¹	AcN:KHP 30:70	12	1.8	na <i>natural waters</i>	1
Develosil LAL (C ₈) 5- μ m 100 \times 6 mm I.D. (Nomura Chemical Co Ltd, Seto, Japan) ²	Almeasure R-3A 100%	6	1.1	3.3 <i>undefined</i>	1
Nova-Pak [®] C ₁₈ 4- μ m 150 \times 3.9 mm I.D. (Waters, Milford, USA) ³	AcN: buffer 20:80	6	0.00002	18 <i>human serum</i>	2

¹ Zhou et al. (1995); Wu et al. (1995)

² Fujita et al. (2004)

³ Lee et al. (1996). The large difference between the LOD and the LOQ is because in this paper the LOD is defined as $3 \times \sigma$ of the baseline noise (which is extremely low) where as the LOQ is defined as $10 \times \sigma$ of the blank.

60/40 methanol/water eluent, so the amount of organic solvent content in the eluent was reduced to 40/60 methanol/water (it is suspected this would also benefit analysis of high ionic strength samples, discussed in section 2.3.1). Results from Lee et al. (1996) were sufficiently similar to those used by Zhou et al. (1995), Wu et al. (1995) and Fujita et al. (2004) for the Nova-Pak[®] to be a good representative column for this analyte, with conditions (e.g. temperature, eluent composition, flow-rate) initially optimised using this column. These conditions were used to compare the relative performance of other columns.

To compare performance, columns with shorter alkyl radicals (or lower carbon content) were checked. Columns with different stationary phases that were available to our lab, and considered appropriate to test, given the above parameters included the Econosphere C₈ 5- μ m 250 \times 4.6 mm I.D. (Alltech Associates, Inc., Deerfield, USA), the Diaspher 110 C₁₀CN 5- μ m 150 \times 4.0 mm I.D. (BioChimMac, Moscow, Russia), L-Column ODS 5- μ m 150 \times 4.6 mm I.D. (Waters, Milford, USA), and the Chromolith[®] RP-18e Performance column.

A comparison of the relative efficiency of these columns under the same separation conditions can be seen in Figure 2.4 (The L-Column is not included as its performance was so poor it did not scale onto the same plot). These conditions were chosen as they were found to be optimal for separation using the Nova-Pak[®] C₁₈ column.

As can be seen in Figure 2.4, there were large differences in peak shape between the different columns tested. The first observation is the relatively poor performance of the columns that did not have end-capped silanol groups (Econosphere C₈ and Diaspher 110 C₁₀CN), showing the importance of a high quality stationary phase for analysis of the Al–lumogallion complex

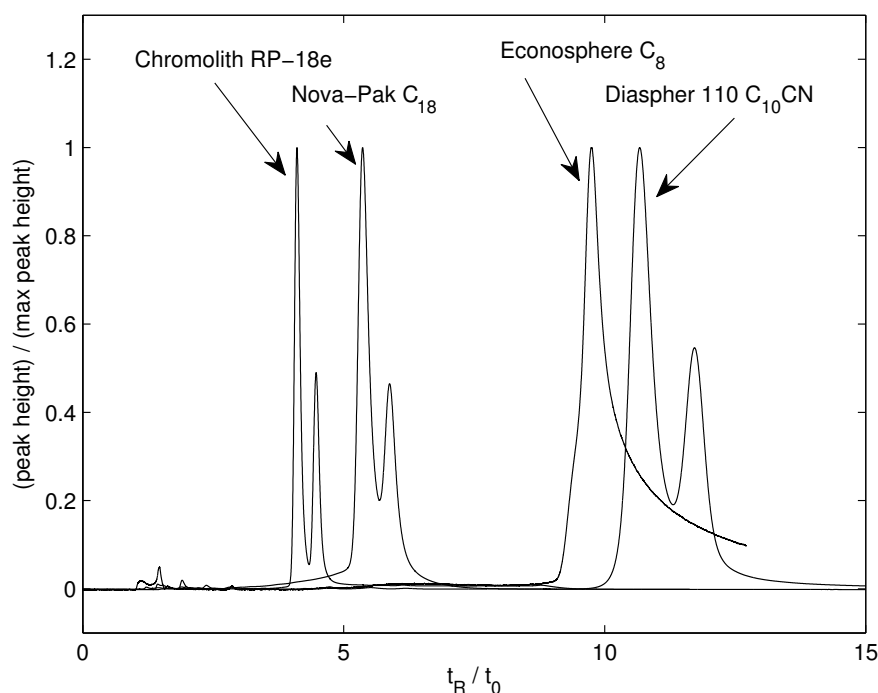


Figure 2.4: Normalised chromatograms of the sample-pre-column reagent mixture obtained using various analytical columns. Separation conditions were maintained as: 40/60 methanol/water (v/v); flow-rate 0.8 mL min^{-1} ; column temperature 40°C ; injection volume $10 \mu\text{L}$. t_R = retention time, t_0 = void time. t_R/t_0 = relative retention time, also known as the retention factor (k). Only the chromolith RP-18e column has endcapped groups, contributing to the improved separation efficiency.

with RP-HPLC. Interestingly, the Econosphere C_8 and Diaspher 110 C_{10}CN columns, both with lower carbon content in the stationary phase than the Nova-Pak[®] C_{18} and the Chromolith[®] RP-18e Performance, provide stronger retention of the Al–lumogallion complex. Two major species of the Al–lumogallion complex were observed, eluted after many other smaller unidentified species. The identity and relevance of these major peaks is discussed in section 2.3.1. Of the columns tested, the Chromolith[®] and the Nova-Pak[®] column performed the best. Compared to the Nova-Pak[®] column, the Chromolith[®] was $\sim 30\%$ faster per run, had $\sim 70\%$ lower backpressure, and had 2.5-fold higher peak efficiency with resolved peaks ($R_S = 1.7$), where the Nova-Pak[®] peaks were not baseline resolved ($R_S < 1.5$). The Chromolith[®] column had much higher performance due to the technological advances gained from its monolithic structure, and was therefore selected as the column of choice. Monolithic columns were not available until relatively recently, hence, the reason they were not investigated in previously described methods.

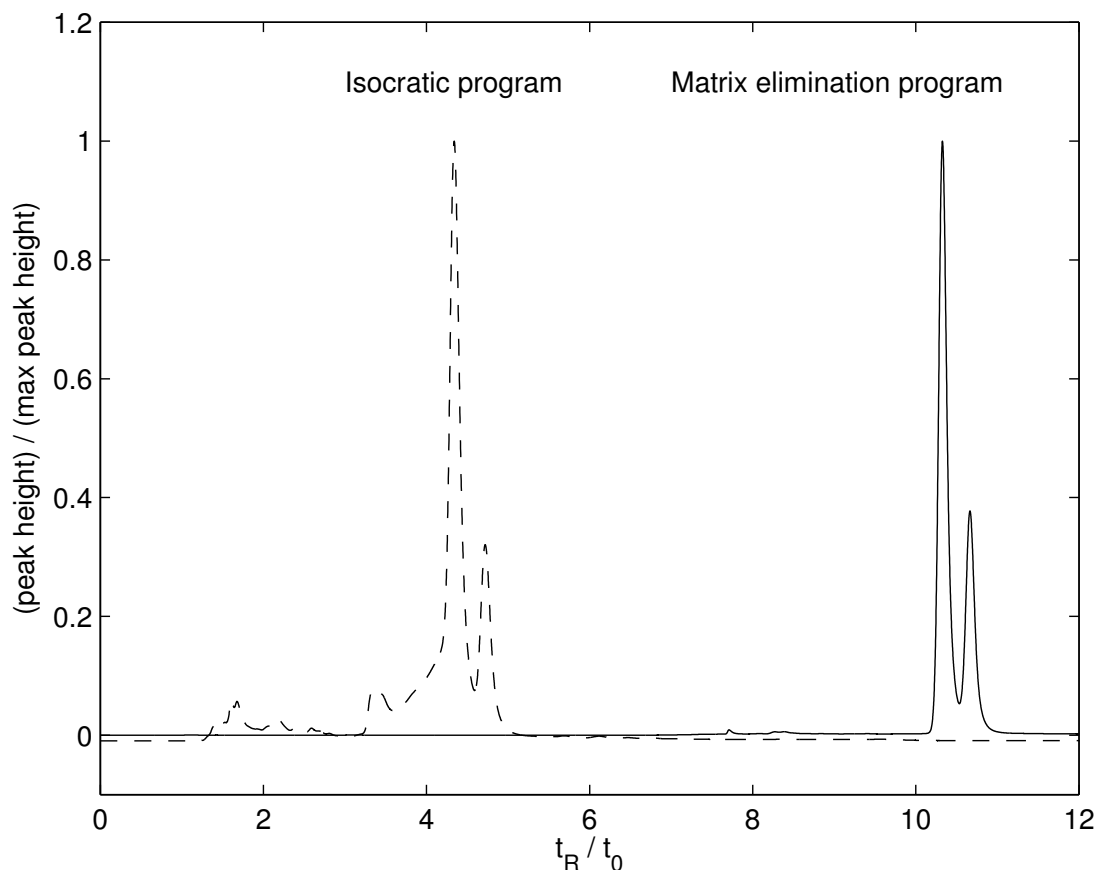


Figure 2.5: Normalised elution profiles obtained using an isocratic and a gradient program (the matrix elimination program). Column = Chromolith® RP-18e Performance column, flow rate 2 mL min^{-1} ; injection volume = $10 \text{ } \mu\text{L}$; temperature 40° ; eluent composition: Isocratic program = methanol/water 40/60 (v/v); Matrix elimination program = methanol/water 5/95 (v/v) for 300 s then methanol/water 40/60 (v/v) for 450 s.

Mobile phase selection

Acetonitrile (AcN) is a common organic mobile phase used in RP-HPLC (Zhou et al., 1995; Wu et al., 1995; Lee et al., 1996). Although AcN was effective as an eluent in this method, it is more expensive than methanol, can be more difficult to obtain, has lower solubility limits for ionic salts relative to methanol (Schellinger and Carr, 2004) and achieves minimal improvement in separation efficiency so methanol was selected instead of AcN.

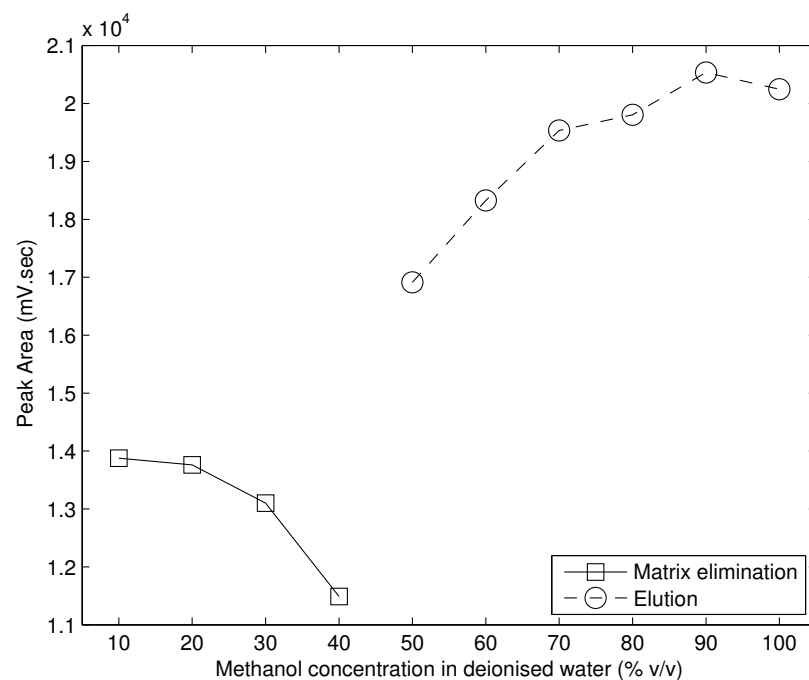
Elution program selection

Complex samples often have high concentrations of ionic salts. This can be problematic, affecting peak shape, efficiency and separation factors.

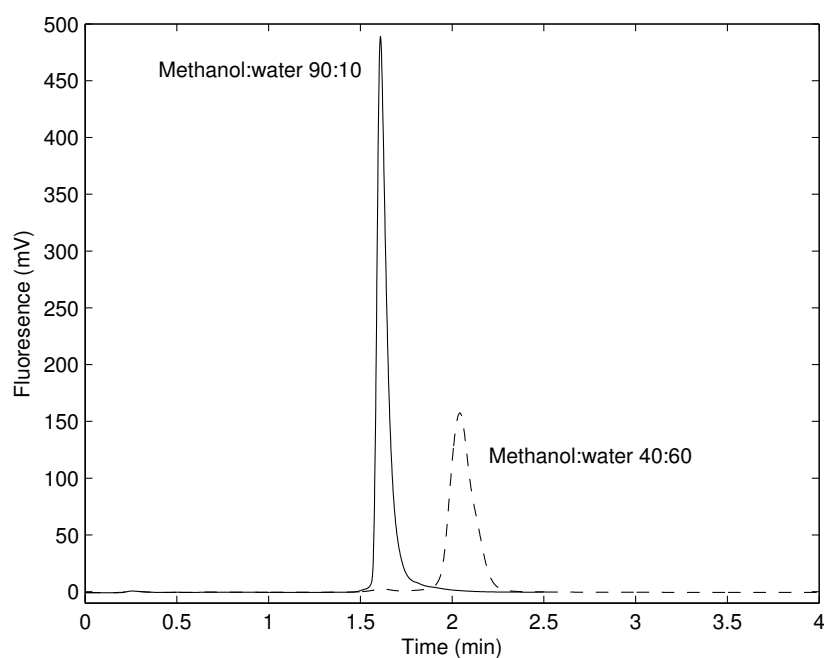
Seawater, given its high ionic strength, was found to induce peak-fronting (where part of the peak is eluted earlier than the main body of the peak), interfering with sample analysis. This is due to the limited solubility of many inorganic salts in the organic solvents used as eluents for RP-HPLC. This problem has not been described or addressed by previous authors. To address this problem, isocratic vs. stepped-gradient elution profiles were investigated using seawater samples spiked with Al^{3+} to ensure artefacts often observed at trace concentrations were avoided.

Inorganic salts and poorly retained organic molecules needed to be removed from the column so they did not interfere with analysis. A comparison of the same seawater sample analysed with an isocratic program vs. a stepped gradient program is presented in Figure 2.5. The gradient program effectively separates the interfering ions from the analytes.

Matrix interference was minimised by using an eluent with a high deionised water fraction for $5 \times$ column-volume, then eluting analytes with a high methanol fraction eluent. To determine the minimum required volume of the matrix elimination step, the effect of the matrix elimination step on analyte peak shape was investigated. Various compositions of methanol/water (10/90, 20/80, 30/70, 40/60 v/v) were tested. As can be seen in the lower-left corner of Figure 2.6a, as the methanol concentration in the eluent increased above 10% (v/v), chromatographic peak area decreased. This is probably due to two mechanisms, the methanol beginning to elute the complex off the column and 'salting out'. 'Salting out' occurs as the composition of the eluent becomes less aqueous. The ionic compounds precipitate and adsorb to the columns active sites, displacing the analyte which elutes earlier, usually with worse peak shape.



(a)



(b)

Figure 2.6: (a) Effect of methanol concentration in the eluent during both the matrix elimination and elution steps of a gradient program on retention time, peak shape and peak area. (b) Comparison of peak shape when the eluent composition is changed from 40/60 to 90/10 (v/v) methanol/water during the elution step of the matrix elimination program.

The favoured composition during matrix elimination was a methanol/water ratio of 5/95 (v/v), to maximise solubility of interfering salts, and minimise the effect on the analyte. The elution step of the gradient program can be optimised in two different ways. Separation of two different species of Al–lumogallion complex, or co-elution of these two species as a single peak.

Although this study and others (Lee et al., 1996; Koshikawa et al., 2010) have found the Al–lumogallion complex to form two major species, their identity has only been hypothesised as $\text{Al}(\text{OH})^{2+}$ –lumogallion and $\text{Al}(\text{OH})_2^+$ –lumogallion (Wu et al., 1995; Zhou et al., 1995; Lee et al., 1996; Fujita et al., 2004), with the second of the two peaks being ignored¹. The structure of the lumogallion–Al complex presented by Wu et al. (1995) is also dubious, as it is an unlikely complex structure. Therefore, the separation at present is not meaningful. As both species respond linearly to Al^{3+} additions, it was supposed the separation of these two species was unnecessary and moved to achieved faster run-times by eluting both as a single peak. This favoured an increase in methanol concentration during the elution step, and a decrease in column length.

The effect of methanol concentration in the eluent on peak area was investigated, and the results are presented in the upper-right corner of Figure 2.6a. As methanol concentration increased towards 90% (v/v), peak area also increased. Figure 2.6b presents how increasing the methanol concentration in the eluent from 40/60 to 90/10 (v/v) methanol/water decreased analysis time by 16%, increased peak height (sensitivity) by more than 3-fold and reduced peak width.

As separation of analytical species was no-longer required, the column could be reduced in length to be a simple pre-concentration and matrix elimination tool. As can be seen in Figure 2.7, a decreased column length and a stronger eluent reduced our run times by > 80% and improved sensitivity 3-fold.

With a run time of 2.5 min, this method is ~75% faster than the next fastest method unaffected by ionic compounds (presented by Zhou et al. (1995) with a run time of 12 min). It is comparable to the

¹With metal-complexes, it is not the metal that interacts with the stationary phase of a reverse-phase column, but the ligand with which it is complexed. As such, the charge of the Al species is not directly relevant to the separation, it is the exact nature (and number) of the ligands with which it forms the complex. The identities described by Lee et al. (1996) are shorthand descriptions of Al–lumogallion complexes that may involve many lumogallion molecules (a very high ratio of lumogallion:Al is required after all). The different charge of the Al species may result in very different complexes with very different hydrophobicities. Postulations on the exact nature of the two peaks were not extended outside of those previously published by Lee et al. (1996) as no data is available on the structure of the Al–lumogallion complex and investigating this was outside the scope of this study.

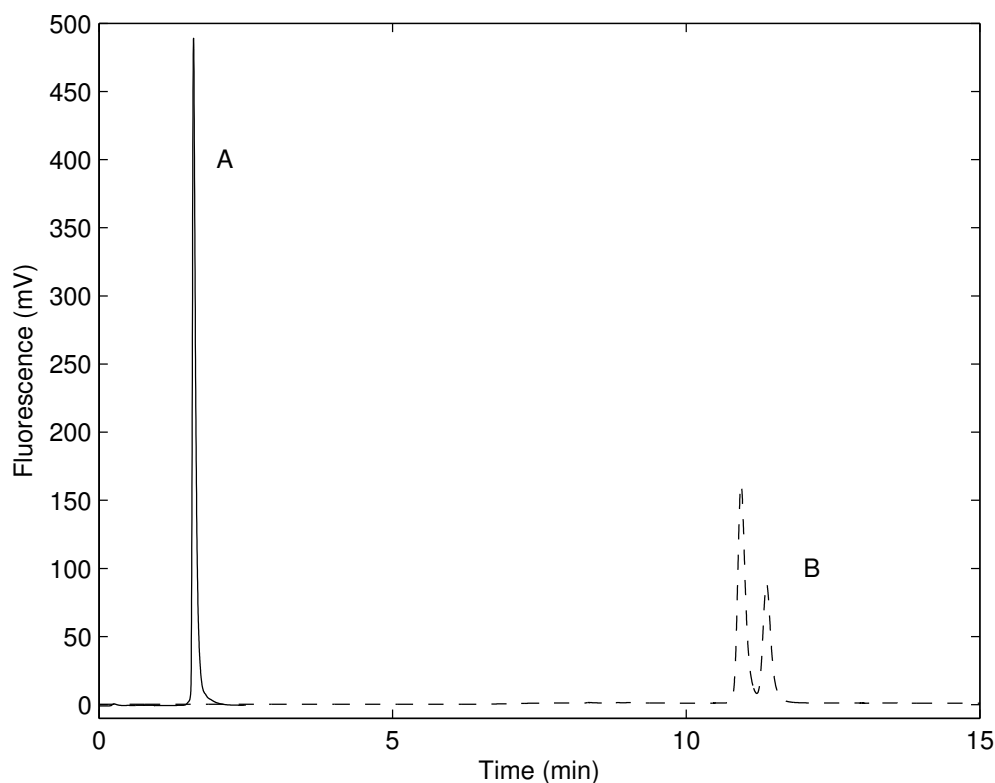


Figure 2.7: Effect of reduced column length and increased methanol concentration in the eluent on peak shape and analysis time. Flow rate = 2.0 mL min^{-1} . Injection volume = $10 \text{ }\mu\text{L}$. Other conditions: A) temperature = 25° ; column = Chromolith® RP-18e Guard column (length = 1 cm); matrix elimination step = methanol/water 5/95 (v/v) for 60 s; elution step = methanol/water 90/10 (v/v) for 90 s. B) temperature 40° ; column = Chromolith® RP-18e Performance column (length = 10 cm); matrix elimination step = methanol/water 5/95 (v/v) for 300 s; elution step = methanol/water 40/60 (v/v) for 450 s.

overall fastest method (presented by [Nagae and Sato \(2005\)](#) with a run time of 2.5 min), although, [Nagae and Sato \(2005\)](#) do not eliminate ionic compounds, and as such, peak shape is negatively affected when this method is used for complex samples such as seawater.

For a suite of 10 seawater samples analysed in triplicate, this represents a reduction in total analytical time of 285 min ($10 \times 3 \times 9.5 \text{ min}$) compared to [Zhou et al. \(1995\)](#). Decreasing the column length from 100 to 10 mm also reduced the cost of the column by ~ 10 fold.

2.3.2 Column temperature and flow rate selection

The manufacturer of the Chromolith® RP-18e type columns recommends using column temperatures below 45°C . Above this temperature the stationary phase can detach from the column

housing. Column temperature was tested from 25 to 40 °C, with a < 5% increase in peak efficiency or peak area across that range, so all further experiments were conducted at 25 °C, which is a temperature consistent with previous methods (Zhou et al., 1995; Wu et al., 1995; Lee et al., 1996).

Flow rate was tested from 0.5 to 4 mL min⁻¹. The best compromise between speed and peak shape was found at 2 mL min⁻¹ for these analytes.

2.3.3 Pre-column-reaction chemistry

Buffer selection and concentration

The optimal pH for Al–lumogallion complex formation is 5.5±0.1 (Resing and Measures, 1994; Clarke et al., 1996; Tria et al., 2008a,b; Brown and Bruland, 2008). Buffers that have been used in other methods include ammonium-acetate (logK_{Al} ~2 (Ohyoshi et al., 1999)), potassium hydrogen phthalate (logK_{Al} ~3 (Hedlund et al., 1988)) and MES (no data or evidence of complex formation was obtained (Good et al., 1966)) (Resing and Measures, 1994; Wu et al., 1995; Lee et al., 1996; Nagae and Sato, 2005; Brown and Bruland, 2008; Tria et al., 2008a). MES was selected here because it does not co-ordinate with metals (unlike ammonium-acetate and phthalate), is non-hazardous, easy to handle and can be easily purified (see section 3.2.2). NaOH was selected instead of NH₄OH because it is non-volatile and therefore more stable over time, although NH₄OH can be purified more easily and may be required for trace-level work.

Formation time

To ensure sensitivity was consistent during the period of analysis of the first to the last samples, the time required for the reaction to go to completion was investigated. A single sample was analysed multiple times over a 3-day period. The Al–lumogallion complex formation was found to be complete and stable after 10 h. This is consistent with previous methods (Wu et al., 1995; Zhou et al., 1995; Lee et al., 1996).

2.3.4 Comparison between RP-HPLC and FAAS for analysis of Al³⁺ in a tea-infusion

Six aliquots (4.50, 4.45, 4.40, 4.35, 4.30, 4.25 mL) of 15.84 mM nitric acid were spiked with various volumes (0, 0.05, 0.10, 0.15, 0.20, 0.25 mL) of 37.1 mM Al³⁺ standard in 15.84 mM nitric acid to

make up Al^{3+} standard additions of 0, 3.7, 7.4, 11.1, 14.8 and 18.5 μM in 15 mM nitric acid. Each of these standards were then spiked with 0.5 mL of prepared sample, diluting the sample 10-fold.

Reverse-phase HPLC fluorescence determined the concentration of Al in the tea infusion to be $83.92 \pm 2.9 \mu\text{M}$. As can be seen in Figure 2.8a, this method had excellent correlation with a linear calibration curve, where $R^2 = 0.9992$ and slope = 58.02. These results compare well with those determined in this study by FAAS with $84.87 \pm 9.7 \mu\text{M}$, with $R^2 = 0.9995$, LOD = 30.0 μM , LOQ = 0.11 mM. Variability between the two methods was insignificant at $P=0.95$.

Signal:noise was excellent (> 700), evident in Figure 2.8b, with a LOD ($3 \times \sigma$ of blank) of 250 nM, and a LOQ ($\text{blank} + 10 \times \sigma$ of blank) of 720 nM.

As the blank-level of this method is directly related to the level of contamination in the pre-column reagent and the DIW used, efforts to reduce contamination, will result in a reduction of blank signal, reducing the LOQ. It was believed there was significant capacity for this as the MES could be purified further, and the NaOH could be replaced with either a higher purity option, or replaced with another, more trace-clean solution such as SEASTAR™ Baseline® Ammonia Solution (Ammonium Hydroxide). However, development of this method for use in trace clean applications is beyond the scope of this paper.

These results compare well with those produced by comparative RP-HPLC methods (Zhou et al., 1995; Wu et al., 1995; Lee et al., 1996) with similar limits of detection and quantification, linearity and precision.

Recovery was assessed by analysing a tea-infusion of known Al concentration and the same tea-infusion spiked with a 1.484 mM standard addition of Al, each made up with pre-column reagent in quintuplet vials, and each vial analysed in triplicate. This determined a recovery of $97.5\% \pm 3.2\%$, $n=5$, $P=0.95$.

Our RP-HPLC fluorescence technique has excellent linearity, is not affected by ionic compounds (even in high concentrations), has a working range from 0.25 to 300 μM (which is similar to other methods (Zhou et al., 1995; Wu et al., 1995; Lee et al., 1996)) and achieves this in much shorter run times. The lower limit of this method is the LOQ, and could be improved by using stock reagents of higher purity and trace clean protocols during analysis, as is the case for other methods mentioned in Cutter et al. (2010), although this does require further investigation.

The upper LOD of this method is controlled by peak shape and the elution period length. This method has a peak with a slight tail. Carry-over between samples occurs when the analyte load exceeds the capacity of the elution period to remove all residual analyte from the column (i.e. extends the length of the tail), raising the baseline and the area of the following injection. If analysis of higher concentration samples is required, this could be addressed by increasing the time period of the elution-step, or increasing the elution-strength of the system-wash between samples, or dilution of samples to within the operating range.

2.4 Conclusions

We have developed a method for the determination of Al using RP-HPLC that is 50–75% faster and considerably cheaper than previously published methods, while maintaining equivalent accuracy, precision and sensitivity. This is achieved by using an ultra-short monolithic column in the place of a conventional longer column.

Future work includes: the applicability of this method at trace-levels in seawater, through further development, with the aim to apply this method to open-ocean samples for biogeochemical studies; and to identify the two major species of the Al–lumogallion complex and determine if these different species are useful for determining Al speciation in aqueous samples.

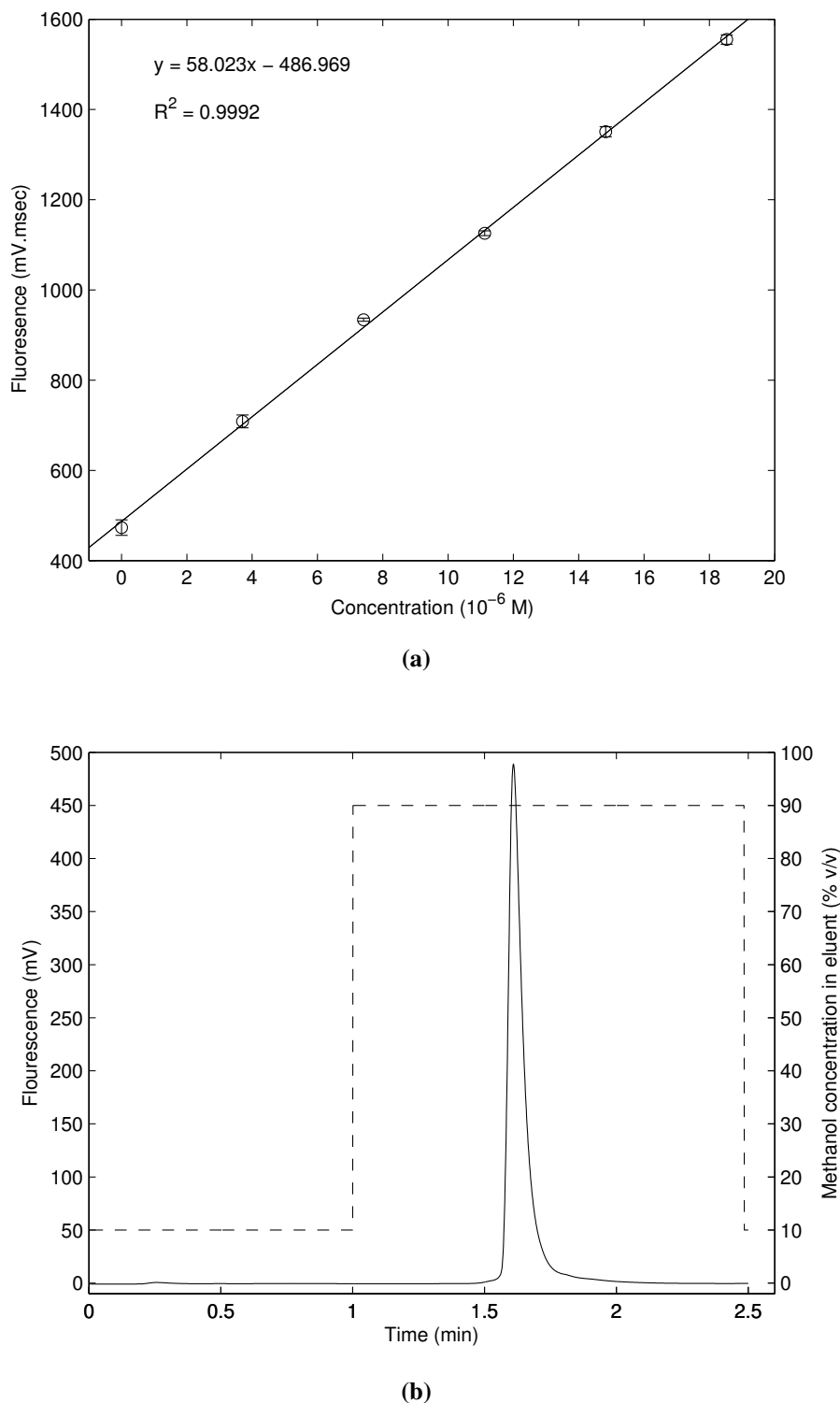


Figure 2.8: (a) Determination of Al by standard addition in a black tea-infusion treated with pre-column reagent using RP-HPLC with fluorescence detection. (b) Solid line = A typical chromatogram of a tea-infusion analysed using this method, column = Chromolith® RP-18e Guard column; flow rate = 2.0 mL min⁻¹; temperature = 25°; injection volume = 10 μ L; eluent see dashed line; Dashed line = matrix elimination methanol gradient program used for this method, matrix elimination step = methanol/water 5/95 (v/v) for 60 s; elution step = methanol/water 90/10 (v/v) for 90 s.

Chapter

3

RP-HPLC determination of dAl in open ocean seawater

[This is a complete type script of [Remenyi et al. \(2012\)](#), apologies for duplication in the introduction and methods sections of this chapter. These were left unaltered for emphasis and clarity, as the variations are small but important.]

3.1 Introduction

The international GEOTRACES program ([Frank et al., 2003](#); [SCOR Working Group, 2006, 2007, 2012](#)) has coordinated many of the world's biogeochemical oceanographic research programs, resulting in large increases in the number of samples to be analysed, as well as the number of key parameters regularly targeted per sample. The application of existing chemical analysis methods from various disciplines (eg. medical, environmental, industrial) to the open ocean environment is of recent interest to the chemical oceanographic community as improvements in analytical efficiencies are sought to match the improvements in sampling technologies and expanded concentration ranges observed (eg. [de Baar et al. \(2008\)](#); [Middag et al. \(2011a,b,c, 2012a\)](#)).

Aluminium is a key parameter of the international GEOTRACES program ([Frank et al., 2003](#); [SCOR Working Group, 2006, 2007, 2012](#)). It is an element that is readily scavenged and has relatively short residence times in dissolved form (dAl) in the surface ocean. This makes it useful as a biogeochemical tracer of watermasses to indicate the level of interaction the target watermass has had with terrestrial sources of trace nutrients (such as wind-blown dust depositing into the ocean ([Measures and Edmond, 1989](#)), although this relationship is limited to surface waters due to sedimentary resuspension ([Moran and Moore, 1991](#); [Middag et al., 2009](#))). Aluminium is ~8% of the earth's crust ([Taylor, 1964](#); [Wedepohl, 1995](#); [Yaroshevsky, 2006](#)), yet is present in natural waters at trace levels, with reported values ranging from ~2.5 μM in rivers ([Upadhyay et al., 2002](#)) to <1 nM in the open ocean ([Hydes and Liss, 1976, 1977b](#); [Caschetto and Wollast, 1979](#); [Hydes, 1979](#); [Stoffyn and Mackenzie, 1982](#); [Hydes, 1983](#); [Measures et al., 1984](#); [Kremling, 1985](#); [Orians and Bruland, 1985, 1986](#); [Jickells, 1986](#); [Hydes et al., 1986](#); [Measures et al., 1986](#); [Hydes et al., 1988](#); [Hydes, 1989](#); [Measures and Edmond, 1989, 1990](#); [Kremling and Hydes, 1988](#); [Hydes](#)

and Kremling, 1993; Moran and Moore, 1992; Moran et al., 1992; Narvekar and Singbal, 1993; Kremling and Streau, 1993; Helmers and Vanderloeff, 1993; Upadhyay and Sen Gupta, 1994; Jickells et al., 1994; Gelado-Caballero et al., 1996; Measures and Vink, 1999; VanBeusekom et al., 1997; Chou and Wollast, 1997; Measures, 1999; Measures and Vink, 2000; Measures, 2002; Bowie et al., 2002; Sanudo-Wilhelmy et al., 2002; Johnson et al., 2003; Obata et al., 2004; Measures et al., 2005, 2006; Obata et al., 2007, 2008; Measures et al., 2008c,a,b; Han et al., 2008; Brown and Bruland, 2009; Brown et al., 2010; Measures et al., 2010; Middag, 2010; Hendry et al., 2010; Middag et al., 2011a,b,c, 2012b; Roeske et al., 2012). The extremely low levels in the open ocean are due to the very low solubility of Al in the highly complex seawater matrix and geographic isolation from continental sources of Al. As a GEOTRACES key parameter, the number of samples per oceanographic cast and cruise have dramatically increased since the 1990s, requiring greater efficiency of analytical methods.

Current popular shipboard techniques have known limitations discussed in Chapter 2. To reduce sample volume requirements and improve the capacity for automation, the method presented by Remenyi et al. (2011) was adapted to determine dissolved Al at trace levels in seawater. This development provided increased efficiencies in required sample volume, automation and robustness compared to the most popular techniques currently used.

3.2 Methods and Procedures

3.2.1 Apparatus

The sample and reagent were stirred using a Fisher Brand Whirlimixer®. pH was measured with a labCHEM-pH meter (TPS Pty Ltd, Brisbane, Australia). Sample management was achieved with an Alliance 2690 HPLC system (Waters, Milford, USA), dwell volume = 1.2 mL. Analyte concentration and separation was achieved on a reversed phase, C₁₈, end-capped Chromolith® RP-18e Guard (10 × 4.6 mm) column. The Al-lumogallion (Al-lumogallion) complex was detected using a scanning fluorescence detector model 474 (Waters, Milford, USA), gain = 100, λ_{ex} = 505 nm bandwidth = 18 nm, λ_{em} = 574 nm bandwidth = 18 nm, with control and signal processing achieved using Empower® software (Waters, Milford, USA).

Sample and reagent bottles were Nalgene® low-density poly-ethylene (LDPE) and analysis vials were Dionex® polypropylene (PP). All were cleaned using trace metal protocols described in Cutter et al. (2010).

3.2.2 Reagents

All ultra-high purity water was from a Milli-Q® Elix® and Gradient® coupled system (Millipore, Billerica, USA).

The solvent was ultra-high purity water and Supragradient® HPLC grade methanol (Scharlau Chemie S.A., Sentmenat, Spain).

Lumogallion (97%, powdered, Pfaltz & Bauer Inc. Waterbury, USA) was made up to 5 mM in ultra-high purity water (0.0517 g / 30 mL).

2-(N-morpholino)ethanesulfonic acid, also known as solid MES hydrate 99.5% (Sigma-Aldrich, St Louis, USA), was made up to 1 M in ultra-high purity water (19.523 g / 100 mL, this solution has a pH <3). It was then purified with respect to transition elements by passing it through a 200×4.6 mm I.D. column packed with Diphonix® resin, particle size 75-150 µm (Eichrom Technologies Inc., Lisle, USA) at 0.2 mL min⁻¹ [Tria et al. \(2008b\)](#). MES solutions at higher concentrations than 1 M created precipitates when stored below 4 °C.

Lumogallion is a ligand that forms a fluorescent complex with Al. The reagent prepared was 2.0 mM lumogallion in 0.9 M MES in DIW at pH 6.1 ± 0.1. MES buffer was used to adjust the pH of the sample-reagent mixture to optimise the reaction yield (the target was pH 5.3 ([Resing and Measures, 1994](#); [Brown and Bruland, 2008](#); [Tria et al., 2008b](#))). The pH was measured on sub-samples so as to not contaminate the working reagent.

Adjustment of pH was done using 16 M SEASTAR™ Baseline® nitric acid, and SEASTAR™ Baseline® ammonia solution (ammonium hydroxide), Seastar Chemicals Inc. (British Columbia, Canada) .

All standards were made up using a commercial standard 1000 mg.L⁻¹ (0.371 M) Al³⁺ in 0.5 M nitric acid (Merck KGaA, Darmstadt, Germany).

All stock solutions were stored in the dark at ~4 °C.

3.2.3 Sample collection and analysis protocols

Samples were collected and analysed using trace metal clean GEOTRACES protocols at every stage of sampling and analysis (with special emphasis on those specific for Al), as suggested in [Bowie and Lohan \(2009\)](#) and [Cutter et al. \(2010\)](#).

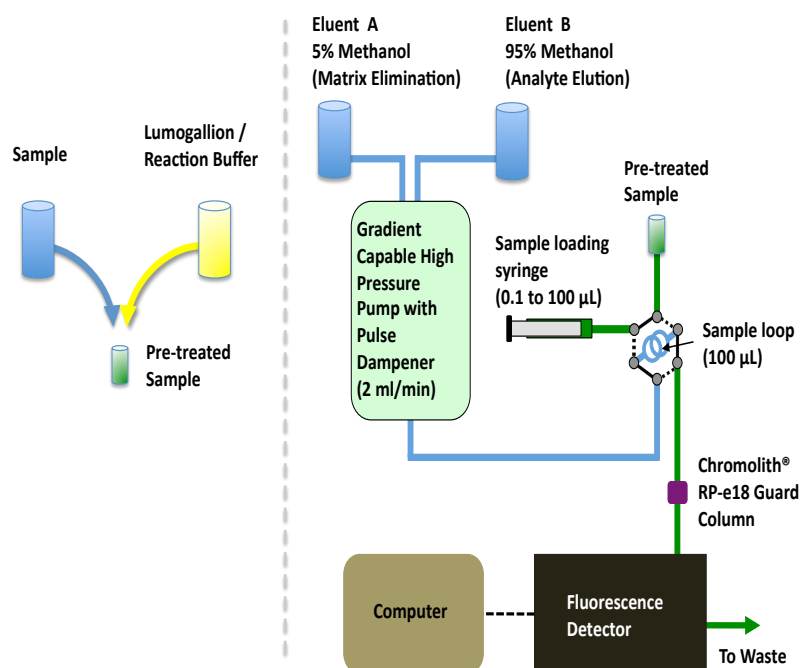


Figure 3.1: Schematic of the sample analysis procedure: Reaction of the sample with the reagent (lumogallion/reaction buffer solution) is performed before injection of 10 μL of this mixture into the RP-HPLC method (NB: injections of 1–100 μL is possible with this system). During injection (column loading and matrix elimination) ‘Eluent A’ is used. During elution of the Al–lumogallion complex to the detector ‘Eluent B’ is used. Flow rate is maintained at 2 $\text{mL}\cdot\text{min}^{-1}$ throughout. Fluorescence detector settings: λ_{ex} = 505 nm (bandwidth = 18 nm), λ_{em} = 574 nm (bandwidth = 18 nm).

3.2.4 Sample analysis

Formation of the lumogallion-Al complex

The ratio of reagent to sample was 1:3. In practice this was a 125 μL aliquot of reagent with a 375 μL aliquot of sample/standard. These were added to a 600 μL polypropylene vial, stirred using a Fisher Brand Whirlimixer® for 60 s and then loaded into the auto-sampler. The solutions were then left overnight (>10 h) at room temperature, after which time the reaction was complete and the complex remained stable for at least 3 days.

Preparation of 100 samples required ~ 120 min.

Analysis of the prepared sample

A schematic of the sample analysis system is presented in Figure 3.1. Two eluents were used in the sample analysis in a stepped-gradient elution program, visualised as the dashed line in Figure 3.2. Eluent A was a 5/95 (v/v) methanol/water mixture, used to load the analyte onto the column and simultaneously eluting the saline matrix off the column. Eluent B was a 90/10 (v/v) methanol/water mixture, applied to remove the analyte from the column and pass it into the detector. More details of this system can be found in Remenyi et al. (2011).

After complex formation was complete, prepared samples were analysed. 10 μL of the prepared sample was injected onto the column. At a constant flow rate of 2 mL min^{-1} , the stepped-gradient elution program was applied, with a matrix elimination step (Eluent A for 60 s), followed by an isocratic elution step (Eluent B for 60 s), followed by column preparation for the next injection (Eluent A for 30 s). Each vial was analysed in triplicate. A six-point calibration (0, 1, 2, 4, 8, 16 nM) and twelve-sample station required 202 min (11.2 min per triplicate analysis).

Preliminary work showed that the co-elution of the seawater matrix with the analyte interfered with the fluorescence response of the Al–lumogallion complex (see Figures 2.5 and 2.6 and Remenyi et al. (2011)). Although this is not a problem at higher concentrations (see Giesbrecht (2007)), it was suspected it may be an issue $< 1 \text{ nM}$ and therefore the matrix elimination program was optimised and used.

3.3 Assessment

3.3.1 Blank estimation

The baseline for RP-HPLC method is the sum of: the composition and flow rate of the eluent changing the refraction of stray light, altering the intensity entering the detector; the presence of fluorescent contaminants in the eluent emitting light at the target wavelength; and electronic noise. The absence of a fluorescent ligand in the eluent means the baseline signal is almost zero. There is virtually no background signal until the analyte plug (containing the reagent contribution and the sample contribution of the Al–lumogallion complex measured) passes through the detector. The blank is the reagent contribution to the concentration of Al–lumogallion complex, along with any leaching of Al from the HPLC system during analysis. Estimating this contribution is not straight forward.

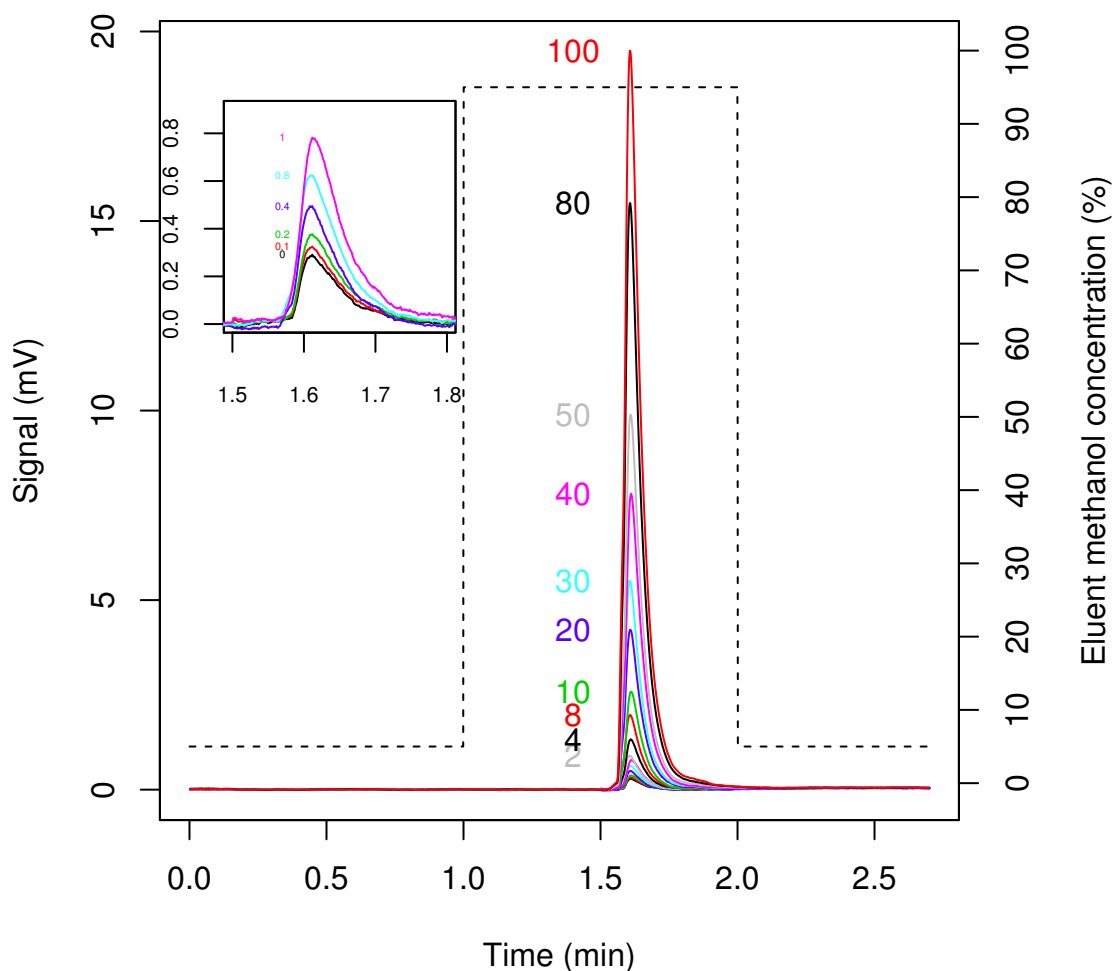


Figure 3.2: Chromatograms of a calibration of the SAlFe reference sample. A representative collection to demonstrate signal-to-noise and peak shape over four orders of magnitude, from 0.1–100 nM. The dashed line is the methanol concentration during the stepped-gradient elution program.

The slope of calibration curves in DIW and seawater were different. A blank DIW sample in the place of seawater resulted in signal intensities much greater than those for spiked seawater samples. This was expected to be due to differences in the fluorescence yield. This is a fundamental difference to the FIA method which incorporates the fluorescent ligand (lumogallion) into the eluent, obviously resulting in a background/baseline signal orders of magnitude higher than the RP-HPLC system. This means the estimation of the blank in the two systems needs to be very different. In the FIA system, blanks can be estimated through the analysis of DIW, as matrix elimination occurs prior to

complex formation. However, for the RP-HPLC system, matrix elimination occurs after complex formation. Complex formation appears to be affected by the matrix of the sample. Therefore, blank estimation was achieved by injecting 2.5 μL of the reagent only. This is the volume of reagent when injecting 10 μL of prepared samples, given the 1:3 ratio of reagent:sample. As an injection of the same volume of reagent normally injected ($\frac{1}{4}$ of the prepared sample volume injected) is the best estimation the blank. This is expected to be an overestimate, since the fluorescence yield of the Al–lumogallion complex is higher in the reagent matrix (MES buffer and DIW) than in the sample matrix (MES buffer and seawater), which has additional interferences present that appear to quench the fluorescence signal.

3.3.2 Calibration and limit of detection

Ultra-high purity water could not be used for calibration or blank estimation. The fluorescent response of the Al–lumogallion complex was quenched by seawater compared to ultra-high purity water. The matrix effect of seawater is significant, and therefore must be used for calibration.

Calibration linearity range was tested from 0.1 to 100 nM, see Figures 3.2 and 3.3. Above 100 nM the lumogallion concentration in the reagent should be increased to maintain linearity. The upper concentration tested was 18.53 mM, column capacity had not yet been reached but the Al–lumogallion complex became unstable for analysis (forming what appeared to be a gel). Standards made up at <1 nM were highly unstable (changing within minutes of production) and required immediate analysis to achieve linearity (Maeve Lohan and Rob Middag both found this same phenomena using the FIA method). This instability is expected to be interfering ions within the seawater matrix altering the equilibration chemistry of Al^{+3} whilst at the ultra-trace levels <1 nM. At concentrations >1 nM, Al^{+3} appeared to dominate effects by these other ions. Samples were stable, probably because they were equilibrated well before they were removed from the sea. It is also likely the stable species of Al available for analysis is a weakly bound complex, rather than the Al^{+3} standard used for calibration. This problem would be applicable to all methods that calibrate with a Al^{+3} standard. As the RP-HPLC system is completely automated, the instability of the low-level standards was not acceptable. To eliminate this error, calibration standards >1 nM were used.

Limit of detection was assessed as: $\frac{3 \times \sigma_{\text{blank}}}{\text{calibration slope}}$ (n= 30 in triplicate)

Limit of detection was 0.13 ± 0.05 nM.

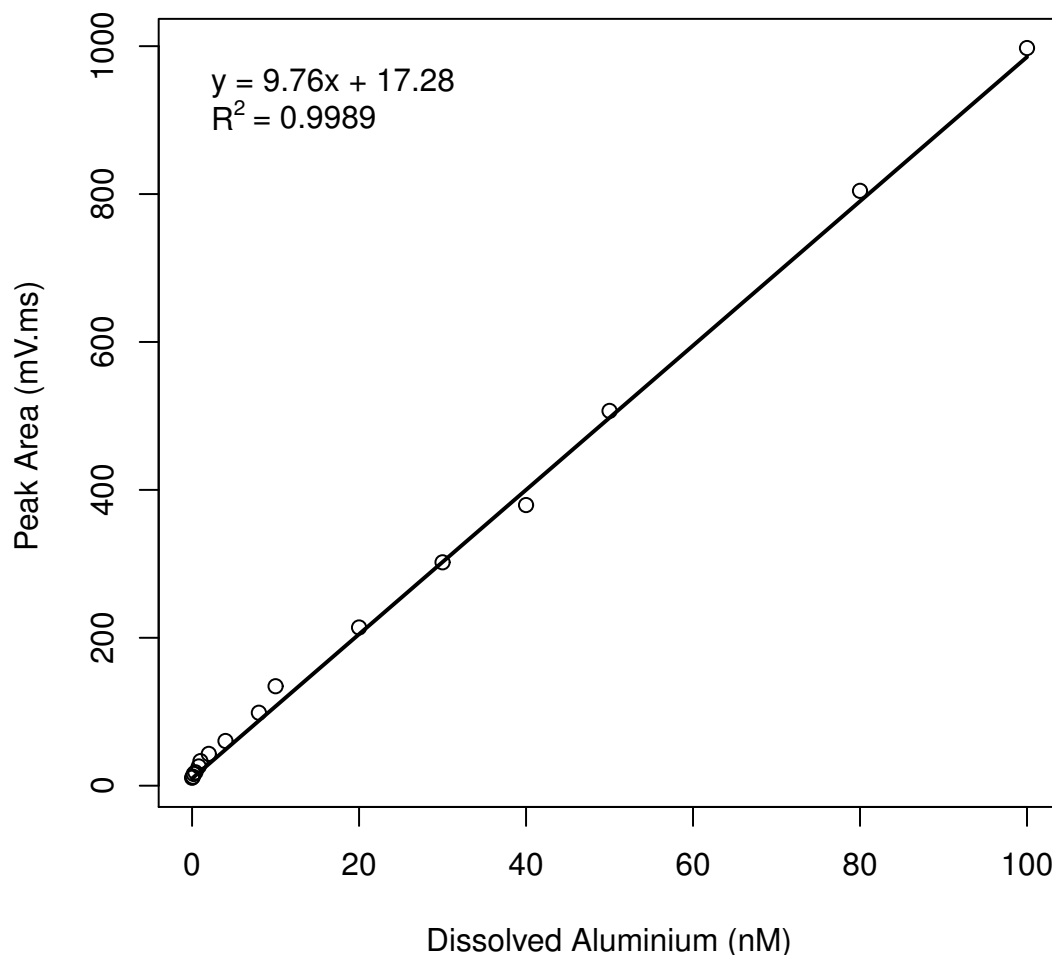


Figure 3.3: Representative 16-point calibration curve of dAl (nM).
Sample = SAFe – S-441.

3.3.3 Accuracy and precision

Accuracy and precision of the method was evaluated by analysing the SAFe reference standard and comparing the results to the Agreed Values presented by [Bruland et al. \(2012\)](#). Results of the 13 SAFe sub-samples analysed are presented in Table 3.2. Agreement with SAFe reference samples was within $4.6 \pm 4.6\%$ ($n = 13$). All analyses were within 15% and most analyses within 5%. This is within similar tolerances to those presented by [Brown and Bruland \(2008\)](#) and [Sohrin et al. \(2008\)](#). The highest percentage deviations were associated with the lowest concentration sub-samples (SAFe–D1). Given the high precision on each set of replicates, it is expected the

Table 3.1: Blank values as concentrations used to calculate the LOD of the RP-HPLC system.

Vial	rep1	rep2	rep3	σ	LOD	Vial	rep1	rep2	rep3	σ	LOD
1	0.179	0.076	0.072	0.061	0.183	16	0.139	0.067	0.160	0.049	0.146
2	0.112	0.146	0.143	0.019	0.057	17	0.180	0.154	0.101	0.040	0.121
3	0.106	0.099	0.113	0.007	0.021	18	0.158	0.112	0.101	0.030	0.091
4	0.173	0.141	0.135	0.021	0.062	19	0.078	0.041	0.099	0.029	0.088
5	0.160	0.173	0.115	0.030	0.091	20	0.186	0.072	0.098	0.060	0.179
6	0.115	0.165	0.068	0.049	0.146	21	0.174	0.024	0.060	0.079	0.236
7	0.140	0.094	0.095	0.026	0.079	22	0.209	0.153	0.180	0.028	0.084
8	0.132	0.158	0.052	0.055	0.165	23	0.181	0.201	0.249	0.035	0.105
9	0.170	0.100	0.084	0.046	0.137	24	0.217	0.086	0.068	0.082	0.245
10	0.162	0.113	0.081	0.041	0.122	25	0.059	0.174	0.148	0.060	0.181
11	0.176	0.118	0.128	0.031	0.092	26	0.196	0.092	0.153	0.052	0.157
12	0.142	0.120	0.113	0.015	0.045	27	0.162	0.099	0.145	0.033	0.098
13	0.141	0.149	0.073	0.042	0.125	28	0.289	0.193	0.139	0.076	0.228
14	0.165	0.086	0.178	0.050	0.150	29	0.193	0.050	0.092	0.074	0.221
15	0.146	0.137	0.104	0.022	0.066	30	0.126	0.182	0.180	0.032	0.096

subsamples are slightly contaminated. Further investigation was not possible due to a limited supply of SAFe–D1 sub-samples.

Precision was calculated on SAFe–D2: mean value of 1.08 nM \pm 0.3 nM (2.7%). Mean precision of SAFe analyses was 1.7 \pm 0.8%, with all analyses within 3.5% relative standard deviation.

SAFe–D2-128 was analysed five times in triplicate to investigate the potential influence of cleaning/handling/analysis protocols (including the use of polypropylene analysis vials) on the final concentration determined. The influence of cleaning/handling/analysis protocols was found to be minimal. Four of the vials had excellent agreement (mean = 1.06 nM; rsd% = 1.2) indicating there is no significant systematic error. However, one of the vials was 0.06 nM higher than the average. This presents a potential error from protocols of \sim 0.06 nM. This accounts for the bulk of the disagreement with the SAFe agreed values. This is considered acceptable by the authors, as to be environmentally relevant as a biogeochemical tracer (beyond indicating the absence of recent aeolian deposition events to the region of interest), dAl concentrations should be at least an order of magnitude larger than this error.

Table 3.2: Analysis of the various SAFe sub-samples using the RP-HPLC.

Agreed values described by [Bruland et al. \(2012\)](#).

All values reported in nM (except where specified as %).

SAFe sub-sample	rep. 1	rep. 2	rep. 3	rsd%	mean	agreed value	error%
SAFe – S-559	1.72	1.72	1.73	0.3	1.72	1.71	0.6
SAFe – S-441	1.77	1.75	1.79	1	1.77	1.71	3.5
SAFe – S-260	1.86	1.8	1.84	1.6	1.83	1.71	7.0
SAFe – S-129	1.68	1.72	1.71	1.2	1.7	1.71	-0.6
SAFe – D2-128-1	1.09	1.07	1.09	1.3	1.08	1.06	1.9
SAFe – D2-128-2	1.05	1.1	1.03	3.5	1.06	1.06	0.0
SAFe – D2-128-3	1.13	1.12	1.1	1.3	1.12	1.06	5.7
SAFe – D2-128-4	1.07	1.02	1.05	2.5	1.05	1.06	-0.9
SAFe – D2-128-5	1.09	1.05	1.06	1.8	1.06	1.06	0.0
SAFe – D2-174	1.09	1.12	1.1	1.6	1.11	1.06	4.7
SAFe – D2-426	0.96	0.95	0.98	1.2	0.96	1.06	-9.4
SAFe – D1-381	0.75	0.73	0.72	2.4	0.73	0.64	14.1
SAFe – D1-165	0.71	0.73	0.7	2.3	0.71	0.64	10.9

3.3.4 Synthesis of the lumogallion-Al complex

pH to achieve optimal derivative yield

Optimum yield of the Al–lumogallion complex is achieved at pH 5.0–5.5 ([Resing and Measures, 1994](#); [Wu et al., 1995](#); [Lee et al., 1996](#); [Brown and Bruland, 2008](#)). Therefore, the reagent pH must be adjusted to account for the pH of the sample of interest. In this study, all samples were collected and then stored at pH 1.8, as prescribed in [Cutter et al. \(2010\)](#). The reagent mixture needed to be adjusted to pH 6.1 to achieve a pH of 5.3 when mixed with the acidified sample.

3.4 Discussion

A comparison of various performance parameters of the RP-HPLC method with methods also used to determine dAl concentration in the SAFe reference samples is presented in [Table 3.3](#).

The RP-HPLC technique is very similar in chemistry and application to the FIA method, which is also a single analyte, shipboard capable technique utilising the fluorescence reaction of the Al–lumogallion complex. As such, in practice the RP-HPLC technique could be used as an

Table 3.3: Comparison of various performance parameters of three methods used for determining dAl in seawater.

Parameter	RP-HPLC ¹	FIA ²	ICP-MS ³
LOD (nM)	0.13	0.10	0.27
Precision (%)	2.7 at 1 nM	2.5 at 5 nM	<9.0 at 1 nM ⁴
Pre-treatment time per 100 samples (hr)	10	0	200
Analysis time per replicate (min)	2.7	7.8	3.3
Operator time per 100 samples (h)	3	39 ⁵	8 ⁶
Sample volume (mL) ⁷	1.5	36	120

¹ This paper.² [Brown and Bruland \(2008\)](#)³ [Sohrin et al. \(2008\)](#)⁴ Interpreted from the statement:

Our data showed excellent agreement with the certified values, except that there was no certified value for Al. The RSD of our data were less than 9%.

where samples analysed were: SAFe-S1, SAFe-D2, NASS-5, CASS-4.

⁵ Operator must be at least partially attentive, if not fully occupied by the analysis

Time calculation: $\frac{100\text{samples} \times 7.8\text{min} \times 3\text{replicates}}{60\text{min}} = 39\text{h}$

⁶ Assuming the use of an auto-sampler during pre-concentration.⁷ Per triplicate analysis, including all rinses.

alternative method to the FIA technique. Major differences are the sample treatment. The FIA method's major advantage is standardising the sample interaction time with the reagent before detection. This is achieved by performing all sample manipulations in-line, after sample injection. This limits contamination, standardises sample pretreatment (as it is all automated) and allows the use of heat to reduce the time required for Al-lumogallion complex formation ([Resing and Measures, 1994](#); [Brown and Bruland, 2008](#)). This major advantage is also the major disadvantage, as the in-line sample treatment complicates the system. The pre-concentration mechanism and the detection mechanism are intricately linked, limiting the options available for each process. Isolating parameter effects is difficult as one parameter has flow on effects to others, making optimisation and trouble-shooting difficult and requiring a high level of experience to operate efficiently. With regard to this, pH stability of all reagents and maintenance of flow ratios are critical for maintaining system stability.

The disadvantages of the FIA method were key to selecting the RP-HPLC method. The chemistry employed in the FIA method was clearly superior to alternatives ([Ahmed and Hossan, 1995](#);

Mulon et al., 2005; Tria et al., 2008a) (and references there in), however, the analytical set-up had many limitations. Changing the in-line sample treatment (as employed in the FIA method) with a pre-column (batch) reagent mixing step, separated the detection mechanism (formation of the Al–lumogallion complex) from the concentration mechanism (the focusing of the Al–lumogallion complex onto the C₁₈ guard column), allowing independent optimisation. Changing the buffer used from the toxic and volatile ammonium-acetate to the non-toxic and non-volatile MES, improved reagent pH stability over time. Replacing a peristaltic pump with a high pressure pump, removed potential backpressure issues, reduced baseline variability, decreased dead volumes and improved the range of column types and flow rates that could be applied. Removing lumogallion from the eluent (and therefore the baseline) allowed greater capacity to quantify the blank, as it was injected as a discrete sample.

The RP-HPLC method achieved similar LOD and precision to the FIA method. This is expected as the chemistry is very similar and blanks/LOD of both systems are dominated by reagent contamination levels. Total analysis times were similar, although required operator times were much lower for the RP-HPLC method, due to the capacity for reliable automation, attributed to robustness (discussed further in section 3.4.1).

Comparison of the RP-HPLC method to the ICP-MS method in Table 3.3 was for illustrative purposes only, as it was also used for analysing the SAFe reference sample. However, they cannot be considered as direct alternatives to each other. The RP-HPLC technique does not have multiple analyte capacity and the ICP-MS method is an impractical method to take to sea. A similarity of both methods is the use of off-line sample pretreatment steps that require significant periods of time (although not labour intensive). This approach decouples chemical mechanisms used for concentration and detection, allowing greater control over each mechanism. However the ICP-MS method must optimise for multiple elements, which can decrease precision at low concentrations for difficult low atomic mass elements like Al. The RP-HPLC method had improved LOD, precision and total analysis times relative to the ICP-MS method. However, required operator time is similar for both methods.

The RP-HPLC method had relatively similar performance to the existing methods. LOD and precision were similar across all methods. Pretreatment time per 100 samples was highly varied. The ICP-MS method required substantial sample preparation before injection into the ICP-MS, however this is offset by the multiple element capability. The RP-HPLC method requires 120 min of labour, followed by 8 h of equilibration time before the start of the analysis sequence, this is much less time than the ICP-MS method and 10 h more than required for the FIA method. Analysis

time per replicate were of the same order of magnitude, however, if these values are converted into operator time per 100 samples, the values are very different.

For the RP-HPLC method, the operator prepares a sample set of 100, loads them into the autosampler and enters sample details into the program's run-sheet (total time about 3 h). The operator can now leave and come back in 13.5 h when the analysis is finished.

For the FIA method, the operator needs to watch the instrument regularly, as it is not robust enough to leave unattended for long periods of time. This requires at least partial attention during every run, and hence requires ~39 h operator time per 100 samples.

For the ICP-MS system, operator requirements for the ICP-MS system were not available through first-hand accounts (as they were for FIA and RP-HPLC methods). An estimate is made assuming an autosampler was used for preconcentration (requiring 2 h), with an operator required to be in attendance (or close at hand) during analysis with an ICP-MS (requiring 6 h).

These differences in operator time are substantial and highlight the advantages of using robust chemical techniques over less robust systems.

3.4.1 Robustness and automation

Method robustness was defined "as the sensitivity of the method to small changes in influencing factors". The advantages of applying robust instrumentation to existing, proven chemistry is demonstrated with the RP-HPLC method presented here. Small changes in sample pH, buffer concentration, system backpressure, fluorescence settings, and laboratory temperature made little difference to signal intensity. As there are no mixing points, the only variable between samples was time since reagent was added, with the impact insignificant between calibrations. Changing over columns had no significant effect. The blank was significantly affected by lumogallion concentration (which is expected), and therefore, was minimised.

The authors experience with the FIA method ([Brown and Bruland, 2008](#)) was that it exhibited high sensitivity to buffer concentration and pH, pump tubing integrity, system backpressure, column used (as they were made in-house as opposed to commercially produced products), mixing coil temperature stability and sample pH. Limited robustness resulted in a requirement for regular (if not constant) attention and significant training to operate efficiently. This lack of robustness is a common acknowledgement by users of FIA methods (not limited to those discussed here).

The RP-HPLC method was very robust and easily automated. It was used to successfully analyse ~300 samples within one week (inclusive of troubleshooting, which was mostly attributed to operator error). The system could be left unattended until completion once the automated analysis program was initiated. Operation and trouble-shooting assistance during development was available through free-access on-line communities.

An example depth profile is presented in Figure 3.4 (GEOTRACES cruise GIPY6 along the SR3 meridional transect, station N20, 144°E, 49.3°S, within the Polar Frontal Zone of the SO). Features include: enrichment at the surface due to supply from aeolian deposition (albeit limited) or advection of waters entrained with dAl; depletion with depth as this is scavenged throughout the water column; enrichment approaching the ocean floor due to supply of dAl from sediments, although this is quite limited. Concentrations are extremely low in this region relative to the the global range due to geographic and atmospheric isolation from continental sources coupled with diatom dominated communities at the surface. Some values were close to the detection limit (displayed as the feint dotted line) but maintained oceanographic consistency, and excellent precision. Oceanographic features include: enrichment at the surface due to supply from aeolian deposition (albeit limited) or advection of waters entrained with dAl; depletion with depth due to scavenging and mixing throughout the water column; enrichment approaching the ocean floor due to supply of dAl from sediments (although this is quite limited). Concentrations are extremely low in this region relative to the global range due to geographic and atmospheric isolation from continental sources coupled with diatom dominated communities in surface polar waters.

3.4.2 Required sample volume

Relative to previously published methods, applying this RP-HPLC technique reduces the required sample volume significantly (as can be seen in Table 3.3), by ~20-fold and ~60-fold in the case of FIA and ICP-MS respectively. This is due to the combination of the extremely sensitive fluorescence detection system and the advantages of HPLC such as low system dead volumes, excellent analyte focusing on highly efficient columns and little band broadening. However, as discussed earlier, comparison with ICP-MS in this case is not fair, as that is a multi-element technique.

3.5 Conclusions

A major limitation of this technique is the time required for sample pre-treatment. This is a function of the slow reaction kinetics of Al (Eigen, 1963). Resing and Measures (1994) and Brown and Bruland (2008) have shown how the heating of the reagent-sample mixture would increase

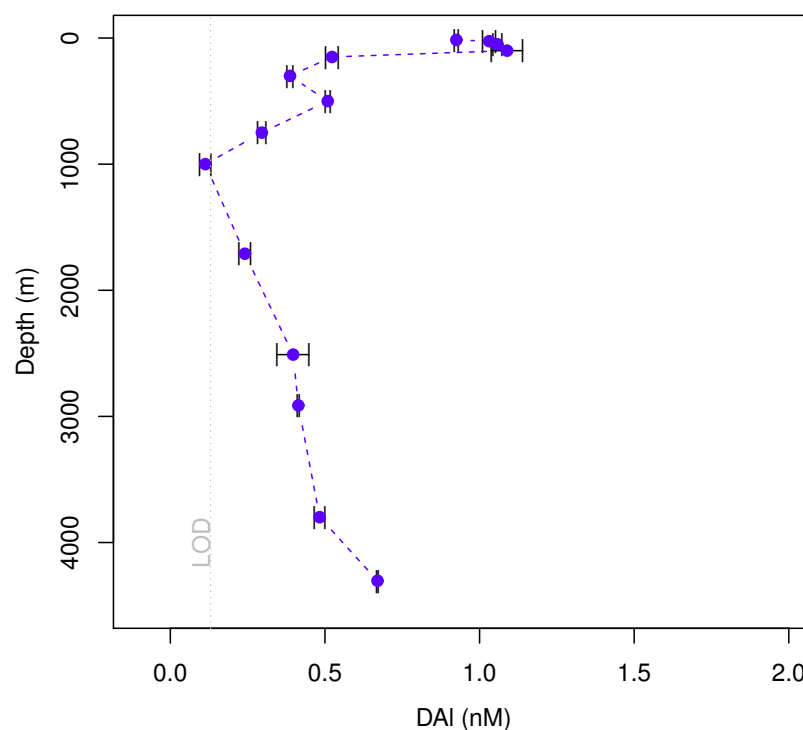


Figure 3.4: Example depth profile of dAl from the SR3 transect (Station N20, 144°E, 49.3°S, within the Polar Frontal Zone of the SO, sampled in April 2008 as part of the International Polar Year - GEOTRACES program).

the kinetics of the Al–lumogallion complex formation. However, it also increases the rate of complex decomposition. Therefore, increasing the rate of kinetics requires in-line systems that can standardise the time between mixing with the reagent and detection (such as those used by [Resing and Measures \(1994\)](#) and [Brown and Bruland \(2008\)](#)). The HPLC system available to the authors at the time of development was not capable of automating the addition of the reagent to the sample hence a more conservative approach to sample pretreatment was adopted, focusing on the long-term stability of the Al–lumogallion complex.

The use of an automated sample dosing and injection system would reduce the time required for complex formation, whilst maintaining the large gains in robustness and automation. The authors would also expect an increase in sensitivity, as the time of maximum complex yield could be targeted.

The RP-HPLC method is an excellent technique to use for the determination of dAl in open ocean

seawater. It employs similar chemistry to the FIA method and has good agreement with agreed values for the SAFe standard reference material. Therefore, open ocean dAl data produced with RP-HPLC are compatible for comparison with the existing global data set. The RP-HPLC method is recommended for future work for those determining Al in seawater due its robustness, sample volume requirements and automation capacity, while achieving comparable LOD, precision and accuracy to existing methods.

Chapter

4

Using dissolved aluminium concentrations to constrain trace element supply to the subantarctic SO south of Australia

4.1 Introduction

In the high-nutrient, low-chlorophyll (HNLC) regions of the ocean, primary production is significantly influenced by micronutrient supply ([Martin and Fitzwater, 1988](#); [Martin et al., 1990](#)). Therefore, constraining the relative contributions of the various sources and sinks of micronutrients is important for understanding the biogeochemical cycling in these regions.

The SAZ is a circumpolar HNLC region and is the interface of the major ocean basins to the SO. The SAZ has phytoplankton concentrations that are relatively high for the SO, exhibit low seasonality and regional variability and are controlled by a complex interplay between light, mixed layer depth (MLD), micronutrient and silicic acid supply and grazing pressure ([Rintoul and Trull, 2001](#); [Bowie et al., 2011a,b](#); [Ebersbach et al., 2011](#)).

The SAZ-Sense (Sensitivity of the Subantarctic Zone to Environmental Change, GEOTRACES cruise GIPY2) project aim was to examine the links between circulation, macro- and micronutrient supply, microbial ecology, and carbon cycling ([Bowie et al., 2011a](#)). Three process stations were identified (see [Figure 4.1](#): two in the SAZ just to the south-west (P1) and the south-east (P3) of Tasmania to compare the east-west gradient; and a third (P2) just poleward of the Polar Front (PF), due south of Tasmania, as it was representative of source waters into both P1 and P2 and to provide a reference water body. P1 was expected to be typical of the present-day SAZ, while P3 was expected to be more characteristic of the zone under the influence of future climate change ([Bowie et al., 2011a](#)). P1 was expected to be of lower biomass, and P3 was expected to be of higher biomass.

Key parameters (identified by the international GEOTRACES program) were analysed at each station in an attempt to elucidate the relative magnitude of micronutrient supplies and sinks. Aeolian deposition is thought to be an important source of micronutrients (such as Iron, Fe) to the open ocean ([Martin, 1990](#); [Martin et al., 1990](#); [Martin, 1991](#); [Duce and Tindale, 1991](#); [Boyd et al., 1996, 2000](#);

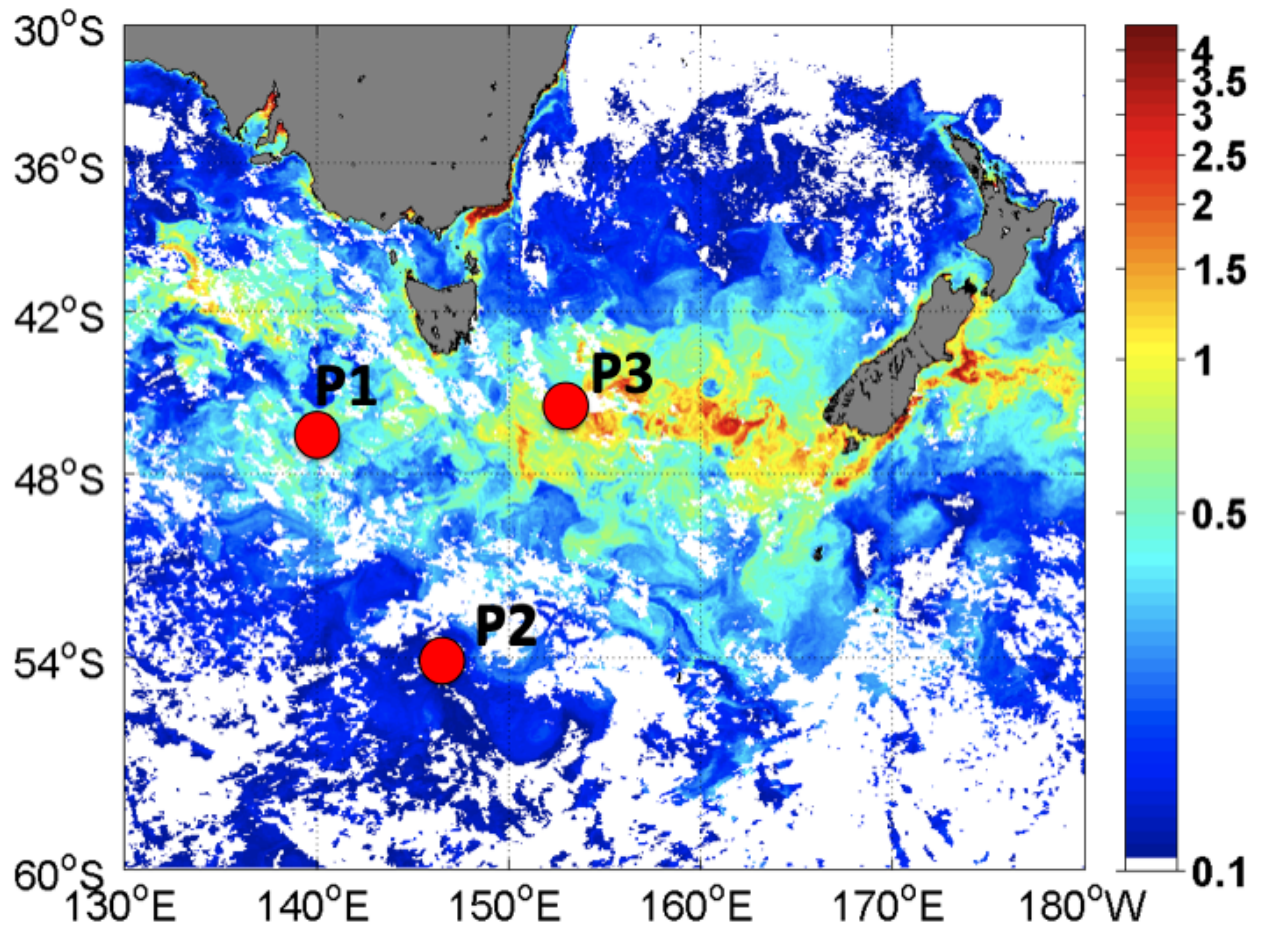


Figure 4.1: 8-day composite MODIS image of chlorophyll-a concentrations from 18-Feb-2007, from [Mongin et al. \(2011b\)](#). Chlorophyll-a (as a proxy for biomass) concentrations were $P3 \gg P1 > P2$. Process station locations were selected to discern the physical and biogeochemical drivers of regional differences in biomass and primary production.

[Bowie et al., 2009](#)). However, estimating the contribution of aeolian dust to the micronutrient budget of the SAZ and SO is difficult due to: the sporadic and variable nature of these events ([Gabric et al., 2010](#)); the remote location of the target region; the high instance of cloud (reducing the usefulness of satellites); and the biogeochemistry of the target micronutrients (e.g. biologically active, poor solubility in seawater, short residence times (weeks) ([Frank et al., 2003](#); [SCOR Working Group, 2006, 2007, 2012](#))).

Al is a GEOTRACES key parameter, used to identify the relative magnitude of aeolian deposition events. Al is $\sim 8\%$ of earth's crust ([Taylor, 1964](#); [Wedepohl, 1995](#); [Yaroshevsky, 2006](#)) and is readily transported in dust during deposition events to the open ocean ([Duce and Tindale, 1991](#); [Arimoto, 2001](#); [Arimoto et al., 2003](#); [Jickells et al., 2005](#); [Bowie et al., 2009](#)). Its role as a nutrient

in seawater is assumed to be insignificant and it is an element that is readily scavenged (Paces, 1978; Stoffyn, 1979; Mackin and Aller, 1984c; Walker et al., 1988; Moran and Moore, 1988, 1992; VanBeusekom et al., 1997). As it is readily scavenged it has a relatively short residence time in the surface ocean, generally assumed to be <3 years (Stoffyn, 1979; Stoffyn and Mackenzie, 1982; Orians and Bruland, 1985, 1986), but can range from days to weeks in region of high productivity to >3 years in regions of low productivity (Orions and Bruland, 1986; Moran and Moore, 1988; Brown et al., 2010). This makes it useful as a biogeochemical tracer of watermasses over these timescales. Al can indicate the level of interaction the target watermass has had with terrestrial sources of micronutrients, such as aeolian deposition into the ocean (Measures and Edmond, 1989), although this relationship is limited to surface waters due to sedimentary resuspension (Moran and Moore, 1991; Middag et al., 2009). dAl concentrations in the ocean can be used as inputs into the MADCOW model (Measures and Vink, 2001) to estimate the aeolian dust deposition rate ($g.m^{-2}.y^{-1}$), and therefore, the relative magnitude of dust as a source of micronutrients compared to upwelling and lateral advection (Measures and Edmond, 1989).

Within this context, dAl concentrations were determined at each station (both transect and process stations) and in combination with other parameters used in an effort to constrain micronutrient supply mechanisms to each process station (P1, P2 and P3).

4.2 Methods

4.2.1 Voyage track and strategy

The SAZ–Sense voyage (RSV *Aurora Australis* 2006/07) took place in the late austral summer, 21 January – 19 February 2007. Additional voyage information can be obtained from the Australian Antarctic Division Data Centre (http://data.aad.gov.au/aadc/voyages/display_voyage.cfm?voyage_id=336). The SAZ–Sense voyage was built around a mix of process and transect stations (Bowie et al., 2011a,b), see Figure 4.2. The process stations were occupied within a Lagrangian framework for several days to fully characterise the water body and its short-term variability. The voyage track was orientated by the locations of the three process stations (P1, P2, P3). Transect legs were nominally the direct line between two process stations, or between a process station and the port of Hobart.

Absolute.Salinity [g/kg] @ Depth [dbar]=first

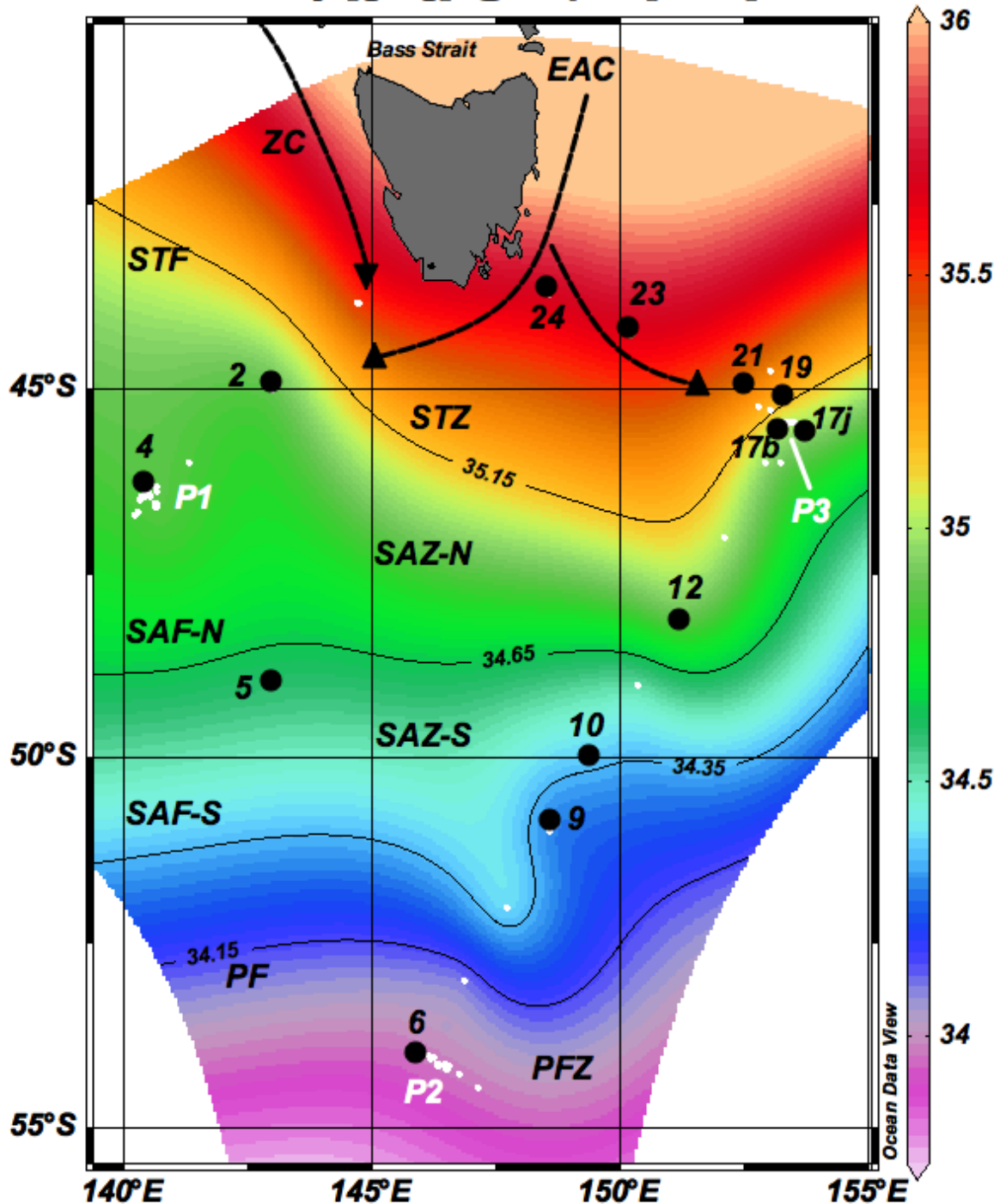


Figure 4.2: SAZ-Sense station locations (● = trace element stations; ○ = CTD stations) relative to the relevant oceanographic features highlighted using absolute salinity values (“[dbar]=first” is 0 dbar, the surface value). ZC = Zeehan Current; EAC = East Australian Current; STF = Subtropical Front; STZ = Subtropical Zone; SAF-N = Subantarctic Front - North; SAZ-N = Subantarctic Zone - North; SAF-S = Subantarctic Front - South; SAZ-S = Subantarctic Zone - South; PF = Polar Front; PFZ = Polar Frontal Zone; AZ = Antarctic Zone.

4.2.2 Oceanographic Setting

Study region

The oceanographic setting is described in [Bowie et al. \(2011a\)](#). Figure 4.2, presents the SAZ-Sense station locations, south of Tasmania, Australia, with the relevant oceanographic features superimposed on an iso-surface of absolute salinity at 0 dbar (the surface). The major currents (and their flows) to consider are the: East Australian Current (EAC, 9.4 Sv ([Ridgway and Godfrey, 1994](#); [Ridgway, 2007](#))) ; Zeehan Current (ZC, 2.4 Sv ([Cirano and Middleton, 2004](#); [Ridgway, 2007](#))) ; and the Antarctic Circumpolar Current (ACC, 147 Sv ([Rintoul and Sokolov, 2001](#)), not shown). Approximate summer locations of the major oceanographic features within the ACC are shown: Subantarctic Front (SAF, 105 Sv ([Rintoul and Sokolov, 2001](#))), which is split into north (SAF-N) and south (SAZ-S); and the Polar Front (PF, 5 Sv ([Rintoul and Sokolov, 2001](#))). These frontal systems separate the distinct watermasses: Subtropical Zone (STZ); Subantarctic Zone north (SAZ-N); Subantarctic Zone south (SAZ-S); Polar Frontal Zone (PFZ).

Currents

The ACC dominates the SO, flowing from West to East ([Rintoul and Sokolov, 2001](#)). It is a composite of many smaller fronts and currents (which all vary in position through space and time), those relevant to this region have been mentioned above.

The EAC, is a well defined north-south current off the eastern coast of Australia, ~200 km wide ([Nilsson and Cresswell, 1980](#); [Mulhearn, 1983](#); [Cresswell and Legeckis, 1986](#); [Ridgway and Godfrey, 1994, 1997](#)). In comparison to the ZC, the adjacent coastal region is densely populated, with farm land and forests that are subject to seasonal bush fires, which may be a source of highly soluble forms of micronutrients to the open ocean ([Guieu et al., 2005](#); [Sholkovitz et al., 2009](#); [Ito, 2011](#); [Sholkovitz et al., 2012](#)). Soils are younger and rich in organic material and minerals easily soluble in water ([Strand et al., 2002](#)). The EAC passes through the middle of the SE atmospheric pathway (see Figure 4.3) ([Mackie et al., 2008](#); [McGowan and Clark, 2008](#); [Strong et al., 2011](#)) and is the beneficiary of aeolian dust transported off the Australian continent over the coastal zone ([Mackie et al., 2008](#)). It also interacts with shelf waters, which could entrain trace elements into the upper water column through vertical mixing. Physical entrainment of shelf waters has been observed by [Baird and Ridgway \(2012\)](#). As the EAC passes Bass Strait, it can incorporate Bass Strait Waters (BSW) as a discrete sub-surface lense inside anticyclonic eddies ([Tomczak, 1981, 1985, 1987](#); [Tomczak and Tanner, 1989](#); [Baird and Ridgway, 2012](#)). BSW are defined as waters

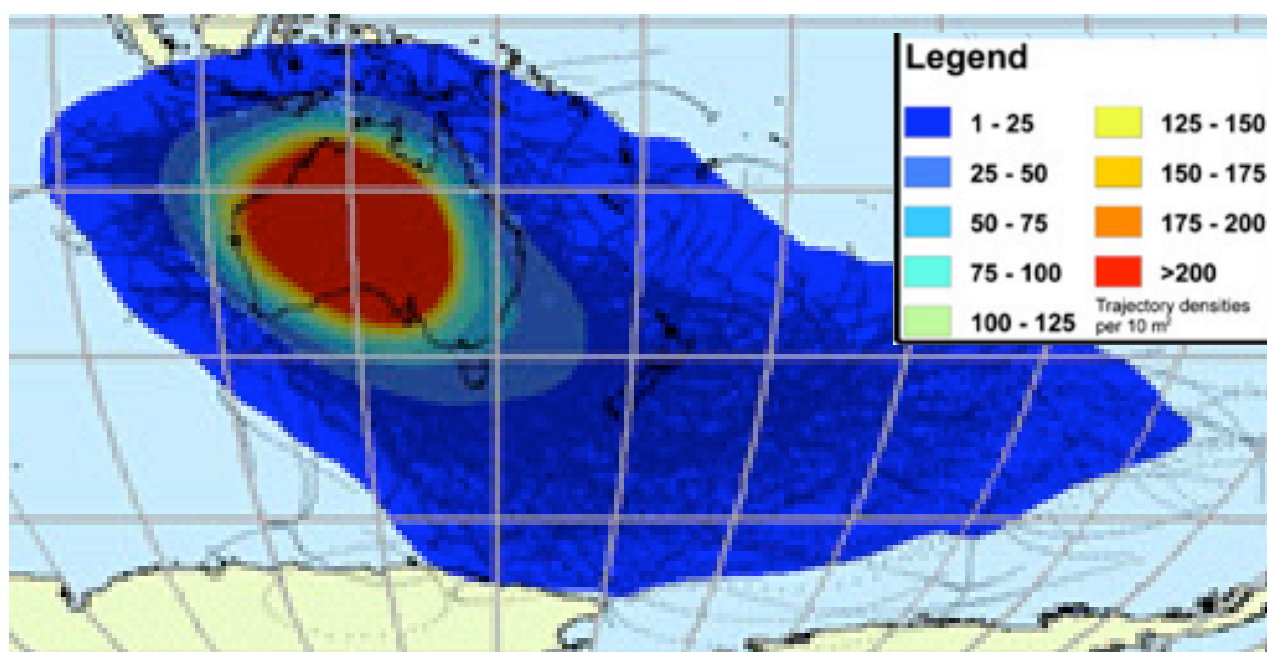


Figure 4.3: A representation of the major atmospheric pathways over AUstralia by McGowan and Clark (2008) using the HYSPLIT model. This represents the potential deposition field of dust from Australia into the Tasman Sea and the Southern Ocean. Most trajectories do not venture far offshore. The atmospheric pathways are referred to as the North West (towards Asia) and South East (towards New Zealand) components.

over the Australian continental shelf (depth <100 m) separating Tasmania from mainland Australia (Harris et al., 2005). Naturally they are in close proximity to terrestrial sources from both Tasmania and Victoria, with high likelihood of trace element enrichment from both aeolian and shelf sediment sources.

The ZC is a continuation of the Leuwin Current and flows from west to east along the southern edge of the Australian continent, before turning south down the west coast of Tasmania (Ridgway and Condie, 2004). In comparison to the EAC, the adjacent coastal region is sparsely populated, mostly of lightly vegetated desert, with soils that are enriched with insoluble minerals (as the soils are old and have been heavily processed by erosive forces) (Mackie et al., 2008, and references therein). The instance of industrial pollution and bush fires (both of which generate particles with a greater soluble fraction (Guieu et al., 2005; Sholkovitz et al., 2009; Ito, 2011; Sholkovitz et al., 2012)) is lower than on the east coast of Australia. The ZC flows along the south eastern edge of the SE Atmospheric pathway (see Figure 4.3) (Mackie et al., 2008; McGowan and Clark, 2008), where the proportion of aeolian deposition is expected to be lower than in the middle of the pathway. Together all these factors reduce the potential trace element yield from aeolian dust deposited into the ZC.

Station 2

Station 2 was on the South-Western edge of a region with a strong seasonal signature in its dynamics, dominated by the ZC in winter and the EAC in summer (where the two currents are 180° out of phase) (Ridgway, 2007). As such, the source waters of this region originate from totally different locations in summer compared to winter. The ZC, driven by the flow of the Leeuwin Current (on the Australian continental west coast), dominates from May to July (austral winter) driving waters from the Great Australian Bight down the west coast and around the southern tip of Tasmania, creating southerly and easterly flows (Ridgway, 2007). A weakening of the ZC in September, coupled with a strengthening of the EAC in October results in the EAC extension rounding the southern tip of Tasmania in November, where northerly and westerly flows then dominate the region until March (Ridgway, 2007).

The meeting of the ZC, the EAC and the northern component of the ACC (at the STF) is a region of dynamic and dispersive oceanographic features (Herraiz-Borreguero and Rintoul, 2011a), where lateral and vertical mixing could rapidly reduce the concentration of trace elements supplied to this region by the ZC and the EAC. MLDs are 150–200 m in winter and 50–100 m in summer (Herraiz-Borreguero and Rintoul, 2011b).

Process station one (P1), station 4

P1 was in the middle of the SAZ, as were stations 5, 10 and 12 (see Figure 4.2). It was expected to be exclusively under the influence of the ACC. The strong westerly winds that dominate the area make it an oceanic region with limited terrestrial influence. Although stations 5, 9, 10 and 12 are not near P1, they are within the SAZ, affected by similar oceanographic and atmospheric conditions between the PF and the STF. MLDs are 500–700 m in winter and 50–100 m in summer (Herraiz-Borreguero and Rintoul, 2011b).

Process station two (P2), station 6

P2 was in the AZ. It was under the influence of the PFZ and the ACC and given its remoteness from the continents, has limited terrestrial influence. MLDs are 200–300 m in winter and 50–100 m in summer (Herraiz-Borreguero and Rintoul, 2011b).

Process station three (P3), stations 17b and 17j

P3 was in a region with highly complex oceanographic features where the EAC extension interacts with the STF. Stations 19, 21, 23 and 24 were under the influence of similar oceanographic conditions as they were also within the EAC/STZ. The southern Tasman Sea, between Tasmania and New Zealand, is a region of relatively slow moving water, separated from the relatively fast ACC by the STF (Herraiz-Borreguero and Rintoul, 2011a). The STF has much slower velocities at P3 compared to its velocity near station 2 and P1. Meso-scale eddies, transported south in the EAC, enter the region and can persist for weeks to months (Mongin et al., 2011a,b). The entire region falls within the SE atmospheric pathway (Mackie et al., 2008). The slow moving nature of the watermasses increase the probability of aeolian deposition events to each watermass in the region. MLDs are 150–200 m in winter and 50–100 m in summer (Herraiz-Borreguero and Rintoul, 2011b).

4.2.3 Sampling and processing

The guiding principle for collection of seawater samples, and any subsequent step from sample processing through to final analysis, was the prevention of contamination. Guidelines coming from the GEOTRACES project (summarised in Bowie and Lohan (2009)) were followed. Water samples were taken from the surface (15 m was the shallowest depth to avoid contamination from the ship) down to 1000 m with acid-cleaned, Teflon-coated, externally sprung, 5-L PVC bottles (Niskin 1010X, General Oceanics, USA). The Niskin bottles were as supplied, apart from replacement of the original taps with PTFE stop-taps (Cole Parmer, USA), replacement of metal crimps with nylon crimps, and replacement of the supplied external springs with teflon coated springs. They were deployed on an autonomous rosette (Niskin Model 1018, General Oceanics, USA) from a winch spooled with 6-mm diameter kevlar hydroline (Strongrope, Australia). The rosette typically had twelve Niskin bottles mounted, but for six casts out of thirteen for dissolved metals, a Falmouth Scientific Instruments (USA) micro-conductivity-temperature-depth (CTD) unit occupied one position. Once the rosette was recovered, the bottles were transferred as quickly as possible into a ‘clean container’ with HEPA-filtered air. Further processing was carried out under an ISO Class 5 trace-metal-clean laminar flow hood. Details on the optimisation of the rosette system (borrowed from the National Institute for Water and Atmospheric Research, NIWA, New Zealand) for trace-metal sampling and the subsequent protocols for processing the samples can be obtained from Ellwood et al. (2008) and Lannuzel et al. (2011a).

During sample processing, seawater came in contact only with Teflon (PTFE), C-Flex (proprietary thermoplastic elastomer; Cole Parmer, USA) and low-density polyethylene (LDPE) screw-cap 60-

mL bottles for storage (Nalgene, USA). All materials had been scrupulously acid-washed before use; the procedures are detailed in [Bowie and Lohan \(2009\)](#). Seawater subsamples were propelled through a short length of C-Flex tubing by over-pressuring each Niskin bottle with nitrogen (<10 kPa; 0.2- μ m filtered) and were filtered through 0.2- μ m pore-size, acid-washed capsules (Pall Supor membrane, Acropak 200, USA). The filtrates were collected in the 60 mL LDPE bottles, and acidified later (<1 week) to pH \sim 1.8 in a land-based ISO Class 3.5 Clean Laboratory using high-purity 12 M hydrochloric acid (Seastar Baseline, Canada). All samples were then stored for a minimum of three months before being analysed to allow for complete equilibration under acid conditions.

4.2.4 Analysis

Samples were analysed using reversed phase high performance liquid chromatography (RP-HPLC) with fluorescence detection ([Remenyi et al., 2012](#)). Acidified seawater samples were pretreated with a reagent containing MES (2-(N-morpholino)ethanesulfonic acid) and lumogallion and left until formation of the fluorescent Al–lumogallion derivative was complete (10 h). The mixture was then injected onto a Chromolith® RP-18e Guard (10 \times 4.6 mm) column with 5% methanol (for analyte pre-concentration and matrix elimination) and then eluted with 95% methanol into a fluorescence detector (λ_{ex} = 505 nm, λ_{em} = 574 nm). Sample pre-treatment required 10 h (>100 samples can be prepared simultaneously) and sample analysis required 10 μ L and 2.7 min per replicate. Total required sample volume (including rinses) was 1.5 mL. The limit of detection was 0.13 ± 0.05 nM, with mean precision of 2.7% at 1 nM (on SAFe–D2 reference samples). Agreement with SAFe reference samples was within $4.6 \pm 4.6\%$ (n = 13).

4.2.5 Air mass trajectory analysis

Thibaut Wagener produced the Figures [4.4](#) and [4.13](#). These are reproductions from [Bowie et al. \(2009, supp.\)](#). Quotes of methods used for figure production follow. Figure [4.4](#) was produced in this manner:

In order to provide a qualitative indication of preferential dust sources to the sampled areas, back trajectories of hypothetical air masses were calculated using the HYSPLIT (HYbrid Single Particle Lagrangian Integrated Trajectory) model developed at the NOAA Air Resource Laboratory ([Draxler and Rolph, 2012](#)), with re-analysed archived meteorological data from the Global Data Assimilation System (see Figure [4.4](#)).

Trajectories were hindcast at four different heights within the atmospheric boundary layer (10, 100, 500 and 1000 m) up to 120 h back in time. For each sampling day, a trajectory was calculated with a finishing point at the position of the ship at 12:00 (UTC). Moreover, from September 2004 to February 2007, trajectories were calculated at 100 m up to 240 h back in time for every 24 h for the three finishing points at P1, P2 and P3. Even though errors on 10 day back trajectories may be significant (Draxler and Rolph, 2012), they provide a reasonable qualitative indication of preferential dust sources to the SAZ-Sense region.

Note that these trajectories are only used as a qualitative measure to highlight that interaction with landmasses is highly unlikely for most of the stations and possible in the northerly most stations.

Figure 4.13 was produced in this manner:

Bush fire locations detected from MODIS Terra and Aqua satellite sensors (data from <http://maps.geog.umd.edu/firms>), and UV Aerosol Index (AI) from the OMI instrument on the same day (data from <http://disc.sci.gsfc.nasa.gov/techlab/giovanni>).

HYSPLIT dispersion density modelling (Draxler and Rolph, 2012) of smoke plumes from known bush fire locations in Tasmania and Victoria were created using similar methods to those used for Figure 4.4, except trajectories were forecast (rather than hindcast).

4.2.6 Model for estimating annual aeolian deposition rates

Estimates of aeolian deposition were made using the simple one dimensional model presented by both Measures and Brown (1996) and Measures and Vink (2000) called MADCOW. Equation is defined as:

$$G = S \times A \quad (4.1)$$

Where:

G = aeolian deposition rate in $g\ m^{-2}\ yr^{-1}$

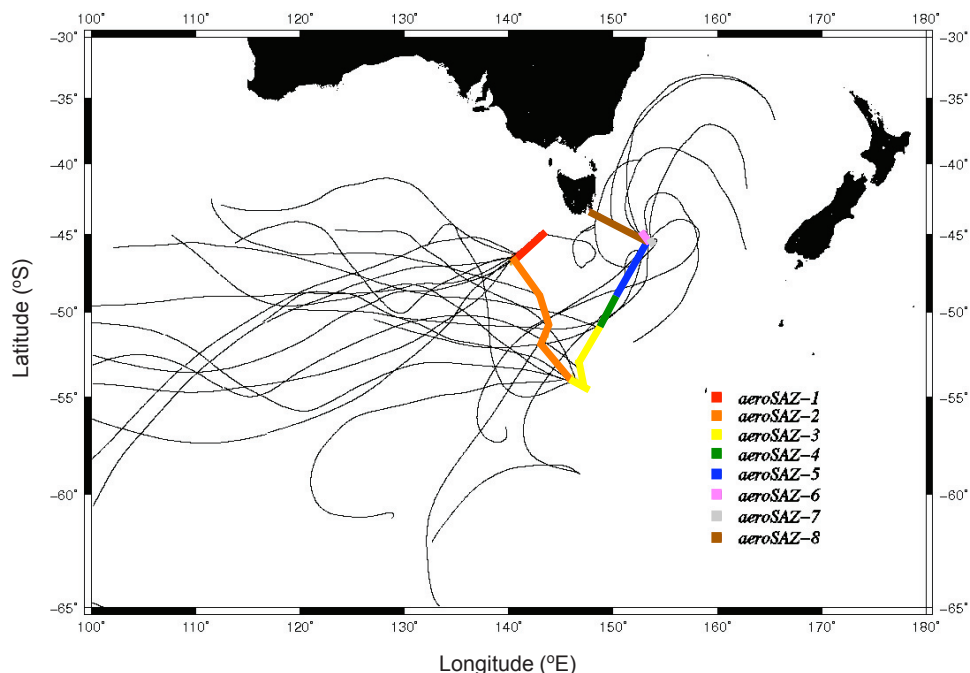


Figure 4.4: AereoSAZ sample collection transits (coloured) overlain with HYSPLIT airmass back trajectories for 5 days prior to each station occupation. In general, stations south of the STF had influence from airmasses over the SO. Stations at or north of the STF had influence from airmasses over Australia, New Zealand and the Tasman Sea, from [Bowie et al. \(2009, supp.\)](#).

S = solubility coefficient. Based on the characterisation of Australian dust by ([Mackie et al., 2008](#)), a relatively low solubility (1.5%) was expected, where $S = 0.133$. The solubility of the particulate Al in the dust source can be set at either 1.5% or 5%, with subsequent coefficients of 0.133 or 0.04 respectively (suggested coefficients from [Measures and Vink \(2000\)](#)).

A = dAl in the ML.

4.3 Results and Discussion

4.3.1 Summary of all results

Depth profiles in the top 1000 m were collected at 13 stations, resulting in 148 samples that were analysed for dAl. dAl was generally depleted with more than half the values < 1 nM and all values < 7.5 nM. This range agrees generally with previously observed values in the SO ([Measures and Edmond, 1990](#); [Middag, 2010](#)). The lowest values were below detection limits (LOD = 0.13 nM), located well below the ML of the SAZ-S and PFZ. The values reflected the complexity of the study region, especially in the north-east sector, where adjacent stations had very different profiles.

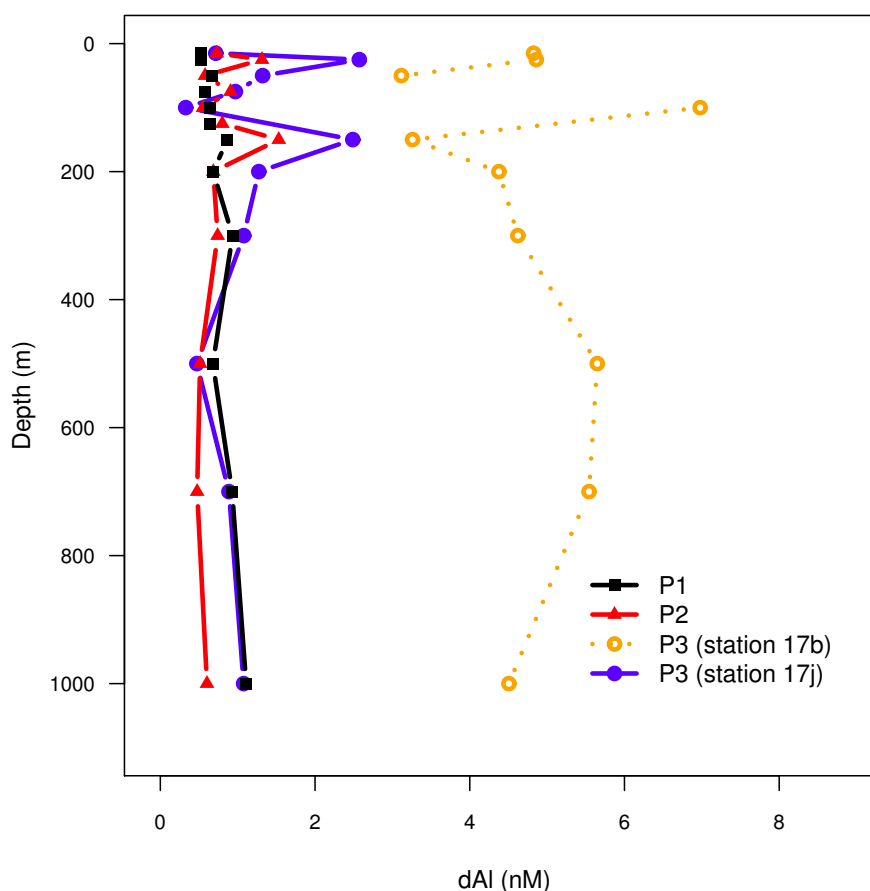


Figure 4.5: Depth profiles for dAl from each process station. Station 17b and 17j at P3 targeted adjacent eddies. These eddies clearly have different histories with regards to Al, discussed in section 4.3.4.

Suspected contamination was detected as values greater than 2 standard deviations from the mean of each profile, then these points were assessed for oceanographic consistency (Boyle et al., 1977b,a) to decide whether they should be included or excluded.

At the three process stations, differences were observed at the surface, with similarity observed at depth (see Figure 4.5). P1 had the lowest surface dAl concentrations of the entire data set, with a slight enrichment with depth observed. P2 had a relatively uniform dAl depth profile, except for samples at 25 m and 200 m, which are discussed later. P3 was a complex site where two profiles were collected. Two adjacent eddies were targeted, with significantly differing dAl profiles observed. Both had enriched surface concentrations compared to both P1 and P2, with further enriched surface values, again observed at 25 m and 200 m (it is possible these bottles suffered from low level contamination).

The transect section of the surface 400 m from P2 to P3 is presented in Figures 4.6, 4.7 and 4.8.

Parameters presented are conservative temperature (Θ), absolute salinity (S_A), potential density (σ), phosphate, nitrate, silicic acid, oxygen, fluorescence, photosynthetically available radiation (PAR), ammonium, Fe and Al. Θ , S_A and σ identify the different watermasses, best visualised by S_A with strong gradients observed at 52.5°S (PF), 51.5°S (SAF-S), 49.0°S (SAF-N) and 47°S (STF) (between 49°S and 51.5°S there is a meander of the SAF-S front, with the return to PFZ water clearly evident). Waters change from cold and fresh in the PFZ (more dense) to warm and salty in the STZ (less dense) near Tasmania, where the water from further north is advected south in the EAC extension. σ reveals the summer MLD was ~ 80 m across the entire section, although north of SAZ-N there was an additional shallow lens of <20 m at the surface, so two MLs were present (Bowie et al., 2011a; Westwood et al., 2011). Only the deeper ML was used for this study. Phosphate and nitrate co-varied, enriched and non-limiting in the SAZ and PFZ, they were depleted approaching nutrient limitation in the ML of the STZ (Bowie et al., 2009). Silicic acid was limiting at the surface over the entire region, although re-supply from below was possible in the PFZ. This was coupled with deepest light penetration ($\text{PAR} = 1 \mu\text{E m}^{-2} \text{s}^{-1}$), enhanced fluorescence throughout the PFZ ML and ammonium enrichment at the bottom of the ML. This suggests that at the southern extremity of our survey zone, either the bloom was already in a state of senescence or, that primary producers take advantage of the favourable nutrient conditions at the bottom of the ML coupled with a deeper photic zone in the PFZ (Parslow et al., 2001). Closer inspection reveals that the ammonium maximum is immediately below the $\text{PAR} = 1 \mu\text{E m}^{-2} \text{s}^{-1}$, suggesting remineralisation was enhanced beneath the photic zone.

Dissolved Fe (dFe) concentrations were decoupled from all of the parameters above, as well as dAl. dFe (discussed in Bowie et al. (2009) and Lannuzel et al. (2011a)) was enriched to ~ 0.4 nM below the ML in the PFZ, and relatively depleted in the surface. It was depleted throughout the water column of the SAZ. dFe was enriched in the STZ around P3, probably due to the influence of the EAC and proximity to the SE atmospheric pathway. Station 24, the closest station to Tasmania was depleted in dFe relative to other measurements in the STZ. This may be from one of three potential mechanisms. (1) The divergence of the EAC into two streams, creating an upwelling of Fe depleted waters at station 24. (2) The ZC can creep around the southern tip of Tasmania, very close to the coast and station 24 may have been in waters from the ZC rather than the EAC. (3) Stations 23 and 24 targeted two different eddies, one that had interacted with the sediments and one that had not.

dAl was compared to a range of oceanographic parameters (Θ , S_A , σ , nitrate, phosphate, oxygen, fluorescence, PAR, ammonium, Fe, Co, Cu, Pb, Ni, Zn, chlorophyll). No significant relationships were found. Decoupling from silicic acid was also observed, similar to observations in the Atlantic sector of the SO (Middag, 2010). Silicic acid concentrations were depleted in the surface waters

north of the PF, and increased significantly with depth (from $\sim 1\text{--}80\ \mu\text{M}$) as biogenic silica was remineralised. dAl profiles in general showed relative homogeneity with depth (or slight depletion) probably associated with limited supply to the surface, hence a reduced gradient with depth. dAl concentrations exhibit a latitudinal gradient increasing with proximity to Tasmania, especially in the STZ. This gradient was much more pronounced than any trend with depth. The dAl concentrations suggest two regimes, loosely separated by the STF. Relative dAl enrichment was $\text{STZ} \gg \text{SAZ-N} > \text{SAZ-S}$, PFZ and AZ. This supports modelling of the SE Atmospheric pathway by [Mackie et al. \(2008\)](#) and the global aeolian deposition modelling by [Zender et al. \(2003\)](#) and [Han et al. \(2008\)](#), although the contribution from re-suspended sediments (which could be considerable) in the STZ cannot be estimated due to the absence of Mn data.

The annual rate of aeolian dust deposition was estimated using MADCOW ranging from $< 0.05\ \text{g.m}^{-2}.\text{y}^{-1}$ in the SAZ and PFZ to a maximum of $0.98\ \text{g.m}^{-2}.\text{y}^{-1}$ in the STZ. Mean values matched expectations, with annual aeolian deposition greatest in the $\text{STZ} \gg \text{SAZ} > \text{PFZ}$. To provide a measure of variance, $\text{mean}(\text{dAl}_{ML})$, $\text{min}(\text{dAl}_{ML})$, $\text{max}(\text{dAl}_{ML})$ values per station are presented in Table 4.1 and Figure 4.9.

MADCOW estimates of the aeolian dust deposition rate agreed generally with aerosol fluxes estimated from samples collected underway by Thibaut Wagener (see Tables 4.2 and 4.3), ([Bowie et al., 2009](#), supp.). It must be noted that the dAl measurements and the aerosol fluxes represent very different time-scales. Aerosol measurements are discrete in time, collected over about a week during the voyage period, which is then extrapolated to represent a year. Where as dAl in the water is assumed (for the MADCOW model) to be an integration over 5 years, used to then infer dust deposition. Aerosol fluxes/concentrations were found to be greatest in the legs closest to Tasmania, from Station 2 to P1 (aeroSAZ-1) and from P3 back to Port (aeroSAZ-8). Fe solubility differed substantially between these two aerosol samples, with extremely low Fe solubility at P1 (0.5%) and relatively high Fe solubility at P3 (17.7%), indicating they were from different kinds of sources ([Bowie et al., 2009](#)), possibly terrestrial dust for aeroSAZ-1 and bush fire smoke/ash for aeroSAZ-8 discussed in Section 4.3.4. All other aerosol concentrations (aeroSAZ-2 to aeroSAZ-7) were found to be extremely low collected throughout the remainder of the voyage, with low Fe solubility.

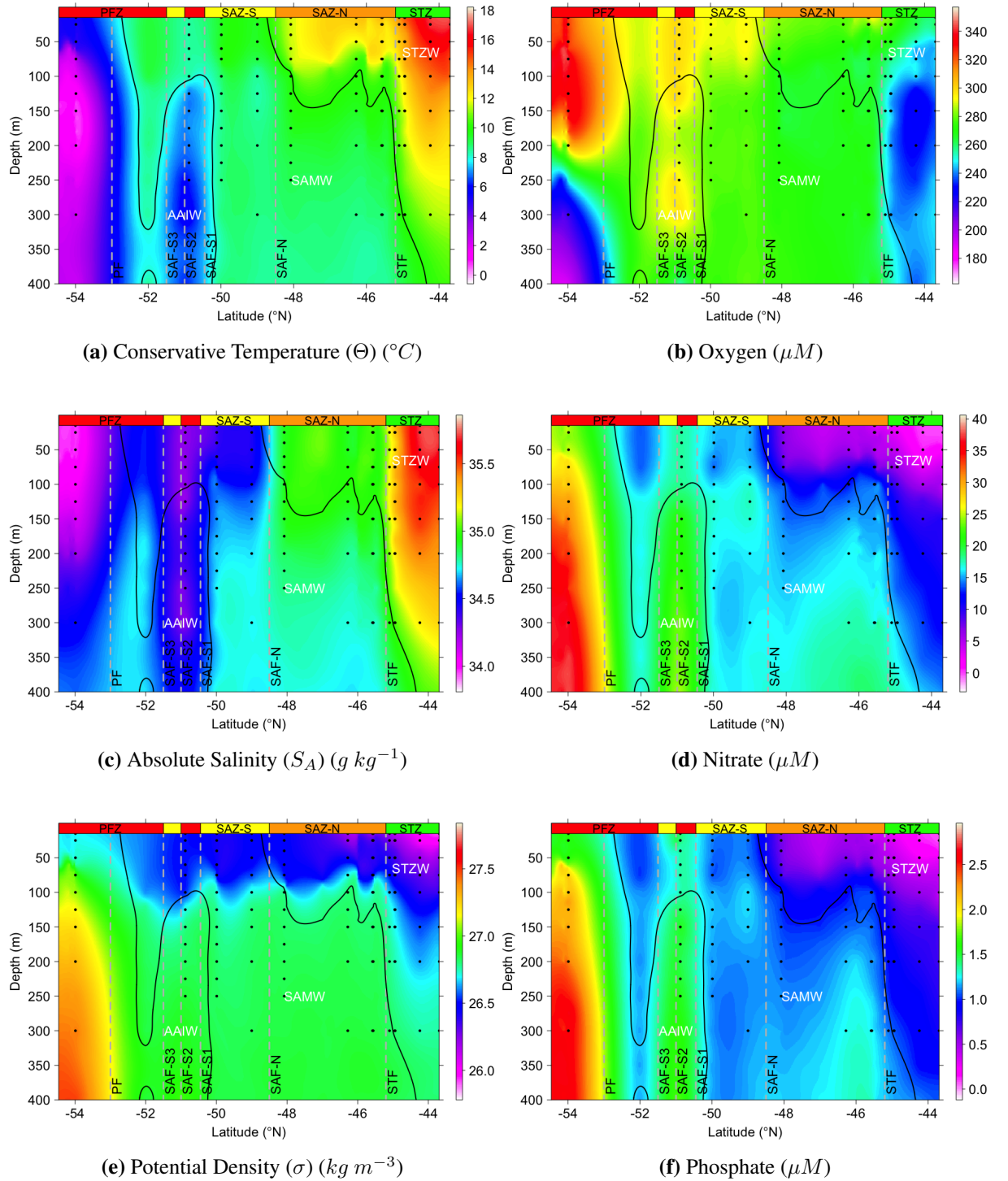


Figure 4.6: Major physical and nutrient parameters of the hydrographic section from P2 (54°S) to P3 (45.5°S) to Tasmania (43°S), in austral summer 2007. • = Trace element sampling point (Data points for hydrographic parameters not shown). Hydrographic parameters courtesy of [Rosenberg \(2007\)](#).

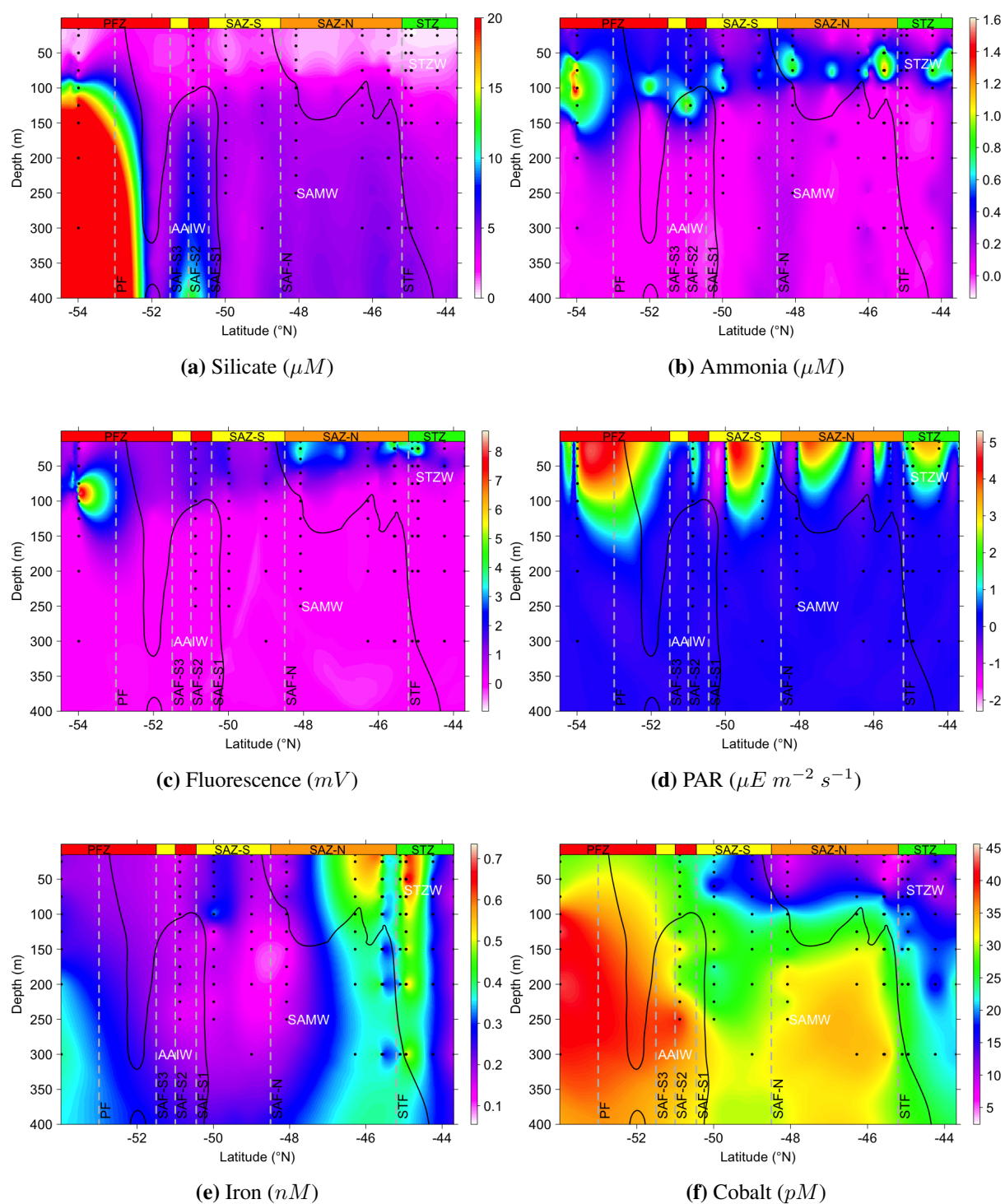


Figure 4.7: Supplementary parameters of the hydrographic section from P2 (54°S) to P3 (45.5°S) to Tasmania (43°S), in austral summer 2007. • = Trace element sampling point (Data points for hydrographic parameters not shown). Hydrographic parameters courtesy of [Rosenberg \(2007\)](#).

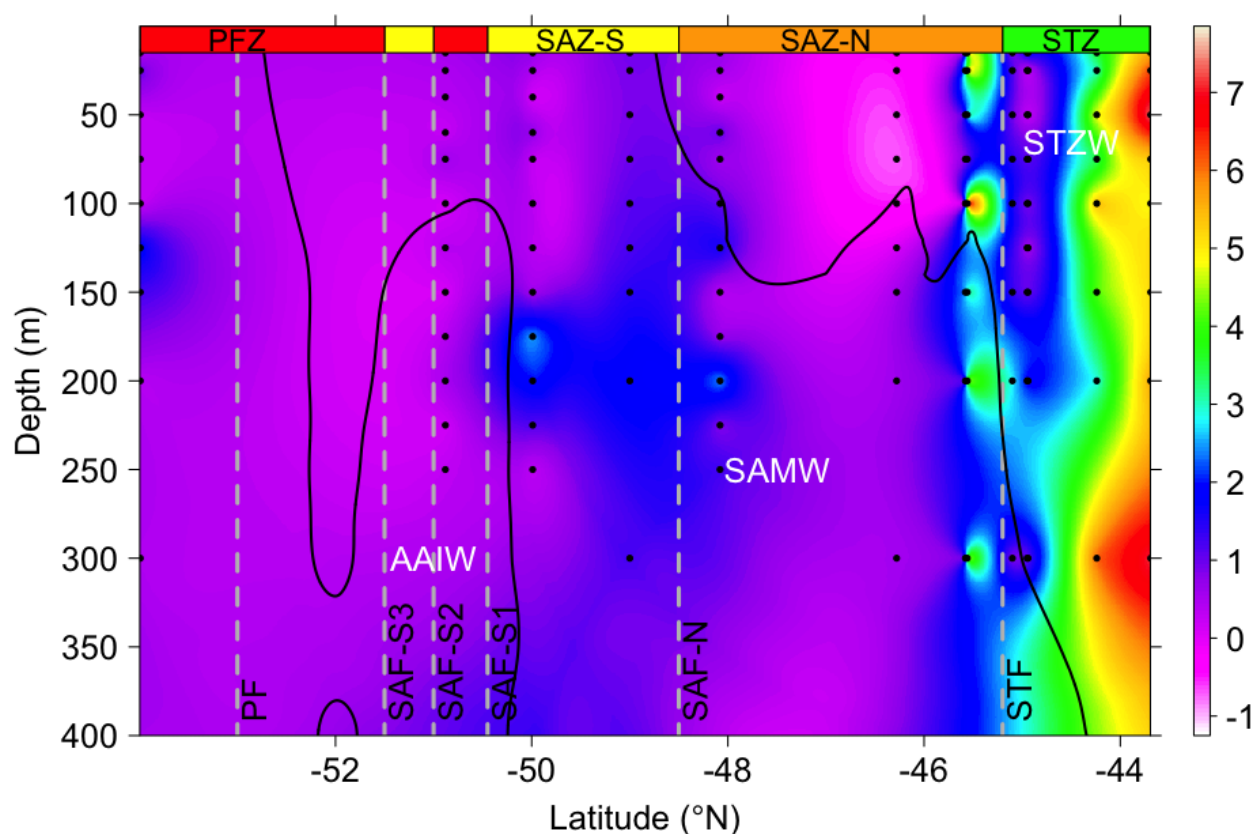


Figure 4.8: Dissolved Al of the hydrographic section along P2–P3–Tasmania in late summer. The strange concentration structure near the STF is effect of 17b and 17j (at the same latitude) on the interpolation algorithm. It appears 17b is an isolated eddy that originated in the EAC. Contours are Θ at 8 °C and 10 °C, these define the boundary between watermasses: STZW = Subtropical Zone Water; SAMW = Subantarctic Mode Water; AAIW = Antarctic Intermediate Water. • = Trace element sampling point. Grey dashed lines represent the oceanographic fronts: PF = Polar Front; SAF-S = Subantarctic Front - South (1,2,3 = multiple crossings over the SAF-S as it meandered relative to the voyage track); SAF-N = Subantarctic Front - North; STF = Subtropical Front. Major oceanographic zones are depicted as coloured bars across the top of the plot: SZ = Southern Zone; PFZ = Polar Frontal Zone; SAZ-S = Southern Subantarctic Zone; SAZ-N = Northern Subantarctic Zone; STZ = Subtropical Zone.

Figure 4.9: Aeolian deposition rates at each station during the SAZ-Sense voyage. Estimates produced using the MADCOW model (Measures and Brown, 1996), and an assumed solubility of 1.5% (coefficient, 0.133).

• = mean, error bars = range (min to max). Range was used instead of standard deviation to give an upper estimate of the error.

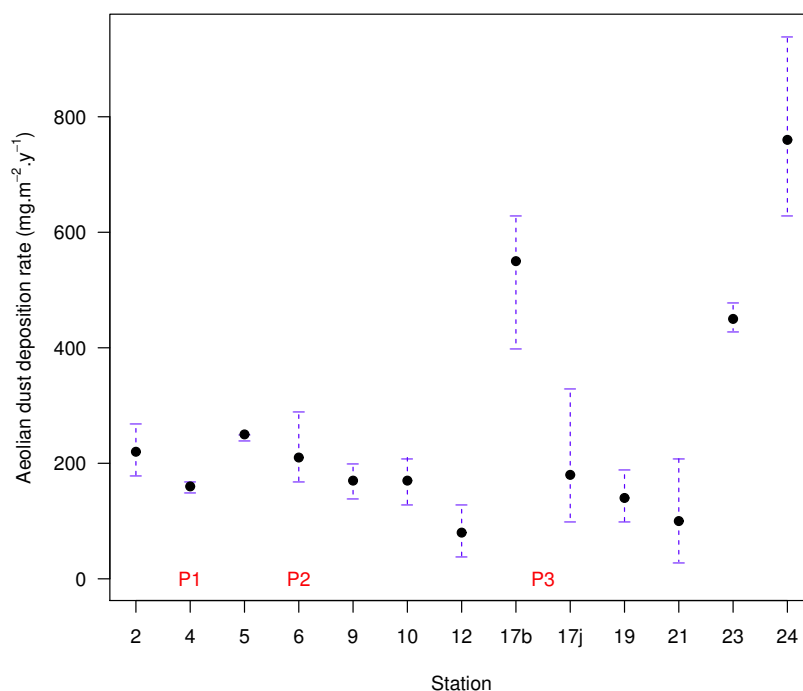


Table 4.1: Table of values plotted in Figure 4.9. Conversion of dAl in the ML at each station to aeolian deposition rate ($mg.m^{-2}.y^{-1}$) using the MADCOW model (Measures and Brown, 1996), and an assumed solubility of 1.5% (coefficient = 0.133). Mean, minimum and maximum dAl values within the true ML were used to constrain the estimates. STZ, SAZ and PFZ+AZ values are the mean, minimum and maximum values of all stations within each zone. For averaging purposes: 17b was assigned to the STZ; 19 and 20 were assigned to the SAZ.

Station	Mean	Min	Max
2	114	81	206
4	108	85	147
5	112	85	202
6	98	63	204
9	79	53	115
10	151	63	356
12	159	65	331
17b	664	434	928
17j	144	44	331
19	241	119	383
20	159	87	246
23	636	399	826
24	741	654	947
STZ	680	399	947
SAZ	136	44	383
PFZ+AZ	88	53	204

4.3.2 Subantarctic Zone – West (SAZ–W): Process station 1 (P1)

P1: dAl concentrations

dAl concentrations at P1 ranged from 0.4 to 1.1 nM. The minimum value was at the surface, which was unexpected. dAl concentrations generally increased with depth. These globally low values agree with previous comments about the region which suggest a limited supply of wind-blown dust (Mackie et al., 2008) or laterally advected shelf waters (Mongin et al., 2011a,b). The low dAl concentrations matched the low concentrations of other trace elements (Fe, Co, Ni, Cu, Cd) investigated at P1 (Bowie et al., 2009; Lannuzel et al., 2011a; Butler et al., 2012, submitted), indicating low trace element supply to this region.

P1: Estimate of aeolian deposition rate

MADCOW estimates of aeolian deposition rate at P1 were within the range of 85–147 $mg.m^{-2}.y^{-1}$ (see Figure 4.9). Globally this was quite low and is expected to be due to the limited terrestrial interaction along the air mass trajectories that dominate the region (see Figure 4.4). These values contrast substantially with aeroSAZ-1, the aerosol sample collected during the transit from station 2 to P1, which observed the highest aerosol concentrations of the voyage (see Table 4.3), corresponding to the highest mass input fluxes of dust and Fe (see Table 4.2). Interestingly, the aeroSAZ-1 aerosols had extremely poor Fe solubility. This suggests the aerosols collected were from older, well processed soils, with minerals that are not readily soluble, and therefore less likely to be biologically available (Mackie et al., 2008).

P1: Trace element sources

Evidence of dust supply to the region was observed, although the soluble proportion was extremely low (see aeroSAZ-1 in Table 4.2 and 4.3). dAl depletion indicates limited supply of soluble Al to the region. Therefore, the low solubility of Fe in the dust supplied observed during SAZ-Sense, may indicate low solubility of other metals, and may be a characteristic feature of dust typically transported to the region. This suggests aeolian supplies of soluble micronutrients to the region are probably low, even if the mass delivered was considerable.

Trace metal station 2 (closest to the ZC-EAC convergence) had some of the lowest dAl and dFe concentrations for the entire sample set, especially at depth, indicating little entrainment of trace

Table 4.2: Aerosol fluxes from at sea measurements during the SAZ-Sense voyage. Generated by Thibaut Wagener, Reproduced with permissions from (Bowie et al., 2009, supp.).

	P1		P2		P3		SO	
Sample	aeroSAZ-1		aeroSAZ-3		aeroSAZ-6–7		aeroSAZ-2–7	
Dust flux ($mg.m^{-2}.y^{-1}$)								
Dry	625	±264	46	±18	129	±60	117	±51
Wet	97	±68	7	±5	20	±15	18	±13
Total	723	±332	54	±24	149	±75	135	±64
Iron flux ($nmol.m^{-2}.d^{-1}$)								
Dry	421	±332	249	±152	306	±178	307	±150
Wet	65	±54	38	±28	47	±42	47	±38
Total	488	±386	288	±180	354	±212	354	±188
Total dFe flux	2.4	±2.1	4	±3.2	7.4	±4.3	4.6	±3.1

elements from the Tasmanian shelf into the ZC, with very limited (if any) supply of trace elements to this region west of Tasmania through advection from either of the ZC or EAC.

This allows us to constrain the major supply of micronutrients to P1 as the lateral and upward transport of deep ACC waters to the surface, either by the deepening ML over winter (to >500 m (Herraiz-Borreguero and Rintoul, 2011b)), or upward Ekman transport within eddies of the ACC. Lateral or upward transport mechanisms were supported by the depth profiles that were either stable or increasing with depth for most trace elements measured at P1 (dAl, dFe, dCo, dNi, dCu, dCd (Lannuzel et al., 2011a; Butler et al., 2012, submitted)).

4.3.3 Polar Front Zone (PFZ): Process station 2 (P2)

P2: dAl concentrations

dAl concentrations at P2 ranged from 0.4 to 1.5 nM. Surface concentrations were low, with two maxima at 25 m and 175 m depth, which may have been from low level contamination (although these bottles did not exhibit contamination at other stations). However they do correlate with spikes in the transmissivity and enriched NH_4 concentrations, that may have increased remineralisation from particulates due to higher pH in the micro-environment, but evidence for this is weak. Excluding these two values, dAl concentrations were very similar to those at P1.

Table 4.3: Aerosol concentrations collected at sea during the SAZ-Sense voyage. Generated by Thibaut Wagener, Reproduced with permissions from (Bowie et al., 2009, supp.).

Sample	Al ($ng.m^{-3}$)		Fe ($ng.m^{-3}$)		Dust ($ng.m^{-3}$)		Fe solubility (%)
AeroSAZ-1	61.6	± 11.1	11	± 8	801	± 144	0.5
AeroSAZ-2	17.3	± 3.2	NA	225	± 42	NA	
AeroSAZ-3	4.6	± 1.1	6.5	± 3.1	60	± 14	1.4
AeroSAZ-4	19	± 3.5	17	± 7	248	± 45	0.2
AeroSAZ-5	3.1	± 0.9	6.7	± 2.1	41	± 12	1.5
AeroSAZ-6	12.4	± 2.3	5	± 1.6	162	± 30	1.6
AeroSAZ-7	13	± 3.4	6	± 2.5	170	± 44	2.5
AeroSAZ-8	53.9	± 13.2	5.1	± 2.6	700	± 171	17.7

P2: Estimate of aeolian deposition rate

MADCOW estimates the aeolian deposition at P2 were within the range of 63–203 $mg.m^{-2}.y^{-1}$. This was a larger range than found at P1, but was still quite low on a global scale. Terrestrial interaction was expected to very limited, as was evident from the air mass trajectories that dominate the region (see Figure 4.4). HYSPLIT modelling of air mass trajectories and dispersion density deposition fields (see Figure 4.14a) shows that transport of continental dust was more probable to be further east, due south of New Zealand, rather than at P2 (see Figures 4.4 and 4.14a).

P2: Trace element sources

As expected (Sedwick et al., 2008; Bowie et al., 2009, 2011a,b; Lannuzel et al., 2011a), due to the geographical and meteorological isolation of the PFZ from the continents, evidence of significant aeolian deposition to the PFZ was not found in either aerosol samples or dAl concentrations. dAl depletion in Winter Water, along with dFe enrichment with depth (Lannuzel et al., 2011a) supports the hypothesis by Sedwick et al. (2008), Bowie et al. (2009) and Lannuzel et al. (2011a) that micronutrient supply of Fe to the PFZ south of Tasmania was controlled by the extent of ML deepening over winter and the rate of upward Ekman-transport. This was consistent with profiles of nitrate, phosphate and silicic acid, all of which are enriched at depth below the summer ML and depleted within the ML at P2, a typical feature of the PFZ (Parslow et al., 2001).

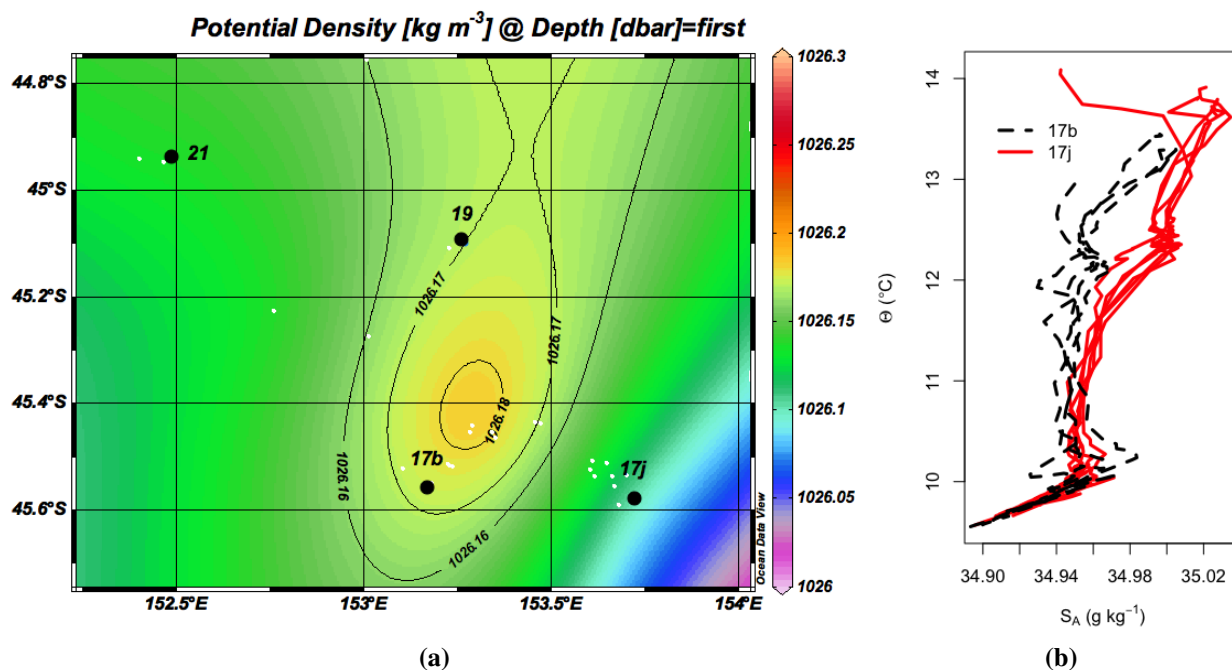


Figure 4.10: (a) Iso-surface of potential density at the surface around P3 (● = trace element station, ○ = CTD stations), stations 23 and 24 are outside of the mapped space. 17b appears to be in the middle of an eddy that has migrated south into the SAZ from the STZ. (b) Θ vs S_A at stations 17b and 17j reveals the different properties of the watermass at each station.

4.3.4 Subantarctic Zone–East (SAZ–E): Process station 3 (P3)

P3: dAl concentrations

dAl concentrations at P3 ranged from 0.3 to 7.4 nM. Two different watermasses at P3 were targeted 5 days apart, labelled stations 17b and 17j in Figures 4.2 and 4.10. The potential density isosurface (Figure 4.10) and dAl profiles (Figure 4.11) clearly indicate watermasses with different life-histories with regards to Al. The highest dAl values were all within the centre of a downwelling eddy (station 17b), possibly advected south from the STZ. The lowest concentrations were all within the dynamic boundary of the neighbouring up-welling eddy (station 17j), more typical of the SAZ. Both profiles were relatively uniform with depth. This suggests the STZ has a greater supply of trace elements, from the atmospheric or sedimentary sources, relative to the SAZ.

P3: Estimate of aeolian deposition rate

MADCOW estimates the aeolian deposition at P3 were within the range of $144\text{--}928\text{ mg.m}^{-2}.\text{y}^{-1}$. This large range was because of the two separate casts having very different ML dAl concentrations.

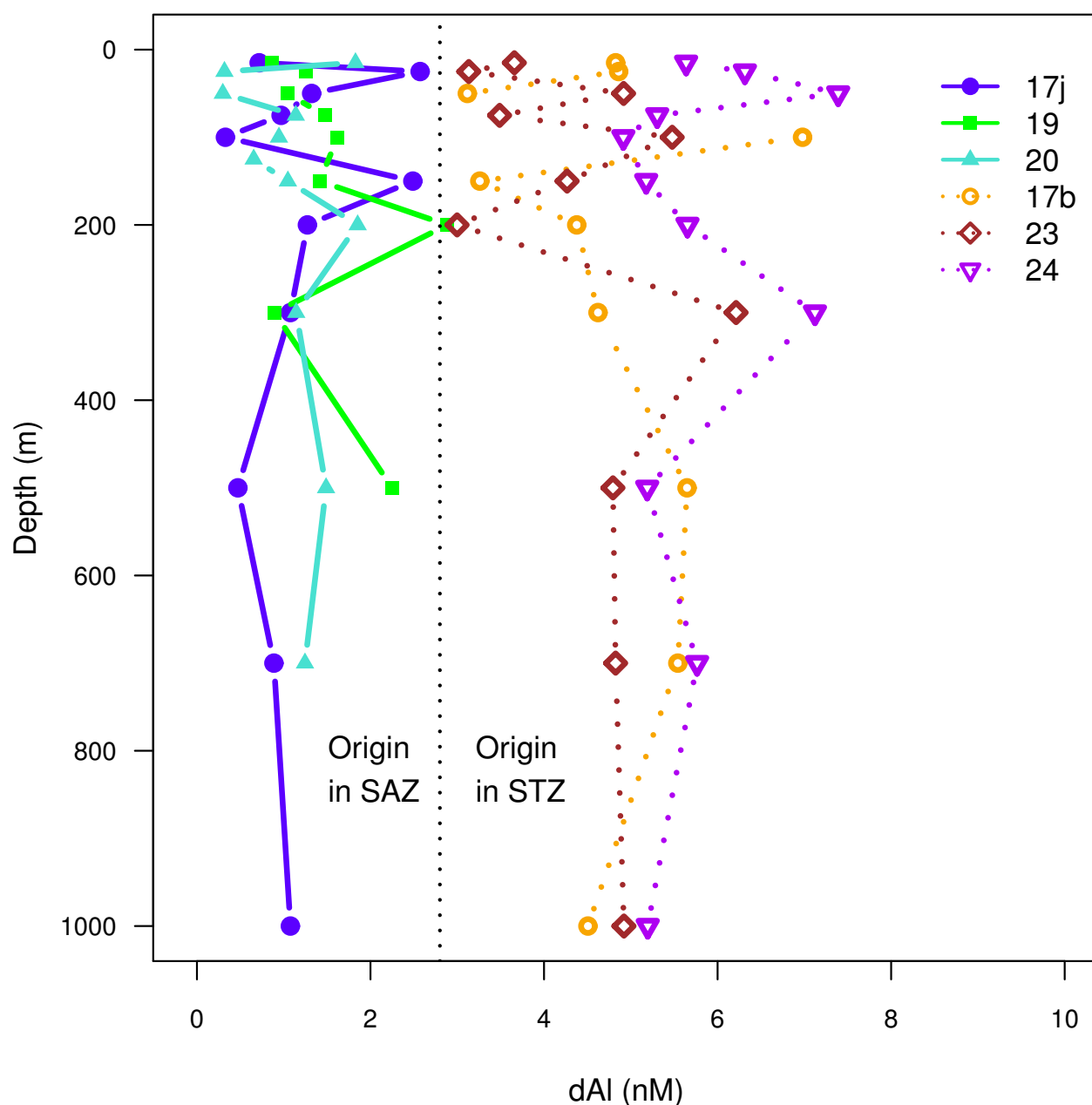


Figure 4.11: Comparison of dAl depth profiles at stations around P3. Stations 17j, 19 and 21 cluster at lower concentrations. Stations 17b, 23 and 24 cluster at higher concentrations. This suggests 17b targeted a watermass that originated in the STZ, where as 17j targeted a watermass that originated in the SAZ.

Aeolian deposition from either of Australia or New Zealand is probable, as seen by the airmass trajectories that dominate the region (see Figure 4.4), although New Zealand is not typically a major source region for dust. P3 also lies within the middle of the SE atmospheric pathway. The aerosol data from P3 (aeroSAZ-6 and aeroSAZ-7) did not support direct aeolian deposition, although this could be due to a temporal mismatch between sampling period and the interval of deposition to

surface waters captured in the eddies.

P3: Trace element sources

A comparison of the depth profiles in the NE sector of the study region is presented in Figure 4.11. This confirms the existence of two regimes: SAZ-N waters with depth profiles relatively depleted in dAl (stations 17j, 19 and 21); and STZ waters with depth profiles enriched with dAl (stations 17b, 23 and 24). This suggests that STZ waters experience higher aeolian deposition from the SE Atmospheric pathway than the waters in the SAZ-N (see MADCOW estimates of aeolian deposition in Figure 4.9). However, these stations are very close to each other and there was no significant atmospheric boundary preventing the delivery of dust across the STF. Therefore, the bulk of the signal must be from trace element enrichment further north (either by aeolian deposition or entrainment from sediments), followed by advection south, rather than from direct aeolian deposition to the region. A comparison of the potential density iso-surface around P3 (see Figure 4.10), coupled with the dFe and dAl concentrations within 17b and 17j (see Figure 4.12) provides evidence to support this. Station 17b, inside a downwelling eddy, was depleted in dFe and enriched in dAl, suggesting trace element input has occurred, but the micronutrients have been consumed prior to sampling. This is consistent with a hypothesis that the watermass was originally in the STZ and has advected south into the SAZ-N. As Mn concentrations were not available, determining if the original source was from the atmosphere or from reducing sediments was not possible.

Station 17j, inside the up welling eddy probably originating in the SAZ-N, was enriched in dFe and depleted in dAl, suggesting the trace element input was relatively recent (since concentrations have not been depleted by biological activity). The delivery mechanism of the dFe was unclear. It cannot be from below, as concentrations decrease with depth. Sources from lateral advection are not obvious. Aeolian deposition to the watermass of bush fire ash high in soluble Fe and low in Al was possible and is discussed in section 4.3.4.

dAl measurements indicate significant dust inputs, however, they appear to be occurring north of the sampled region of the STF, deeper inside the SE atmospheric pathway, before being advected south. This leaves the advection of EAC waters to be the most dominant source of trace elements to P3 over the summer. This supports modelling by [Mongin et al. \(2011b\)](#), which found EAC advection to be extensive (transporting with it trace elements resuspended from the shelf). However, [Mongin et al. \(2011b\)](#) found this mechanism alone was not enough to account for the extent of the bloom in the Tasman Sea and eastern SAZ more generally, discussed in [Bowie et al. \(2009\)](#).

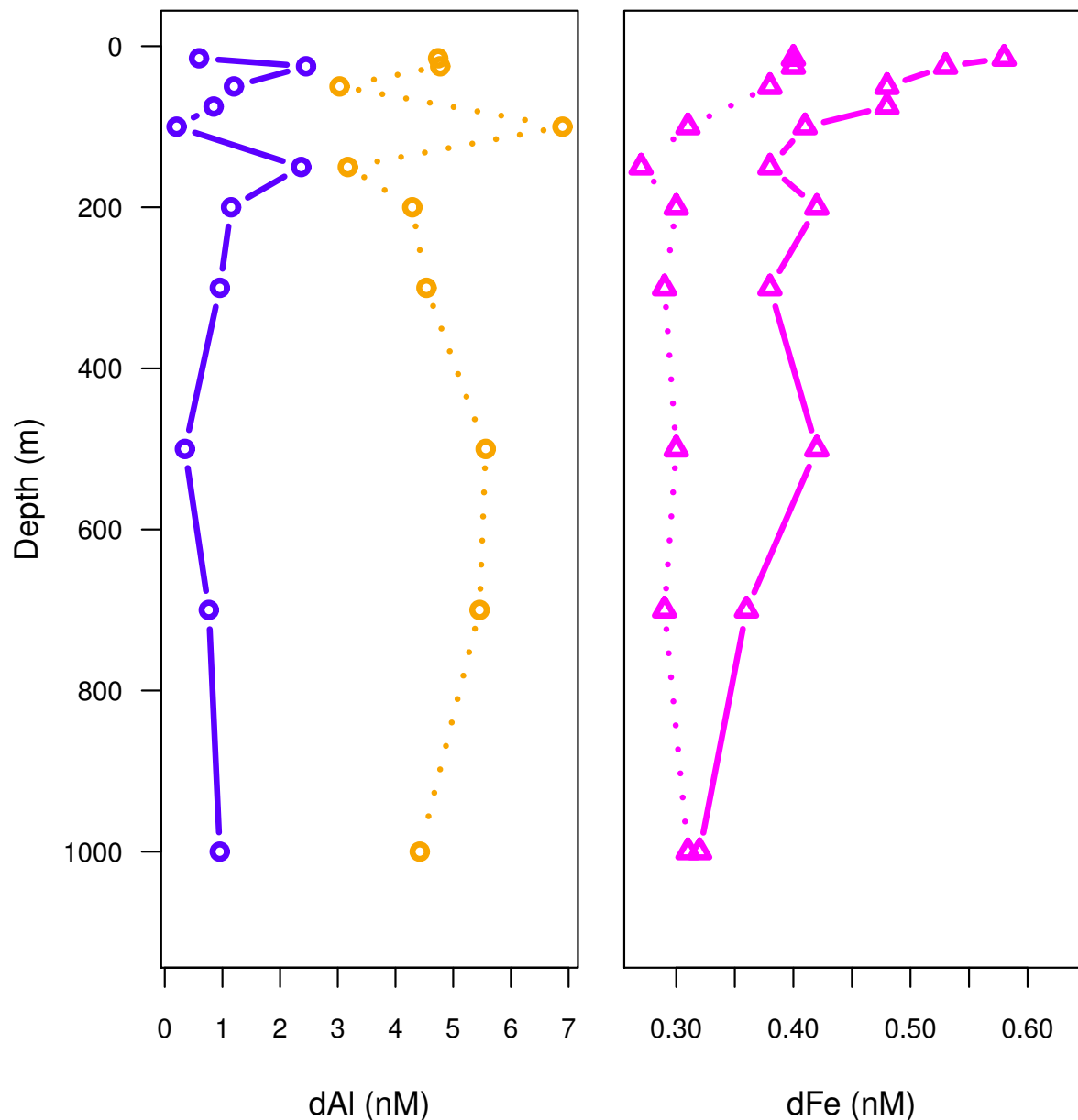


Figure 4.12: Comparison of dAl and dFe profiles at 17b (dashed lines) and 17j (solid lines). 17b was relatively Fe depleted and Al enriched, indicating a significant influence of dust, but some time ago (as the Fe has been consumed). 17j was relatively Fe enriched and Al deplete, this suggests the supply of Fe to this watermass was not from wind-blown dust, but was also unlikely to be from depth, as dFe concentrations decrease with depth. This suggests the source may be from lateral advection, although the original source to those waters remains unclear. The decrease with depth could also be from mixing of low dFe and high dFe waters or water column scavenging.

P3: Potential of bush fire as a source of trace elements to the surface ocean

Given the dynamics observed at P3, the northern part of the bloom in the Tasman Sea could be supported by aeolian inputs, and the southern bloom could be supported by upward Ekman transport

within some eddies of the EAC that interact with the STF. Aeolian inputs could be enhanced by bush fire events, mobilising dust, as well as generating ash. Bush fires are a seasonal event in Eastern Australia and therefore could provide a mechanism for micronutrient delivery to the open ocean communities during their growing season (Ito, 2011). Combustion aerosols are expected to have much higher soluble portion of trace elements relative to non-combustion aerosols, and therefore, could account for a significant portion of the aeolian trace element supply (Streets et al., 2009; Sholkovitz et al., 2009; Ito, 2011; Sholkovitz et al., 2012, and references therein). The composition of combustion aerosols, is also expected to be different to dust given the differing composition of the ash and soils, and could account for the decoupling of dAl and dFe inside the eddies targeted at P3.

During the period from October 2006 to February 2007 in Australia, bush fires burned continuously for 69 days across Victoria. There were also shorter more isolated events in Tasmania (see Figure 4.13). The aerosSAZ-8 sample was collected during this time on approach to Tasmania. This sample showed the second highest aerosol concentrations, with a mineral composition that had 17.7% soluble Fe. This was much greater (35-fold) than the solubility at P1. HYSPLIT dispersion modelling of smoke plumes from known bushfire locations in Tasmania (see Figure 4.14a) (Draxler and Rolph, 2012; Rolph, 2012) show it is probable the aerosSAZ-8 sample was collecting ash particles, which could account for the higher Fe solubility. This dispersion modelling also shows it was possible for ash from bush fires in either Tasmania or Victoria to have been deposited at or near P3, however, no signature was observed on the aerosSAZ-6 and aerosSAZ-7 samples and no methods were employed to accurately decouple a marine signature of bush fire from dust.

Images from further north (not shown) clearly show smoke being transported off the coast of Victoria, over the Tasman Sea (and the EAC), however, images further south were not useful due to extensive cloud cover. Satellite estimates of precipitation events using CMORPH products (Joyce et al., 2004) found 13 precipitation events (defined as $>1.5 \text{ mm.hr}^{-1}$) during the bush fire period that passed over P3 and surrounding areas. This would have provided an opportunity for wet deposition into the ocean of any aerosols that were present in the overlying atmosphere. Wet deposition is expected to increase the solubility of trace elements relative to dry deposition (Jickells et al., 2005). Given the duration of the bush fire events during the 2006/2007 season, it is probable they are responsible for a significant proportion of the dAl signal (as well as delivery of other trace elements) (Hawas et al., 2003; McMeeking et al., 2005; Saarnio et al., 2010; Ito, 2011).

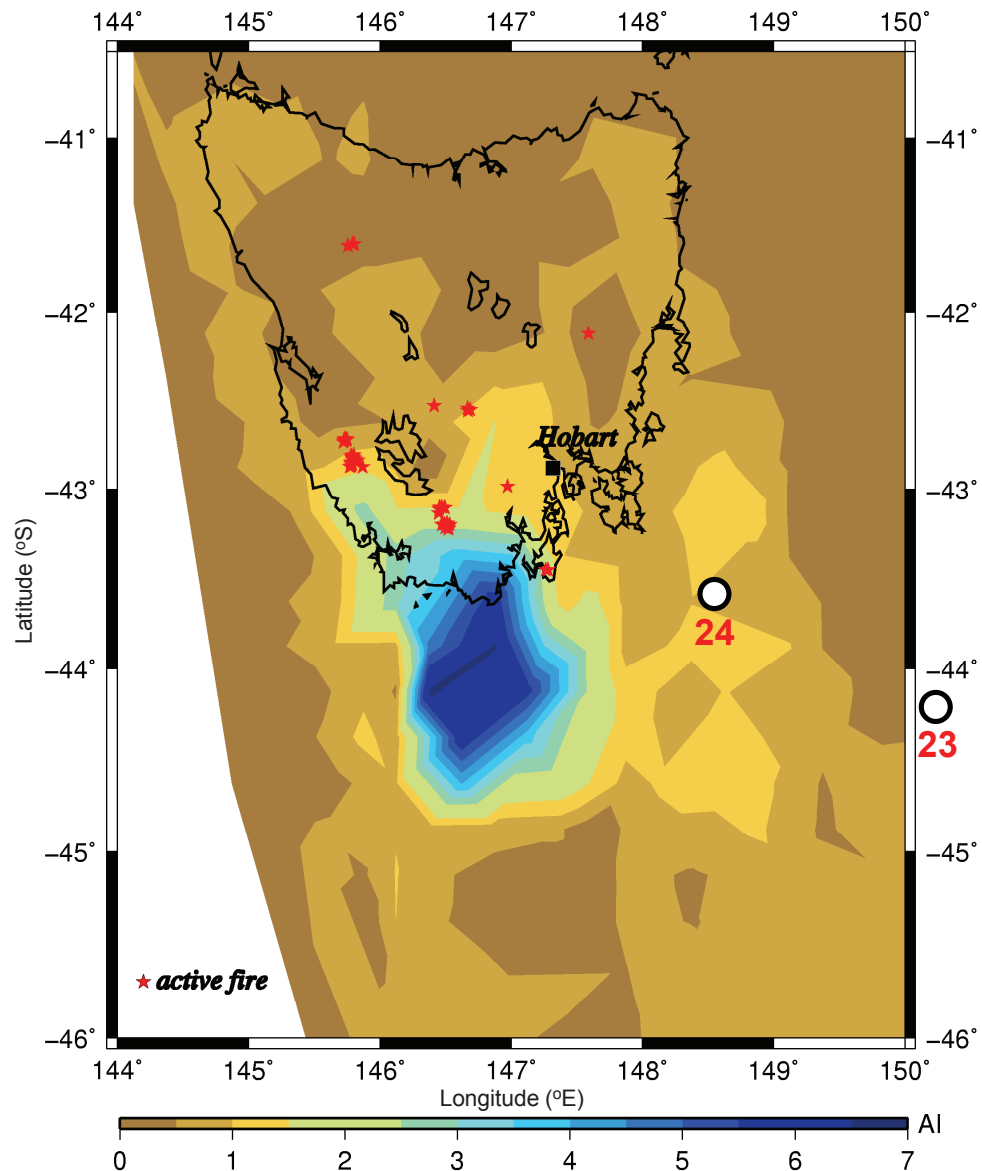


Figure 4.13: Active fires in Tasmania on the 18 February 2007 indicating an important smoke plume while sampling AeroSAZ-8. Locations of transect stations 23 and 24 are shown (white circles). Reproduced with permissions from [Bowie et al. \(2009, supp.\)](#).

P3: Seasonal impact of each delivery mechanism

The trace element supply mechanisms have differing seasonal cycles: upward mixing of enriched parameters via a deepening ML occurs over winter; aeolian dust/ash deposition was strongest in late spring/early summer (during the bush fire season and the influence of drying, northerly winds); advection and upward Ekman transport inside eddies strengthens with the extension of the EAC

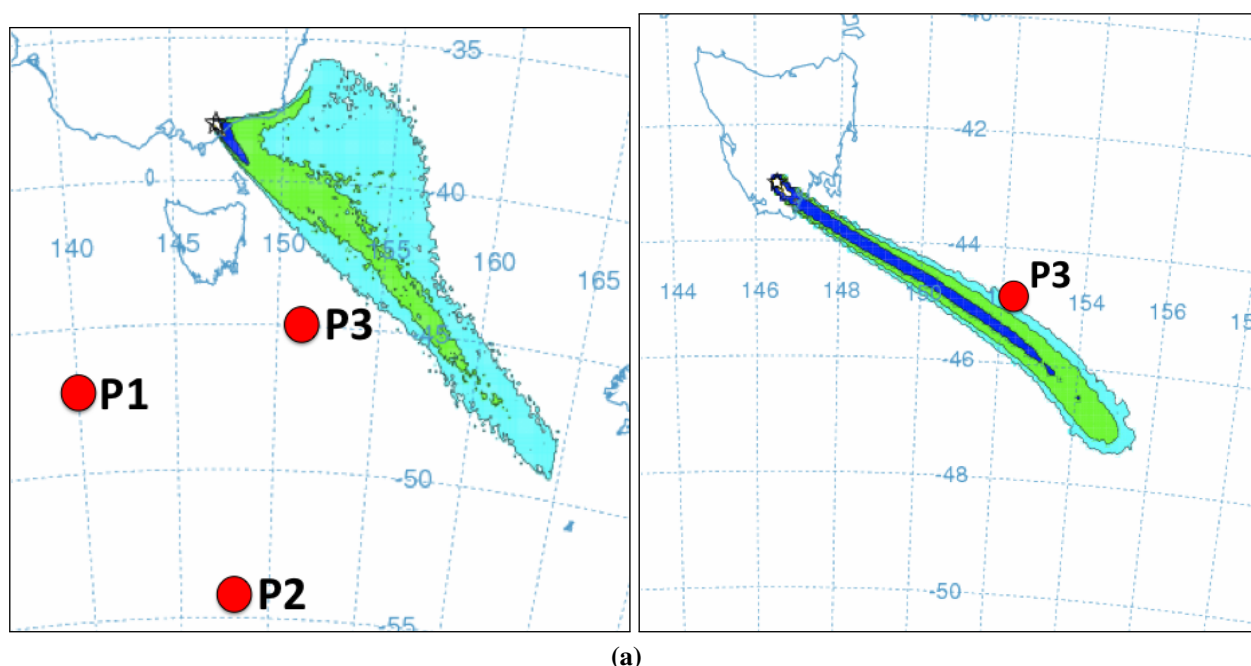


Figure 4.14: HYSPLIT dispersion density modelling of smoke plumes from known bush fire sites in Victoria and Tasmania for 48 h from 0000 hrs 18-Feb-2007. Both show the possibility of aeolian transport of bush fire ash to the STZ, SAZ-N and region surrounding P3.

further south and east, peaking in late summer. These cycles may be complementary, maintaining a relatively stable supply of micronutrients to the surface waters throughout the year at P3.

4.3.5 Process Station Comparisons

Stations P1 and P2 had very similar dAl distributions indicating similar trace element sources to these sites, controlled by upward Ekman transport within eddies, and the deepening of the ML over winter.

The slightly elevated values immediately below the ML (~150 m) may be due to incorporation into diatom frustules (as discussed in section 4.3.3), followed by dissolution with depth. dAl remineralisation may occur rapidly due to the extremely low dAl concentrations in seawater coupled with the potentially high concentrations inside the frustules due to bio-accumulation, similar to the dissolution kinetics observed when DIW is added to a glass vial (dAl concentrations increase rapidly).

P1 had very different dAl distributions to P3. P3 was enriched at all targeted stations relative to P1. This suggests a greater influence from terrestrial material at P3 relative to P1. Supply of

trace elements to P1 appears to be controlled by upward Ekman transport within eddies, and the deepening of the ML over winter. P3 does not appear to have a clearly dominant trace element delivery mechanism, with evidence of aeolian deposition, advection and upwelling all contributing at different times throughout the annual cycle. It is probable this was a contributing factor for enhanced biomass around P3 relative to P1, where supply was dominated by the deepening of the ML over winter.

NPZD modelling by [Kidston et al. \(2011\)](#) could account for much, but not all of the difference in biomass between P1 and P3, leading them to suggest differing supply of Fe to the two regions may account for this observed difference. Results from this study support this hypothesis, as dAl concentrations are enriched at P3 relative to P1. However, eddy-driven stratification, a new mechanism presented by [Mahadevan et al. \(2012\)](#), could account for the discrepancy between the modelled and the observed features, decreasing the importance of micronutrient budgets. This was because the winter MLDs and the relative influence and characteristics of eddies of the two regions were quite different. [Mahadevan et al. \(2012\)](#) suggest subtle differences in the parameters used to model stratification may significantly influence the timing of ML formation. Therefore, the magnitude of ML formation as a driver of primary productivity in the NPZD model as used by [Kidston et al. \(2011\)](#) may be underestimated. An adaption of the existing NPZD model would be required to investigate this possibility.

P2 was depleted in dAl relative to P3. As discussed previously, P3 had multiple possible sources all operating in concert, differing in relative strengths from winter to summer. In contrast supply of dAl to the surface at P2 was dominated by the physical ocean dynamics in winter entraining the relatively trace element enriched waters from below. These underlying waters were enriched either due to remineralisation of particulates, or, lateral advection from a sedimentary source (such as Kerguelen Island).

4.4 Conclusions

Dissolved aluminium concentrations collected throughout the SAZ-Sense voyage were determined, with maximum values obtained closest to Tasmania and within the influence of the East Australian Current. The dAl were successfully used to identify the major trace element supply mechanisms at various stations. Process stations 1 and 2 were supplied by the upwelling of underlying trace element enriched watermasses by upward Ekman transport in summer and the deepening of the ML in winter. Process station 3 was supplied by a combination of sources. Direct and indirect aeolian deposition to the study region (evidence from investigation of different eddies). Upwelling of

underlying waters masses seems less likely as a source, due to depletion of trace elements with depth, although advection of micronutrient enriched EAC and non-EAC waters appears likely. The seasonal cycles of delivery processes are expected to be complementary at P3, resulting in lower seasonal variability in trace element supplies at P3. This may go some way to explaining the higher average primary production observed in the NE sector of the study region, especially north of the STF. The presence of diatoms may influence the biogeochemical behaviour of dAl, which may reduce its usefulness as a proxy for quantifying aeolian deposition to those areas of the ocean.

Chapter

5

The distribution and biogeochemistry of Al along the WOCE SR3 repeat transect (GEOTRACES voyage GIPY6)

5.1 Introduction

This is the first dAl study in the full water column of the Australian sector of the SO along the WOCE repeat section SR3. The primary purpose of this section within WOCE was to investigate the exchange between the Indian and Pacific Oceans south of Australia. It was a contribution to the GEOTRACES and International Polar Year programs (cruise GIPY6) as it was expected to provide insight into the biogeochemistry of trace elements in terrestrially remote parts of the SO, as well as being one of the few transects routinely investigated and well characterized in the SO. 294 samples were collected at 27 stations from 65.5°S to 44.0°S with up to 15 depths (0–4440 m) between Antarctica and Tasmania (Australia) along the 140°E meridian.

There are few studies that have investigated the distribution of dAl in the SO south of 40° S. A summary of most of the published data is presented in Table 5.1. The major full water column studies have been in the South Atlantic (including Drake Passage) ([Middag et al., 2011a, 2012a](#)), Ross Sea ([Measures, 2002](#)) and in proximity of the Crozet and Kerguelen Islands ([VanBeusekom et al., 1997](#)). In general, dAl concentrations in the SO are ≤ 2 nM, which is low compared to the equatorial and subtropical regions of the ocean, but comparable to the Arctic and North Pacific ([Hydes and Liss, 1976, 1977b](#); [Caschetto and Wollast, 1979](#); [Hydes, 1979](#); [Stoffyn and Mackenzie, 1982](#); [Hydes, 1983](#); [Measures et al., 1984](#); [Kremling, 1985](#); [Orians and Bruland, 1985, 1986](#); [Jickells, 1986](#); [Hydes et al., 1986](#); [Measures et al., 1986](#); [Hydes et al., 1988](#); [Hydes, 1989](#); [Measures and Edmond, 1989, 1990](#); [Kremling and Hydes, 1988](#); [Hydes and Kremling, 1993](#); [Moran and Moore, 1992](#); [Moran et al., 1992](#); [Narvekar and Singbal, 1993](#); [Kremling and Streau, 1993](#); [Helmers and Vanderloeff, 1993](#); [Upadhyay and Sen Gupta, 1994](#); [Jickells et al., 1994](#); [Gelado-Caballero et al., 1996](#); [Measures and Vink, 1999](#); [VanBeusekom et al., 1997](#); [Chou and Wollast, 1997](#); [Measures, 1999](#); [Measures and Vink, 2000](#); [Measures, 2002](#); [Bowie et al., 2002](#); [Sanudo-Wilhelmy et al., 2002](#); [Johnson et al., 2003](#); [Obata et al., 2004](#); [Measures et al., 2005, 2006](#); [Obata et al., 2007, 2008](#); [Measures et al., 2008c,a,b](#); [Han et al., 2008](#); [Brown and Bruland, 2009](#); [Brown](#)

Table 5.1: Observed dAl concentrations (nM) in the ocean south of 40°S.

Publication	Location	Min	Max	Mean	n=
	Open Ocean				
Middag et al. (2012a)	Drake Passage	0.1	2–5 ¹	~1	~230
Middag et al. (2011a)	South Atlantic	0.1	6	~1	470
Dammshauser et al. (2011)	South Atlantic (surface only)	na	na	5	~20
Vink et al. (2000)	South Atlantic (surface only)	na	na	0.5	na ²
VanBeusekom et al. (1997)	Crozet / Kerguelen Islands	0.3	4	1	~330
Obata et al. (2004)	South Indian / Australian Sector	0.1	4	0.7	15 ²
Obata et al. (2008)	Tasman Sea	4	11	6	9 ²
Measures (2002)	Ross Sea	0.2	3	0.7	~630
Sanudo-Wilhelmy et al. (2002)	Weddell Sea (surface only)	1.7	4.5	3	~20
Moran et al. (1992)	Weddell Sea	1	6	~3	~50
Vanbennekom et al. (1991)	Weddell Sea	1	3	na	na
	sea ice				
Lannuzel et al. (2011b)	Australian Sector (sea ice)	1.3	7	3	~40
Hendry et al. (2010)	Marguerite Bay (sea ice)	17	41	26	~20
	Marguerite Bay (under sea ice)	2	27	~10	16

¹ The exact maximum in the ocean is unclear, as there is a sharp gradient observed with distance from the coast, where the maximum value is >14 nM, from fluvial sources.

² Only the most southern station (at ~40° S) of the data set is considered. This may not be in the SO, but is included for completeness.

et al., 2010; Measures et al., 2010; Middag, 2010; Hendry et al., 2010; Middag et al., 2011a,b,c, 2012b; Roeske et al., 2012). The short residence time of Al in seawater means high concentrations near source regions are not long-lived, with only remnant signals observable at >1000 km. In the SO, concentrations are depleted due to: limited aeolian deposition of dust (see Figure 5.1); the dust delivered is relatively enriched in insoluble Al-minerals (Mackie et al., 2008); and the low temperature surface seawater (20–30°C less than in the tropics and sub-tropics) further reduces the already slow kinetics of Al present as soluble minerals (Eigen, 1963).

5.1.1 Source regions of dust to the SO

Aeolian deposition to the SO is extremely limited, 2–3 orders of magnitude lower than to the equatorial regions. In the Australian sector of the SO, the terrestrial sources are South America and Australia (see Figure 5.1) (Mahowald et al., 2007). Dust that is supplied from Australia is low in soluble minerals as the soils are well processed and highly weathered because of their geological age. Atmospheric processing of dust is an important, but unconstrained, factor in the eventual solubility of aeolian deposited dust.

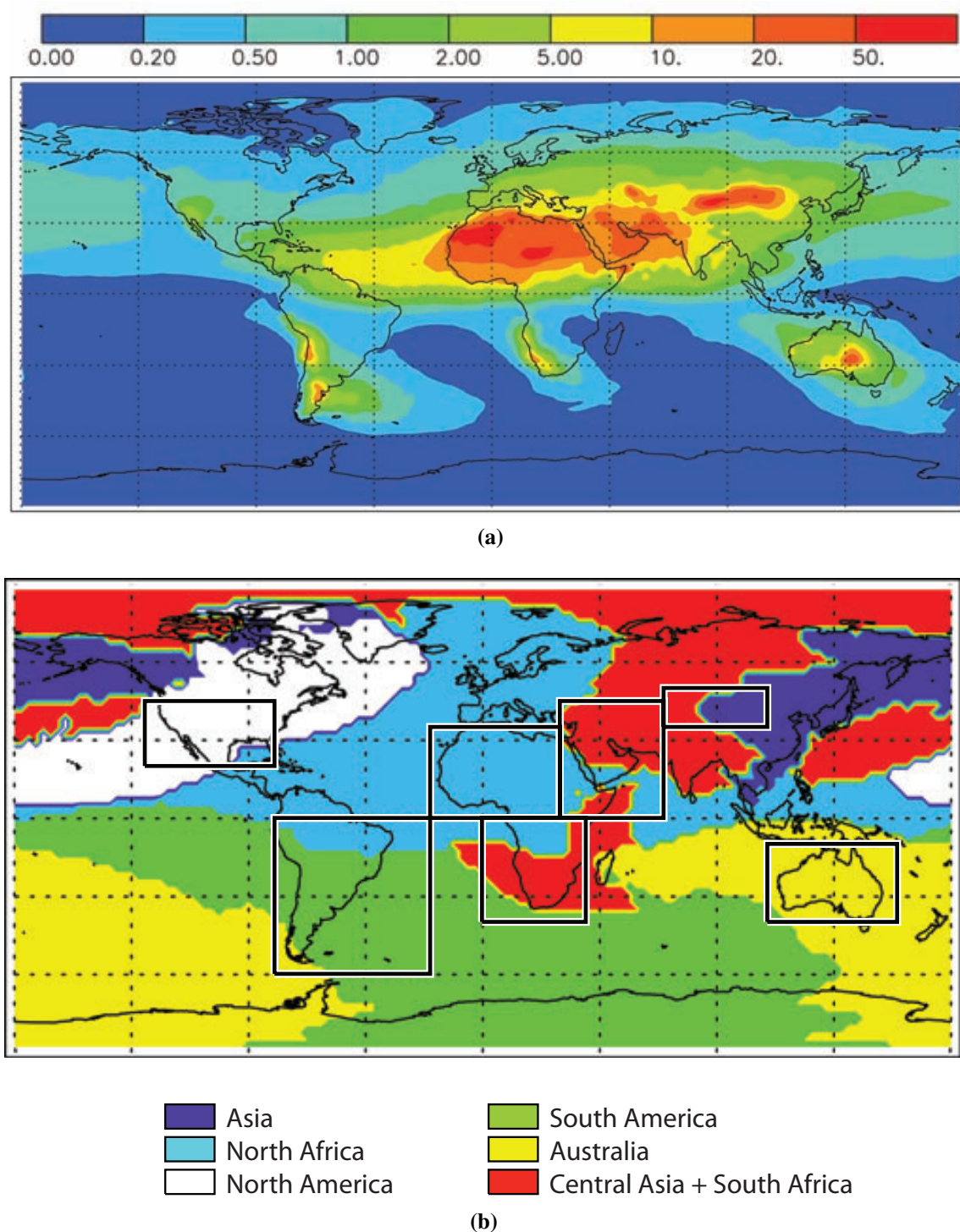


Figure 5.1: (a) Figure from [Jickells et al. \(2005\)](#), this is a composite of outputs from three modelling studies ([Duce, 1991](#); [Ginoux et al., 2001](#); [Hand et al., 2004](#)). Output from these models (as presented by [Jickells et al. \(2005\)](#)) is extremely similar to that from DEAD ([Zender et al., 2003](#)); (b) Source apportionment study from ([Mahowald et al., 2007](#)) based on the model used in ([Mahowald et al., 2006](#)). Colours show which regions dominate the deposition at a given location.

Table 5.2: Definitions of oceanographic fronts, zones and sub-zones along the SR3 transect.

(a) Approximate latitudes where each oceanographic front crosses the SR3 repeat transect
Frontal positions as described by [Sokolov and Rintoul \(2009a,b\)](#).

Latitude	Front name	Acronym
46.6°S	Subtropical Front	STF
51.4°S	Northern Subantarctic Front	NSAF
52.2°S	Middle Subantarctic Front	MSAF
54.0°S	Southern Subantarctic Front	SSAF
54.8°S	Northern Polar Front 1	NPF1
56.0°S	Northern Polar Front 2	NPF2
57.2°S	Northern Polar Front 3	NPF3
60.0°S	Middle Polar Front	MPF
61.8°S	Southern Polar Front	SPF
63.4°S	Northern South Antarctic Circumpolar Current Front	NSACCF
64.0°S	Southern South Antarctic Circumpolar Current Front	SSACCF

(b) Definition of each oceanographic zone and sub-zone separated by the fronts. The IPFZ is previously described in [Parslow et al. \(2001\)](#). The EMLDZ is a zone specially defined for this discussion.

Latitude boundaries	Frontal boundaries	Zone name	Acronym
46.6–43.0°S	North of the STF	Subtropical Zone	STZ
51.4–46.6°S	NSAF–STF	Subantarctic Zone-North	SAZ-N
54.8–51.4°S	NPF–NSAF	Subantarctic Zone-South	SAZ-S
	MSAF–NSAF	Subantarctic Frontal Zone-North	SAFZ-N
	SSAF–MSAF	Subantarctic Frontal Zone-South	SAFZ-S
	NPF–SSAF	Interpolar Frontal Zone	IPFZ
61.8–54.8°S	SPF–NPF	Polar Frontal Zone	PFZ
	MPF–NPF	Polar Frontal Zone-North	PFZ-N
	SPF–MPF	Polar Frontal Zone-South	PFZ-S
66.0–61.8°S	South of the SPF	Southern Zone	SZ
	NSACCF–SPF	Southern Zone-North	SZ-N
	SSACCF–NSACCF	Southern Zone-Middle	SZ-M
	Coast–SSACCF	Southern Zone-South	SZ-S
52.2–49.0°S	MSAF–~49.0°S	Extreme MLD Zone	EMLDZ

One aspect known to increase solubility is the acidity within clouds before deposition. Cloud vapour acidity is linked to anthropogenic aerosols (such as SO_x and NO_x species), which are expected to be lower over the SO ([Sholkovitz et al., 2009, 2012](#)). Therefore, the proportion of dust that is converted to dAI is expected to always be relatively low ($\leq 1\%$) ([Mackie et al., 2008](#)).

5.1.2 Oceanographic setting

The region between Antarctica and Tasmania is dominated by the ACC. The various fronts within the ACC extend from the surface to the sea floor and have been well defined by [Sokolov and Rintoul \(2002, 2009a](#), and references within). Approximate latitudes at which each front crossed the SR3 transect are presented in Table 5.2a. These fronts then subdivide the ocean into zones and sub-zones. These are defined in Table 5.2b, with the sub-zones also presented in Figure 5.2a.

Watermasses

The watermasses of interest are: Subtropical Zone Water (STWZ), Subantarctic Mode Water (SAMW), Antarctic intermediate water (AAIW), Winter Water (WW), Upper Circumpolar Deep Water (UCDW), Lower Circumpolar Deep Water (LCDW), Antarctic Surface Water (AASW), Shelf Water (SHW) and Antarctic Bottom Water (AABW). Note the absence of North Atlantic Deep Water (NADW), which by this longitude has been incorporated into LCDW. Shelf water is loosely defined as waters over the Antarctic Continental Shelf. Defining characteristics of these watermasses are presented in Table 5.3, with their relative positions on a T-S diagram presented in Figure 5.3. The hydrographic parameters, major nutrients and oxygen values observed along SR3 are presented in Figure 5.4. Of particular interest to this study is silicon (Si) (presented as Silicic acid in Figure 5.4f) which follows a typical nutrient profile south of the NPF. However, depletion to bio-limiting levels is observed north of the NPF, corresponding with a shift in the community structure from siliceous organisms in the south, to carbonaceous organisms in the north ([de Salas et al., 2011](#); [Westwood et al., 2011](#), Simon Wright, unpublished data).

Oceanographic fronts

The oceanographic fronts within the ACC meander significantly following the major bathymetric features. They also exhibit latitudinal variability on seasonal and decadal timescales. The frequency with which the three main fronts (MSAF, MPF, NSACCF) occupy a certain location is presented in Figure 5.2b. Although the frontal positions do vary (and sometimes converge), each occupies a relatively well defined latitudinal range at any one longitude. Figure 5.2b also demonstrates the influence of bathymetric features: the MSAF and the MPF diverge north and south respectively around the Kerguelen Plateau; at $\sim 140^\circ$ E the MPF and the NSACCF meander sharply northward as they are deflected by the continuation of the South East Indian Ridge; and at $\sim 160^\circ$ E the MSAF is deflected southward by the Campbell Plateau. The divergence of the MSAF and the MPF leads

to the formation of the IPFZ, first postulated and described by Parslow et al. (2001). This sub-zone has been found to exhibit characteristics unlike those of the SAZ and PFZ, such as a subsurface chlorophyll maximum (with a significantly different community to that found at the surface) and low north-to-south advection velocities (Parslow et al., 2001, and references therein).

Specific features along SR3

The mean flow of the ACC is from west to east with a velocity varying between sub-zones. Maximum velocity of the ACC along the SR3 transect was $\approx 1 \text{ m.s}^{-1}$ observed within the SAFZ-N, this was at least 5-fold greater than flows in any direction along the rest of the transect. It is this relatively fast west-to-east mean flow that contributes to the maintenance of the strong frontal structure of the ACC and the relatively low north-to-south advection of watermasses. An unusual feature along the 140° E meridian, is the subduction-zone, where SAMW is formed, best visualised as contour $>300 \text{ m}$ (green, yellow and red) in Figure 5.5 (Herraiz-Borreguero and Rintoul, 2011b). This corresponds to the Extreme MLD Zone (EMLDZ), where winter MLs can exceed 500 m depth (Herraiz-Borreguero and Rintoul, 2011b). This is not to be confused with the AAIW, which is only a subsurface feature at this longitude.

Other trace elements of interest

Other GEOTRACES key parameters were also investigated along this SR3 repeat (see Figure 5.6). Cd, Co, Cu, Ni and Zn were investigated by Ed Butler, Roslyn Watson and Jeanette O’Sullivan, and Fe was investigated by Delphine Lannuzel. These are the subject of publications currently under review or inpress. Pb was also investigated but the data set is not considered reliable due to suspected contamination and so was omitted. No significant relationships were observed between Al and any other physical or chemical parameter observed during the SR3 voyage and therefore few are directly discussed. They have been included for the interest of the reader.

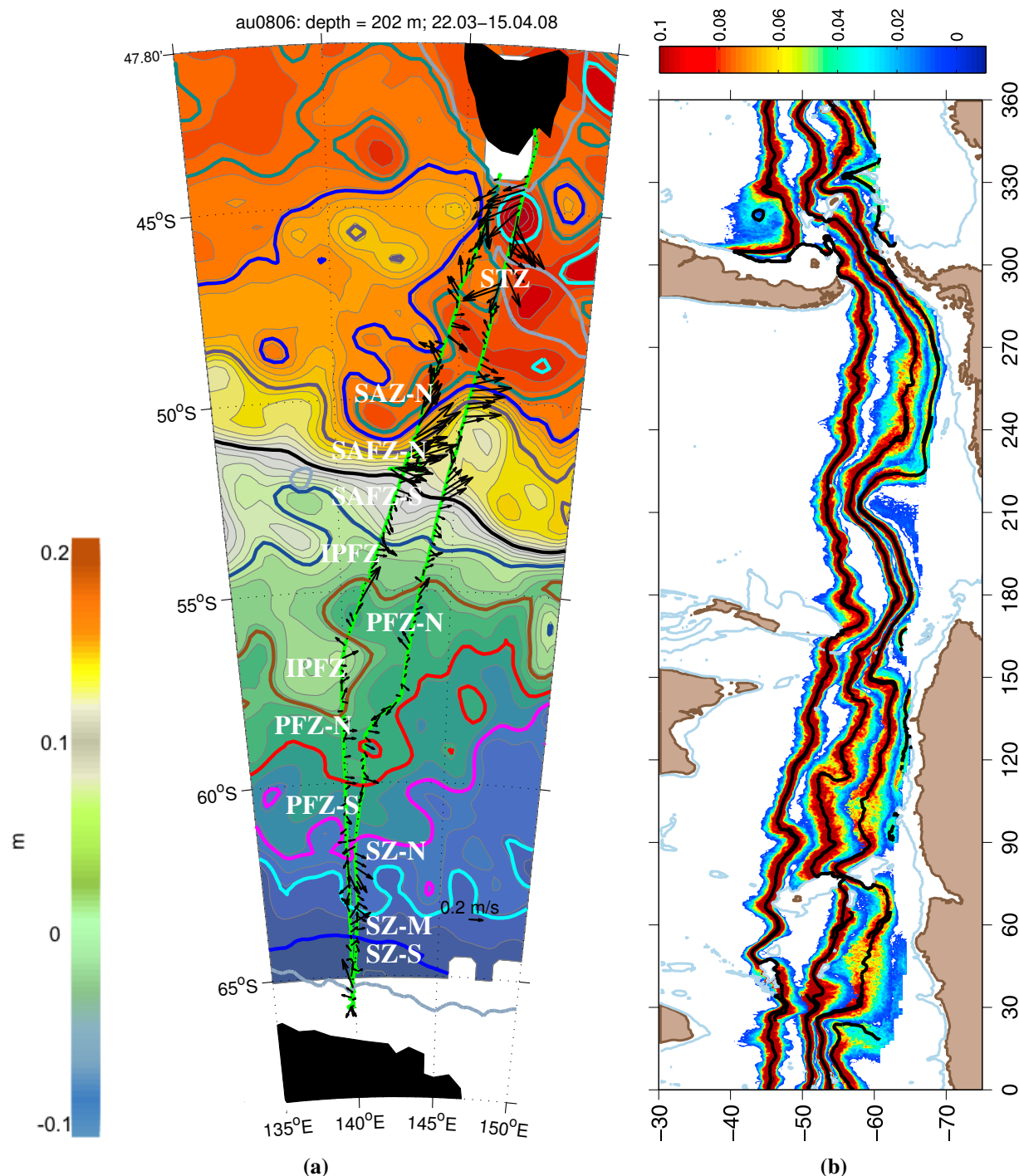


Figure 5.2: Figures unpublished, associated with Sokolov and Rintoul (2009a,b). (a) ADCP data (\uparrow = current velocity, $m\ s^{-1}$, scale bar is near “SZ-M”) superimposed over sea surface height anomaly (SSHA) contours. Oceanographic fronts are presented as bold-coloured lines. From S to N these are: blue = SSACCF; cyan = NSACCF; magenta = SPF; red = MPF; brown = NPF; grey-blue = SSAF; black = MSAF, dark-blue = NSAF. The STF has no signal in SSHA but crosses SR3 at $\sim 46.5^\circ$. White labels identify the sub-zones between the fronts. All acronyms are defined in Tables 5.2a and 5.2b. (b) The frequency of occurrence of the front positions in the SO. Color range reflects occupation from 0.4 to 10% of the time. Only MSAF and MPF and NSACCF are shown. The central thick solid line indicates the mean position of each frontal branch, derived by contouring the mean SSH field. Light blue lines indicate the 2000 m isobath.

Table 5.3: Definitions of watermasses particular to the April 2008 SR3 repeat (Laura Herraiz-Borreguero *pers.comm*).

watermass	Defining features				
	Θ (°C)	S_A (g kg ⁻¹)	γ (kg m ⁻³)	Oxygen (μ M)	Frontal boundary
STZW	>10				
SAMW	8 – 10				
UCDW				< 190	
LCDW	0 – 4	> 34.65		> 190	
WW	< 8	< 34.4			N of SPF
AAIW	0 – 8	34.4 – 34.7		>190	N of NSACCF
AASW		< 34.5			S of SPF
SHW	< 2	> 34.5	<28.27	>250	
AABW	< 0	> 34.5	>28.27		

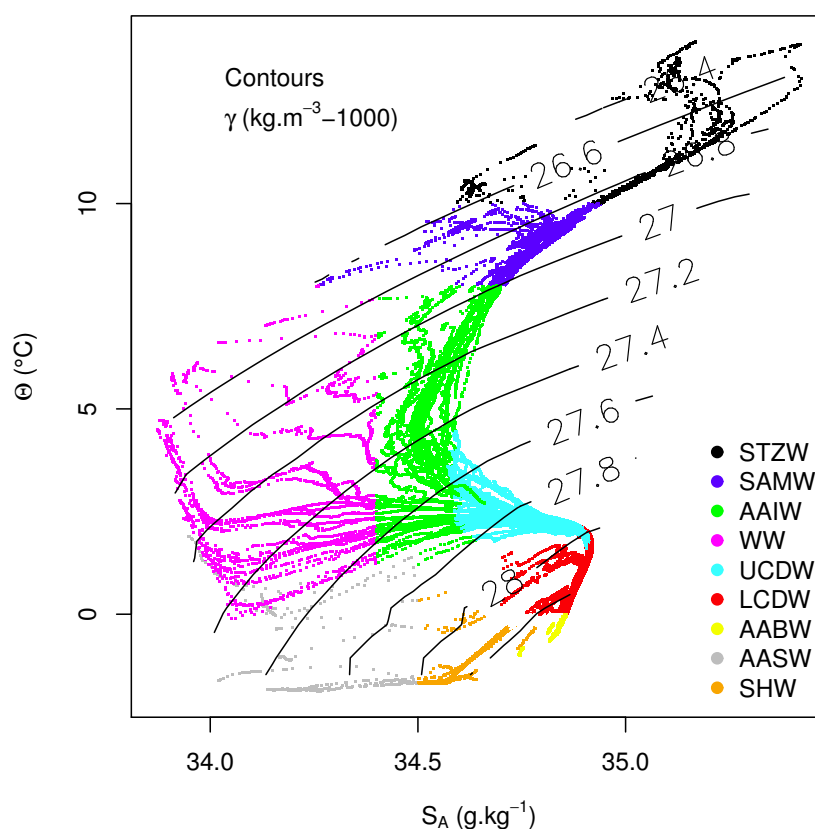


Figure 5.3: Absolute salinity (S_A) vs. conservative temperature (Θ), overlain with neutral density contours (γ). Different colours indicate different watermasses as defined in this study.

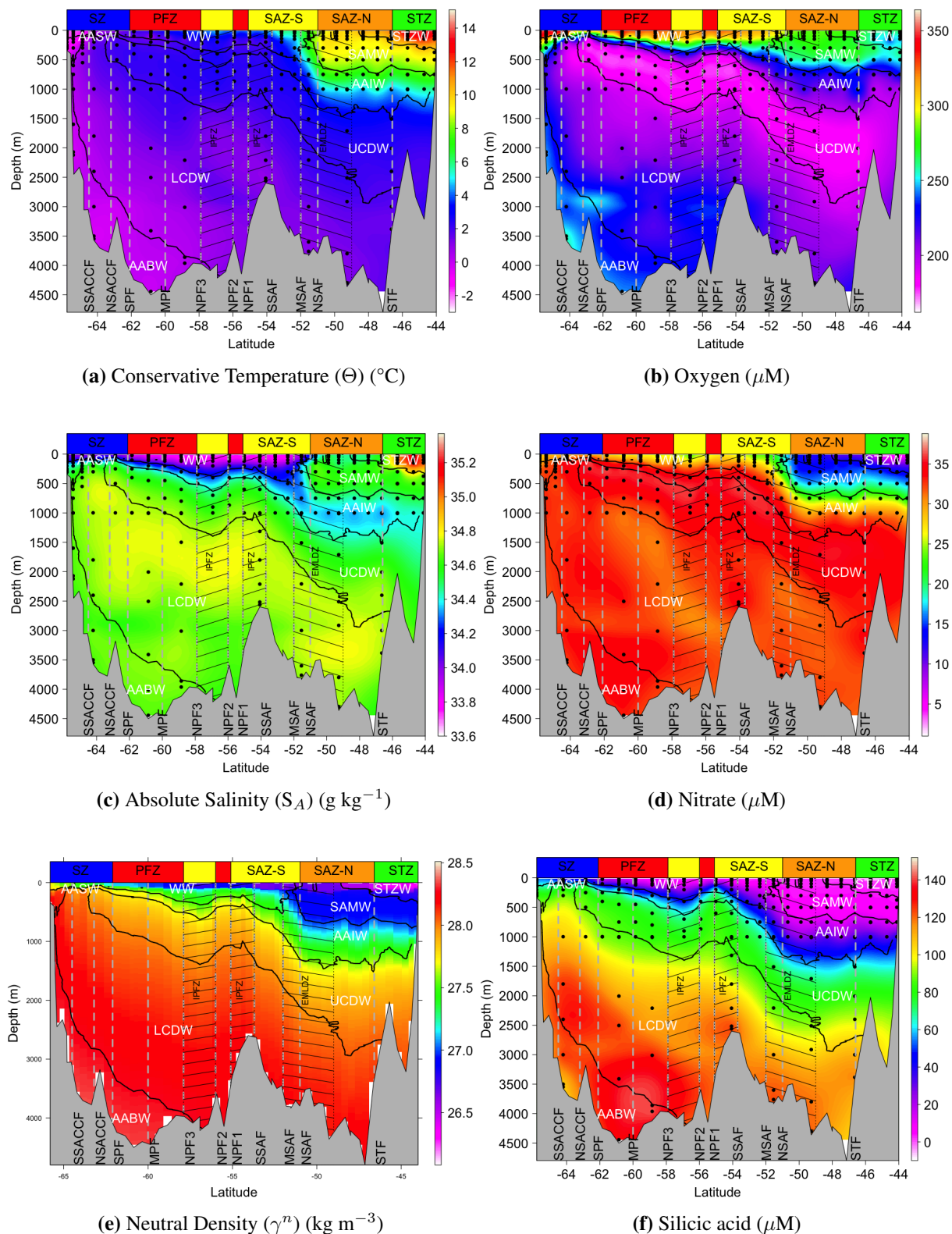


Figure 5.4: Depth vs. latitude section plot of physical and macronutrient parameters along the SR3 transect. Phosphate (range 0.5–2.5 μM) trends were almost identical to nitrate and so omitted. Mean flow was typically eastward (out of the page), with speeds ranging from 0.1–1 m.s^{-1} .

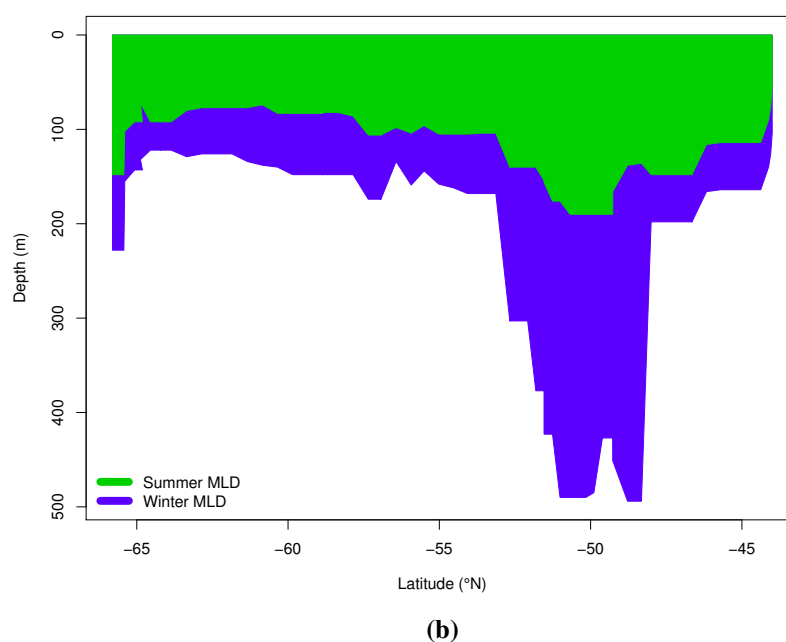
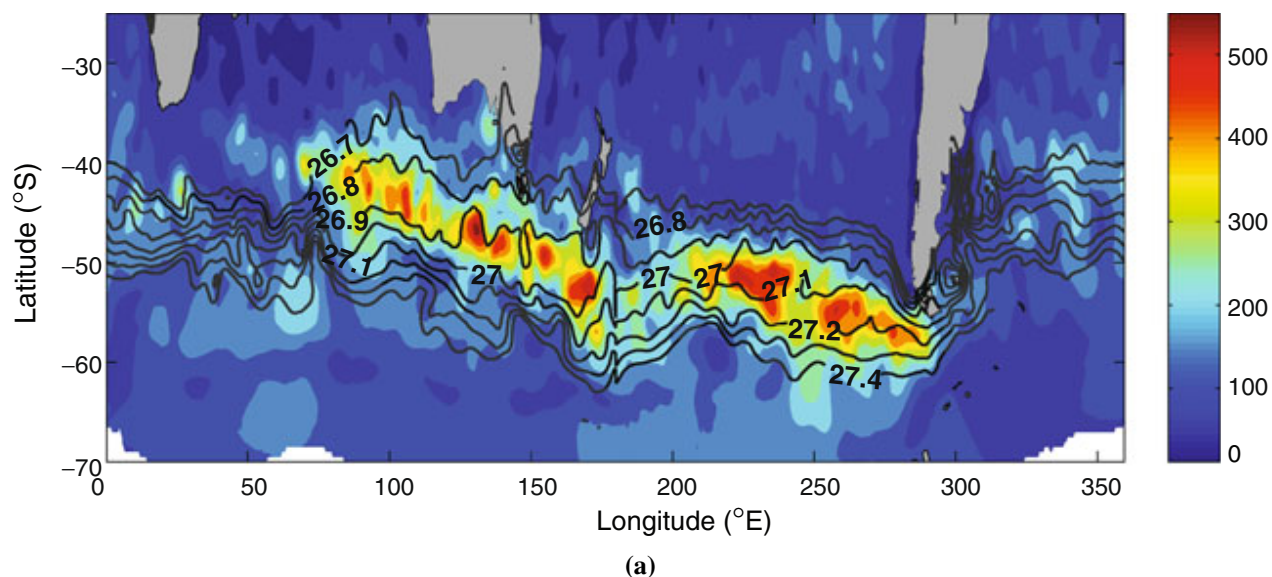


Figure 5.5: (a) MLD calculated following a density difference criterion with a threshold of 0.03 kg m^{-3} from Argo floats, during late winter conditions (September). Figure Reproduced with permissions from [Herraiz-Borreguero and Rintoul \(2011b\)](#). (b) Summer (largest density difference) and winter (second-largest density difference) MLDs from CTD casts along SR3.

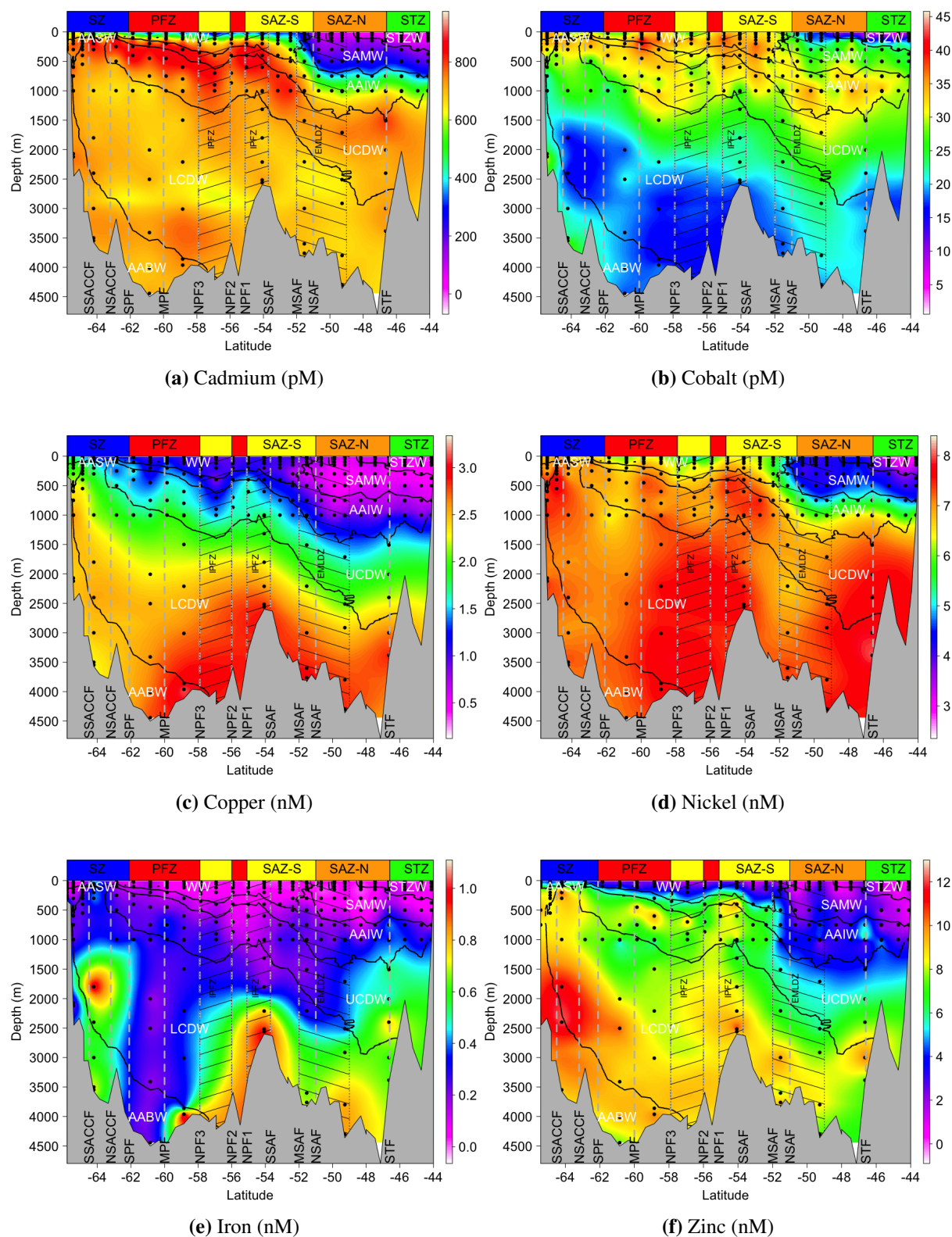


Figure 5.6: Depth vs. latitude section plot of other trace elements measured along the SR3 transect. No significant relationships were observed between these and dAl

5.2 Methods

5.2.1 Voyage track and strategy

The voyage track was defined so as to observe the latitudinal variability of a range of parameters between Antarctica and Tasmania. Trace element casts were limited by personnel availability and sample processing constraints to approximately every 1° of latitude from ~66°S to ~44°S along the SR3 transect. This corresponded to about every second oceanographic CTD cast.

5.2.2 Sampling and processing

All trace metal sampling and analytical procedures followed the protocols recommended for the GEOTRACES expeditions during the International Polar Year as closely as possible (Bowie and Lohan, 2009). The water column at 27 stations was sampled down to 1000 m at a resolution of approximately every 1 degree of latitude (9–12 depths per profile). Sampling was carried out using 6-L externally-closing, Teflon-lined Niskin-1010X bottles deployed on an autonomous 1018 intelligent rosette system (specially adapted for trace metal work, General Oceanics Inc., USA) suspended on Kevlar rope (Bowie et al., 2009). Bottles were tripped as the trace metal rosette was being raised through the water column at approximately 0.1–0.2 $m.s^{-1}$. The validity of this technique has been reported previously (Measures et al. 2008).

In addition, at 8 stations 10-L Niskin bottles specially prepared to be trace metal clean were deployed on the standard CTD rosette to sample from 1000 m to the bottom of the water column (6 depths per profile). For sample bottle firing, the CTD rosette package was raised to the nominal depth, held briefly there for the CTD burst, then lowered at 1 $m.s^{-1}$, whereupon the trace metal bottle was fired in clean' water after approximately 10 s. To assess for possible contamination using the CTD rosette, intercomparison samples taken at 1000 m and for one complete profile using both systems bottle were compared.

All sampling processing was carried out under an ISO class 5 trace-metal-clean laminar flow bench in a clean container, with all materials used for sample handling thoroughly acid-washed. Nitrogen gas passed through an in-line 0.2 m pore-size Teflon membrane filter was used to over-pressurise the water samplers (<10 kPa). Samples were drawn through C-Flex tubing (Cole Parmer) and filtered in-line through 0.2 m pore-size acid-washed capsules (Pall Supor membrane, Acropak 200). All transfer tubes, filtering devices and sample containers were rinsed liberally with sample before final collection. Samples were collected in 60 ml Nalgene LDPE bottles and were acidified with Seastar Baseline HCl (2 $ml.L^{-1}$ sample; approximate final pH 1.8) within 24 h of collection, stored at room temperature. Analysis methods are identical to those described in Sections 3 and 4.2.4.

5.2.3 Model for estimating annual aeolian deposition rates

Aeolian deposition rates were estimated using the MADCOW model (Measures and Brown, 1996), identical to those described in section 4.2.6 (see equation 4.1).

5.3 Results

The dAl concentrations along the SR3 transect are presented as a section in Figure 5.7 and as depth profiles in Figure 5.8 (aggregated per zone, coloured per sub-zone). Values are also plotted on a grid of latitude vs. γ (neutral density) rather than depth in Figure 5.9 (color scaling is also more coarse than in Figure 5.7). Figures 5.7 and 5.9 both reveal no obvious correlation with watermass or density, but a strong correlation with the ocean frontal structure, resulting in a latitudinal pattern of distribution. Maximum concentrations were observed within close proximity to Tasmania and subsurface in the IPFZ. Minimum concentrations were observed in the fastest flowing jet of the SAF (see current vector in Figure 5.2a), corresponding to the EMLDZ (see Figure 5.5) which incorporated the southern part of the SAZ-N and the northern part of the SAZ-S. Slight enrichment at the surface, and near sediments is observed at almost every station outside of the IPFZ (see Figure 5.9), although only minor enrichment relative to overlying waters was observed near sediments. Within the IPFZ enrichment was observed at 200–600 m. The majority of variability occurred in the upper 300 m across the entire transect. Measured dAl concentrations varied from 0.05 (<LOD of 0.13 nM) to 3.97 nM. The sample set has an arithmetic mean of 0.84 ± 0.58 nM and a median of 0.69 nM. Seventy-five percent of the values were found below 1.05 nM. Data was skewed towards low values (see Figure 5.10a). Initial investigation sub-setting the data by zone (STZ, SAZ-N, SAZ-S, PFZ and SZ) did not reveal any obvious trends. Partitioning data by oceanographic fronts into sub-zones (as defined in Table 5.2b) revealed more obvious differences between regions.

5.3.1 Quality assessment

There were only five bad values within the entire data set (1.6%), they all lacked oceanographic consistency and were clear outliers within the overall data set (see Figure 5.10b). They were considered contaminated (probably during storage) and removed before analysis and interpretation. Questionable values were included in all analysis and interpretation as they appeared to be oceanographically consistent (Boyle et al., 1977b,a). When the CTD-mounted 10-L Niskin bottles were deployed for deep sampling, 1000 m was sampled for comparison with samples collected using the General Oceanics autonomous rosette. There was generally good agreement (see Figure 5.10c and 5.10d), especially given the low concentrations observed.

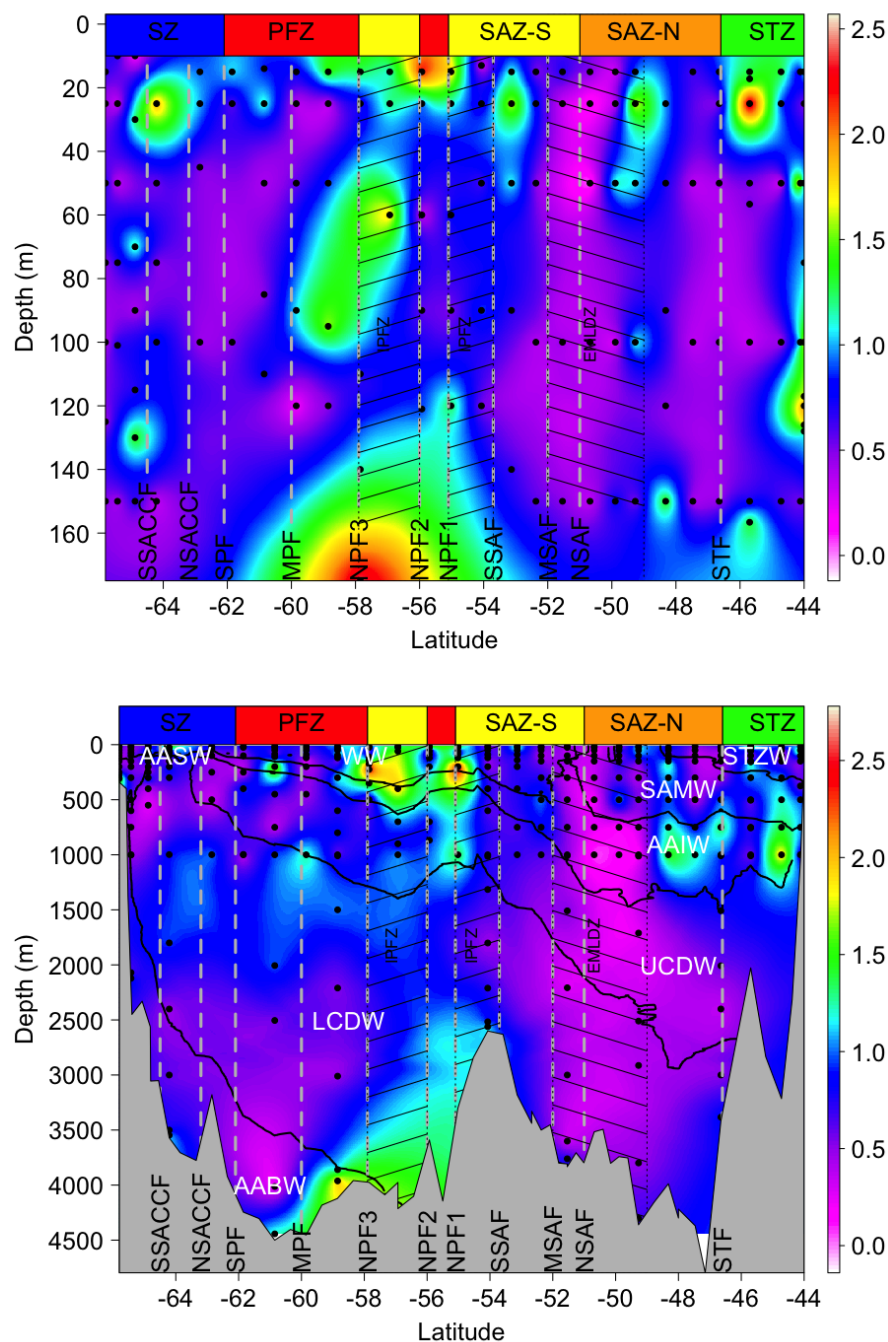


Figure 5.7: Depth vs. latitude section plot of dAl concentrations along the SR3 transect, from Antarctica (left) to Tasmania (right). Contours defining watermasses follow respective values presented in Table 5.3. Frontal positions are defined as by Sokolov and Rintoul (2009a). • = data point. Zones are defined as per Bowie et al. (2011b). Shaded area indicates the region of the EMLDZ and the IPFZ. Concentrations were extremely low across the entire transect, especially in the SAZ-N and SZ. Trends appeared to correlate with sub-zones rather than major zones or watermasses. dAl concentrations were found to be statistically different (t-test p-value <0.05) in adjacent sub-zones across the STF, SSAF and NPF.

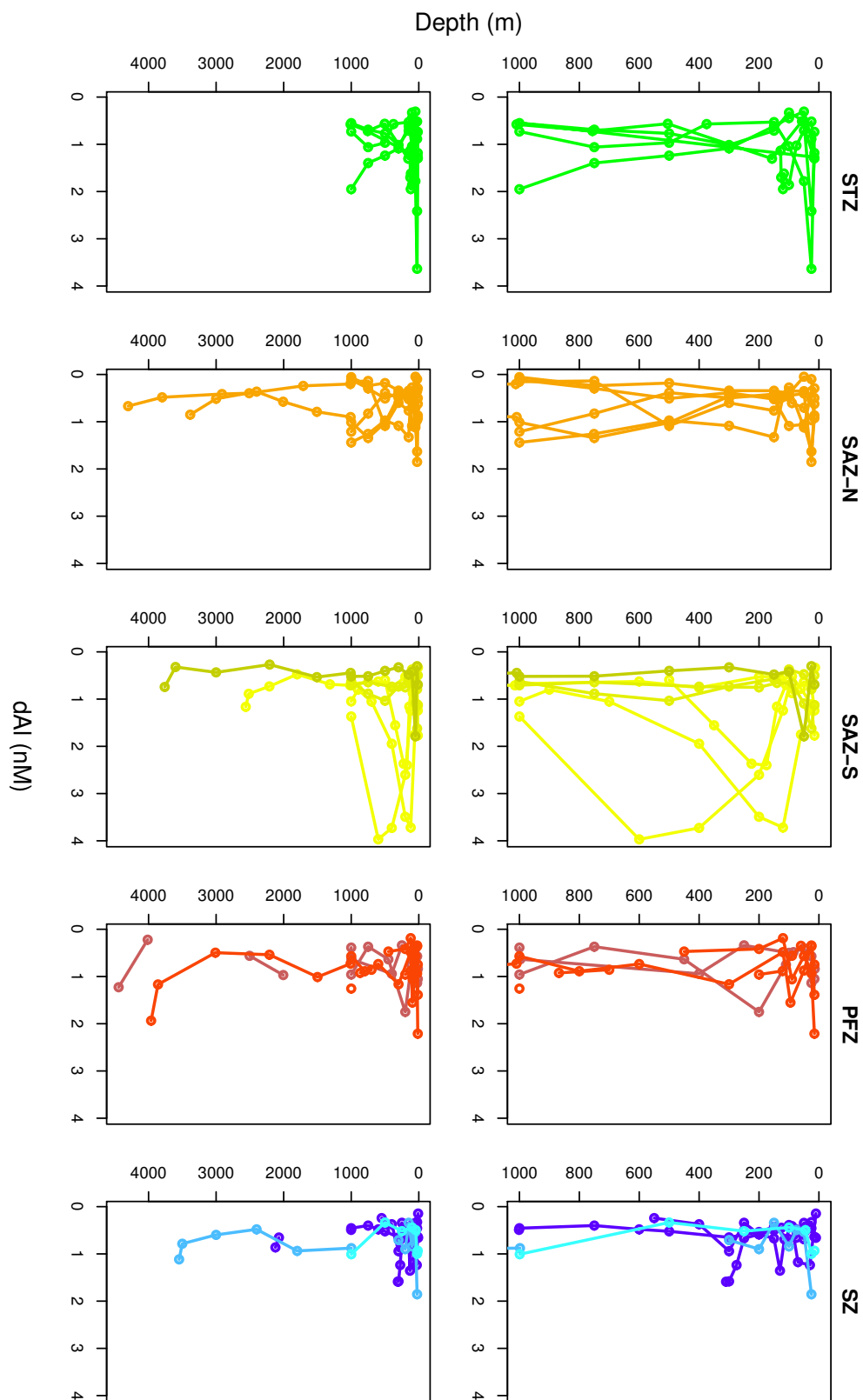


Figure 5.8: Depth profiles of dAl within each major zone. The subsurface maxima observed within SAZ-S (and sub-zone IPFZ) is expected to be the remnant signal from the Kerguelen Plateau.

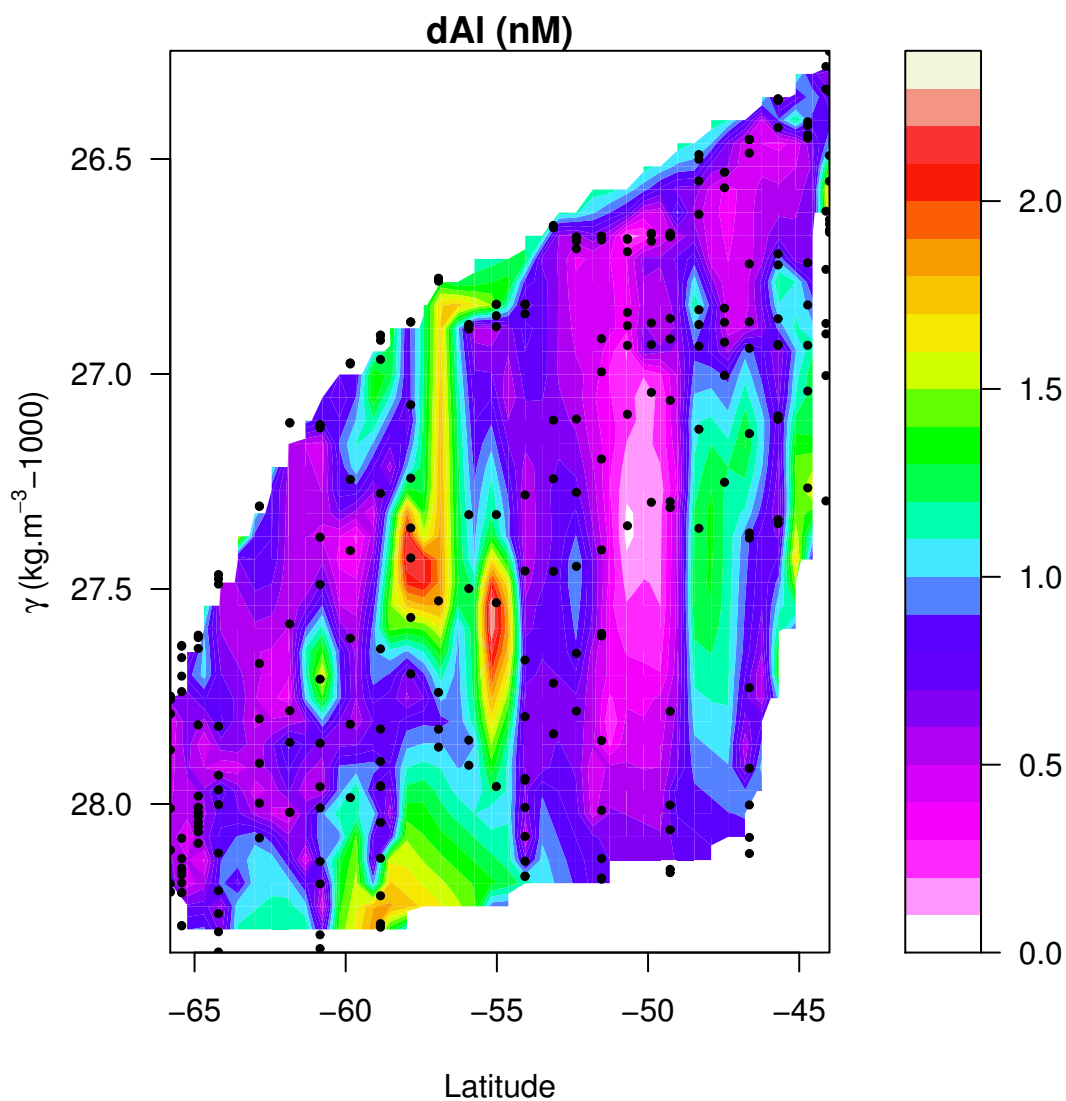


Figure 5.9: Section plot of dAl along SR3, with latitude vs. γ (neutral density) instead of depth, • = data point. Lowest (surface) and highest (bottom) density water per station is generally enriched relative to the intermediate density water. Exceptions are within the IPFZ and 4 samples in the SAZ-N.

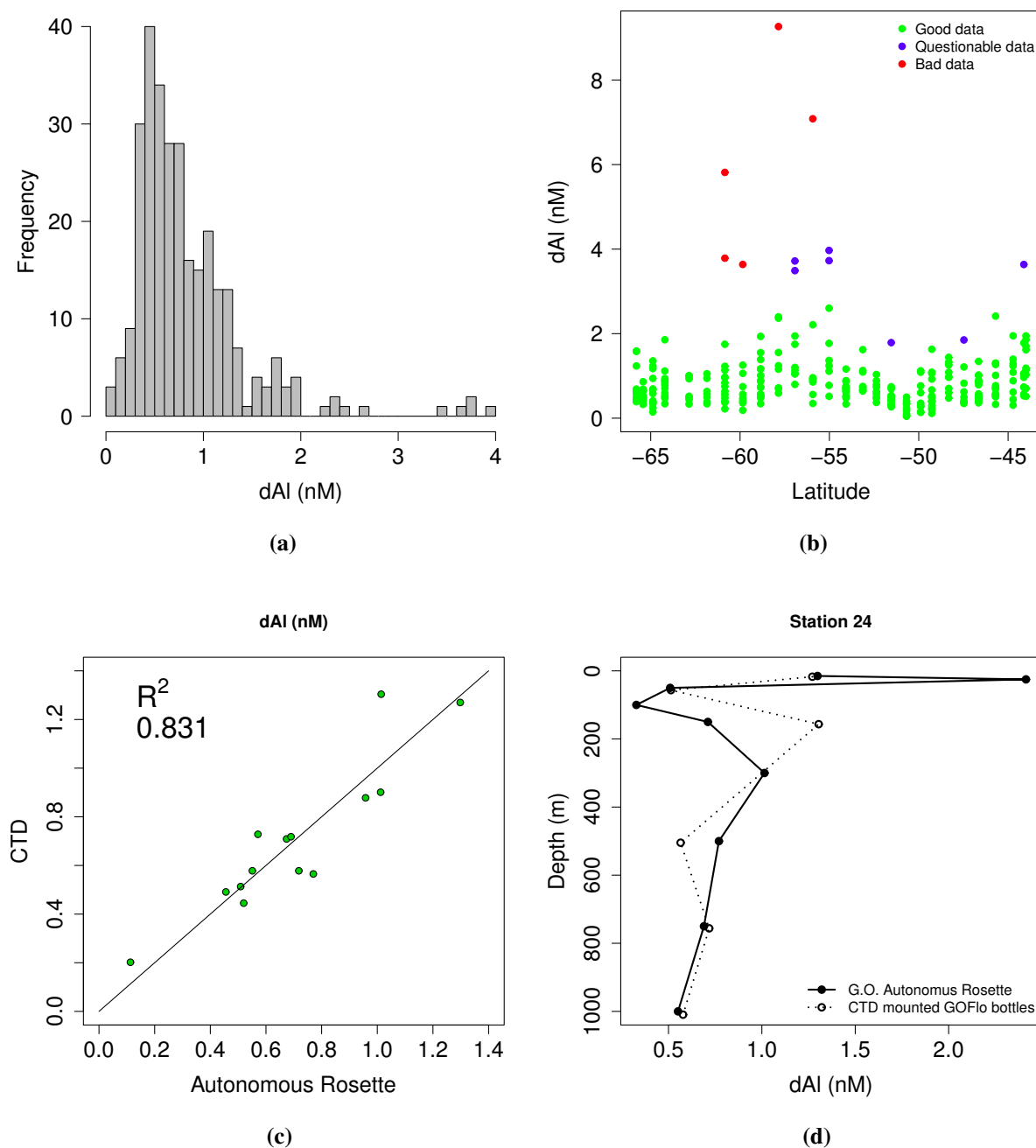


Figure 5.10: (a) Histogram of all good and questionable data. Most of the values were below 1 nM. (b) Visual representation of all dAl data along the SR3 transect. Bad data points were removed from analysis. Questionable data were included. (c) Comparison of all inter-comparison samples collected using both trace element sampling systems. (d) Station 24 depth profiles collected using both trace element sampling systems.

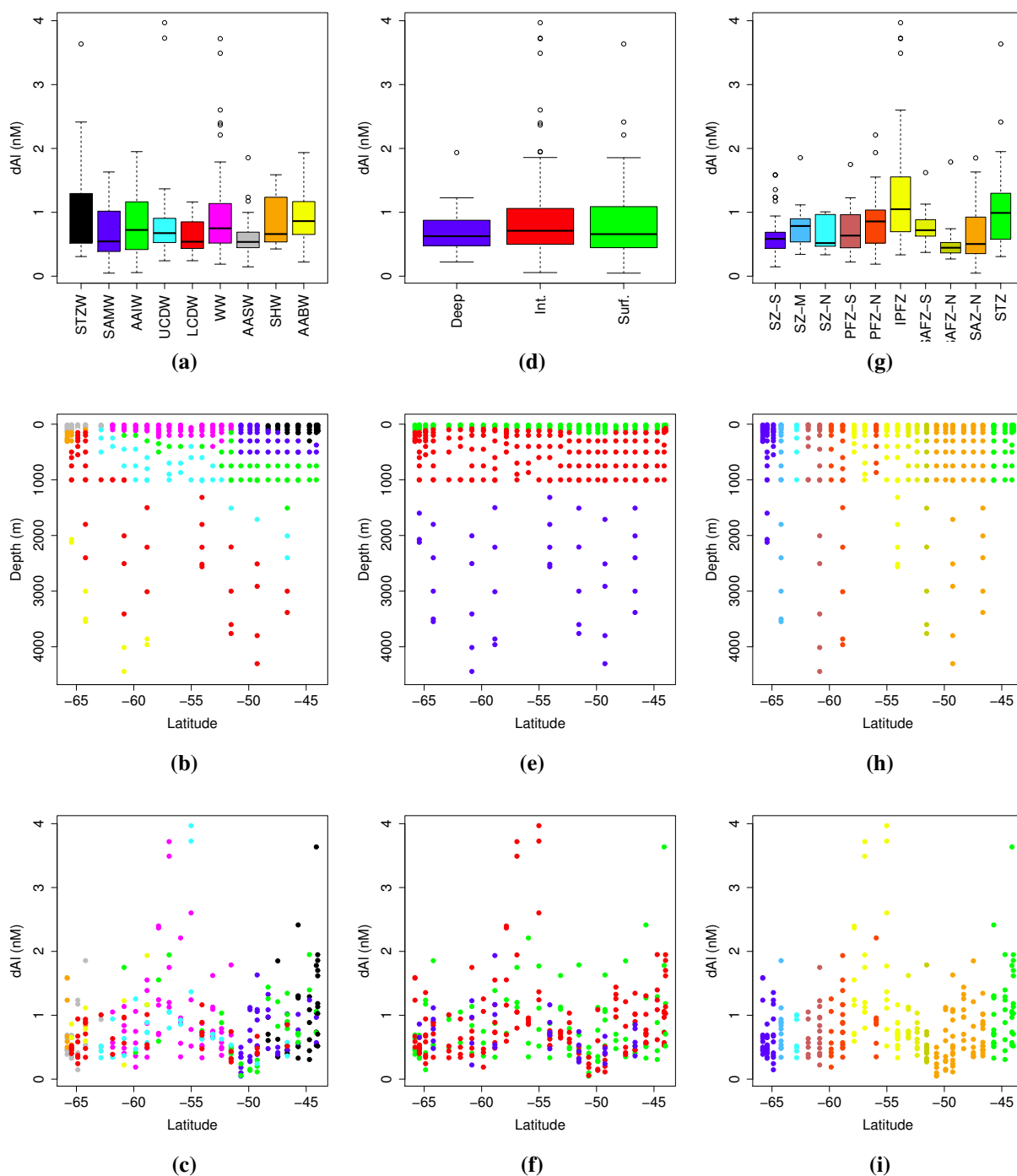


Figure 5.11: Visual representation of the dAI data set, subset by: (a–c) watermass; (d–f) Depth class (where: Deep > 500 m; MLD > Int. < 500 m; Surf. < MLD); and (g–i) Frontal zone. \circ = statistical outliers. Colour schemes of the different subsets are completely independent.

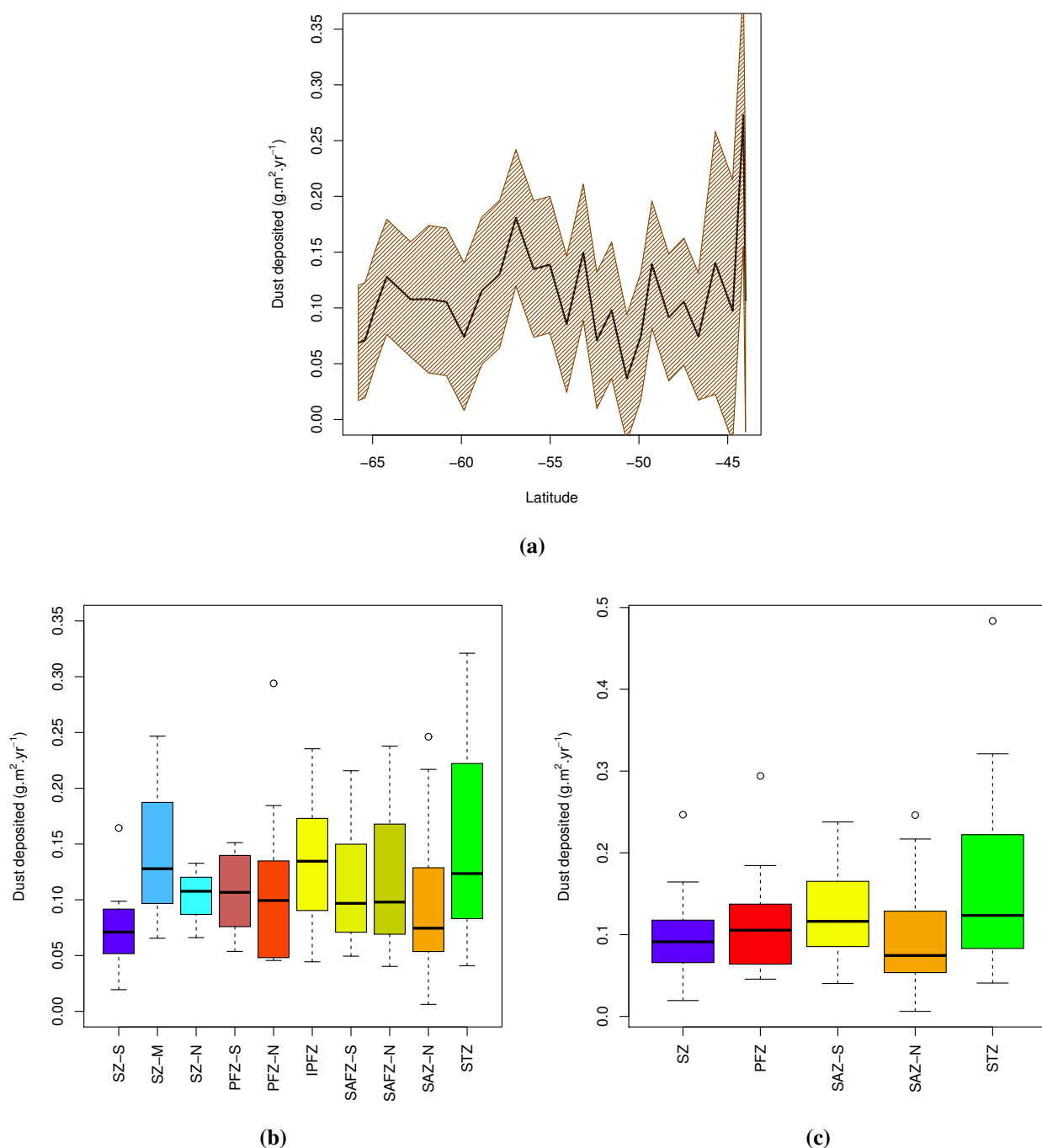


Figure 5.12: MADCOW (solubility = 1.5%) estimates of aeolian deposition by (a) station (shaded area = standard deviation of dAl values within the ML; line = mean of values within the ML); (b) sub-zone; and (c) major zone. \circ = statistical outliers.

Table 5.4: Description of dAl values determined in each watermass.

	Mean	SD	Min	> 25%	Median	> 75%	Max
All data	0.84	0.59	0.05	0.48	0.69	1.05	3.97
STZW	1.01	0.68	0.31	0.52	0.80	1.29	3.64
SAMW	0.68	0.38	0.05	0.39	0.54	1.02	1.63
AAIW	0.80	0.51	0.06	0.42	0.72	1.14	1.95
WW	0.99	0.72	0.19	0.52	0.75	1.14	3.72
UCDW	0.89	0.83	0.24	0.53	0.67	0.91	3.97
LCDW	0.62	0.24	0.24	0.43	0.54	0.85	1.16
AASW	0.67	0.39	0.15	0.45	0.54	0.69	1.86
SHW	0.86	0.44	0.43	0.55	0.66	1.14	1.59
AABW	0.95	0.49	0.22	0.65	0.86	1.17	1.94

Table 5.5: t-test p-values determining if the dAl concentrations within each watermass are statistically different from each other. Values <0.05 were used as the threshold to indicate difference was significant.

	STZW	SAMW	AAIW	WW	UCDW	LCDW	AASW	SHW	AABW
STZW		0.01	0.12	0.84	0.52	0	0.02	0.4	0.76
SAMW	0.01		0.24	0.01	0.19	0.45	0.96	0.25	0.14
AAIW	0.12	0.24		0.14	0.6	0.05	0.27	0.72	0.42
WW	0.84	0.01	0.14		0.6	0	0.01	0.47	0.86
UCDW	0.52	0.19	0.6	0.6		0.08	0.2	0.88	0.79
LCDW	0	0.45	0.05	0	0.08		0.59	0.12	0.08
AASW	0.02	0.96	0.27	0.01	0.2	0.59		0.26	0.15
SHW	0.4	0.25	0.72	0.47	0.88	0.12	0.26		0.68
AABW	0.76	0.14	0.42	0.86	0.79	0.08	0.15	0.68	

5.3.2 Summary of dAl concentrations within each watermass

Values observed within each watermass are summarised in Table 5.4 and presented in Figures 5.11a, 5.11b and 5.11c. Dissolved Al values within each watermass were compared with a t-test (see Table 5.5). Due to the extremely low variance ($\sigma^2 = 0.35$ nM) of the entire data, few watermasses were significantly different from each other. STZW had some of the highest values from the study (although still low on a global scale), whereas SAMW had the lowest values of the study (and some of the lowest values ever observed in the open ocean). LCDW had the lowest mean, median and standard deviation of dAl concentrations, which is expected due to increased scavenging with depth. AASW was also extremely low, probably due to limited supply from the ice-covered Antarctic coupled with enhanced scavenging during periods of high productivity.

Table 5.6: Description of dAl values determined in each depth class.

	Mean	SD	Min.	25%	Median	75%	Max.
Deep	0.70	0.35	0.22	0.48	0.62	0.87	1.94
Int.	0.90	0.66	0.06	0.50	0.71	1.06	3.97
Surf.	0.81	0.55	0.05	0.45	0.66	1.09	3.64

Table 5.7: t-test p-values determining if the dAl concentrations within each depth class are statistically different from each other. Values <0.05 were used as the threshold to indicate difference was significant.

	Deep	Int.	Surf.
Deep	1.00	0.01	0.16
Int.	0.01	1.00	0.24
Surf.	0.16	0.24	1.00

5.3.3 Summary of dAl concentrations within deep, intermediate and surface waters

Values observed within each depth class are summarised in Table 5.6 and presented in Figures 5.11d, 5.11e and 5.11f. The depth classes were: Deep, collected deeper than 1100 m; Intermediate (Int.), collected between 1100 m and the bottom of the ML; and Surface (Surf.), collected shallower than the summer MLD. Most samples were within the intermediate depth class. A t-test (results presented in Table 5.7) revealed deep waters were significantly different to intermediate waters, but were statistically similar to surface waters. There was no systematic distribution pattern with depth across the SR3 transect. Sub-zones exhibited different dAl distributions with depth. Surface waters were enriched relative to intermediate and deep waters in the STZ. The SAZ-N was relatively homogeneous throughout the entire water column. Intermediate waters were enriched relative to both surface and deep waters in the IPFZ. Surface waters were enriched relative to intermediate and deep waters in the SAFZ-N and SAFZ-S. The PFZ and the SZ exhibited similar patterns, relatively homogeneous throughout the water column, with only slight enrichment at the sediment interface, with both depleted and enriched values observed at the surface at different stations.

5.3.4 Summary of dAl concentrations within each major ocean zone

Values observed within each oceanographic zone are summarised in Table 5.8. Concentrations within the STZ were much lower than those observed in this zone during the SAZ-Sense voyage. Concentrations within the SAZ-N were similar to those observed in this zone during the SAZ-Sense voyage, where a latitudinal gradient was observed increasing with proximity to Tasmania. This zone had the lowest values of the entire data set. The SAZ-S had the highest variability, elucidated after

Table 5.8: Description of dAl values determined in each major ocean zone.

	Mean	SD	Min	> 25%	Median	> 75%	Max
All data	0.84	0.59	0.05	0.48	0.69	1.05	3.97
STZ	1.08	0.64	0.31	0.59	0.99	1.30	3.64
SAZ-N	0.63	0.40	0.05	0.35	0.50	0.92	1.85
SAZ-S	1.03	0.82	0.27	0.53	0.73	1.15	3.97
PFZ	0.81	0.43	0.19	0.49	0.75	0.99	2.21
SZ	0.69	0.35	0.15	0.46	0.60	0.87	1.86

Table 5.9: t-test p-values determining if the dAl concentrations within the major ocean zones are statistically different from each other. Values <0.05 were used as the threshold to indicate difference was significant.

	STZ	SAZ-N	SAZ-S	PFZ	SZ
STZ		0.00	0.76	0.03	0.00
SAZ-N	0.00		0.00	0.02	0.40
SAZ-S	0.76	0.00		0.05	0.00
PFZ	0.03	0.02	0.05		0.12
SZ	0.00	0.40	0.00	0.12	
EMLDZ	0.00	0.197	0.00	0.00	0.00

analysis of sub-zones. The polar frontal zone was relatively enriched in dAl, with concentrations comparable to those near Tasmania. dAl values within each zone were compared with a t-test (see Table 5.9). The STZ, SAZ-S and the PFZ found to be statistically similar to each other, as were the SAZ-N and the SZ. SAZ-N and SZ were found to be statistically different from STZ, SAZ-S and the PFZ.

5.3.5 Summary of dAl concentrations within each sub-zone

Values observed within each sub-zone are summarised in Table 5.10 and presented in Figures 5.11g, 5.11h and 5.11i.

There are no minor fronts that partition the STZ or SAZ-N into sub-zones. The SAZ-N had the lowest overall value. The IPFZ had the highest mean, median and overall values. T-test p-values from comparison of dAl values within each sub-zone (see Table 5.11) revealed significant differences across the STF, SSAF and the NPF. Concentrations between the SSAF and the NPF were significantly different from all other regions. The region between the NPF and the MPF was

Table 5.10: Description of dAl values determined in each sub-zone. Each region was defined by the front on its southern boundary.

	Mean	SD	Min	> 25%	Median	> 75%	Max
All data	0.84	0.59	0.05	0.48	0.69	1.05	3.97
STZ	1.08	0.64	0.31	0.59	0.99	1.30	3.64
SAZ-N	0.63	0.40	0.05	0.35	0.50	0.92	1.85
SAFZ-N	0.55	0.37	0.27	0.36	0.44	0.53	1.79
SAFZ-S	0.78	0.29	0.37	0.63	0.72	0.86	1.62
IPFZ	1.32	0.97	0.33	0.70	1.05	1.55	3.97
PFZ-N	0.86	0.46	0.19	0.52	0.86	1.03	2.21
PFZ-S	0.74	0.38	0.22	0.46	0.64	0.96	1.75
SZ-N	0.68	0.29	0.34	0.47	0.52	0.97	1.01
SZ-M	0.80	0.38	0.34	0.54	0.78	0.90	1.86
SZ-S	0.66	0.35	0.15	0.44	0.58	0.69	1.59

Table 5.11: t-test p-values determining if the dAl concentrations within the frontal zones are statistically different from each other. Values <0.05 were used as the threshold to indicate difference was significant. The oceanographic region between the SSAF and the NPF (labeled the NPF) was significantly different from all other regions with significantly higher values. This corresponds to the region of surface silicic acid maxima (from upwelling of underlying waters).

	STZ	SAZ-N	MSAF	SSAF	NPF	MPF	SPF	NSACCF	SSACCF	SPOLE
STZ		0.00	0.00	0.02	0.18	0.10	0.01	0.02	0.07	0.00
SAZ-N	0.00		0.42	0.10	0.00	0.02	0.30	0.74	0.16	0.77
SAZF-N	0.00	0.42		0.06	0.00	0.02	0.14	0.39	0.08	0.33
SSAF	0.02	0.10	0.06		0.00	0.45	0.71	0.45	0.83	0.18
NPF	0.18	0.00	0.00	0.00		0.01	0.00	0.00	0.01	0.00
MPF	0.10	0.02	0.02	0.45	0.01		0.31	0.20	0.70	0.05
SPF	0.01	0.30	0.14	0.71	0.00	0.31		0.67	0.62	0.43
NSACCF	0.02	0.74	0.39	0.45	0.00	0.20	0.67		0.41	0.88
SSACCF	0.07	0.16	0.08	0.83	0.01	0.70	0.62	0.41		0.23
SPOLE	0.00	0.77	0.33	0.18	0.00	0.05	0.43	0.88	0.23	

statistically different from the region south of the SSACCF. Concentrations south of the MPF are statistically similar. Concentrations between the STF and the SSAF are statistically similar.

Table 5.12: Description of aeolian deposition estimates (g/m²/yr) values determined in each major ocean zone using MADCOW (solubility = 1.5%).

	Mean	SD	Min	> 25%	Median	> 75%	Max
All data	0.11	0.07	0.01	0.06	0.09	0.14	0.48
STZ	0.15	0.11	0.04	0.07	0.11	0.17	0.48
SAZ-N	0.09	0.06	0.01	0.05	0.07	0.12	0.25
SAZ-S	0.12	0.06	0.04	0.07	0.10	0.16	0.24
PFZ	0.11	0.07	0.05	0.06	0.10	0.13	0.29
SZ	0.09	0.05	0.02	0.06	0.07	0.09	0.25

5.4 Aeolian deposition estimates using MADCOW

Aeolian deposition rates were calculated using MADCOW, assuming 1.5% solubility of particulate Al supplied (based on observed Fe solubility in aerosols from SAZ-Sense, see Table 4.3). Estimates were made per station, sub-zone and major ocean zone (see Figure 5.12). Only values within the summer ML were considered (calculated per station). Annual aeolian deposition would be expected to occur over larger spatial scales than per station or sub-zone (some of which are quite narrow latitudinal bands), so spatial variability was only investigated on a zonal scale.

Aeolian deposition rate estimates over the entire transect had a mean of 0.11 ± 0.07 g/m²/yr, with minimum and maximum values of 0.01 and 0.48 g/m²/yr respectively.

When separated in major ocean zones, there was a slight positive trend from S to N, although SAZ-N did not follow this trend (see Figure 5.12c and Table 5.12). Mean values for each major ocean zone were very similar, ranging from 0.09 ± 0.05 in the SZ to 0.15 ± 0.11 g/m²/yr in the STZ. Minimum aeolian deposition rates were found in the SAZ-N (within the EMLDZ). Maximum aeolian deposition rates were found in the STZ (close to Tasmania).

Aeolian deposition rates within the STZ were statistically significantly different to those in the SAZ-N and the SZ.

5.5 Discussion

5.5.1 The nature of the overall trends in dAl

In general dAl concentrations were < 1 nM (see Figure 5.10a) and relatively invariant with depth (see Figure 5.7). This suggests extremely limited supply of soluble dust to the surface along the

Table 5.13: t-test p-values determining if the aeolian deposition estimates within major ocean zones are statistically different from each other.

	STZ	SAZ-N	SAZ-S	PFZ	SZ
STZ		0.03	0.97	0.60	0.05
SAZ-N	0.03		0.10	0.27	0.88
SAZ-S	0.97	0.10		0.55	0.13
PFZ	0.60	0.27	0.55		0.33
SZ	0.05	0.88	0.13	0.33	

entire transect which is expected and in agreement with all previous observations and modelling of aeolian deposited dust (Seze et al., 1991; Duce, 1991; Whitehead et al., 1998; Ginoux et al., 2001; Zender et al., 2003; Hand et al., 2004; Jickells et al., 2005; Schulz et al., 2009). Overall the trends were latitudinal correlating with the frontal system of the ACC, rather than with depth or watermass. The ACC is separated by strong frontal systems that act as well-defined physical boundaries, limiting mixing of adjacent watermasses within each sub-zone. Mean flow varies within each of these sub-zones, as does average vertical movement of water (upwelling vs. downwelling). Therefore, the concentration of dAl is probably controlled more by lateral and vertical advection processes, rather than aeolian processes typical of other ocean basins. The relatively homogeneous vertical profiles at most stations suggest the deepening of the ML in winter could be an important control over surface concentrations along SR3, especially within the IPFZ. Maximum values were observed within the STZ and IPFZ. Minimum values were observed within the SZ-S and the EMLDZ.

5.5.2 Comparison to previous observations in the SO

The range of dAl along the SR3 transect is extremely similar to those observed in other regions of the SO (see Table 5.1) with very similar mean ($0.84 \text{ nM} \pm 0.6$), min (0.1 nM) and max (4.0 nM) values. There are only 4 previous transects to compare, Drake Passage, South Atlantic, Ross Sea and between Crozet and Kerguelen Islands (VanBeusekom et al., 1997; Measures, 2002; Middag et al., 2011a, 2012a). In the open ocean, each of these studies exhibited vertical gradients, increasing with depth. This is not what was observed for SR3 at any station along this transect.

In the Drake Passage and South Atlantic, a strong relationship between watermasses and dAl concentrations were observed (Middag et al., 2011a, 2012a). Sedimentary sources were identified. There was a general gradient of dAl to increase with depth. In the northern SAZ a subsurface

maxima of ~ 2 nM was observed between 200–1000 m. Minimum concentrations were observed in the surface of the most southerly stations (65 – 70° S).

Around Crozet and Kerguelen Islands (immediately before the plateau), there was significant latitudinal variability. The southern stations within the PFZ were homogeneous with depth, ~ 0.7 nM, while the northern stations (either SAZ or STZ) ranged from 2–4 nM, with a subsurface maxima of ~ 4 nM. Interpretation is difficult as influence from the South Atlantic, Agulhas current and the Islands is all possible (VanBeusekom et al., 1997). However, it is clear the northern part of the transect was subject to greater supply of Al than the southern region.

The study within the Ross Sea observed distributions most similar to those along SR3 (Measures, 2002). Surface concentrations were low, with a subsurface maximum between 200–1000 m within the IPFZ. Unlike along SR3 there was a general increase with depth, and with maximum concentrations observed at the sediment interface which is probably due to entrainment from sediments as the dense waters from the Ross Sea polynas cascade down the continental shelf.

A subsurface maximum was observed within the IPFZ along SR3. A subsurface maximum of similar magnitude was also observed in the IPFZ of the Ross Sea, the SAZ of the South Atlantic and the SAZ-N of Crozet and Kerguelen Islands. Oceanographic zones were estimated from Figure 5.2b (VanBeusekom et al., 1997; Measures, 2002; Middag et al., 2011a, 2012a). It may be this subsurface maxima is a feature of the SAZ / IPFZ, resulting from remineralisation of particulate organic matter within this productive zone (for the SO). It is possible it is a coincidental feature, with a multitude of sources (depending on the location) and no systematic relevance, but is of local importance as a general supply mechanism to the surface. At present there is insufficient data to draw strong conclusions.

5.5.3 Why was dAl relatively enriched in the IPFZ?

Before delving into the possible explanations for this relative enrichment, it is important to note that the actual values on a global scale were extremely low (max. = 3.97 nM) and the level of enrichment relative to the rest of the transect was minor (1–2 nM). The potential for low-level contamination when attempting to determine dAl in SO sea water was high, however, the pattern observed does not reflect one expected from systematic bottle contamination. If bottle contamination were a problem, it would be evident across the entire data set, rather than concentrated in one specific frontal zone (the IPFZ). This is particularly true because the IPFZ was split by a meander in the NPF, so it was not sampled chronologically, making temporary bottle contamination (such as from handling on the

deck of the ship) less likely (although not impossible). Also, removal of the highest values (those >3 nM) does not alter the trends observed.

Processes considered to potentially result in an apparent regional enrichment are: enhanced entrainment of dAl from sediment or hydrothermal sources; enriched samples have unexpectedly targeted micro regions of biomass senescence; increased residence time of dAl within this sub-zone; and enhanced supply of Al from the atmosphere due to atmospheric divergence.

Unexpected targeting micro-regions of biomass senescence Although dAl is assumed to be oceanographically consistent, dAl is particle reactive and therefore subject to influence of remineralisation processes. Al would be returned to the water column as dAl, especially in the presence of acids or bases associated with decomposition of particulate matter (Al^{3+} and AlOH_4^- are highly soluble in seawater at pH <4.5 and >8 respectively). Given the depletion of dAl along SR3 and timing of the season (Autumn / Fall), it is probable enrichment in isolated samples was due to the unexpected targeting of sinking senescent phytoplankton blooms. If Al in the particles was bound to silica, it is unlikely to be released as silica remineralises very slowly, but sinks quickly. However, siliceous organisms are only a part of the community within this sub-zone so it is possible there was opportunity for Al to be remineralised. The subsurface maximum of dAl was much deeper than the subsurface chlorophyll maxima. Particles could be remineralised below the chlorophyll maxima, but the rate of dissolution would need to be rapid to enrich dAl at this depth, so this is unlikely to be the cause of enrichment for this case.

Enhanced supply of Al from the atmosphere The IPFZ is on the northern boundary of the divergence of two atmospheric cells, the mid-latitude and polar cells. This divergence zone ranges from ~54–62°S and is a region of enhanced precipitation. This could also act as an aerosol concentration mechanism, where two air masses transport dust towards the same region, where it may then be washed out through wet deposition. Wet deposition is expected to increase the solubility of all trace elements relative to dry deposition (Duce and Tindale, 1991; Sholkovitz et al., 2009, 2012). Solubility studies during the SAZ-Sense voyage (see Table 4.3) show solubilities of dry dust collected ranging from 0.2–17%. Increased occurrence of wet deposition could easily increase the solubility of dust deposited by 2-fold (Mackie et al., 2008, and references therein) to account for the relative enrichment observed in the IPFZ. It is not clear why there would be more rain on the northern boundary (54–56°S) of this divergence zone relative to the rest of the divergence zone (56–62°S), and there certainly was no evidence to support this as the case from climatology. It could be that, as found in the equatorial Atlantic, a “rain curtain” washes the dust from the air with dramatic efficiency, hence dAl concentrations are enhanced at the northern edge of this region.

of higher precipitation (Measures and Edmond, 1990; Middag et al., 2012b). Although possible, this is unlikely, as the existence of the well-defined rain curtain in the equatorial Atlantic is due to the equator, a much stronger and well defined atmospheric boundary than any in the SO.

Possible entrainment of dAl from local sediment sources The potential for dAl enrichment throughout the entire water column from entrainment of sedimentary pore waters immediately below seems unlikely, and is not reflected in vertical distribution of dAl in the IPFZ. Bathymetry upstream for 50° of longitude between 54–58°S along SR3 appears too deep for upwelling to bring a source of dAl the required 2500 m to the surface. Even if a hydrothermal supply of Al were present (such as observed for Fe and Mn in other parts of the ocean (Tagliabue et al., 2010; Middag et al., 2011c)), dAl-enriched waters would require significant positive buoyancy to influence surface values.

Possible entrainment of dAl from glacial subsurface meltwaters Subsurface glacial meltwater, transporting freshwater into the ocean at the coast was too distant and a continuous signal of such a supply was not evident in the salinity profiles (Rosenberg, 2008). Opportunistic sampling of iceberg samples during this study (data not presented) also revealed no observable enrichment of dAl within proximity of icebergs (however sampling methods may have been flawed).

Possible entrainment of dAl from distant sediment sources Entrainment of trace elements within sediment pore water into the overlying water column does occur over the Kerguelen Plateau (VanBeusekom et al., 1997; Blain, 2008; Blain et al., 2008). Figure 5.2b presents the frequency of the major fronts within the ACC over the last 15 years. The *white* region between the MSAF and the MPF (the two most northerly bands) is the region of waters that pass over the Kerguelen Plateau on their journey eastward, and has been previously described as the IPFZ (Parslow et al., 2001). Recent studies have shown that the trace elements entrained into these waters from the shelf can be transported >1000 km off the shelf and influence primary production (Sokolov and Rintoul, 2007b; Mongin et al., 2008, 2009). It is possible the dAl enrichment found in the IPFZ was a remnant signal from the Kerguelen Plateau. The low dAl concentrations along the SR3 transect make this remnant signal observable. Assuming a velocity of 0.2 m/s, waters entrained with dAl from shelf sediments of the Kerguelen plateau would travel the 4600 km to reach the SR3 transect in 5–8 months. This is certainly within the time frame of Al residence time in both the surface (1–3 years) and deep waters (10–70 years). Unfortunately, Mn was not analysed to help assess this hypothesis. It has previously been recognised the supply of dFe to the PFZ is dominated from below, as was recognised in the SAZ-Sense voyage. However the original source of this dFe has not been established. It could very likely be the Kerguelen Plateau. However, the similar feature observed north of the Crozet and

Kerguelen Islands suggests another even more distant source may be responsible. Candidates for this source include may be some subsurface portion of the Agulhas Current or maybe a link to South East Atlantic subsurface waters. These alternatives are unlikely (and not exhaustive), but given the absence of data cannot be ruled out just yet.

The most probable explanations for dAl enrichment in the IPFZ The two most likely candidates contributing to dAl enrichment in this zone are enhanced wet aeolian deposition and entrainment from sedimentary pore waters from the Kerguelen Plateau. Both processes theoretically have the potential to contribute the entire dAl enrichment observed. However, the wet aeolian deposition would be expected to influence the entire PFZ, whereas the entrainment from Kerguelen Plateau would be expected to only influence northern boundary. Therefore it is the remnant signal from the Kerguelen Plateau that was most likely to have influenced this region.

5.5.4 Why was dAl relatively enriched in the STZ?

The biogeochemical processes leading to enrichment in the STZ have been presented Chapter 4. It is a complex interplay between aeolian deposition of aerosols (both dust and smoke/ash) and lateral advection and mixing of three main currents, the ACC, EAC and the ZC. The ACC and the ZC appear relatively depleted in trace elements. The EAC is relatively enriched in trace elements, due to entrainment of sedimentary and atmospheric sources as it transits along the east coast of Australia. There was no obvious signal of influence from the EAC during this April repeat of SR3, with the northerly stations more similar to P1 than to P3, suggesting the region is dominated by the ACC (and possibly the ZC). Very close to Tasmania it is probably local sources of Al (both fluvial and aeolian) that begin to have an influence at the surface.

5.5.5 Why was dAl relatively depleted within the SZ-S (the surface of which was defined as AASW)?

Depleted dAl values within the SZ is expected and agrees with previous observational and modelling studies ([Vanbennekom et al., 1991](#); [Measures, 2002](#); [Han et al., 2008](#); [Middag et al., 2011a, 2012a](#); [van Hulst et al., 2012](#)) . In winter, during sea ice formation, the frazzle-ice particles may act as adsorption sites for dAl, so it is stripped out of solution and concentrated into the sea ice ([Lannuzel et al., 2007, 2008](#); [van der Merwe et al., 2009](#); [Lannuzel et al., 2010, 2011b](#); [van der Merwe et al., 2011a,b](#)). Once formed, the sea ice acts as barrier to atmosphere-ocean interaction, collecting aeolian deposited dust. These two processes may explain the enrichment of Al in sea ice relative

to the underlying water column (see the values for sea ice in Table 5.1). When the sea ice melts in summer, the subsequent enhanced particulate concentrations of the spring phytoplankton bloom rapidly scavenges dAl, removing it from the dissolved phase, transporting it to depth. Supply of dAl from sediments appeared limited, which is expected given the stratifying influence of sea ice and the strong downward movement of water due to the formation of AABW in this region (Rintoul et al., 1997; Rintoul and Bullister, 1999; Rintoul and Sokolov, 2001; Rintoul et al., 2002; Rintoul, 2007). Recent evidence presented by Middag et al. (2013) found that within the Weddell Sea, dAl concentrations increased with depth as waters travelled along the continental slope, indicating a supply from sediments. A similar feature is found along SR3, with an increasing trend in dAl concentrations with depth where AASW < SHW < AABW in the SZ (see Figure 5.11a). However, a t-test reveals these watermasses are not significantly different (see Table 5.5). Even so, along SR3 this (quite weak) evidence is only indicative as these three watermasses are not directly connected. The AABW at SR3 is sourced from waters that are subducted from further west, these shallow waters may be slightly enriched relative to the shallow waters along SR3 (eg. AASW / SHW). This may give the illusion of enrichment with depth at SR3 (where: AASW < SHW < AABW) when it may just be the signature of the deeper watermasses, not enrichment from local sedimentary sources.

5.5.6 Why was dAl relatively depleted within the EMLDZ?

The depletion of dAl throughout the entire water column within the EMLDZ was puzzling. Depletion relative to the STZ was expected due to increased distance from terrestrial sources. However, the concentrations at the PFZ indicate sustained supply of Al to at least 56°S.

As previously mentioned, the EMLDZ has the fastest eastward mean flow, the deepest annual MLD (4–5-fold greater than other sub-zones) and also the lowest annual biomass rate of regions along SR3 (as estimated from satellite measurements). Waters within this region have travelled through some of the most terrestrially remote regions of the planet, therefore, the concentration of dAl was expected to be low. Entrainment from Kerguelen Plateau, although possible, is less probable, as the SAF meanders around the plateau rather than over the top of it, limiting potential for entrainment of sedimentary sources. Obata et al. (2004) presents a single, high resolution (15 depths) dAl depth profile at 40° S, 110° E, where below 200 m, values are mostly around 0.7 nM. There is a surface maximum of 4 nM, but that is 1 data point. So dAl concentrations are already depleted further west, at the beginning of the EMLDZ.

Scavenging rate within the EMLDZ can be assumed to be minimal and ignored due to the low annual biomass. Al% in dust and Al% solubility can be assumed to be relatively constant across

the transect, and were assumed to be 8% and 1.5% respectively. However, annual maximum MLD extended down to about 500 m, significantly deeper than within the other sub-zones.

Simple calculations can be used to assess the impact of MLD on converting dust inputs to dAl concentrations. These are investigated in more detail in Chapter 6. The dilution effect of varying MLD along the SR3 transect can explain almost all of the difference observed (~ 3 -fold) between the dAl concentrations in the PFZ and STZ relative to the EMLDZ.

5.5.7 The relationship of Al with other parameters along SR3

Al and Fe along SR3

Al is completely decoupled from Fe along the SR3 transect (compared Figure 5.6 and 5.7), similar to observations in the South Atlantic and the Ross Sea. This is expected, due to the limited aeolian deposition of dust. Sources of trace elements are limited and distant, with ample opportunity for biological processing to decouple the relationship of these two elements at all depths (phytoplankton and bacteria). At depth, sources of Fe may be both hydrothermal and sedimentary, with significant enrichment of dFe observed near the ocean floor. dAl concentrations do not reflect any possible enrichment from hydrothermal sources. De-coupling of Fe and Al in sea ice is probably due to biological processes, where Fe is concentrated and accumulated by biology, while Al is ignored. Fe is readily recycled within the ML, whereas once Al is scavenged to solid phase, it is not readily remineralised and as such is removed from the surface quickly. Also, zooplankton are thought to graze at depth and the surface, accumulating Fe while feeding at the bottom and releasing it to the surface through defecation. This process is not expected to also transport Al, only Fe.

The relationship of Si and Al in the Australian Sector of the SO

A relationship between Al and Si has been observed in the Arctic Ocean (Middag et al., 2009). Terrestrial material is enriched in both Si (most abundant) and Al (third most abundant), at an Al/Si ratio of $\sim 1:3$ (Taylor, 1964; Wedepohl, 1995; Yaroshevsky, 2006), and is the dominant source of these elements to the Arctic Ocean, transported by either fluvial or aeolian processes (reviewed by Middag et al. (2009)). Aluminium and Si have different solubilities in seawater, and therefore the ratio observed of these elements in the dissolved phase can be much lower. Middag et al. (2009) identified a linear relationship between Al and Si with depth in the Arctic Ocean. The slope of this linear relationship is $\sim \frac{1}{455}$, which happens to be the ratio of Al:Si ($\sim 1:455$) in

diatom frustules. [Middag et al. \(2009\)](#) proposed the linear relationship with depth is a consequence of diatom frustules dissolving with depth, imprinting the ratio into the dissolved phase of these elements. A relationship between the two elements is maintained throughout the Atlantic Ocean, with diminishing strength from North to South as dissolved Si concentrations increase in the deeper watermasses disproportionately to dAl.

In the Southern Ocean, this relationship is no longer observable. The short residence time of dAl in the deep ocean (10–70 years) means it does not accumulate in deep water. However, Si has a long residence time ($\sim 15,000$ years) and therefore accumulates in deep ocean waters. Si is relatively depleted in the Arctic Oceans ($1\text{--}10\mu\text{M}$), but enriched in the SO ($140\mu\text{M}$) ([Middag et al., 2011a](#), and references therein). Al and Si are completely decoupled along the SR3 transect. This is in agreement with the recent understanding of the Al and Si biogeochemical cycles ([Middag et al., 2009, 2011a, 2012a](#)). Figure 5.13 shows how the relationship is dominated by one or the other, depending on the watermass. The relationship is also investigated per watermass (see Figure 5.14), where it is clear there is no systematic relationship (except possibly in AASW, where it is a negative relationship, but this is considered a coincidence due to limited data).

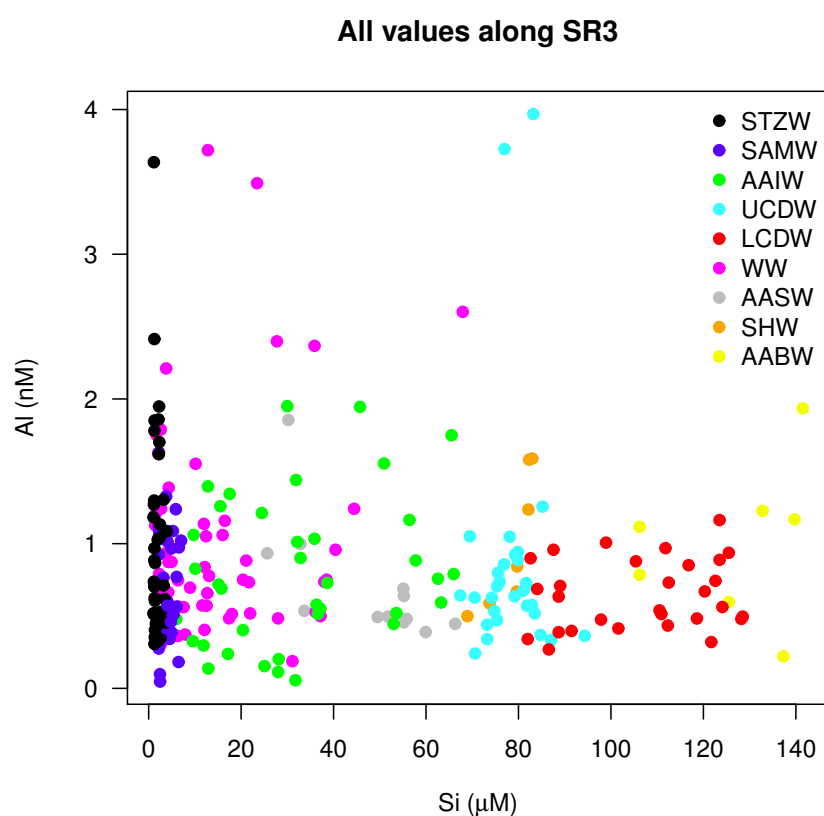


Figure 5.13: Comparison of dissolved Si and Al along the SR3 transect. Different colours represent the different watermasses. There is no significant relationship found.

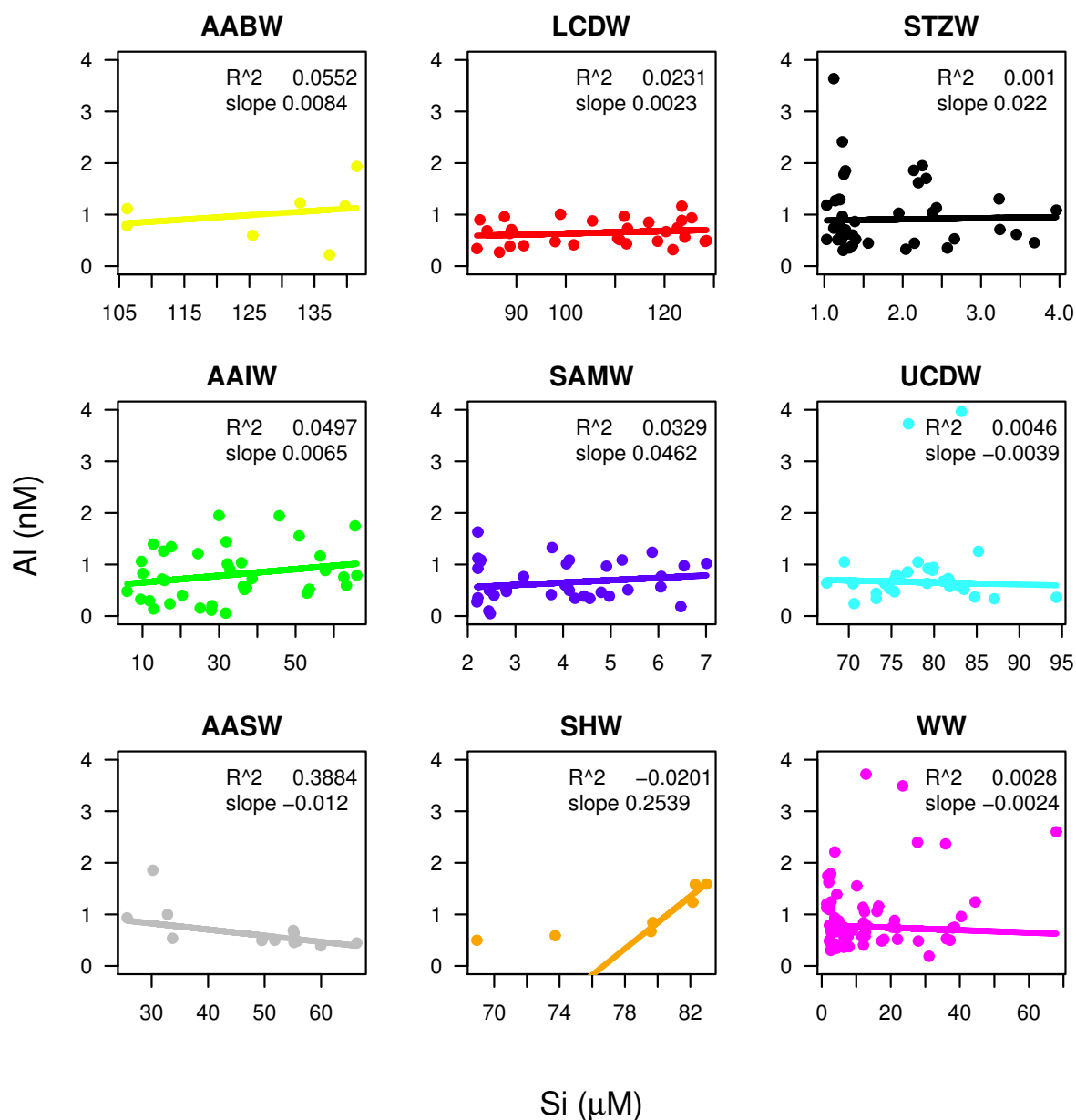


Figure 5.14: Comparison of dissolved Si and Al separated by watermass along the SR3 transect. There were no significant relationships found, which agrees with recent postulations from [Middag et al. \(2011a\)](#).

5.5.8 Aeolian deposition rates

On a global scale, per station aeolian deposition rate estimates were very similar along the SR3 transect. They were certainly within an order of magnitude of current estimates produced by the DEAD and LMDzT-INCA models (Seze et al., 1991; Whitehead et al., 1998; Zender et al., 2003; Schulz et al., 2009) . However, the relatively homogeneous depth profiles (with little gradient between the surface and underlying waters) suggest aeolian deposition may be much lower than those estimated by MADCOW (Measures and Brown, 1996). As predicted by the original authors, the MADCOW model was not designed for use in the SO, with many assumptions that are inappropriate (especially MLD). It needs modification for appropriate estimation, which was attempted in the next chapter.

5.6 Conclusions

dAl was investigated along the SR3 transect. Relative to the global range, concentrations were low ranging from <LOD (0.05) to 3.97 nM. Seventy-five percent of values were ≤ 1 nM. Relatively homogenous with depth, trends were found to be latitudinal matching oceanographic properties (such as annual maximum MLD) within sub-zone between the oceanographic fronts. No correlation was observed with watermass. Distributions were similar to those previously observed in the SO, but not identical.

Concentrations were observed to be depleted in the EMLDZ probably due to dilution and limited supply mechanisms. They were also quite depleted in the SZ-S, probably due to enhanced scavenging by both sea ice and particulate organic matter as well as limited supply mechanism which were inhibited as sea ice acts as a barrier to atmosphere-ocean interactions. Enrichment of dAl within the IPFZ is postulated to arise from entrainment of sedimentary pore waters from the Kerguelen Plateau, although this idea needs confirmation.

Estimates of aeolian deposition rates using MADCOW support output from the atmospheric models DEAD and LMDzT-INCA, however, the use of MADCOW is not appropriate in the SO and requires modifications to the assumptions applied to attain more realistic estimates.

Chapter

6

Comparison of different model estimates of aeolian deposition to the SO

6.1 Introduction

6.1.1 Aims of this chapter

There are three aims of this chapter.

- To compare the model estimates of surface dAl concentrations in the SO from DEAD-MADCOW and LMDzT-INCA-NEMO-PISCES to observations along SR3.
- To compare the model estimates of aeolian deposition of dust in the SO from DEAD and INCA to those estimated by applying MADCOW to dAl determined along SR3.
- To investigate the sensitivity of the MADCOW model to changes in the parameters MLD, scavenging rate and dust solubility.

6.1.2 Background

Aeolian deposition into the open ocean is difficult to measure and estimate. Events are sporadic and are linked strongly to extreme weather events that develop over short timescales (days) relative to the planning required for research expeditions (years) (Mitchell et al., 1992; Ekstrom et al., 2004, and many others). The open ocean is remote, making it difficult and expensive to study. Moorings deployed to investigate surface conditions are still insufficiently robust, especially in regard to their ability to withstand extreme open ocean conditions, so their use in the study of aeolian deposition is impractical (if not still impossible in all but the calmest seas) (from a recent review by Sholkovitz et al. (2012)). Ships of opportunity follow trade routes that are often not environmentally relevant and sample quality can be poor as aerosol sampling is a highly skilled task (Ezat et al., 1991; Radlein and Heumann, 1992; Kolesov et al., 1993). Satellite measurements are often impeded by cloud and in some areas are of little use at all because of this (Hsu et al., 2012).

Furthermore, it has only been in very recent times that the algorithms have become available to adequately correct satellite data to provide reliable aerosol measurements (Hsu et al., 2012). Conversion of satellite-derived aerosol concentrations to surface-ocean-dissolved-trace-element values is poorly understood as the processes that control this are poorly constrained (eg. the solubility of the minerals in the dust, the atmospheric processing (wet vs dry deposition), diffusion and dispersion rates) (Claustre et al., 2002; Hsu et al., 2012; Sholkovitz et al., 2012). All of the above difficulties are much greater when applied to the SO because it is more remote, has rougher seas, more cloud, less sea-traffic and typically lower volumes of dust (Zender et al., 2003; Jickells et al., 2005; Mackie et al., 2008). The primary source of dust to the SO south of Australia is from Australian deserts. These soils are old, weathered and well-processed, where most of the dissolvable minerals have been removed (Mackie et al., 2008).

The above difficulties have been so great that aerosol and dust parameters were excluded from almost all AR4 IPCC models contributing to the 2007 Report on Climate Change as they were too poorly constrained (Pachauri and Reisinger, 2007). In fact, aerosol estimation was considered to be one of the key parameters to improve and include when developing AR5 models (contributing to the up-coming IPCC report) (Pachauri and Reisinger, 2007).

In the absence of observations, estimates of aeolian deposition have been made by computer modelling (Zender et al., 2003; Jickells et al., 2005; van Hulst et al., 2012, and references therein) and by the use of dAl concentrations within the ML as a proxy for annual aeolian deposition (Measures and Edmond, 1989; Measures and Brown, 1996; Measures and Vink, 2000).

6.1.3 Estimates of aeolian deposition to the SO

Atmospheric global circulation models (GCMs) have been well established, characterised and tested since the early 1990s. These models estimate global atmospheric circulation patterns, which provide the transport mechanism for dust from the continents into the ocean (Duce and Tindale, 1991; Duce et al., 1991; Duce, 1991; Zender et al., 2003; Duce et al., 2008; Mackie et al., 2008, and references therein). Modelling of aeolian deposition to the open ocean using different GCMs has produced estimates of remarkable similarity, with differences between models resulting from dust-related assumptions (particle size, source region, uplift rates) as opposed to differences in atmospheric circulation patterns (Duce, 1991; Whitehead et al., 1998; Ginoux et al., 2001; Woodward, 2001; Zender et al., 2003; Hand et al., 2004; Schulz et al., 2009). Textor et al. (2006) state that these estimates have been validated against high-quality observations, although the number of observations and the number of sites were limited.

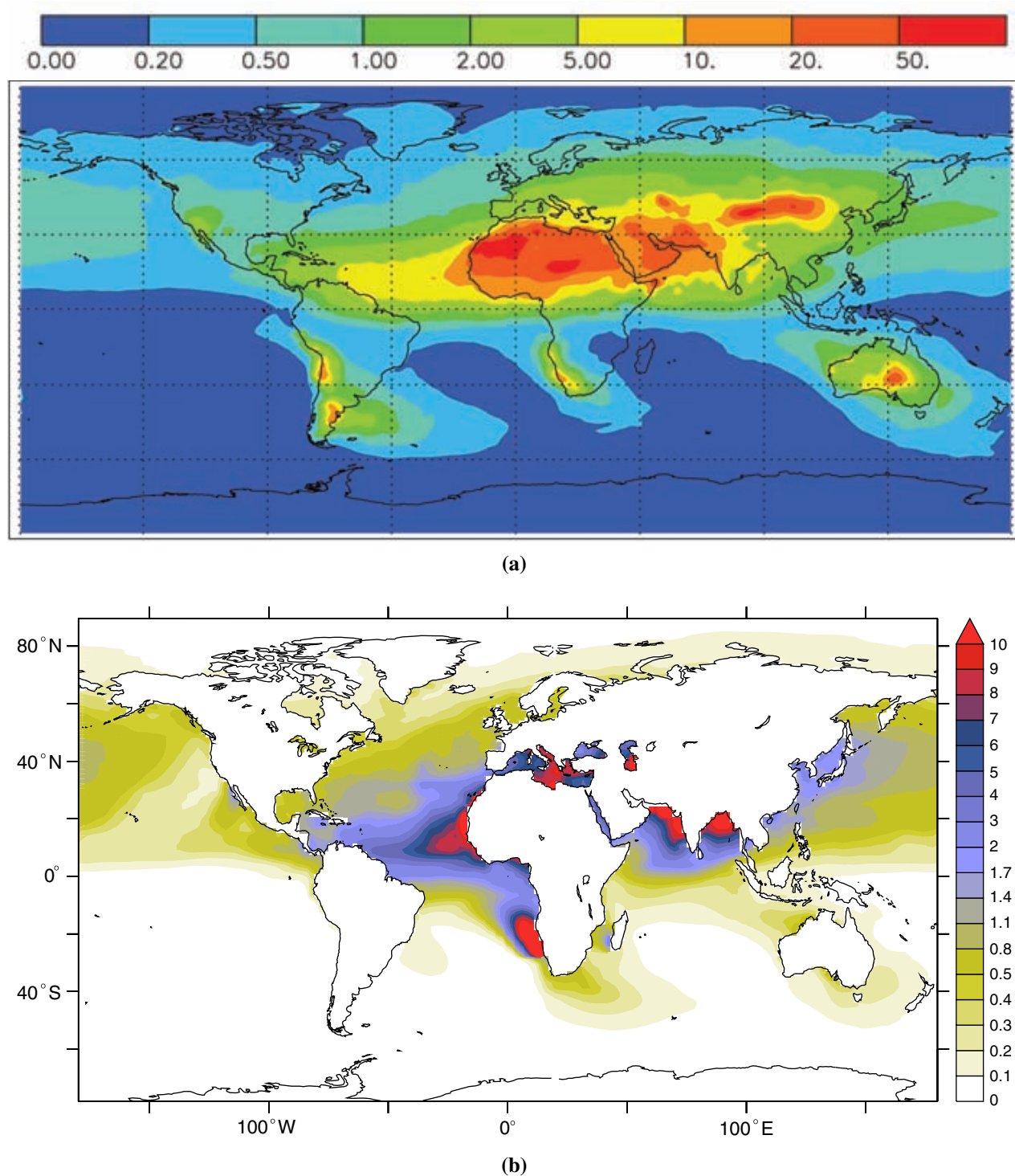


Figure 6.1: Recent modelling of annual aeolian deposition to the ocean surface ($g\ m^{-2}\ yr^{-1}$): (a) predicted by DEAD (Zender et al., 2003). Figure from Jickells et al. (2005) is a composite of outputs from three modelling studies (Duce, 1991; Ginoux et al., 2001; Hand et al., 2004) with output extremely similar to that from DEAD. (b) predicted by INCA (a module of LMDzT) (Seze et al., 1991; Whitehead et al., 1998; Schulz et al., 2009). Figure from van Hulst et al. (2012).

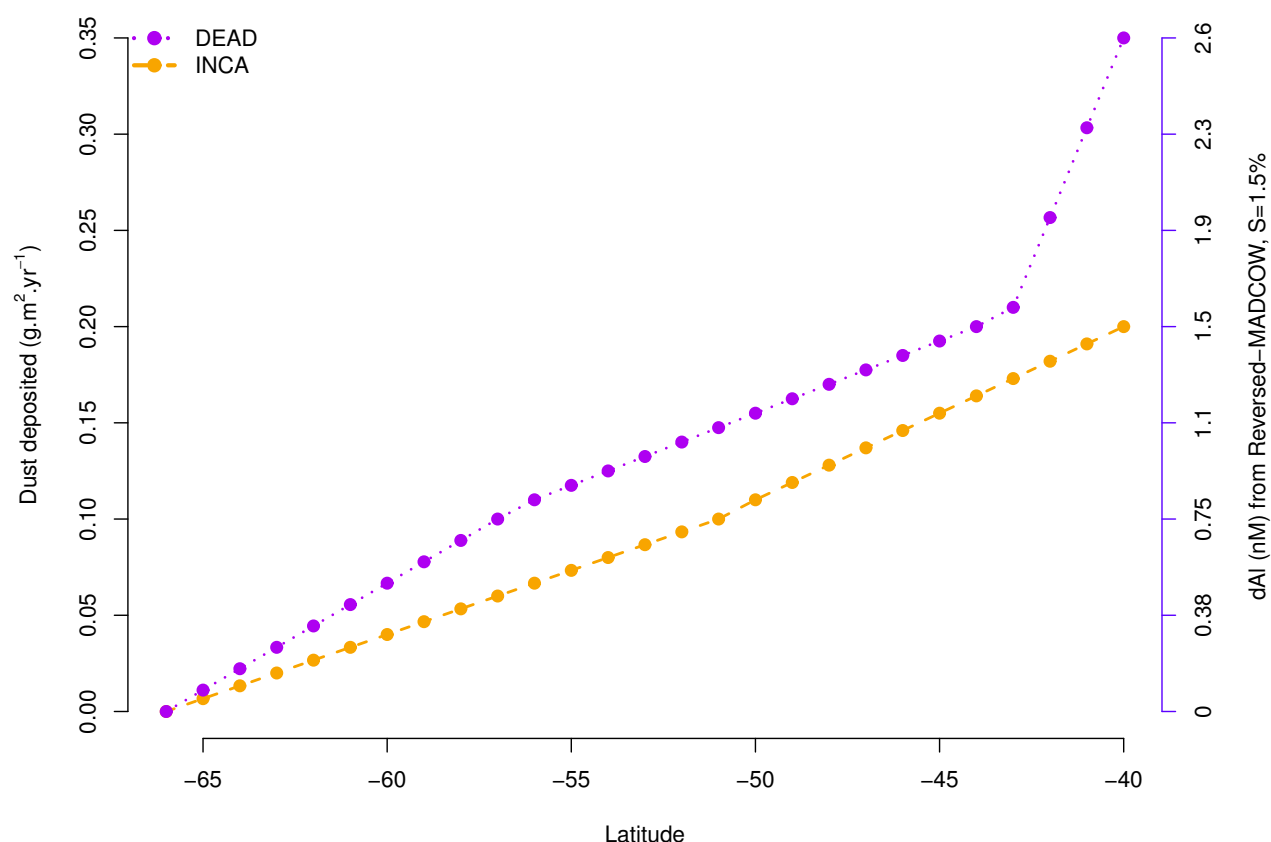


Figure 6.2: Estimates of aeolian deposition along SR3 transect from DEAD Zender et al. (2003) and INCA Aumont et al. (2008). Left-hand y-axis is the model estimate of dust deposition rate. Right-hand y-axis converts the dust deposition rate into the inferred dAl concentration in the ML, calculated using Reversed-MADCOW (Han et al., 2008).

Two of the more recent global annual aeolian deposition models are INCA and DEAD: their global output is presented in Figure 6.1 and specifically along SR3 is presented in Figure 6.2. The estimates from DEAD (Zender et al., 2003) and Jickells et al. (2005) are extremely similar and further discussion treats them as such (NB: Jickells et al. (2005) provided a better figure to compare to INCA due to its map orientation). The INCA and DEAD models do differ significantly over the South Atlantic, however this is not relevant to this study as the models agree quite well over the Indian and Australian sectors of the SO (upstream of and over the SR3 transect). These estimates of aeolian deposition have subsequently been used to estimate dAl concentrations in the ocean.

6.1.4 Estimates of dAl concentrations in the SO

DEAD and INCA have been used by [Han et al. \(2008\)](#) and [van Hulst et al. \(2012\)](#), respectively, to estimate dAl concentrations in the ocean. [Han et al. \(2008\)](#) applied the MADCOW model (Equation 6.1) in reverse, taking global estimates of aeolian dust deposition (G) from DEAD and calculating the expected dAl concentration in the surface ocean (A) (the DEAD-MADCOW estimate along SR3 is presented as the righthand axis in Figure 6.2). Globally the DEAD-MADCOW estimates agreed quite well with observations of surface dAl concentrations in the low and mid latitudes (like MADCOW did with aeolian deposition observations), but appeared to overestimate dAl in low aeolian deposition regions like the SO and the Northern Pacific. The paucity of dAl observations limited testing and interpretation of the model. The DEAD-BEC model of [Moore et al. \(2004\)](#) is not discussed here because DEAD-MADCOW appeared to perform better in the SO. [van Hulst et al. \(2012\)](#) recently investigated the biogeochemical cycling of dAl in the ocean after 1000 model years. They used NEMO-PISCES ([Aumont and Bopp, 2006](#)) with inputs from LMDzT-INCA (aeolian deposition) ([Seze et al., 1991](#); [Whitehead et al., 1998](#); [Aumont et al., 2008](#); [Schulz et al., 2009](#)) and PISCES (sedimentary entrainment based on models for iron) ([Aumont and Bopp, 2006](#)). This was the most comprehensive and complicated global modelling experiment of the biogeochemical cycling of dAl achieved to date, operated in four dimensions (space through time). INCA-NEMO-PISCES estimates were in strong agreement with observations throughout the Atlantic and Northern Pacific Ocean (see Figure 1.11). However, there are a few specific regions in the South Atlantic where agreement was weak [van Hulst et al. \(2012\)](#), possibly due to how sedimentary inputs were parameterised.

6.1.5 Measurement of Aluminium for Dust Calculation in Oceanic Waters: MADCOW

As ground truthing of aeolian deposition models over the ocean is difficult ([Mitchell et al., 1992](#)), [Measures and Edmond \(1990\)](#) suggested dAl could be used as a proxy for aeolian deposition. Following this, the MADCOW model was developed to convert surface ocean dAl concentrations (nM) to aeolian dust deposition rates ($g\ m^{-2}\ yr^{-1}$) ([Measures and Brown, 1996](#); [Measures and Vink, 2000](#)). This steady state model, as presented in [Measures and Brown \(1996\)](#), is:

$$G = \frac{A \times Sc \times M \times 1000}{D \times S} \quad (6.1)$$

The parameters (and their assumed values) as described by [Measures and Brown \(1996\)](#) and [Measures and Vink \(2000\)](#) is presented in Table 6.1, and when used as inputs to the model, MADCOW simplifies to:

Table 6.1: Parameter descriptions and assigned values in the MADCOW model as described in [Measures and Brown \(1996\)](#)

Symbol	Units	Parameter description	Original value	Calculation
G	$g\ m^{-2}\ yr^{-1}$	aeolian deposition rate		Equation 6.1
$Al\%_{dust}$	%	fractional content of Al in dust	8.1	
Al_{Mr}	$mol.g^{-1}$	molar mass of Al	26.982	
D	$mol.g^{-1}$	molar concentration of Al in dust		$Al_{Mr} \times Al\%_{dust}$
S	%	percent solubility of the particulate Al in the dust source	1.5% or 5.0%	
M	m	MLD	30	
R_t	yr	residence time of dAl in ML	5	
Sc	yr^{-1}	fractional scavenging per year	0.2	$\frac{1}{R_t}$
A	$mol.L^{-1}$	dAl concentration in the ML		

$$G = 0.133 \times A \quad (\text{for } 1.5\% \text{ solubility}) \quad (6.2)$$

$$G = 0.04 \times A \quad (\text{for } 5.0\% \text{ solubility}) \quad (6.3)$$

6.2 Methods

6.2.1 Comparing surface dAl concentrations from observations and model outputs

Surface dAl concentrations as estimated by [Han et al. \(2008\)](#) using the DEAD-MADCOW model and [van Hulst et al. \(2012\)](#) using the INCA-NEMO-PISCES model were compared to observations from the SAZ-Sense voyage and along the SR3 transect.

6.2.2 Comparison of dust deposition estimates along the SR3 transect

Comparison of dust deposition estimates along the SR3 transect by the DEAD, INCA and MADCOW models were compared. MADCOW was applied using equation 6.2, using the input variables as defined by [Measures and Brown \(1996\)](#) and [Measures and Vink \(2000\)](#). However, as these definitions/estimates/assumptions were recognised by these authors, to be inappropriate for the SO, alternative and more appropriate definitions/estimates/assumptions were applied. The difference was compared and discussed. The relevant assumptions, definitions and estimations of these alternative input parameters are described below.

6.2.3 Estimating summer MLD (M)

Summer MLDs were calculated following the density difference criterion with a threshold of 0.03 kg m^{-3} (Herraiz-Borreguero and Rintoul, 2011b) (these were identical to those calculated using the largest density difference) applied to the CTD data collected during the same voyage (Rosenberg, 2008).

6.2.4 Estimating scavenging rates (Sc)

In MADCOW, Sc is assumed to be 20% of D (see Table 6.1), calculated from an assumed residence time (R_t) of 5 years. As very little is known about the actual R_t for dAl in the surface ML, the appropriate value within any particular region of the ocean is likely to be within the range 0.1–10 years (Orians and Bruland, 1985, 1986; Measures and Edmond, 1990; Measures and Brown, 1996; Han et al., 2008; van Hulten et al., 2012; Han et al., 2012), so assuming 5 years is not unreasonable. However, Sc is also assumed to be geographically constant and this is not probable (van Hulten et al., 2012), especially along the SR3 transect. Sc for dAl is expected to be proportional to total suspended particulate material (SPM), enhanced when silica-compounds are present, especially as siliceous organisms (Paces, 1978; Stoffyn, 1979; Mackin and Aller, 1984c; Walker et al., 1988; Moran and Moore, 1988; Erofeeva et al., 1989; Lydersen, 1990; Measures and Edmond, 1990; Vanbennekom et al., 1991; Moran and Moore, 1992; Measures and Brown, 1996; VanBeusekom et al., 1997; Measures and Vink, 2000; Ščančar and Milačič, 2006; Siddall et al., 2008; Han et al., 2008; Rutgers V.D. Loeff et al., 2011; Savenko and Savenko, 2011; van Hulten et al., 2012; Han et al., 2012). Observations of both biogenic silica and SPM were unavailable, and therefore, an effort to create a index based on proxies that incorporated the effect of both inorganic and biogenic silica and SPM was developed. The proxies selected were silicic acid and chlorophyll-a (Chla).

Silicic acid concentrations (hereafter referred to as ' Si_M ', for measured Si) were assumed to vary proportionally with biogenic silica concentrations along the SR3 transect. Chla concentrations were assumed to vary proportionally with SPM concentrations. These assumptions only aim to estimate geographical variability along the SR3 transect. Si_M and Chla concentrations in the ML along the SR3 transect collected during various *L' Astrolabe* voyages between 2003–2012 were available from Dr. Simon Wright and his team at the Australian Antarctic Division (unpublished data, papers are in preparation). For both Si and Chla, values were normalised ($\frac{Si_M}{Si_{M \text{ max}}}$ and $\frac{Chla}{Chla_{\text{max}}}$, i.e. all values were between 0 and 1), providing a relative scaling mechanism along the transect. Each of Si_M and Chla was subset into eight latitudinal bands (defined by the position of the oceanographic fronts during each voyage), and the value that equalled the 75th-quartile of each bin was used as

the scavenging index. Maximum values were not used, to discount anomalous measurements or years. The resulting Si_M and Chl a indices were summed together to provide a geographical index with which to estimate Sc and resulted in reasonable values within the range 0.20–0.96 (presented in Table 6.2).

6.2.5 Estimating solubility rates (S)

Solubility rates are thought to be controlled by factors such as the size of the dust particle, mineral composition of the dust delivered, whether it is wet or dry deposition, the level of atmospheric processing (i.e. the acidity of the cloud droplets or the exposure to various levels of radiation, such as UV) and the acidity of the oceanic waters to which it is delivered (Stoffyn, 1979; Stoffyn and Mackenzie, 1982; Measures and Edmond, 1990; Measures and Brown, 1996; Measures and Vink, 2000; Han et al., 2008, 2012; Han, 2012; van Hulten et al., 2012; Sholkovitz et al., 2012).

Sources of dust to the Australian Sector of the SO are primarily from Australia. As previously mentioned, Australian dust sources are old, weathered, highly processed sediments and therefore, the more soluble minerals have already been removed (Mackie et al., 2008). Therefore, solubility of these sources is assumed to be very low (<1%). Average annual radiation exposure and ocean pH are not expected to vary enough along the SR3 transect to influence solubility in any significant way. Average rainfall along SR3 ranges 1–4 $mm\ d^{-1}$, which is low-to-moderate compared to other regions of the ocean (Laboratory, 2013). The northern and southern regions of the SR3 transect are drier relative to the middle portion of the transect, and this could influence the relative solubility of dAl to those regions. Assuming solubility is proportional to precipitation, relatively solubility along the SR3 transect was estimated using an index of rainfall. Annually averaged daily precipitation ($mm\ d^{-1}$) estimates were retrieved from the NASA Goddard Space Flight Centre website (Laboratory, 2013). These estimates were converted to an index (0–1) relative to the maximum global daily precipitation values. As Han et al. (2008) selected 5% solubility to investigate global dAl concentrations using the DEAD-MADCOW model, the index was used to scale the 5% value along the SR3 transect, resulting in reasonable values within the range 0.7–1.2% (presented in Table 6.2).

6.2.6 Estimating stock dAl concentration

The pre-existing dAl concentration before aeolian deposition is difficult to estimate from observed data, and within the MADCOW model is assumed to be balanced by Sc. However, in the SO, where winter MLD can be very deep, entrainment of dAl into the ML from underlying waters must be

accounted for, as Sc has removed it from the summer ML (the season during which the box model is estimated to perform), but it has been returned during deepening of the winter ML. An attempt to quantify this in a relative way is presented below. From the dAl dataset available the mean dAl in the summer (A_s) and winter (A_w) MLs were calculated. A_s was taken as the mean dAl concentration in the summer ML (M_s). A_w was defined as the mean dAl concentration from below the summer ML, but within the winter ML (M_w). A simple subtraction ($A_s - A_w$) was not appropriate, as in this section of the SO, where surface values are very low, A_w was often larger than A_s , resulting in negative values which are not sensible. Therefore, the proportion of dAl in summer ML considered to be from *New Dust* was estimated as:

$$A_R = \frac{A_s}{A_s + A_w} \quad (6.4)$$

This always resulted in a fractional proportion between 0 and 1. When $A_w \ll A_s$, $A_R \approx 1$. This is true for areas of the global ocean where dust deposition is relatively high, like the mid-Atlantic, Mediterranean or north-Indian Oceans, which is where the data was sourced for testing and development of the MADCOW model. When $A_w \gg A_s$, $A_R \approx 0$. This would be typical of the SO, where the ML deepens substantially over winter, entraining underlying waters into the surface layers. The dAl concentration associated with aeolian deposition (now termed A' as it is different to the original A term) then becomes:

$$A' = A_s \times A_R \quad \text{or} \quad A' = \frac{A_s^2}{A_s + A_w} \quad (6.5)$$

Substituting A' into the MADCOW equation results in:

$$G = \frac{A' \times Sc \times M \times 1000}{D \times S} \quad \text{or} \quad G = \frac{A_s^2 \times Sc \times M \times 1000}{(A_s + A_w) \times D \times S} \quad (6.6)$$

6.3 Results and Discussion

6.3.1 Surface dAl concentrations: Comparison of observations to model output.

Estimates of dAl concentrations in the surface ocean along the SR3 transect by [Han et al. \(2008\)](#) and [van Hulst et al. \(2012\)](#) are compared to the observed values from SR3 and SAZ-Sense in

Figure 6.3. While Han et al. (2008) found a general increase from Antarctica to Tasmania, van Hulst et al. (2012) found much less latitudinal variability, with a maximum around -50°N.

The observations from SR3 strongly support estimates by van Hulst et al. (2012) across the entire transect, but especially south of the Polar Front (PF). However, van Hulst et al. (2012) overestimates dAl in the surface of the SAZ relative to both SR3 and SAZ-Sense, although only by about 2-fold, which is well within sampling and analytical error. The discrepancy is likely to be associated with assumptions regarding two parameters, MLD and scavenging rates. These factors are very well approximated south of the PF by their model, but this is not the case further north. The extreme MLD zone (where the largest differences were found between model estimates and observations) is a specific characteristic of the SAZ in the Australian Sector of the SO and is not a general ocean feature. It is not expected to have been considered (or well approximated) in a typical ocean GCM like NEMO. Also, van Hulst et al. (2012) used biogenic silica concentrations as a way of estimating scavenging rates. The SAZ is depleted in dissolved silica in the top 1000 m (see Figure 5.4f) and is bio-limiting in the euphotic zone, resulting in biomass being dominated by non-siliceous organisms (Nelson and Treguer, 1992; Nelson et al., 2002; Franck et al., 2000; de Salas et al., 2011; Westwood et al., 2011). However, this does not indicate limited productivity, with a substantial biomass from spring to autumn. Therefore, the model will have underestimated both the dilution factor (MLD) and the scavenging rate within the SAZ.

Observations did not support the estimates from Han et al. (2008) using DEAD-MADCOW. Agreement with SAZ-Sense observations near Tasmania is probably coincidental, as the evidence presented in Chapter 4 suggests higher values from recent bushfire-ash, or delivery from advected waters rather than dust at those locations. DEAD-MADCOW underestimated dAl concentrations south of -60°N, and overestimated dAl values north of -53°N. Han et al. (2008) applied the 5.0% solubility rate globally (which they acknowledged was probably too high for the SO south of Australia). Assuming 1.5% ($S = 0.133$) instead of 5% ($S = 0.04$) would account for almost all of the discrepancy north of -54°N, but this then further underestimates dAl surface concentrations south of -54°N (see Figure 6.3). Of the parameters used by the DEAD-MADCOW model, $S=1.5\%$ is a relatively good approximation given the current level of understanding. However, $M=30\text{m}$ and $Sc=0.2$ are probably not appropriate, and therefore contribute to the deviation of the model from the observations south of -54°N.

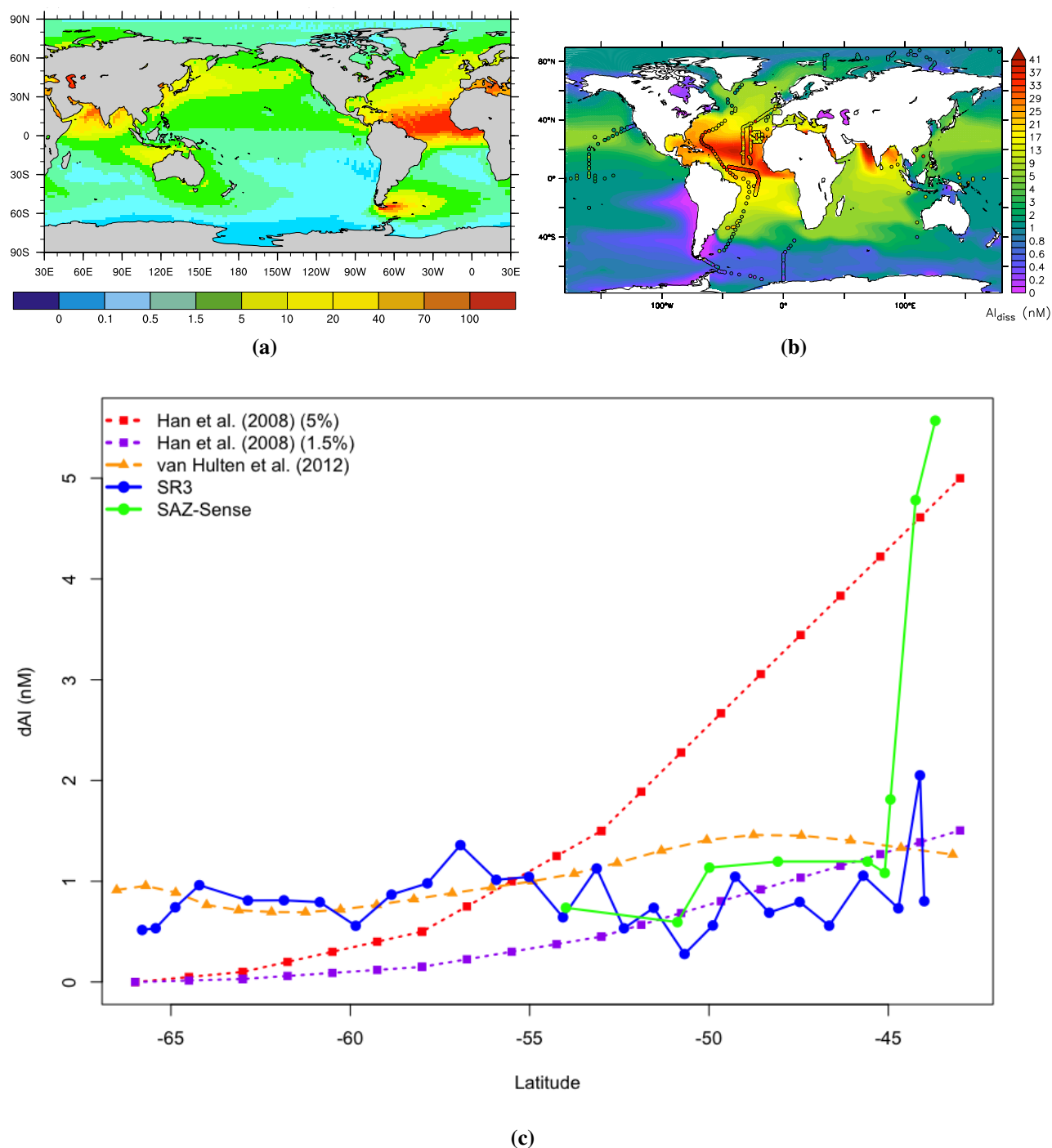


Figure 6.3: (a) Han et al. (2008) dAl concentration in surface oceans (0–30 m) from DEAD-MADCOW. (b) van Hulten et al. (2012) dAl concentration (nM) from the reference experiment at the surface ocean, with respective observations plotted on top of it. (c) Comparison of dAl concentrations observed along the SR3 transect to those estimated by Han et al. (2008) and van Hulten et al. (2012) (NB: Han et al. (2008) only published based on 5% solubility, the 1.5% solubility estimate presented was calculated from the 5% estimate as it is presented here).

Table 6.2: MADCOW input parameter values per station and the associated dust deposition estimates along the SR3 transect. M_s =summer MLD; M_w =winter MLD; Sc =scavenging rate; S =solubility; A =dAl in the summer ML; G_A =dust estimate given A ; A' =dAl in the summer ML additional to that supplied from underlying waters; $G_{A'}$ =dust estimate given A' , G_o =dust estimate given original parameter settings (A ; $M=30m$; $Sc=0.2$; $S=0.015$).

Station	Latitude °N	M_s m	M_w m	Sc % yr^{-1}	S %	A nM	A' nM	G_A $g\ m^{-2}\ yr^{-1}$	$G_{A'}$ $g\ m^{-2}\ yr^{-1}$	G_o $g\ m^{-2}\ yr^{-1}$
N 01	-65.803	148	228	0.956	0.008	0.52	0.25	3.08	1.50	0.07
N 02	-65.426	148	228	0.956	0.008	0.53	0.28	3.19	1.68	0.07
N 03	-64.879	92	143	0.956	0.008	0.74	0.31	2.75	1.16	0.10
N 04	-64.209	92	122	0.659	0.008	0.96	0.51	2.46	1.31	0.13
N 05	-62.855	77	126	0.659	0.010	0.81	0.52	1.38	0.90	0.11
N 06	-61.850	77	126	0.377	0.010	0.81	0.50	0.79	0.49	0.11
N 07	-60.850	74	138	0.377	0.012	0.79	0.45	0.62	0.35	0.11
N 08	-59.849	83	148	0.377	0.012	0.56	0.26	0.49	0.23	0.07
N 09	-58.851	83	148	0.377	0.012	0.87	0.40	0.76	0.35	0.12
N 10	-57.850	86	148	0.377	0.012	0.98	0.50	0.93	0.48	0.13
N 11	-56.930	106	174	0.377	0.012	1.36	0.36	1.59	0.43	0.18
N 12	-55.929	104	159	0.342	0.010	1.01	0.54	1.22	0.65	0.13
N 13	-55.020	105	158	0.342	0.010	1.04	0.48	1.26	0.58	0.14
N 14	-54.071	105	168	0.242	0.010	0.64	0.36	0.55	0.31	0.09
N 15	-53.132	104	168	0.242	0.010	1.13	0.71	1.01	0.64	0.15
N 16	-52.370	140	303	0.202	0.010	0.53	0.24	0.53	0.24	0.07
N 17	-51.540	154	377	0.252	0.010	0.74	0.51	1.01	0.70	0.10
N 18	-50.682	190	490	0.252	0.008	0.28	0.12	0.56	0.25	0.04
N 19	-49.892	190	485	0.252	0.008	0.56	0.27	1.13	0.55	0.07
N 20	-49.270	190	427	0.252	0.008	1.05	0.76	2.11	1.54	0.14
N 21	-48.320	136	494	0.252	0.007	0.69	0.25	1.14	0.41	0.09
N 22	-47.472	148	198	0.252	0.007	0.79	0.52	1.43	0.94	0.11
N 23	-46.650	148	198	0.252	0.007	0.56	0.31	1.01	0.55	0.07
N 24	-45.700	114	164	0.395	0.010	1.06	0.54	1.60	0.82	0.14
N 25	-44.720	114	164	0.395	0.010	0.73	0.40	1.11	0.60	0.10
N 26	-44.118	90	140	0.395	0.010	2.05	1.36	2.46	1.63	0.27
N 27	-43.999	54	104	0.395	0.010	0.80	0.29	0.58	0.21	0.11

6.3.2 Application of reasonable values for M , Sc and S per station using the MADCOW model

The MADCOW model was applied per station, with the values of M , Sc and S approximated as appropriate resulting in the dust deposition rate estimates presented in Table 6.2. These values are significantly different to those originally used by Measures and Brown (1996) and Measures and

Vink (2000) resulting in an order of magnitude increase in the estimated dust deposition rates. The values of M , Sc and S are presented as a relative proportion of the original estimates of MADCOW (where $M=30\text{m}$, $Sc=0.2$, $S=0.015$) in Figure 6.4a.

The individual effect of altering M , Sc and S per station is presented in Figure 6.4b. Between -67° and -60°N , dust deposition rate estimates are controlled in approximately equal measure by both M and Sc whereas between -60° and -43°N , they are controlled mostly by M . The variability of S (as it was defined and estimated by this study) along the SR3 transect was far less significant than the effect of M or Sc , which is not unexpected, given it varied the least from the original MADCOW values (see Figure 6.4a).

The combined impact of M , Sc and S on dust deposition rate estimates as they all co-varied per station is presented in Figure 6.4c. The potential influence of underlying waters potentially is also compared in this figure. Accounting for the influence underlying waters changes the general pattern of dust deposition rates observed, decreasing estimates at the Polar Front ($\sim -54^\circ\text{N}$). While this is significant, it is far less significant than the combined effect of M , Sc and S , which change the dust deposition rate estimates by an order of magnitude. These estimates were compared to those by DEAD and INCA in order to assess if this was reasonable.

6.3.3 DEAD and INCA vs. MADCOW

Dust deposition rate estimates from DEAD, INCA and MADCOW were compared (see Figure 6.5). MADCOW estimates using Equation 6.2 as originally set by Measures and Brown (1996) returned relatively reasonable dust estimates, but the M values are completely unrealistic. MADCOW estimates using geographically appropriate values for M , Sc and S at each station (see Table 6.2) resulted in unreasonable, very high dust deposition rate estimates compared to those from DEAD and INCA (atmospheric models). Stations N01 and N02 (closest to Antarctica) are found to have the highest dust deposition rates along the SR3 transect, which seems highly unreasonable, especially since both DEAD and INCA (and all other dust models actually) estimate that region to have the lowest dust deposition (see Figure 6.5c). This result is due to Sc being assumed to be highest in the highly productive, diatom dominated sea-ice zone (where $Chla$ and Si_M values were highest) and S is assumed to be lowest (due to very low rainfall). Both of these changes have a positive effect on dust deposition rates within the MADCOW model. M is also deeper than 30 m at those stations, which is also a positive effect.

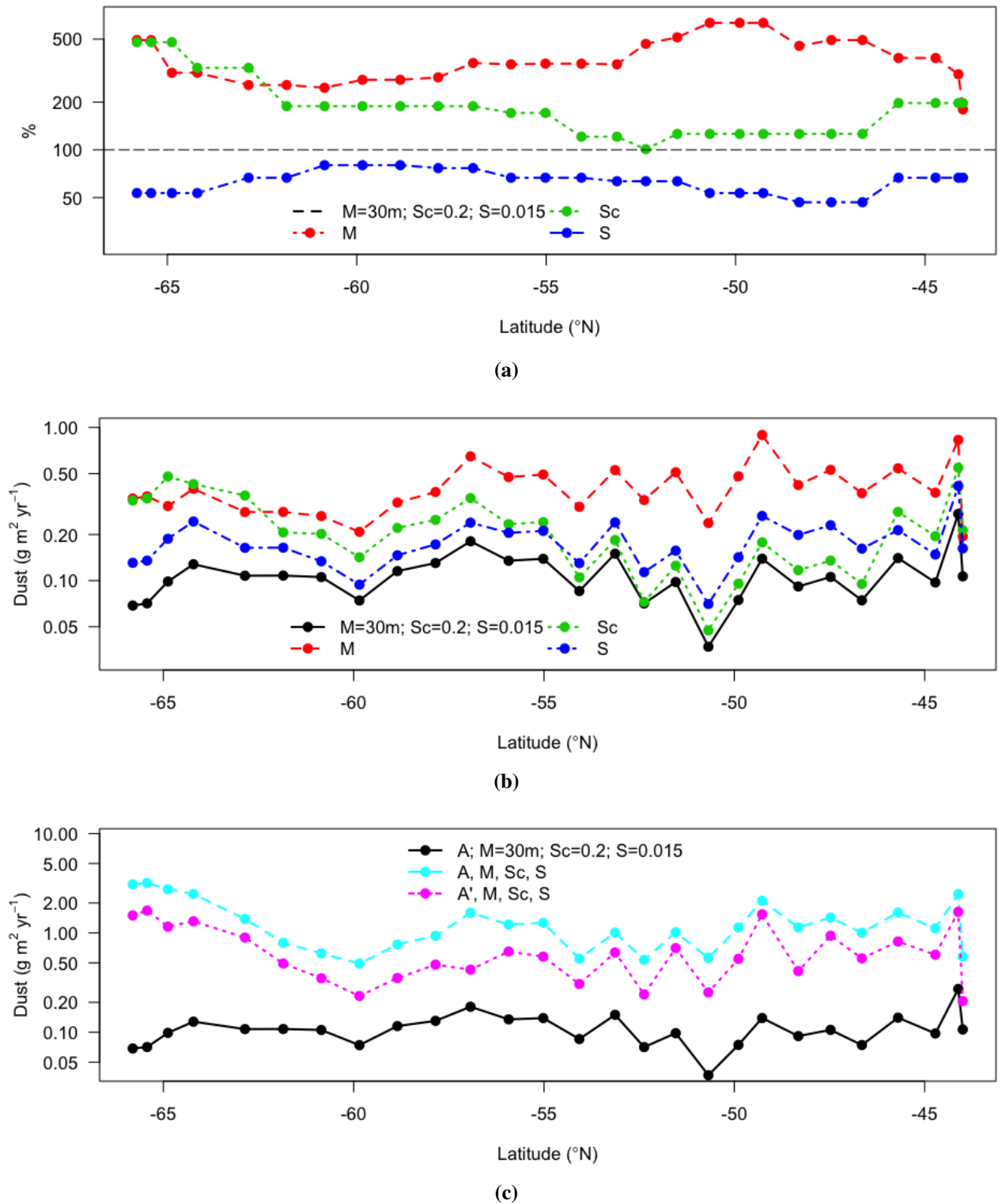


Figure 6.4: (a) Percentage change of M , Sc and S at each station relative to the original settings of the MADCOW model. (b) Individual impact of adjusting either M , Sc or S per station on the dust deposition rate estimates provided by the MADCOW model. (c) Combined impact of adjusting either M , Sc or S per station on the dust deposition rate estimates provided by the MADCOW model. The potential influence of underlying waters during winter is also compared (i.e. A vs. A').

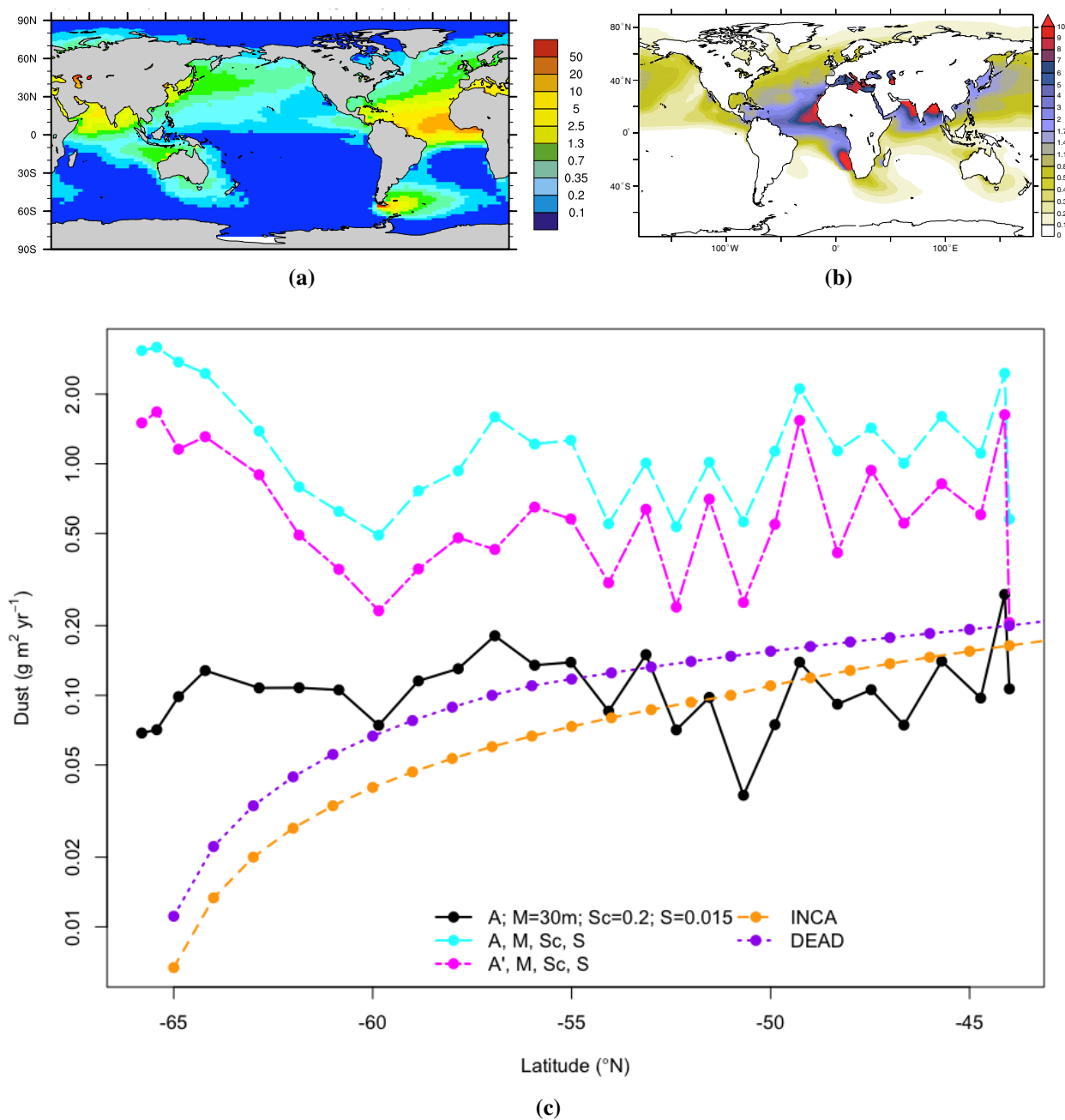


Figure 6.5: Comparison of aeolian deposition rate estimates ($g\ m^{-2}\ yr^{-1}$) from DEAD, INCA and MADCOW models.

The relatively poor performance of the MADCOW model when the variables are altered for the conditions in the SO requires a bit of investigation. As Sc and S were approximated in a coarse and simplistic manner, their relative effect can be discounted due to poor parameterisation and scaling. However, as discussed in Section 6.3.2, M has a very large influence on dust deposition rate estimates when applied in MADCOW. This is the result of very deep summer MLDs along SR3, resulting in high dilution factors when converting dAl to dust. Measures and Brown (1996) defend their choice to use the summer MLD (where $M=30\text{m}$) as the majority of scavenging is likely to occur during spring and summer due to increased SPM.

Although it is also expected that the majority of scavenging in the SO would occur in summer, it overlooks the fact that dilution effects during deepening of the ML could be far greater than the effect of scavenging in this region. In a real world sense, this is further compounded by the fact that if $R_t \geq 1$ then the dilution factor of interest should not be the summer ML, but the winter ML (as $M_s \ll M_w$ in some regions, such as the EMLDZ). When only real values of M are applied (i.e. Sc and S are kept constant) the MADCOW model converted some of the lowest surface dAl values (eg. Station N18, N19 and N21) into some of the the highest dust deposition estimates (data not presented).

As the MADCOW model assumes all dAl in the summer ML has been delivered by atmospheric dust deposition. Resupply from underlying waters during the deepening of the ML is not considered important. In regions of high dust deposition, it would not seem important, as entrainment of underlying waters would usually result in a decrease of surface dAl, not an increase. However, in the SO, the opposite may be true (as observed in the IPFZ). This does not need to rely on sedimentary sources eventually being entrained into the surface waters (such as is postulated to occur in the IPFZ), as the surface dAl is so depleted in the SO that globally low dAl concentrations (around 1–2 nM) in the underlying waters could actually resupply the surface (i.e. some dAl profiles in the SO exhibit a nutrient-like distribution). Underlying waters may accumulate dAl as SPM remineralises (especially when scavenged by non-siliceous particles) and these waters are then entrained into the dAl-depleted surface waters.

In this study, Sc was scaled relative to quasi-proxies of SPM. However, this attempt is admittedly inaccurate due to the failure of both Chla to accurately estimate SPM and Si_M to accurately represent biogenic silica formation in surface waters. These proxies also make no attempt to estimate SPM export from the ML (which is the actual mechanism of dAl removal). Although it would seem reasonable to assume SPM export is proportional to biomass, evidence from sediment traps along SR3 do not strictly support this assumption (Trull et al., 2001c,a,b, 2008b,a). Therefore

if the Sc term is instead used simply to offset the effect of the deeper ML (implying a longer residence time in surface waters): $Sc \sim 0.05$ (an R_t of ~ 20 years) where $M=80$ m (the average summer MLD along SR3); or $Sc \sim 0.033$ (an R_t of ~ 30 years) where $M=200$ m (the average winter MLD along SR3). Along the SR3 transect, during summer the MLD ranges ~ 50 – 200 m and in winter this range is ~ 100 – 500 m (Rosenberg, 2007, 2008; Herraiz-Borreguero and Rintoul, 2010, 2011a,b). The MADCOW model is not equipped to deal with this level of variability in the MLD, especially where the scavenging rate would be expected to increase (not decrease as is necessary to maintain reasonable estimates) in the regions where the estimates are most unreasonable (i.e. the sea-ice zone).

Given the investigation above it appears a few basic assumptions of the MADCOW model may not be met by conditions in the SO:

“... On the oceanic side, the main concern is sensitivity i.e., there must be a significant input into a relatively low background signal...” (Measures and Brown, 1996)

“... We have however eliminated data from the upwelling zone off N.W. Africa and at the equator since the Al poor upwelled waters cannot be considered to be in steady state with atmospheric input...” (Measures and Brown, 1996)

“The most serious short coming of our model is that it ignores the effect of advection of surface waters from one region to another. Clearly a water mass moving from a high[-dust] to a low[-dust] region is not in steady state and will reflect some average of the dust loadings in the two zones. In addition, a dust input calculated on the basis of a surface water Al content is an input to a parcel of water, rather than to a fixed geographic position. The short residence time of Al in surface waters will mitigate this problem. At this stage, we cannot eliminate these variables and accept that they will contribute to inaccuracy of predictions.” (Measures and Brown, 1996)

The MADCOW model is more the 20 years old and at that time the range of dAl concentrations available for comparison was very sparse indeed. As such, no attempt was made by Measures and Brown (1996) to define what a *significant input* or a *relatively low background signal* might be. It appears that the SO may provide a good example of a region with *insignificant inputs* relative to the *background signal* (in fact, the Australian Sector of the SO might be a region where the background signal of dAl might be estimated).

The deep winter MLDs within the SO may equate to a similar mechanism as the upwelling zone off N.W. Africa, especially in the EMLDZ, where surface concentrations are not in steady state with

the atmosphere due to interaction and influence from the deeper underlying waters, especially over periods greater than 1 year (which are required for use of the MADCOW model).

The fast moving ACC may influence the ability of the MADCOW model to accurately perform as the water masses are moving (and mixing) much faster than the assumed residence time (1–5 years), and especially if the residence time is closer to 20 years, which is not impossible (e.g. waters can be transported from near Kerguelen Island to the SR3 transect south of Tasmania, ~1500 km, in 6–7 months).

Any one of these assumptions not being met would seriously compromise the validity of using the MADCOW model to convert dAl concentrations into reliable dust deposition rate estimates. As it appears all three of these assumptions are not met, it appears the MADCOW model cannot be used to estimate dust deposition to the Australian sector of the Southern Ocean. Dissolved Al concentrations do have other uses in understanding the biogeochemistry of the Southern Ocean, however, it is the conclusion of this thesis that quantifying dust deposition is not one of them.

6.4 Conclusion

Model estimates of surface dAl concentrations by [van Hulst et al. \(2012\)](#) using the INCA-NEMO-PISCES model were well supported by observations along the SR3 transect. Deviations were largest in the SAZ, where the within model parameterisation of scavenging rates and MLDs did not match with the local conditions.

Model estimates of surface dAl concentrations by [Han et al. \(2008\)](#) using the DEAD-MADCOW model were not supported by observations along the SR3 transect. The DEAD-MADCOW model output produced a decreasing trend with increasing latitude, whereas observed dAl concentrations were relatively uniform across the SR3 transect, with minimal increasing or decreasing trends.

Dust deposition rate estimates were reasonable using the MADCOW model as presented by [Measures and Brown \(1996\)](#) and [Measures and Vink \(2000\)](#), (i.e. $G = 0.133 * A$ where $S=1.5\%$, intended for use in the mid-Atlantic). These estimates were in relatively good agreement with both DEAD and INCA model estimates of dust deposition rates along SR3. However, application of the model with parameters that were more appropriate for the SO resulted in extremely high dust deposition rate estimates and these were considered unreasonable. Investigation revealed the lack of variance of dAl observations with depth and latitude along the SR3 transect, coupled with the physical oceanographic conditions in the Australia sector of the SO invalidate many of the assumptions required by the MADCOW model. Therefore, dAl concentrations in the SO cannot be reliably used to quantify dust deposition rates into the SO.

Chapter

7

Conclusion and Future Work

7.1 Key goals and tasks

The goal of this project was to investigate the impact of aeolian deposition to the Australian Sector of the SO using dAl concentrations. This was broken down into five major aims which were:

- (i) To overcome the shortcomings of existing methods used for the determination of dAl in open ocean seawater samples.
- (ii) To investigate the distribution of dAl in the Australian sector of the SO.
- (iii) To conduct biogeochemical and oceanographic interpretation of these dAl concentrations to elucidate the relative contribution of various supply mechanisms to the waters sampled.
- (iv) To compare dAl observations in the SO to model estimates.
- (v) To estimate aeolian deposition of dust to the SO using dAl concentrations as a proxy (using MADCOW, or if necessary develop an alternative model) and subsequently compare these estimates to those from atmospheric models.

The problems addressed, the solutions found, the impact of these solutions and the subsequent future directions relating to each of these aims are described below.

7.1.1 To overcome the shortcomings of existing methods used for the determination of dAl in open ocean seawater samples

At the beginning of this project significant effort to establish either an FIA or HPCIC system (as previously described by [Resing and Measures \(1994\)](#); [Brown and Bruland \(2008\)](#); [Tria et al. \(2008b\)](#)) was unsuccessful, with both lacking robustness and reliability at sub-nM levels of Al in

seawater. This led to the novel application of monolithic column technology using a RP-HPLC technique. Previous methods using RP-HPLC had detection limits of around 20 nM and analysis times of 6–12 min per analysis depending on the method. These issues were addressed separately in two stages: (1) Reduction of analysis time (Chapter 2); (2) Reduction of the LOD (Chapter 3).

Analysis time was reduced from 6 min to 3 min by increasing the flow rate and co-eluting (instead of separating) the two species of Al-lumogallion complex. The use of a monolithic-silica-column in the place of a packed-bed-column achieved an improvement in separation efficiency (see Figure 2.4) and a decrease in analysis time from 6 to 5 min (or 17%). An investigation into the character of the two peaks observed found they both behaved linearly from 1 to 10,000 nM. There was no need to separate the two species, so analysis times were finally reduced from 6 to 3 min (or 50%) and this also improved the signal-to-noise ratio from >300 to >700. This work was published as [Remenyi et al. \(2011\)](#). Compared to the relevant FIA method by [Brown and Bruland \(2008\)](#), the RP-HPLC method was 65% faster (3 vs. 7.8 min) and used 95% less sample (1.5 vs. 36 mL) due to the comparatively low dead volumes possible within a HPLC system. However, the LOD was still not adequate to apply to open ocean samples.

Once analysis times had been reduced, an investigation into the sources of contamination influencing the LOD were conducted. To this point, trace-element-clean protocols had not been applied, as it was unnecessary during early stages of method development. Operating using trace-element-clean protocols required the simultaneous adaption of apparatus and reagents. Apparatus were changed from glass or metal to acid-cleaned-plastic (either LDPE or PP). All work was conducted under a laminar-flow-hood. *Analytical-grade* acids and bases were replaced with those of the highest available quality with regards to trace-element purity. The MES buffer was passed through a diphonix resin that significantly reduced the concentrations of almost all metals (certainly Al). These steps resulted in an improvement of the LOD from 250 to 0.13 nM (or 99.9%). This work was published as [Remenyi et al. \(2012\)](#).

The final RP-HPLC method presented in Chapters 2 and 3 is a robust, easily automated, fast method that minimises sample and reagent consumption relative to methods previously published. It provides a potential platform for the rapid shipboard analysis of large sample-sets (as it is yet to be tested at sea). It demonstrates the benefit of combining improved technology with well-developed existing chemistry to achieve improved analytical performance. This approach could easily be applied to other constituents of interest to the oceanographic community. However, this method is not perfect and should be viewed as a progressive step towards more controlled, robust and comprehensive multi-element approaches that can be applied shipboard or on autonomous samplers.

Future Work

Many questions and opportunities presented themselves during the development of the RP-HPLC system. These avenues for future investigation are presented below.

As discussed in Chapter 3, a major disadvantage of the RP-HPLC method described is the required pre-treatment time before analysis. The use of an automated sample dosing and injection system would reduce the time required for complex formation, whilst maintaining the large gains in robustness and automation. The authors would also expect an increase in sensitivity, as the time of maximum complex-yield could be targeted.

Two analytical species of Al–lumogallion complex were observed during the early stages of method development (see Figures 2.4, 2.5 and 2.7). These have been previously reported and subsequently ignored by Zhou et al. (1995); Wu et al. (1995); Lee et al. (1996). This project established (through fraction collection and re-injection) that they were two stable and different complexes. Attempts to structurally characterise and identify these two species were limited and unsuccessful. After preliminary tests failed (QTOF-MS, crystallisation, UV-Vis and fluorimetric spectral analysis) this was not pursued further as it was not within the scope of this project. Further work to structurally characterise and identify these species would determine if they could be of use as additional tools for environmental or medical studies.

As silica is most likely to be contaminated for Al, the successful application of a silica-monolith to determine dAl at <1 nM proves the purity of the silica-monolith used in Merck Chromolith® columns is excellent. Contamination problems with respect to other trace elements would be unexpected. The ability of IDA functional groups to selectively bind transition metals under low pH - high ionic strength conditions — such as sea water (NaCl 0.6 M) sampled for trace elements — has been well established (Nesterenko and Jones, 1996, 1997; Nesterenko and Shpigun, 2002; Sugrue et al., 2004; Jones and Nesterenko, 2008; Dias et al., 2010; Moyna et al., 2012). Tria et al. (2008b), described the success of using IDAS in a HPLC system to determine dAl. Nesterenko et al. (2012) took this idea further, functionalising a Chromolith® RP-18e Performance (100 × 4.6 mm) column with IDA groups, applied for the simultaneously determination of dissolved Mg, Ca and Sr concentrations in seawater. There are at least three potentially useful applications of this technology:

(1) The performance of a short monolithic column functionalised with IDA as a solid phase extraction component should be evaluated relative to those currently in common usage (eg. ICP-MS (Sohrin et al., 2008; Milne et al., 2010), FIA (Obata et al., 1993; de Jong et al., 1998; Brown

and Bruland, 2008)). These can be used with low-pressure pumps (Victory et al., 2004) and would probably improve inter-column performance (as the stationary phase is produced commercially), as well as improving extraction efficiency due to increased surface area.

(2) Development of a ship-board, multi-element analytical method for determination of transition-row elements in sea water. The performance should be evaluated of a Chromolith® RP-18e Performance (100 × 4.6 mm) column functionalised with IDA coupled with a non-selective detection system for metals (Williams and Barnett, 1992) to determine GEOTRACES key parameters in seawater after direct injection.

(3) Investigate the performance of the short monolithic column functionalised with IDA to directly pre-concentrate trace elements in seawater whilst *in situ*. If performance is sufficient and stable over time these could be deployed on moorings, recovered and analysed by ICP-MS (Milne et al., 2010; Sohrin et al., 2008), to obtain data on the seasonal variability of trace elements at target locations such as the time-series sites off Maria Island, or the Pulse mooring (~140°E, 45°S).

There are many analytical techniques available that have not yet been broadly applied to oceanographic analyses. Two of particular note are capillary electrophoresis and the use of plate readers. Preliminary studies to further the work by Riaz et al. (2003); Riaz and Chung (2005) are currently underway, investigating the use of capillary electrophoresis for direct determination of a range of transition metals in seawater. This work is led by Assoc. Prof. Michael Breadmore at the University of Tasmania. For progress please contact him directly. Plate readers are analytical instruments that take advantage of rapid, sensitive chemical reactions to analyse large sample-sets (~100) in short time periods (~1 hr). Recent work by Dr. Zanna Chase and her student Axel Durand investigates the application of plate reader techniques for the direct analysis of coastal seawater (Durand et al., 2013). There is significant scope for the adaption of such an approach for the deployment on autonomous vehicles for the investigation of trace metals in estuarine and coastal systems. The LOD of this technique is currently limited without incorporating preconcentration, so the application to open ocean environments is less probable at this stage.

7.1.2 To investigate the distribution of dAl in the Australian sector of the SO

The distribution of dAl in the Australian sector of the SO has not been investigated prior to this project. This represented a major deficiency in the understanding of the global biogeochemical cycling of Al.

The first high-resolution data-set of dAl in the Australian sector of the SO was generated by this project. Over 440 samples were collected from 40 stations between Antarctica and Tasmania in

Summer 2007 and Autumn 2008. This project determined the dAl concentration in each of these samples and contributed this data-set to the GEOTRACES Data Centre (GDAC) and is intended to be included in the *Intermediate Data Product* from GDAC to be released in 2014. This data will be openly accessible.

This project found the range of dAl in the Australian sector of the SO was from ~ 0.1 nM (below LOD) to ~ 4.0 nM, which is very low compared to other ocean basins (0.1–180 nM, see Figure 1.10a). Concentrations were relatively uniform across the entire transect due to the extremely low concentrations. However the trends that were observed were latitudinal, with major differences observed between the sub-zones separated by the oceanographic fronts.

The generation of this dAl data-set provides a baseline study for future work. It provides observations that can now be compared to model estimates, so that current biogeochemical mechanisms that influence Al can be tested and improved.

Future Work

This study is the first investigation into the distribution of dAl in the Australian Sector of the SO. However, there are many regions within this sector that require further study. How the continental shelf influences the biogeochemical cycling of Al in coastal and open ocean waters is poorly understood. In order to better understand these processes and how they impact on the productivity of Australia's Exclusive Economic Zone (EEZ) requires more field observations to constrain current models.

The international GEOTRACES program has been very successful in standardising analytical methods and protocols to produce high quality, inter-comparable data. However, the methods and protocols to handle, manipulate and estimate error associated with the data produced are not yet standardised. Addition of suggested data processing methods to the GEOTRACES cook book (possibly in the form of *functions* such as the *GSW 3.0* package (by Trevor McDougall et. al.), used by physical oceanographers for data handling in MATLAB) would be beneficial to the community, as would agreement on what the most appropriate methods are for data processing and error estimation. Using the open source program *R* as a repository could be a possible part of the solution, given the recent work by *Dan E. Kelley* to develop the *oce* package, for manipulation and visualisation of oceanographic data sets (<http://cran.r-project.org/web/packages/oce/index.html>).

7.1.3 To conduct biogeochemical oceanographic interpretation of these dAl concentrations to elucidate the relative contribution of various supply mechanisms to the waters sampled

Through the creation of the high-resolution data-set discussed above, an investigation into the biogeochemical cycling of Al in the Australian sector of the SO was conducted. The trends observed in the dAl data set were compared to previously observed physical and biogeochemical mechanisms in SO to assess their relevance to dAl distribution.

Concentrations of dAl were very low, which is assumed to be associated with limited aeolian deposition of dust (but could also be due to the scavenging rates exceeding the rate of supply). As dust is limited, the distribution of dAl was primarily controlled through watermass movements (lateral advection and upwelling). Mean flow in an west-to-east direction is relatively strong within the ACC and this resulted in latitudinal gradients observed in the dAl distribution between Antarctica and Tasmania (no evidence of north-south lateral advection influencing the dAl signature was observed).

However, north of the STF, the north-south lateral advection of waters within the EAC were found to dramatically influence dAl concentrations, this may have also influenced the northern part of the SAZ if eddies managed to cross the STF. The EAC is likely to be entrained with dAl from fluvial, sedimentary and aeolian sources as it travels along the east-coast of Australia. Influence from fluvial sources into the EAC are unlikely to be observed by 40° S. However, sedimentary and aeolian sources can be transported great distances once entrained. Sedimentary sources along the Australian Continental Shelf especially within the highly dynamic and shallow region called the Bass Strait, can become incorporated in the EAC and is transported south past Tasmania. However, the contribution of resuspended sediments to the dAl pool was not elucidated due to the absence of Mn data. Aeolian deposition into the EAC is also probable, as it passes through the SE-atmospheric pathway (Mackie et al., 2008; Boyd et al., 2010). So significant enrichment of the EAC is expected, and concentrations of dAl seemed to reflect this.

The highest concentrations of dAl observed during this study were observed in the STZ, closest to Tasmania during the SAZ-Sense process study. Associated observations from satellite measurements, field aerosol observations (the aeroSAZ samples) and HYSPLIT reanalysis modelling all suggest it is likely bushfire ash could have influenced dAl concentrations between Tasmania and P3 (and beyond). This could also explain the heterogeneous nature of the dAl distribution in the region, as the ash would not be expected to be distributed uniformly. Unfortunately, the aeroSAZ samples collected were not analysed for black carbon, which could have given further support to these ideas.

Maximum concentrations within the SO were observed in surface waters close to Tasmania and surprisingly within the IPFZ. Upwelling within the IPFZ was observed to increase surface dAl concentrations, similar to patterns observed in other trace elements and nutrients. This is expected to be due to a distant sub-surface supply of dAl being upwelled, rather than its use as a micronutrient and subsequent redissolution (although possible). The IPFZ has been postulated to be a cohesive pathway of waters that crosses over the Kerguelen Plateau before meandering towards its intersection with 140°E (Parslow et al., 2001). The strong zonal demarcation of the ACC, coupled with the fastflow from west-to-east makes the sedimentary supply of dAl from the Kerguelen Plateau to the IPFZ at 140°E unexpectedly probable, but this does agree with the postulations from Parslow et al. (2001) and Sokolov and Rintoul (2007a,b).

Minimum concentrations were observed within the EMLDZ of the SAZ probably due to the diluting effect of the deeper ML during winter. As Al has a residence time of 1-3 years in the surface layers, it is unsurprising such a strong physical annual feature influences deep into the water column, rather than just the surface. This is the first investigation to observe and report a significant influence of the EMLDZ on a biogeochemical constituent.

Concentrations were also extremely low in the SZ correlating with sea ice formation. This may be due to a combination of limited aeolian supply and enhanced scavenging in the region. In winter, during sea ice formation, the frazzle-ice particles may act as adsorption sites for dAl, so it is stripped out of solution. Once formed, the sea ice acts as a lid, collecting aeolian deposited dust. These two processes may explain the enrichment of Al in sea ice relative to the underlying watercolumn. Then when the sea ice melts in summer, the subsequent enhanced particulate concentrations of the spring phytoplankton bloom rapidly scavenges dAl, removing it from the dissolved phase, and transporting it to depth.

The first biogeochemical interpretation of dAl in the Australian Sector of the SO has provided a basis upon which current ideas can be revised, or new ideas can be introduced. The suggestion that sedimentary sources of dAl can be transported large distances from the Kerguelen Plateau is novel but requires further investigation and validation. It must be noted this effect is only observable because of the extremely low concentrations across the entire transect. A similar process elsewhere may be undetectable due to the dominance of fluvial or aeolian supply mechanisms (either absent, or limited in the IPFZ).

Future Work

The effect of the EMLDZ on biological process has not been investigated. Modelling of NPDZ characteristics of the SAZ-Sense process study by Kidston et al. (2011) did not incorporate this

aspect, or eddy-induced ML formation (as presented by [Mahadevan et al. \(2012\)](#)) as these ideas were not yet available. Re-analysis of the NPDZ model after incorporating these mechanisms may explain the difference in biomass from P1 vs. P3, without the need for different trace element supply mechanisms.

Trace elemental composition of bushfire smoke and ash is currently very poorly delineated. Bushfires (wild fires) as a source of trace elements to the ocean have not been thoroughly investigated in the literature (with a few exceptions ([Guieu et al., 2005](#); [Luo et al., 2008](#); [Ito, 2011](#)), but even then the data available is extremely limited). This is an area that could use more work. Tracers of bushfire ash in seawater have not been characterised or investigated and would be useful in quantifying trace element delivery mechanisms, and the impact of bushfires on ocean productivity and biomass.

The concentration of dAl observed from SAZ-Sense and SR3 were extremely low with little variability with depth. This prompted the questions: *What is the background concentration of dAl in the seawater?*, and *When is dAl no longer useful as a proxy for dust?*. A theoretical framework, or model to assess the validity of using dAl as a proxy for dust needs to be developed. This may include regional assessment of parameters such as: dAl concentration (too low and it becomes qualitative, simply indicating very limited dust); scavenging rates (above which dAl no longer represents dust inputs); solubility rates (too low and the error associated with dust estimation becomes too large); and biological uptake rates (if proven).

7.1.4 To compare dAl observations in the SO to model estimates

Although there have been many recent attempts to model the biogeochemical cycling of Al through the Australian sector of the SO, data to assess the validity of the assumptions and estimates within the models was not available at the beginning of this project. Observed surface dAl concentrations along the SR3 transect were compared to the most recent modelling studies by [Han et al. \(2008\)](#) and [van Hulst et al. \(2012\)](#).

Modelling by [Han et al. \(2008\)](#) (DEAD-MADCOW) overestimated surface dAl concentrations in the SO. This was probably because it overestimated the solubility of Al delivered in dust and underestimated dilution (MLD) and scavenging rates. Modelling by [van Hulst et al. \(2012\)](#) (NEMO-PISCES) was much more sophisticated and consequently had much better agreement with observations. Agreement between the NEMO-PISCES model and the observed data is excellent south of the Polar Front, where the model assumptions and mechanisms are appropriate (where [van](#)

[Hulten et al. \(2012\)](#) use biogenic silica concentrations to estimate scavenging). However, differences between observations and model estimates are much greater in the SAZ and surrounding Tasmania. In the EMLDZ of the SAZ, the NEMO-PISCES model overestimated dAl, probably because the dilution factor applied in their model is too low. However around Tasmania, the model substantially underestimates dAl. This could be due to either an underestimate of sources, or an overestimate of sinks. The biogenic silica field used to estimate scavenging in the NEMO-PISCES model is ~ 5 -fold greater than observations in the SAZ and the STZ ([Rosenberg, 2007, 2008](#)). The associated scavenging rate will also be too large (interestingly this does not correct the overestimated values observed in the EMLDZ of the SAZ). It is likely that the source mechanisms in the NEMO-PISCES model underestimate entrainment within the EAC, and almost certainly do not account for supply from bushfires.

Future Work Further understanding and methods for estimating scavenging / redissolution rates are required for accurate modelling. Within the NEMO-PISCES model, [van Hulten et al. \(2012\)](#) estimate scavenging using biogenic silica concentrations. This approach is obviously not appropriate in regions dominated by carbonaceous organisms, and therefore, scavenging estimates are underestimated. By developing an index that incorporates both biogenic silica and seasonal biomass estimates from some other measure (such as ocean colour from satellite measurements) a more accurate estimate of scavenging in non-siliceous dominated phytoplankton communities may be achieved, improving the performance of the NEMO-PISCES model. Incorporating parameters for bushfire and sedimentary sources of Al is difficult as observations and associated understanding of these process are extremely limited.

7.1.5 To estimate aeolian deposition of dust to the SO using dAl concentrations as a proxy (using MADCOW, or if necessary develop an alternative model) and subsequently compare these estimates to those from atmospheric models

It is not currently practical to directly measure the rate of aeolian deposition of dust to the SO so a variety of methods to indirectly estimate it have been developed. These indirect methods invariably have greater uncertainty over the polar regions than over the equatorial regions and as such, comparison of these methods with each other is useful to constrain their uncertainty. Surface dAl concentrations from the open ocean have been demonstrated to be a good proxy of dust deposition using the MADCOW model ([Measures and Brown, 1996](#)).

Dust deposition rate estimates using the MADCOW model without adjusting the original parameters (intended for use in the mid-Atlantic) were reasonable, and in relatively good agreement with both

DEAD and INCA model estimates. However, application of the model with M , Sc and S parameters that were more appropriate for the SO resulted in extremely high dust deposition rate estimates and these were considered unreasonable. Investigation revealed the lack of variance of dAl observations with depth and latitude along the SR3 transect, coupled with the physical oceanographic conditions in the Australia sector of the SO invalidate many of the assumptions required by the MADCOW model. Therefore, dAl concentrations in the SO cannot be used as inputs to the MADCOW model to quantify dust deposition rates into the SO.

Given the lack of quality satellite observation of dust deposition over the SO and the infrequent collection of aerosol concentrations in the SO, there are currently no reliable methods for estimating dust deposition to the SO. The best estimates of trace element availability in the SO is from direct measurement of water samples.

APPENDIX A – COST OF THERMAL PERFORMANCE IMPROVEMENTS

Appendix A contains:

Cost of design changes to achieve a rating of 5-6 stars

Appendix

A

Dissolved Aluminium Data collected during this project

Table A.1: Dissolved aluminium data collected during the SAZSense voyage (GEOTRACES voyage GIPY2). Samples were collected using the Trace Metal Rosette (TMR). These were separate operations to the CTD casts, and as such have different station numbers.

QF = Quality Flag; 0 = *good*; 2 = *<LOD*; 4 = *suspect*; 8 = *bad*.

Cruise	Station No.		Date & Time	Lon. (°E)	Lat. (°N)	Depth (m)	dAl (nM)	QF
	TMR	CTD						
AA0307	2b	4	2007-01-20T16:53	143.03	-44.95	15	0.88	0
AA0307	2b	4	2007-01-20T16:53	143.03	-44.95	25	0.37	0
AA0307	2b	4	2007-01-20T16:53	143.03	-44.95	50	0.52	0
AA0307	2b	4	2007-01-20T16:53	143.03	-44.95	75	0.59	0
AA0307	2b	4	2007-01-20T16:53	143.03	-44.95	100	0.41	0
AA0307	2b	4	2007-01-20T16:53	143.03	-44.95	125	0.31	0
AA0307	2b	4	2007-01-20T16:53	143.03	-44.95	150	0.29	0
AA0307	2b	4	2007-01-20T16:53	143.03	-44.95	200	0.58	0
AA0307	2b	4	2007-01-20T16:53	143.03	-44.95	300	0.48	0
AA0307	2b	4	2007-01-20T16:53	143.03	-44.95	500	0.42	0
AA0307	2b	4	2007-01-20T16:53	143.03	-44.95	700	0.64	0
AA0307	2b	4	2007-01-20T16:53	143.03	-44.95	1000	1.23	0
AA0307	4a	11	2007-01-22T18:25	140.46	-46.28	15	0.29	0
AA0307	4a	11	2007-01-22T18:25	140.46	-46.28	25	0.29	0
AA0307	4a	11	2007-01-22T18:25	140.46	-46.28	50	0.43	0
AA0307	4a	11	2007-01-22T18:25	140.46	-46.28	75	0.34	0
AA0307	4a	11	2007-01-22T18:25	140.46	-46.28	100	0.41	0
AA0307	4a	11	2007-01-22T18:25	140.46	-46.28	125	0.40	0
AA0307	4a	11	2007-01-22T18:25	140.46	-46.28	150	0.63	0
AA0307	4a	11	2007-01-22T18:25	140.46	-46.28	200	0.45	0
AA0307	4a	11	2007-01-22T18:25	140.46	-46.28	300	0.70	0
AA0307	4a	11	2007-01-22T18:25	140.46	-46.28	500	0.45	0

Continued on next page

Table A.1 – continued from previous page

Cruise	Station No.		Date & Time	Lon. (°E)	Lat. (°N)	Depth (m)	dAl (nM)	QF
	TMR	CTD						
AA0307	4a	11	2007-01-22T18:25	140.46	-46.28	700	0.69	0
AA0307	4a	11	2007-01-22T18:25	140.46	-46.28	1000	0.88	0
AA0307	5	36	2007-01-29T23:15	143.00	-49.00	15	0.64	0
AA0307	5	36	2007-01-29T23:15	143.00	-49.00	25	0.70	0
AA0307	5	36	2007-01-29T23:15	143.00	-49.00	50	0.85	0
AA0307	5	36	2007-01-29T23:15	143.00	-49.00	75	1.47	0
AA0307	5	36	2007-01-29T23:15	143.00	-49.00	100		8
AA0307	5	36	2007-01-29T23:15	143.00	-49.00	125	0.36	0
AA0307	5	36	2007-01-29T23:15	143.00	-49.00	150	0.44	0
AA0307	5	36	2007-01-29T23:15	143.00	-49.00	200	0.54	0
AA0307	5	36	2007-01-29T23:15	143.00	-49.00	300	0.64	0
AA0307	5	36	2007-01-29T23:15	143.00	-49.00	500	0.58	0
AA0307	5	36	2007-01-29T23:15	143.00	-49.00	700	0.58	0
AA0307	5	36	2007-01-29T23:15	143.00	-49.00	1000	1.24	0
AA0307	6a	38	2007-02-01T08:53	145.92	-53.99	15	0.43	0
AA0307	6a	38	2007-02-01T08:53	145.92	-53.99	25	1.01	0
AA0307	6a	38	2007-02-01T08:53	145.92	-53.99	50	0.28	0
AA0307	6a	38	2007-02-01T08:53	145.92	-53.99	75	0.28	0
AA0307	6a	38	2007-02-01T08:53	145.92	-53.99	100	0.25	0
AA0307	6a	38	2007-02-01T08:53	145.92	-53.99	125	1.84	0
AA0307	6a	38	2007-02-01T08:53	145.92	-53.99	150	1.23	0
AA0307	6a	38	2007-02-01T08:53	145.92	-53.99	200	0.38	0
AA0307	6a	38	2007-02-01T08:53	145.92	-53.99	300	0.44	0
AA0307	6a	38	2007-02-01T08:53	145.92	-53.99	500	0.11	2
AA0307	6a	38	2007-02-01T08:53	145.92	-53.99	700	0.17	0
AA0307	6a	38	2007-02-01T08:53	145.92	-53.99	1000	0.30	0
AA0307	9	64	2007-02-08T06:52	148.65	-50.88	15	0.55	0
AA0307	9	64	2007-02-08T06:52	148.65	-50.88	25	0.45	0
AA0307	9	64	2007-02-08T06:52	148.65	-50.88	40	0.41	0
AA0307	9	64	2007-02-08T06:52	148.65	-50.88	60	0.24	0
AA0307	9	64	2007-02-08T06:52	148.65	-50.88	75	0.61	0
AA0307	9	64	2007-02-08T06:52	148.65	-50.88	100	0.11	2

Continued on next page

Table A.1 – continued from previous page

Cruise	Station No.		Date & Time	Lon. (°E)	Lat. (°N)	Depth (m)	dAl (nM)	QF
	TMR	CTD						
AA0307	9	64	2007-02-08T06:52	148.65	-50.88	125	0.38	0
AA0307	9	64	2007-02-08T06:52	148.65	-50.88	150	0.10	2
AA0307	9	64	2007-02-08T06:52	148.65	-50.88	175	0.36	0
AA0307	9	64	2007-02-08T06:52	148.65	-50.88	200	0.52	0
AA0307	9	64	2007-02-08T06:52	148.65	-50.88	225	0.16	0
AA0307	9	64	2007-02-08T06:52	148.65	-50.88	250	0.32	0
AA0307	10	66	2007-02-09T00:45	149.43	-49.99	15	0.69	0
AA0307	10	66	2007-02-09T00:45	149.43	-49.99	25	0.45	0
AA0307	10	66	2007-02-09T00:45	149.43	-49.99	40	0.13	0
AA0307	10	66	2007-02-09T00:45	149.43	-49.99	60	0.71	0
AA0307	10	66	2007-02-09T00:45	149.43	-49.99	75	0.27	0
AA0307	10	66	2007-02-09T00:45	149.43	-49.99	100	0.33	0
AA0307	10	66	2007-02-09T00:45	149.43	-49.99	125	0.35	0
AA0307	10	66	2007-02-09T00:45	149.43	-49.99	150	0.59	0
AA0307	10	66	2007-02-09T00:45	149.43	-49.99	175	2.47	0
AA0307	10	64	2007-02-09T00:45	149.43	-49.99	200	1.95	0
AA0307	10	66	2007-02-09T00:45	149.43	-49.99	225	1.14	0
AA0307	10	66	2007-02-09T00:45	149.43	-49.99	250	0.32	0
AA0307	12	71	2007-02-10T03:05	151.19	-48.08	15	0.67	0
AA0307	12	71	2007-02-10T03:05	151.19	-48.08	25	0.56	0
AA0307	12	71	2007-02-10T03:05	151.19	-48.08	40	0.19	0
AA0307	12	71	2007-02-10T03:05	151.19	-48.08	60	1.02	0
AA0307	12	71	2007-02-10T03:05	151.19	-48.08	75	0.59	0
AA0307	12	71	2007-02-10T03:05	151.19	-48.08	100	1.04	0
AA0307	12	71	2007-02-10T03:05	151.19	-48.08	125	1.59	0
AA0307	12	71	2007-02-10T03:05	151.19	-48.08	150	0.39	0
AA0307	12	71	2007-02-10T03:05	151.19	-48.08	175	0.67	0
AA0307	12	71	2007-02-10T03:05	151.19	-48.08	200	2.40	0
AA0307	12	71	2007-02-10T03:05	151.19	-48.08	225	0.85	0
AA0307	12	71	2007-02-10T03:05	151.19	-48.08	250	1.28	0
AA0307	17b	79	2007-02-11T15:15	153.17	-45.56	15	4.74	0
AA0307	17b	79	2007-02-11T15:15	153.17	-45.56	25	4.78	0

Continued on next page

Table A.1 – continued from previous page

Cruise	Station No.		Date & Time	Lon. (°E)	Lat. (°N)	Depth (m)	dAl (nM)	QF
	TMR	CTD						
AA0307	17b	79	2007-02-11T15:15	153.17	-45.56	50	3.03	0
AA0307	17b	79	2007-02-11T15:15	153.17	-45.56	75		8
AA0307	17b	79	2007-02-11T15:15	153.17	-45.56	100	6.89	0
AA0307	17b	79	2007-02-11T15:15	153.17	-45.56	150	3.17	0
AA0307	17b	79	2007-02-11T15:15	153.17	-45.56	200	4.29	0
AA0307	17b	79	2007-02-11T15:15	153.17	-45.56	300	4.54	0
AA0307	17b	79	2007-02-11T15:15	153.17	-45.56	500	5.56	0
AA0307	17b	79	2007-02-11T15:15	153.17	-45.56	700	5.46	0
AA0307	17b	79	2007-02-11T15:15	153.17	-45.56	1000	4.42	0
AA0307	19	85	2007-02-13T19:05	153.27	-45.10	15	0.81	0
AA0307	19	85	2007-02-13T19:05	153.27	-45.10	25	1.19	0
AA0307	19	85	2007-02-13T19:05	153.27	-45.10	50	0.98	0
AA0307	19	85	2007-02-13T19:05	153.27	-45.10	75	1.41	0
AA0307	19	85	2007-02-13T19:05	153.27	-45.10	100	1.56	0
AA0307	19	85	2007-02-13T19:05	153.27	-45.10	150	1.35	0
AA0307	19	85	2007-02-13T19:05	153.27	-45.10	200	2.82	0
AA0307	19	85	2007-02-13T19:05	153.27	-45.10	300	0.83	0
AA0307	19	85	2007-02-13T19:05	153.27	-45.10	500	2.19	0
AA0307	21	93	2007-02-14T14:40	152.49	-44.94	15	1.79	0
AA0307	21	93	2007-02-14T14:40	152.49	-44.94	25	0.28	0
AA0307	21	93	2007-02-14T14:40	152.49	-44.94	50	0.26	0
AA0307	21	93	2007-02-14T14:40	152.49	-44.94	75	1.10	0
AA0307	21	93	2007-02-14T14:40	152.49	-44.94	100	0.91	0
AA0307	21	93	2007-02-14T14:40	152.49	-44.94	125	0.62	0
AA0307	21	93	2007-02-14T14:40	152.49	-44.94	150	1.01	0
AA0307	21	93	2007-02-14T14:40	152.49	-44.94	200	1.82	0
AA0307	21	93	2007-02-14T14:40	152.49	-44.94	300	1.11	0
AA0307	21	93	2007-02-14T14:40	152.49	-44.94	500	1.45	0
AA0307	21	93	2007-02-14T14:40	152.49	-44.94	700	1.21	0
AA0307	17j	96	2007-02-17T01:15	153.72	-45.58	15	0.59	0
AA0307	17j	96	2007-02-17T01:15	153.72	-45.58	25	2.45	0
AA0307	17j	96	2007-02-17T01:15	153.72	-45.58	50	1.20	0

Continued on next page

Table A.1 – continued from previous page

Cruise	Station No.		Date & Time	Lon. (°E)	Lat. (°N)	Depth (m)	dAl (nM)	QF
	TMR	CTD						
AA0307	17j	96	2007-02-17T01:15	153.72	-45.58	75	0.85	0
AA0307	17j	96	2007-02-17T01:15	153.72	-45.58	100	0.20	0
AA0307	17j	96	2007-02-17T01:15	153.72	-45.58	150	2.37	0
AA0307	17j	96	2007-02-17T01:15	153.72	-45.58	200	1.15	0
AA0307	17j	96	2007-02-17T01:15	153.72	-45.58	300	0.95	0
AA0307	17j	96	2007-02-17T01:15	153.72	-45.58	500	0.35	0
AA0307	17j	96	2007-02-17T01:15	153.72	-45.58	700	0.76	0
AA0307	17j	96	2007-02-17T01:15	153.72	-45.58	1000	0.95	0
AA0307	23	105	2007-02-18T17:30	150.20	-44.24	15	3.55	0
AA0307	23	105	2007-02-18T17:30	150.20	-44.24	25	3.02	0
AA0307	23	105	2007-02-18T17:30	150.20	-44.24	50	4.80	0
AA0307	23	105	2007-02-18T17:30	150.20	-44.24	75	3.38	0
AA0307	23	105	2007-02-18T17:30	150.20	-44.24	100	5.37	0
AA0307	23	105	2007-02-18T17:30	150.20	-44.24	150	4.15	0
AA0307	23	105	2007-02-18T17:30	150.20	-44.24	200	2.89	0
AA0307	23	105	2007-02-18T17:30	150.20	-44.24	300	6.10	0
AA0307	23	105	2007-02-18T17:30	150.20	-44.24	500	4.68	0
AA0307	23	105	2007-02-18T17:30	150.20	-44.24	700	4.71	0
AA0307	23	105	2007-02-18T17:30	150.20	-44.24	1000	4.81	0
AA0307	24	108	2007-02-19T16:45	148.58	-43.69	15	5.59	0
AA0307	24	108	2007-02-19T16:45	148.58	-43.69	25	6.27	0
AA0307	24	108	2007-02-19T16:45	148.58	-43.69	50	7.34	0
AA0307	24	108	2007-02-19T16:45	148.58	-43.69	75	5.26	0
AA0307	24	108	2007-02-19T16:45	148.58	-43.69	100	4.87	0
AA0307	24	108	2007-02-19T16:45	148.58	-43.69	150	5.13	0
AA0307	24	108	2007-02-19T16:45	148.58	-43.69	200	5.61	0
AA0307	24	108	2007-02-19T16:45	148.58	-43.69	300	7.08	0
AA0307	24	108	2007-02-19T16:45	148.58	-43.69	500	5.14	0
AA0307	24	108	2007-02-19T16:45	148.58	-43.69	700	5.72	0
AA0307	24	108	2007-02-19T16:45	148.58	-43.69	1000	5.15	0

Table A.2: Dissolved aluminium data collected during the WOCE SR3 repeat transect voyage (GEOTRACES voyage GIPY6). Samples were collected using the Trace Metal Rosette (TMR). These were separate operations to the CTD casts, and as such have different station numbers.

QF = Quality Flag; 0 = *good*; 2 = *<LOD*; 4 = *suspect*; 8 = *bad*.

Cruise	Station No.		Date & Time	Lon. (°E)	Lat. (°N)	Depth (m)	dAl (nM)	QF
	TMR	CTD						
Au 08 / 06	N 01	4	2008-03-28T22:00	139.68	-65.80	15	0.64	0
Au 08 / 06	N 01	4	2008-03-28T22:00	139.68	-65.80	25	0.46	0
Au 08 / 06	N 01	4	2008-03-28T22:00	139.68	-65.80	50	0.69	0
Au 08 / 06	N 01	4	2008-03-28T22:00	139.68	-65.80	75	0.48	0
Au 08 / 06	N 01	4	2008-03-28T22:00	139.68	-65.80	100	0.39	0
Au 08 / 06	N 01	4	2008-03-28T22:00	139.68	-65.80	125	0.45	0
Au 08 / 06	N 01	4	2008-03-28T22:00	139.68	-65.80	150	0.50	0
Au 08 / 06	N 01	4	2008-03-28T22:00	139.68	-65.80	200	0.59	0
Au 08 / 06	N 01	4	2008-03-28T22:00	139.68	-65.80	250	0.67	0
Au 08 / 06	N 01	4	2008-03-28T22:00	139.68	-65.80	275	1.24	0
Au 08 / 06	N 01	4	2008-03-28T22:00	139.68	-65.80	300	1.58	0
Au 08 / 06	N 01	4	2008-03-28T22:00	139.68	-65.80	310	1.59	0
Au 08 / 06	N 02	7	2008-03-29T10:00	139.84	-65.43	10	0.66	0
Au 08 / 06	N 02	7	2008-03-29T10:00	139.84	-65.43	25	0.33	0
Au 08 / 06	N 02	7	2008-03-29T10:00	139.84	-65.43	50	0.34	0
Au 08 / 06	N 02	7	2008-03-29T10:00	139.84	-65.43	75	0.66	0
Au 08 / 06	N 02	7	2008-03-29T10:00	139.84	-65.43	101	0.69	0
Au 08 / 06	N 02	7	2008-03-29T10:00	139.84	-65.43	150	0.43	0
Au 08 / 06	N 02	7	2008-03-29T10:00	139.84	-65.43	200	0.54	0
Au 08 / 06	N 02	7	2008-03-29T10:00	139.84	-65.43	300	0.65	0
Au 08 / 06	N 02	7	2008-03-29T10:00	139.84	-65.43	500	0.52	0
Au 08 / 06	N 02	7	2008-03-29T10:00	139.84	-65.43	600	0.48	0
Au 08 / 06	N 02	7	2008-03-29T10:00	139.84	-65.43	750	0.40	0
Au 08 / 06	N 02	7	2008-03-29T10:00	139.84	-65.43	1000	0.46	0
Au 08 / 06	N 02	7	2008-03-29T09:35	139.84	-65.43	1001	0.49	0
Au 08 / 06	N 02	7	2008-03-29T09:35	139.84	-65.43	1600		8
Au 08 / 06	N 02	7	2008-03-29T09:35	139.84	-65.43	2070	0.65	0
Au 08 / 06	N 02	7	2008-03-29T09:35	139.84	-65.43	2122	0.86	0
Au 08 / 06	N 03	10	2008-03-30T09:30	140.21	-64.88	10	0.15	0

Continued on next page

Table A.2 – continued from previous page

Cruise	Station No.		Date & Time	Lon. (°E)	Lat. (°N)	Depth (m)	dAl (nM)	QF
	TMR	CTD						
Au 08 / 06	N 03	10	2008-03-30T09:30	140.21	-64.88	30	1.24	0
Au 08 / 06	N 03	10	2008-03-30T09:30	140.21	-64.88	70	1.17	0
Au 08 / 06	N 03	10	2008-03-30T09:30	140.21	-64.88	90	0.41	0
Au 08 / 06	N 03	10	2008-03-30T09:30	140.21	-64.88	115	0.69	0
Au 08 / 06	N 03	10	2008-03-30T09:30	140.21	-64.88	130	1.35	0
Au 08 / 06	N 03	10	2008-03-30T09:30	140.21	-64.88	150	0.67	0
Au 08 / 06	N 03	10	2008-03-30T09:30	140.21	-64.88	200	0.58	0
Au 08 / 06	N 03	10	2008-03-30T09:30	140.21	-64.88	250	0.34	0
Au 08 / 06	N 03	10	2008-03-30T09:30	140.21	-64.88	300	0.94	0
Au 08 / 06	N 03	10	2008-03-30T09:30	140.21	-64.88	400	0.37	0
Au 08 / 06	N 03	10	2008-03-30T09:30	140.21	-64.88	550	0.24	0
Au 08 / 06	N 04	13	2008-03-31T02:00	139.84	-64.21	11		8
Au 08 / 06	N 04	13	2008-03-31T02:00	139.84	-64.21	15		8
Au 08 / 06	N 04	13	2008-03-31T02:00	139.84	-64.21	25	1.85	0
Au 08 / 06	N 04	13	2008-03-31T02:00	139.84	-64.21	50	0.54	0
Au 08 / 06	N 04	13	2008-03-31T02:00	139.84	-64.21	75	0.49	0
Au 08 / 06	N 04	13	2008-03-31T02:00	139.84	-64.21	100	0.84	0
Au 08 / 06	N 04	13	2008-03-31T02:00	139.84	-64.21	150	0.34	0
Au 08 / 06	N 04	13	2008-03-31T02:00	139.84	-64.21	200	0.90	0
Au 08 / 06	N 04	13	2008-03-31T02:00	139.84	-64.21	300	0.71	0
Au 08 / 06	N 04	13	2008-03-31T02:00	139.84	-64.21	500		8
Au 08 / 06	N 04	13	2008-03-31T02:00	139.84	-64.21	750		8
Au 08 / 06	N 04	13	2008-03-31T02:00	139.84	-64.21	1000		8
Au 08 / 06	N 04	13	2008-03-30T19:44	139.84	-64.21	998	0.88	0
Au 08 / 06	N 04	13	2008-03-30T19:44	139.84	-64.21	1800	0.94	0
Au 08 / 06	N 04	13	2008-03-30T19:44	139.84	-64.21	2401	0.48	0
Au 08 / 06	N 04	13	2008-03-30T19:44	139.84	-64.21	3000	0.60	0
Au 08 / 06	N 04	13	2008-03-30T19:44	139.84	-64.21	3500	0.79	0
Au 08 / 06	N 04	13	2008-03-30T19:44	139.84	-64.21	3548	1.12	0
Au 08 / 06	N 05	17	2008-03-31T20:00	139.86	-62.85	15	0.93	0
Au 08 / 06	N 05	17	2008-03-31T20:00	139.86	-62.85	25	1.00	0
Au 08 / 06	N 05	17	2008-03-31T20:00	139.86	-62.85	45	0.50	0

Continued on next page

Table A.2 – continued from previous page

Cruise	Station No.		Date & Time	Lon. (°E)	Lat. (°N)	Depth (m)	dAl (nM)	QF
	TMR	CTD						
Au 08 / 06	N 05	17	2008-03-31T20:00	139.86	-62.85	100	0.44	0
Au 08 / 06	N 05	17	2008-03-31T20:00	139.86	-62.85	250	0.52	0
Au 08 / 06	N 05	17	2008-03-31T20:00	139.86	-62.85	500	0.34	0
Au 08 / 06	N 05	17	2008-03-31T20:00	139.86	-62.85	999	1.01	0
Au 08 / 06	N 06	19	2008-04-01T10:30	139.85	-61.85	11		8
Au 08 / 06	N 06	19	2008-04-01T10:30	139.85	-61.85	15	1.05	0
Au 08 / 06	N 06	19	2008-04-01T10:30	139.85	-61.85	25	0.57	0
Au 08 / 06	N 06	19	2008-04-01T10:30	139.85	-61.85	60		8
Au 08 / 06	N 06	19	2008-04-01T10:30	139.85	-61.85	100	0.50	0
Au 08 / 06	N 06	19	2008-04-01T10:30	139.85	-61.85	250	0.34	0
Au 08 / 06	N 06	19	2008-04-01T10:30	139.85	-61.85	400	0.94	0
Au 08 / 06	N 06	19	2008-04-01T10:30	139.85	-61.85	997	0.63	0
Au 08 / 06	N 06	19	2008-04-01T10:30	139.85	-61.85	1000	0.39	0
Au 08 / 06	N 07	21	2008-04-02T00:00	139.85	-60.85	14	0.84	0
Au 08 / 06	N 07	21	2008-04-02T00:00	139.85	-60.85	25	1.14	0
Au 08 / 06	N 07	21	2008-04-02T00:00	139.85	-60.85	50	0.40	0
Au 08 / 06	N 07	21	2008-04-02T00:00	139.85	-60.85	85	0.48	0
Au 08 / 06	N 07	21	2008-04-02T00:00	139.85	-60.85	110	0.75	0
Au 08 / 06	N 07	21	2008-04-02T00:00	139.85	-60.85	200	1.75	0
Au 08 / 06	N 07	21	2008-04-02T00:00	139.85	-60.85	450	0.64	0
Au 08 / 06	N 07	21	2008-04-02T00:00	139.85	-60.85	750	0.37	0
Au 08 / 06	N 07	21	2008-04-02T00:00	139.85	-60.85	1000	0.96	0
Au 08 / 06	N 07	21	2008-03-30T19:44	139.84	-60.85	1007	3.79	8
Au 08 / 06	N 07	21	2008-03-30T19:44	139.84	-60.85	2006	0.97	0
Au 08 / 06	N 07	21	2008-03-30T19:44	139.84	-60.85	2505	0.56	0
Au 08 / 06	N 07	21	2008-03-30T19:44	139.84	-60.85	3410	5.82	8
Au 08 / 06	N 07	21	2008-03-30T19:44	139.84	-60.85	4013	0.22	0
Au 08 / 06	N 07	21	2008-03-30T19:44	139.84	-60.85	4443	1.23	0
Au 08 / 06	N 08	24	2008-04-02T00:00	139.86	-59.85	15	0.75	0
Au 08 / 06	N 08	24	2008-04-02T00:00	139.86	-59.85	25	0.36	0
Au 08 / 06	N 08	24	2008-04-02T00:00	139.86	-59.85	50	0.56	0
Au 08 / 06	N 08	24	2008-04-02T00:00	139.86	-59.85	90	1.06	0

Continued on next page

Table A.2 – continued from previous page

Cruise	Station No.		Date & Time	Lon. (°E)	Lat. (°N)	Depth (m)	dAl (nM)	QF
	TMR	CTD						
Au 08 / 06	N 08	24	2008-04-02T00:00	139.86	-59.85	120	0.19	0
Au 08 / 06	N 08	24	2008-04-02T00:00	139.86	-59.85	200	0.42	0
Au 08 / 06	N 08	24	2008-04-02T00:00	139.86	-59.85	450	0.47	0
Au 08 / 06	N 08	24	2008-04-02T00:00	139.86	-59.85	750	3.64	8
Au 08 / 06	N 08	24	2008-04-02T00:00	139.86	-59.85	1000	1.26	0
Au 08 / 06	N 09	26	2008-04-03T00:00	139.84	-58.85	15	1.39	0
Au 08 / 06	N 09	26	2008-04-03T00:00	139.84	-58.85	25	0.34	0
Au 08 / 06	N 09	26	2008-04-03T00:00	139.84	-58.85	50	0.87	0
Au 08 / 06	N 09	26	2008-04-03T00:00	139.84	-58.85	95	1.55	0
Au 08 / 06	N 09	26	2008-04-03T00:00	139.84	-58.85	120	0.48	0
Au 08 / 06	N 09	26	2008-04-03T00:00	139.84	-58.85	300	1.16	0
Au 08 / 06	N 09	26	2008-04-03T00:00	139.84	-58.85	600	0.74	0
Au 08 / 06	N 09	26	2008-04-03T00:00	139.84	-58.85	800	0.89	0
Au 08 / 06	N 09	26	2008-04-03T00:00	139.84	-58.85	1000	0.57	0
Au 08 / 06	N 09	26	2008-04-03T07:26	139.84	-58.85	1010	0.73	0
Au 08 / 06	N 09	26	2008-04-03T07:26	139.84	-58.85	1499	1.01	0
Au 08 / 06	N 09	26	2008-04-03T07:26	139.84	-58.85	2210	0.54	0
Au 08 / 06	N 09	26	2008-04-03T07:26	139.84	-58.85	3011	0.50	0
Au 08 / 06	N 09	26	2008-04-03T07:26	139.84	-58.85	3860	1.17	0
Au 08 / 06	N 09	26	2008-04-03T07:26	139.84	-58.85	3962	1.94	0
Au 08 / 06	N 10	29	2008-04-04T00:00	139.85	-57.85	15	1.24	0
Au 08 / 06	N 10	29	2008-04-04T00:00	139.85	-57.85	25	0.72	0
Au 08 / 06	N 10	29	2008-04-04T00:00	139.85	-57.85	80	9.27	8
Au 08 / 06	N 10	29	2008-04-04T00:00	139.85	-57.85	110	0.70	0
Au 08 / 06	N 10	29	2008-04-04T00:00	139.85	-57.85	140	1.16	0
Au 08 / 06	N 10	29	2008-04-04T00:00	139.85	-57.85	175	2.40	0
Au 08 / 06	N 10	29	2008-04-04T00:00	139.85	-57.85	225	2.37	0
Au 08 / 06	N 10	29	2008-04-04T00:00	139.85	-57.85	350	1.55	0
Au 08 / 06	N 10	29	2008-04-04T00:00	139.85	-57.85	500	0.59	0
Au 08 / 06	N 11	32	2008-04-04T00:00	139.85	-56.93	15	1.13	0
Au 08 / 06	N 11	32	2008-04-04T00:00	139.85	-56.93	25	1.20	0
Au 08 / 06	N 11	32	2008-04-04T00:00	139.85	-56.93	60	1.75	0

Continued on next page

Table A.2 – continued from previous page

Cruise	Station No.		Date & Time	Lon. (°E)	Lat. (°N)	Depth (m)	dAl (nM)	QF
	TMR	CTD						
Au 08 / 06	N 11	32	2008-04-04T00:00	139.85	-56.93	120	3.72	4
Au 08 / 06	N 11	32	2008-04-04T00:00	139.85	-56.93	200	3.49	4
Au 08 / 06	N 11	32	2008-04-04T00:00	139.85	-56.93	400	1.95	0
Au 08 / 06	N 11	32	2008-04-04T00:00	139.85	-56.93	700	1.05	0
Au 08 / 06	N 11	32	2008-04-04T00:00	139.85	-56.93	900	0.80	0
Au 08 / 06	N 11	32	2008-04-04T00:00	139.85	-56.93	1000	1.05	0
Au 08 / 06	N 12	34	2008-04-05T00:00	140.41	-55.93	15	2.21	0
Au 08 / 06	N 12	34	2008-04-05T00:00	140.41	-55.93	25	0.94	0
Au 08 / 06	N 12	34	2008-04-05T00:00	140.41	-55.93	60	0.35	0
Au 08 / 06	N 12	34	2008-04-05T00:00	140.41	-55.93	90	0.56	0
Au 08 / 06	N 12	34	2008-04-05T00:00	140.41	-55.93	121	0.88	0
Au 08 / 06	N 12	34	2008-04-05T00:00	140.41	-55.93	200	0.96	0
Au 08 / 06	N 12	34	2008-04-05T00:00	140.41	-55.93	400	7.08	8
Au 08 / 06	N 12	34	2008-04-05T00:00	140.41	-55.93	700	0.86	0
Au 08 / 06	N 12	34	2008-04-05T00:00	140.41	-55.93	868	0.92	0
Au 08 / 06	N 13	36	2008-04-06T00:00	141.02	-55.02	15	1.77	0
Au 08 / 06	N 13	36	2008-04-06T00:00	141.02	-55.02	25	1.11	0
Au 08 / 06	N 13	36	2008-04-06T00:00	141.02	-55.02	60	0.78	0
Au 08 / 06	N 13	36	2008-04-06T00:00	141.02	-55.02	90	0.52	0
Au 08 / 06	N 13	36	2008-04-06T00:00	141.02	-55.02	120	1.24	0
Au 08 / 06	N 13	36	2008-04-06T00:00	141.02	-55.02	200	2.60	0
Au 08 / 06	N 13	36	2008-04-06T00:00	141.02	-55.02	400	3.73	4
Au 08 / 06	N 13	36	2008-04-06T00:00	141.02	-55.02	600	3.97	4
Au 08 / 06	N 13	36	2008-04-06T00:00	141.02	-55.02	1000	1.37	0
Au 08 / 06	N 14	38	2008-04-06T00:00	141.60	-54.07	13	0.33	0
Au 08 / 06	N 14	38	2008-04-06T00:00	141.60	-54.07	25	0.73	0
Au 08 / 06	N 14	38	2008-04-06T00:00	141.60	-54.07	50	0.64	0
Au 08 / 06	N 14	38	2008-04-06T00:00	141.60	-54.07	90	0.87	0
Au 08 / 06	N 14	38	2008-04-06T00:00	141.60	-54.07	120	0.51	0
Au 08 / 06	N 14	38	2008-04-06T00:00	141.60	-54.07	200	0.53	0
Au 08 / 06	N 14	38	2008-04-06T00:00	141.60	-54.07	400	0.76	0
Au 08 / 06	N 14	38	2008-04-06T00:00	141.60	-54.07	600	0.63	0

Continued on next page

Table A.2 – continued from previous page

Cruise	Station No.		Date & Time	Lon. (°E)	Lat. (°N)	Depth (m)	dAl (nM)	QF
	TMR	CTD						
Au 08 / 06	N 14	38	2008-04-06T00:00	141.60	-54.07	1000	0.67	0
Au 08 / 06	N 14	38	2008-04-06T15:23	141.60	-54.07	1015	0.71	0
Au 08 / 06	N 14	38	2008-04-06T15:23	141.60	-54.07	1315	0.69	0
Au 08 / 06	N 14	38	2008-04-06T15:23	141.60	-54.07	1801	0.47	0
Au 08 / 06	N 14	38	2008-04-06T15:23	141.60	-54.07	2211	0.73	0
Au 08 / 06	N 14	38	2008-04-06T15:23	141.60	-54.07	2517	0.89	0
Au 08 / 06	N 14	38	2008-04-06T15:23	141.60	-54.07	2561	1.16	0
Au 08 / 06	N 15	41	2008-04-07T00:00	142.14	-53.13	15	1.13	0
Au 08 / 06	N 15	41	2008-04-07T00:00	142.14	-53.13	25	1.62	0
Au 08 / 06	N 15	41	2008-04-07T00:00	142.14	-53.13	50	1.09	0
Au 08 / 06	N 15	41	2008-04-07T00:00	142.14	-53.13	90	0.67	0
Au 08 / 06	N 15	41	2008-04-07T00:00	142.14	-53.13	140	0.66	0
Au 08 / 06	N 15	41	2008-04-07T00:00	142.14	-53.13	200	0.75	0
Au 08 / 06	N 15	41	2008-04-07T00:00	142.14	-53.13	400	0.74	0
Au 08 / 06	N 15	41	2008-04-07T00:00	142.14	-53.13	750	0.64	0
Au 08 / 06	N 15	41	2008-04-07T00:00	142.14	-53.13	1000	0.71	0
Au 08 / 06	N 16	44	2008-04-08T00:00	142.53	-52.37	15	0.50	0
Au 08 / 06	N 16	44	2008-04-08T00:00	142.53	-52.37	25	0.79	0
Au 08 / 06	N 16	44	2008-04-08T00:00	142.53	-52.37	50	0.47	0
Au 08 / 06	N 16	44	2008-04-08T00:00	142.53	-52.37	100	0.37	0
Au 08 / 06	N 16	44	2008-04-08T00:00	142.53	-52.37	150	0.57	0
Au 08 / 06	N 16	44	2008-04-08T00:00	142.53	-52.37	300	0.73	0
Au 08 / 06	N 16	44	2008-04-08T00:00	142.53	-52.37	500	1.03	0
Au 08 / 06	N 16	44	2008-04-08T00:00	142.53	-52.37	750	0.88	0
Au 08 / 06	N 16	44	2008-04-08T00:00	142.53	-52.37	1000	0.63	0
Au 08 / 06	N 17	47	2008-04-10T00:00	143.00	-51.54	15	0.69	0
Au 08 / 06	N 17	47	2008-04-10T00:00	143.00	-51.54	25	0.30	0
Au 08 / 06	N 17	47	2008-04-10T00:00	143.00	-51.54	50	1.79	4
Au 08 / 06	N 17	47	2008-04-10T00:00	143.00	-51.54	100	0.42	0
Au 08 / 06	N 17	47	2008-04-10T00:00	143.00	-51.54	150	0.48	0
Au 08 / 06	N 17	47	2008-04-10T00:00	143.00	-51.54	300	0.33	0
Au 08 / 06	N 17	47	2008-04-10T00:00	143.00	-51.54	500	0.40	0

Continued on next page

Table A.2 – continued from previous page

Cruise	Station No.		Date & Time	Lon. (°E)	Lat. (°N)	Depth (m)	dAl (nM)	QF
	TMR	CTD						
Au 08 / 06	N 17	47	2008-04-10T00:00	143.00	-51.54	750	0.52	0
Au 08 / 06	N 17	47	2008-04-10T00:00	143.00	-51.54	1000	0.52	0
Au 08 / 06	N 17	47	2008-04-09T20:31	142.99	-51.54	1009	0.45	0
Au 08 / 06	N 17	47	2008-04-09T20:31	142.99	-51.54	1509	0.53	0
Au 08 / 06	N 17	47	2008-04-09T20:31	142.99	-51.54	2208	0.27	0
Au 08 / 06	N 17	47	2008-04-09T20:31	142.99	-51.54	3000	0.43	0
Au 08 / 06	N 17	47	2008-04-09T20:31	142.99	-51.54	3601	0.32	0
Au 08 / 06	N 17	47	2008-04-09T20:31	142.99	-51.54	3761	0.74	0
Au 08 / 06	N 18	51	2008-04-10T00:00	143.42	-50.68	15	0.50	0
Au 08 / 06	N 18	51	2008-04-10T00:00	143.42	-50.68	25	0.10	2
Au 08 / 06	N 18	51	2008-04-10T00:00	143.42	-50.68	50	0.05	2
Au 08 / 06	N 18	51	2008-04-10T00:00	143.42	-50.68	100	0.40	0
Au 08 / 06	N 18	51	2008-04-10T00:00	143.42	-50.68	150	0.34	0
Au 08 / 06	N 18	51	2008-04-10T00:00	143.42	-50.68	300	0.34	0
Au 08 / 06	N 18	51	2008-04-10T00:00	143.42	-50.68	500	0.18	0
Au 08 / 06	N 18	51	2008-04-10T00:00	143.42	-50.68	750	0.24	0
Au 08 / 06	N 18	51	2008-04-10T00:00	143.42	-50.68	1000	0.06	2
Au 08 / 06	N 19	54	2008-04-11T00:00	143.80	-49.89	15	0.29	0
Au 08 / 06	N 19	54	2008-04-11T00:00	143.80	-49.89	25	0.35	0
Au 08 / 06	N 19	54	2008-04-11T00:00	143.80	-49.89	50	1.12	0
Au 08 / 06	N 19	54	2008-04-11T00:00	143.80	-49.89	100	0.28	0
Au 08 / 06	N 19	54	2008-04-11T00:00	143.80	-49.89	150	0.77	0
Au 08 / 06	N 19	54	2008-04-11T00:00	143.80	-49.89	300	0.60	0
Au 08 / 06	N 19	54	2008-04-11T00:00	143.80	-49.89	500	1.09	0
Au 08 / 06	N 19	54	2008-04-11T00:00	143.80	-49.89	750	0.14	0
Au 08 / 06	N 19	54	2008-04-11T00:00	143.80	-49.89	1000	0.15	0
Au 08 / 06	N 20	56	2008-04-12T00:00	144.10	-49.27	15	0.93	0
Au 08 / 06	N 20	56	2008-04-12T00:00	144.10	-49.27	25	1.63	0
Au 08 / 06	N 20	56	2008-04-12T00:00	144.10	-49.27	50	1.06	0
Au 08 / 06	N 20	56	2008-04-12T00:00	144.10	-49.27	100	1.09	0
Au 08 / 06	N 20	56	2008-04-12T00:00	144.10	-49.27	150	0.52	0
Au 08 / 06	N 20	56	2008-04-12T00:00	144.10	-49.27	300	0.39	0

Continued on next page

Table A.2 – continued from previous page

Cruise	Station No.		Date & Time	Lon. (°E)	Lat. (°N)	Depth (m)	dAl (nM)	QF
	TMR	CTD						
Au 08 / 06	N 20	56	2008-04-12T00:00	144.10	-49.27	500	0.51	0
Au 08 / 06	N 20	56	2008-04-12T00:00	144.10	-49.27	750	0.30	0
Au 08 / 06	N 20	56	2008-04-12T00:00	144.10	-49.27	1000	0.11	2
Au 08 / 06	N 20	56	2008-04-11T19:52	144.10	-49.27	1012	0.20	0
Au 08 / 06	N 20	56	2008-04-11T19:52	144.10	-49.27	1711	0.24	0
Au 08 / 06	N 20	56	2008-04-11T19:52	144.10	-49.27	2510	0.40	0
Au 08 / 06	N 20	56	2008-04-11T19:52	144.10	-49.27	2913	0.41	0
Au 08 / 06	N 20	56	2008-04-11T19:52	144.10	-49.27	3799	0.48	0
Au 08 / 06	N 20	56	2008-04-11T19:52	144.10	-49.27	4303	0.67	0
Au 08 / 06	N 21	59	2008-04-12T00:00	144.53	-48.32	25	0.97	0
Au 08 / 06	N 21	59	2008-04-12T00:00	144.53	-48.32	50	0.70	0
Au 08 / 06	N 21	59	2008-04-12T00:00	144.53	-48.32	90	0.60	0
Au 08 / 06	N 21	59	2008-04-12T00:00	144.53	-48.32	120	0.48	0
Au 08 / 06	N 21	59	2008-04-12T00:00	144.53	-48.32	150	1.33	0
Au 08 / 06	N 21	59	2008-04-12T00:00	144.53	-48.32	300	1.08	0
Au 08 / 06	N 21	59	2008-04-12T00:00	144.53	-48.32	500	0.97	0
Au 08 / 06	N 21	59	2008-04-12T00:00	144.53	-48.32	751	1.26	0
Au 08 / 06	N 21	59	2008-04-12T00:00	144.53	-48.32	1000	1.44	0
Au 08 / 06	N 22	62	2008-04-13T00:00	144.90	-47.47	15	0.62	0
Au 08 / 06	N 22	62	2008-04-13T00:00	144.90	-47.47	25	1.85	4
Au 08 / 06	N 22	62	2008-04-13T00:00	144.90	-47.47	50	0.35	0
Au 08 / 06	N 22	62	2008-04-13T00:00	144.90	-47.47	100	0.35	0
Au 08 / 06	N 22	62	2008-04-13T00:00	144.90	-47.47	150	0.42	0
Au 08 / 06	N 22	62	2008-04-13T00:00	144.90	-47.47	300	0.50	0
Au 08 / 06	N 22	62	2008-04-13T00:00	144.90	-47.47	500	0.39	0
Au 08 / 06	N 22	62	2008-04-13T00:00	144.90	-47.47	750	0.83	0
Au 08 / 06	N 22	62	2008-04-13T00:00	144.90	-47.47	1000	1.21	0
Au 08 / 06	N 23	64	2008-04-13T00:00	145.25	-46.65	15	0.87	0
Au 08 / 06	N 23	64	2008-04-13T00:00	145.25	-46.65	25	0.52	0
Au 08 / 06	N 23	64	2008-04-13T00:00	145.25	-46.65	50	0.40	0
Au 08 / 06	N 23	64	2008-04-13T00:00	145.25	-46.65	100	0.45	0
Au 08 / 06	N 23	64	2008-04-13T00:00	145.25	-46.65	150	0.46	0

Continued on next page

Table A.2 – continued from previous page

Cruise	Station No.		Date & Time	Lon. (°E)	Lat. (°N)	Depth (m)	dAl (nM)	QF
	TMR	CTD						
Au 08 / 06	N 23	64	2008-04-13T00:00	145.25	-46.65	300	0.46	0
Au 08 / 06	N 23	64	2008-04-13T00:00	145.25	-46.65	500	1.02	0
Au 08 / 06	N 23	64	2008-04-13T00:00	145.25	-46.65	750	1.34	0
Au 08 / 06	N 23	64	2008-04-13T00:00	145.25	-46.65	1000	1.01	0
Au 08 / 06	N 23	64	2008-04-13T16:11	145.25	-46.65	1009	0.90	0
Au 08 / 06	N 23	64	2008-04-13T16:11	145.25	-46.65	1508	0.79	0
Au 08 / 06	N 23	64	2008-04-13T16:11	145.25	-46.65	2008	0.58	0
Au 08 / 06	N 23	64	2008-04-13T16:11	145.25	-46.65	2400	0.36	0
Au 08 / 06	N 23	64	2008-04-13T16:11	145.25	-46.65	3000	0.51	0
Au 08 / 06	N 23	64	2008-04-13T16:11	145.25	-46.65	3383	0.85	0
Au 08 / 06	N 24	67	2008-04-14T00:00	145.66	-45.70	15	1.30	0
Au 08 / 06	N 24	67	2008-04-14T00:00	145.66	-45.70	25	2.41	0
Au 08 / 06	N 24	67	2008-04-14T00:00	145.66	-45.70	50	0.51	0
Au 08 / 06	N 24	67	2008-04-14T00:00	145.66	-45.70	100	0.33	0
Au 08 / 06	N 24	67	2008-04-14T00:00	145.66	-45.70	150	0.71	0
Au 08 / 06	N 24	67	2008-04-14T00:00	145.66	-45.70	300	1.01	0
Au 08 / 06	N 24	67	2008-04-14T00:00	145.66	-45.70	500	0.77	0
Au 08 / 06	N 24	67	2008-04-14T00:00	145.66	-45.70	750	0.69	0
Au 08 / 06	N 24	67	2008-04-14T00:00	145.66	-45.70	1000	0.55	0
Au 08 / 06	N 24	67	2008-04-14T06:52	145.66	-45.70	17	1.27	0
Au 08 / 06	N 24	67	2008-04-14T06:52	145.66	-45.70	57	0.51	0
Au 08 / 06	N 24	67	2008-04-14T06:52	145.66	-45.70	157	1.30	0
Au 08 / 06	N 24	67	2008-04-14T06:52	145.66	-45.70	505	0.56	0
Au 08 / 06	N 24	67	2008-04-14T06:52	145.66	-45.70	756	0.72	0
Au 08 / 06	N 24	67	2008-04-14T06:52	145.66	-45.70	1010	0.58	0
Au 08 / 06	N 25	69	2008-04-14T00:00	146.05	-44.72	15	1.29	0
Au 08 / 06	N 25	69	2008-04-14T00:00	146.05	-44.72	25	0.89	0
Au 08 / 06	N 25	69	2008-04-14T00:00	146.05	-44.72	50	0.31	0
Au 08 / 06	N 25	69	2008-04-14T00:00	146.05	-44.72	100	0.45	0
Au 08 / 06	N 25	69	2008-04-14T00:00	146.05	-44.72	150	0.62	0
Au 08 / 06	N 25	69	2008-04-14T00:00	146.05	-44.72	300	1.09	0
Au 08 / 06	N 25	69	2008-04-14T00:00	146.05	-44.72	500	1.24	0

Continued on next page

Table A.2 – continued from previous page

Cruise	Station No.		Date & Time	Lon. (°E)	Lat. (°N)	Depth (m)	dAl (nM)	QF
	TMR	CTD						
Au 08 / 06	N 25	69	2008-04-14T00:00	146.05	-44.72	750	1.40	0
Au 08 / 06	N 25	69	2008-04-14T00:00	146.05	-44.72	1000	1.95	0
Au 08 / 06	N 26	71	2008-04-15T00:00	146.22	-44.12	15	0.74	0
Au 08 / 06	N 26	71	2008-04-15T00:00	146.22	-44.12	25	3.64	4
Au 08 / 06	N 26	71	2008-04-15T00:00	146.22	-44.12	50	1.78	0
Au 08 / 06	N 26	71	2008-04-15T00:00	146.22	-44.12	100	1.04	0
Au 08 / 06	N 26	71	2008-04-15T00:00	146.22	-44.12	150	0.53	0
Au 08 / 06	N 26	71	2008-04-15T00:00	146.22	-44.12	375	0.57	0
Au 08 / 06	N 26	71	2008-04-15T00:00	146.22	-44.12	500	0.97	0
Au 08 / 06	N 26	71	2008-04-15T00:00	146.22	-44.12	750	1.06	0
Au 08 / 06	N 26	71	2008-04-15T00:00	146.22	-44.12	1000	0.73	0
Au 08 / 06	N 27	73	2008-04-15T00:00	146.32	-44.00	15	1.18	0
Au 08 / 06	N 27	73	2008-04-15T00:00	146.32	-44.00	25	0.52	0
Au 08 / 06	N 27	73	2008-04-15T00:00	146.32	-44.00	50	0.70	0
Au 08 / 06	N 27	73	2008-04-15T00:00	146.32	-44.00	75	1.03	0
Au 08 / 06	N 27	73	2008-04-15T00:00	146.32	-44.00	100	1.86	0
Au 08 / 06	N 27	73	2008-04-15T00:00	146.32	-44.00	117	1.62	0
Au 08 / 06	N 27	73	2008-04-15T00:00	146.32	-44.00	120	1.95	0
Au 08 / 06	N 27	73	2008-04-15T00:00	146.32	-44.00	126	1.70	0
Au 08 / 06	N 27	73	2008-04-15T00:00	146.32	-44.00	128	1.13	0

References

- Ahmed, M. J., and Hossan, J., 1995: Spectrophotometric determination of aluminium by morin. *Talanta.*, **42**, 1135–1142.
- Alonso, A., Almendral, M., Porras, M., Curto, Y., and Garca de Mara, C., 2001: Flow-injection solvent extraction with and without phase separation: Fluorimetric determination of aluminium in water. *Anal. Chim. Acta.*, **447(1-2)**, 211–217.
- Alonso, J. I. G., Garcia, A. L., Sanzmedel, A., Gonzales, E. B., Ebdon, L., and Jones, P., 1989: Flow-injection and liquid chromatographic determination of aluminum based on its fluorimetric reaction with 8-hydroxyquinoline-5-sulphonic acid in a micellar medium. *Anal. Chim. Acta.*, **225(0)**, 339 – 350.
- Anders, A. M., Sletten, R. S., Derry, L. A., and Hallet, B., 2003: Germanium/silicon ratios in the Copper River Basin, Alaska: Weathering and partitioning in periglacial versus glacial environments. *J. Geophys. Res.*, **108(F1)**, 6005–.
- Arimoto, R., 2001: Eolian dust and climate: relationships to sources, tropospheric chemistry, transport and deposition. *Earth-sci. Rev.*, **54(1-3)**, 29–42.
- Arimoto, R., Duce, R. A., Ray, B. J., and Tomza, U., 2003: Dry deposition of trace elements to the western North Atlantic. *Global. Biogeochem. Cy.*, **17(1)**, 1010.
- Aumont, O., and Bopp, L., 2006: Globalizing results from ocean in situ iron fertilization studies. *Global. Biogeochem. Cy.*, **20(2)**, GB2017.
- Aumont, O., Bopp, L., and Schulz, M., 2008: What does temporal variability in aeolian dust deposition contribute to sea-surface iron and chlorophyll distributions? *Geophys. Res. Lett.*, **35(7)**, L07607.

- Baird, M. E., and Ridgway, K. R., 2012: The southward transport of sub-mesoscale lenses of Bass Strait Water in the centre of anti-cyclonic mesoscale eddies. *Geophys. Res. Lett.*, **39**, L02603.
- Bennetto, H. P., and Caldin, E. F., 1971a: Kinetics of solvent exchange and ligand substitution reactions of metal ions in relation to structural properties of the solvent. *J. Chem. Soc. A*, **1**, 2198–2207.
- Bennetto, H. P., and Caldin, E. F., 1971b: Kinetics of the reaction of nickel(II) ions with 2,2[prime or minute]-bipyridyl in water-methanol mixtures. *J. Chem. Soc. A*, **1**, 2207–2210.
- Bennetto, H. P., and Caldin, E. F., 1971c: Solvent effects on the kinetics of the reactions of nickel(II) and cobalt(II) ions with 2,2[prime or minute]-bipyridyl and 2,2[prime or minute],2[double prime]-terpyridyl. *J. Chem. Soc. A*, **1**, 2191–2198.
- Bi, S. P., Gan, N., Lu, X. C., Ni, H. Y., Lin, H., Wang, X. L., and Wei, Z. B., 2003: Evaluation of aluminum speciation in surface waters in China and its environmental risk assessment. *Environ. Geol.*, **45**, 65–71, 10.1007/s00254-003-0847-5.
- Bidigare, R. R., Kennicutt, M. C., and Brooks, J. M., 1985: Rapid-determination of Chlorophylls and Their Degradation Products By High-performance Liquid-chromatography. *Limnol. Oceanogr.*, **30**(2), 432–435.
- Blain, S., 2008: Natural iron fertilization in the ocean and GEOTRACES. *Geochim. Cosmochim. Ac.*, **72**(12), A88–A88.
- Blain, S., Sarthou, G., and Laan, P., 2008: Distribution of dissolved iron during the natural iron-fertilization experiment KEOPS (Kerguelen Plateau, Southern Ocean). *Deep-Sea. Res. Pt. II.*, **55**(5-7), 594–605.
- Bowie, A. R., Griffiths, F. B., Dehairs, F., and Trull, T. W., 2011a: Oceanography of the subantarctic and Polar Frontal Zones south of Australia during summer: Setting for the SAZ-Sense study. *Deep-Sea. Res. Pt. II.*, **58**(21-22), 2059–2070.
- Bowie, A. R., Lannuzel, D., Remenyi, T. A., Wagener, T., Lam, P. J., Boyd, P. W., Guieu, C., Townsend, A. T., and Trull, T. W., 2009: Biogeochemical iron budgets of the Southern Ocean

- south of Australia: Decoupling of iron and nutrient cycles in the subantarctic zone by the summertime supply. *Global. Biogeochem. Cy.*, **23**, GB4034.
- Bowie, A. R., and Lohan, M. C., 2009: Analysis of Iron in Seawater. O. Wurl, Ed., *Practical Guidelines for the Analysis of Seawater*, CRC Press, chap. Analysis of Iron in Seawater, 235–257, ISBN: 9781420073065 ISBN 13: 1420073060 Total number of pages: 408.
- Bowie, A. R., Trull, T. W., and Dehairs, F., 2011b: Estimating the sensitivity of the subantarctic zone to environmental change: The SAZ-Sense project. *Deep-Sea. Res. Pt. II.*, **58(21-22)**, 2051–2058.
- Bowie, A. R., Whitworth, D. J., Achterberg, E. P., Mantoura, R. F. C., and Worsfold, P. J., 2002: Biogeochemistry of Fe and other trace elements (Al, Co, Ni) in the upper Atlantic Oceans. *Deep-Sea. Res. Pt. I.*, **49(4)**, 605–636.
- Boyd, P. W., Mackie, D. S., and Hunter, K. A., 2010: Aerosol iron deposition to the surface ocean - Modes of iron supply and biological responses. *Mar. Chem.*, **120(1-4)**, 128–143.
- Boyd, P. W., Muggli, D. L., Varela, D. E., Goldblatt, R. H., Chretien, R., Orians, K. J., and Harrison, P. J., 1996: In vitro iron enrichment experiments in the NE subarctic Pacific. *Mar. Ecol-Prog. Ser.*, **136(1-3)**, 179–193.
- Boyd, P. W., Watson, A. J., Law, C. S., Abraham, E. R., Trull, T., Murdoch, R., Bakker, D. C. E., Bowie, A. R., Buesseler, K. O., Chang, H., Charette, M., Croot, P., Downing, K., Frew, R., Gall, M., Hadfield, M., Hall, J., Harvey, M., Jameson, G., LaRoche, J., Liddicoat, M., Ling, R., Maldonado, M. T., McKay, R. M., Nodder, S., Pickmere, S., Pridmore, R., Rintoul, S., Safi, K., Sutton, P., Strzepek, R., Tanneberger, K., Turner, S., Waite, A., and Zeldis, J., 2000: A mesoscale phytoplankton bloom in the polar Southern Ocean stimulated by iron fertilization. *Nature.*, **407(6805)**, 695–702.
- Boyd, P. W., Wong, C. S., Merrill, J., Whitney, F., Snow, J., Harrison, P. J., and Gower, J., 1998: Atmospheric iron supply and enhanced vertical carbon flux in the NE subarctic Pacific: Is there a connection? *Global. Biogeochem. Cy.*, **12(3)**, 429–441.
- Boyle, E. A., Edmond, J. M., and Sholkovitz, E. R., 1977a: Mechanism of iron removal in estuaries. *Geochim. Cosmochim. Ac.*, **41(9)**, 1313–1324.

- Boyle, E. A., Sclater, F. R., and Edmond, J. M., 1977b: Distribution of dissolved copper in Pacific. *Earth. Planet. Sc. Lett.*, **37(1)**, 38–54.
- Brand, L. E., 1991: Minimum Iron Requirements of Marine-phytoplankton and the Implications For the Biogeochemical Control of New Production. *Limnol. Oceanogr.*, **36(8)**, AMER SOC LIMNOL & OCEANOGR.
- Broecker, W. S., 1984: Carbon-dioxide circulation through ocean and atmosphere. *Nature.*, **308(5960)**, 602–602.
- Broecker, W. S., Takahashi, T., Simpson, H. J., and Peng, T. H., 1979: Fate of fossil-fuel carbon-dioxide and the global carbon budget. *Science.*, **206(4417)**, 409–418.
- Brown, M. T., and Bruland, K. W., 2008: An improved flow-injection analysis method for the determination of dissolved aluminum in seawater. *Limnol. Oceanogr.-Meth.*, **6**, 87–95.
- Brown, M. T., and Bruland, K. W., 2009: Dissolved and particulate aluminum in the Columbia River and coastal waters of Oregon and Washington: Behavior in near-field and far-field plumes. *Estuar. Coast. Shelf. S.*, **84(2)**, 171–185.
- Brown, M. T., Lippiatt, S. M., and Bruland, K. W., 2010: Dissolved aluminum, particulate aluminum, and silicic acid in northern Gulf of Alaska coastal waters: Glacial/riverine inputs and extreme reactivity. *Mar. Chem.*, **122(1-4)**, 160–175.
- Bruland, K., Brown, M., Middag, R., de Baar, H., Sohrin, Y., Ren, J., Cullen, J., and Giesbrecht, T., 2012: Dissolved Aluminum values in nmol/kg, Consensus values (1 std. dev.) for SAFe Reference Samples as of November 2011. Data viewed online, 28 June, 2012.
- Buck, C. S., Landing, W. M., Resing, J. A., and Measures, C. I., 2010: The solubility and deposition of aerosol Fe and other trace elements in the North Atlantic Ocean: Observations from the A16N CLIVAR/CO(2) repeat hydrography section. *Mar. Chem.*, **120(1-4)**, 57–70.
- Butler, E. C. V., OSullivan, J. E., Watson, R. J., Bowie, A. R., Remenyi, T. A., and Lannuzel, D., 2012: Trace metals Cd, Co, Cu, Ni, Zn and Pb in waters of the Subantarctic and Polar Frontal Zones south of Tasmania during the SAZSense Project. submitted to Marine Chemistry, February 2012.

- Caschetto, S., and Wollast, R., 1979: Vertical distribution of dissolved Aluminum in the Mediterranean Sea. *Mar. Chem.*, **7(2)**, 141–155.
- Chaudry, M., Noor-Ul-Islam, and Yasin, Z., 1988: Separation and analysis of aluminium(III) by cation exchange ion chromatography. *J. Radioanal. Nucl. Ch.*, **122**, 43–50, 10.1007/BF02037161.
- Chisholm, S. W., 2000: Oceanography: Stirring times in the Southern Ocean. *Nature*, **407(6805)**, 685–687.
- Chou, L., and Wollast, R., 1997: Biogeochemical behavior and mass balance of dissolved aluminum in the western Mediterranean Sea. *Deep-Sea. Res. Pt. II.*, **44(3-4)**, 741–768.
- Cirano, M., and Middleton, J. F., 2004: Aspects of the Mean Wintertime Circulation along Australia's Southern Shelves: Numerical Studies. *J. Phys. Oceanogr.*, **34(3)**, 668–684.
- Clarke, N., Danielsson, L. G., and Sparén, A., 1996: Analytical methodology for the determination of aluminium fractions in natural fresh waters (technical report). *Pure. Appl. Chem.*, **68(8)**, 1597–1638.
- Claustre, H., Morel, A., Hooker, S. B., Babin, M., Antoine, D., Oubelkheir, K., Bricaud, A., Leblanc, K., Queguiner, B., and Maritorena, S., 2002: Is desert dust making oligotrophic waters greener? *Geophys. Res. Lett.*, **29(10)**, 1469.
- Cresswell, G., and Legeckis, R., 1986: Eddies off southeastern Australia. *Deep-Sea. Res.*, **33(11-12)**, 1527 – 1562.
- Cutter, G., Anderson, P., Codispoti, L., Croot, P., Francois, R., Lohan, M., Obata, H., and Rutgers van der Loeff, M., 2010: Sampling and Sample-handling Protocols for GEOTRACES Cruises. Tech. rep., GEOTRACES.
- Dammshauser, A., Wagener, T., and Croot, P. L., 2011: Surface water dissolved aluminum and titanium: Tracers for specific time scales of dust deposition to the Atlantic? *Geophys. Res. Lett.*, **38**, L24601.
- de Baar, H. J. W., Boyd, P. W., Coale, K. H., Landry, M. R., Tsuda, A., Assmy, P., Bakker, D. C. E., Bozec, Y., Barber, R. T., Brzezinski, M. A., Buesseler, K. O., Boye, M., Croot, P. L.,

- Gervais, F., Gorbunov, M. Y., Harrison, P. J., Hiscock, W. T., Laan, P., Lancelot, C., Law, C. S., Levasseur, M., Marchetti, A., Millero, F. J., Nishioka, J., Nojiri, Y., van Oijen, T., Riebesell, U., Rijkenberg, M. J. A., Saito, H., Takeda, S., Timmermans, K. R., Veldhuis, M. J. W., Waite, A. M., and Wong, C. S., 2005: Synthesis of iron fertilization experiments: From the iron age in the age of enlightenment. *J. Geophys. Res-Oceans.*, **110**(C9), C09S16.
- de Baar, H. J. W., Timmermans, K. R., Laan, P., De Porto, H. H., Ober, S., Blom, J. J., Bakker, M. C., Schilling, J., Sarthou, G., Smit, M. G., and Klunder, M., 2008: Titan: A new facility for ultraclean sampling of trace elements and isotopes in the deep oceans in the international Geotraces program. *Mar. Chem.*, **111**(1-2), 4 – 21.
- de Jong, J. T. M., den Das, J., Bathmann, U., Stoll, M. H. C., Kattner, G., Nolting, R. F., and de Baar, H. J. W., 1998: Dissolved iron at subnanomolar levels in the Southern Ocean as determined by ship-board analysis. *Anal. Chim. Acta.*, **377**(2-3), 113–124.
- de Salas, M. F., Eriksen, R., Davidson, A. T., and Wright, S. W., 2011: Protistan communities in the Australian sector of the Sub-Antarctic Zone during SAZ-Sense. *Deep-Sea. Res. Pt. II.*, **58**(21-22), 2135–2149.
- Dias, J. C., Kubota, L. T., Nesterenko, P. N., Dicinoski, G. W., and Haddad, P. R., 2010: A new high-performance chelation ion chromatographic system for the direct determination of trace transition metals in fuel ethanol. *Anal. Method.*, **2**(10), 1565–1570.
- Dickson, A. G., and Goyet, C., 1994: Handbook of methods for the analysis of the various parameters of the carbon dioxide system in sea water - version 2. Tech. Rep. ORNL/CDIAC-74, U. S. Department of Energy.
- Draxler, R., and Rolph, G., 2012: HYSPLIT (HYbrid Single-Particle Lagrangian Integrated Trajectory). Model access via NOAA ARL READY Website. NOAA Air Resources Laboratory, Silver Spring, MD.
- Duce, R., 1991: The atmospheric input of trace species to the World ocean. *Global. Biogeochem. Cy.*, **5**(3), 193–259, cited By (since 1996) 717.

- Duce, R. A., LaRoche, J., Altieri, K., Arrigo, K. R., Baker, A. R., Capone, D. G., Cornell, S., Dentener, F., Galloway, J., Ganeshram, R. S., Geider, R. J., Jickells, T., Kuypers, M. M., Langlois, R., Liss, P. S., Liu, S. M., Middelburg, J. J., Moore, C. M., Nickovic, S., Oschlies, A., Pedersen, T., Prospero, J., Schlitzer, R., Seitzinger, S., Sorensen, L. L., Uematsu, M., Ulloa, O., Voss, M., Ward, B., and Zamora, L., 2008: Impacts of atmospheric anthropogenic nitrogen on the open ocean. *Science.*, **320(5878)**, 893–897.
- Duce, R. A., Tindale, N., and Zhuang, G., 1991: Atmospheric iron and its impact on marine biological productivity and chemical cycling. *Abstr. Pap. Am. Chem. S.*, **201(Part 2)**, 20–NUCL.
- Duce, R. A., and Tindale, N. W., 1991: Atmospheric Transport of Iron and Its Deposition In the Ocean. *Limnol. Oceanogr.*, **36(8)**, 1715–1726.
- Durand, A., Chase, Z., Remenyi, T., and Queroue, F., 2013: Microplate-reader method for the rapid analysis of copper in natural waters with chemiluminescence detection. *Front. Microbio.*, **3(437)**.
- Ebersbach, F., Trull, T. W., Davies, D. M., and Bray, S. G., 2011: Controls on mesopelagic particle fluxes in the Sub-Antarctic and Polar Frontal Zones in the Southern Ocean south of Australia in summer-Perspectives from free-drifting sediment traps. *Deep-Sea. Res. Pt. II.*, **58(21-22)**, 2260–2276.
- Eigen, M., 1963: Fast elementary steps in chemical reaction mechanisms. *Pure. Appl. Chem.*, **6(1)**, 97–116.
- Ekstrom, M., McTainsh, G. H., and Chappell, A., 2004: Australian dust storms: Temporal trends and relationships with synoptic pressure distributions (1960-99). *Int. J. Climatol.*, **24(12)**, 1581–1599.
- Ellwood, M. J., Boyd, P. W., and Sutton, P., 2008: Winter-time dissolved iron and nutrient distributions in the Subantarctic Zone from 40-52S; 155-160E. *Geophys. Res. Lett.*, **35(11)**, L11604.
- Erdemoğlu, S. B., and Güçer, Ş., 2005: Selective Determination of Aluminum Bound with Tannin in Tea Infusion. *Anal. Sci.*, **21(8)**, 1005–1008.

- Erofeeva, E. A., Savenko, V. S., and Fazlullin, S. M., 1989: On solubility of aluminum hydroxide in the sea-water. *Okeanologiya+*, **29(3)**, 421–422.
- Ezat, U., Dulac, F., Gaudry, A., and Buat-menard, P., 1991: Sample preparation and analysis-methods for studying mineral aerosol in the Southern-Hemisphere (Amsterdam Island). *Analisis*, **19(6)**, 180–183.
- Flaten, A. K., and Lund, W., 1997: Speciation of aluminium in tea infusions studied by size exclusion chromatography with detection by post-column reaction. *Sci. Total. Environ.*, **207(1)**, 21 – 28.
- Franck, V., Brzezinski, M., Coale, K., and Nelson, D., 2000: Iron and silicic acid concentrations regulate Si uptake north and south of the Polar Frontal Zone in the Pacic sector of the Southern Ocean. *Deep-Sea. Res. Pt. II.*, **47**, 33153338.
- Frank, M., Jeandel, C., Anderson, R., Henderson, G., Francos, R., and Sharma, M., 2003: GEOTRACES: Studying the global marine biogeochemistry of trace elements and isotopes. *EOS T. Am. Geophys. Union.*, **84(34)**, –.
- Fujita, N., Kobayashi, H., Enami, T., Nagae, N., and Charleston, N., 2004: Sensitive determination of aluminum in parenteral solutions and injections by HPLC with fluorescence detection using lumogallion. *Bunseki. Kagaku.*, **53(1)**, 17–23.
- Gabelich, C. J., Chen, W. R., Yun, T. I., Coffey, B. M., and Suffet, I. H., 2005: The role of dissolved aluminum in silica chemistry for membrane processes. *Desalination*, **180(1-3)**, 307–319.
- Gabric, A. J., Cropp, R. A., McTainsh, G. H., Johnston, B. M., Butler, H., Tilbrook, B., and Keywood, M., 2010: Australian dust storms in 2002-2003 and their impact on Southern Ocean biogeochemistry. *Global. Biogeochem. Cy.*, **24**, 0–0.
- Gao, L. A., Tao, D. Y., Shan, Y. C., Liang, Z., Zhang, L. H., Huo, Y. S., and Zhang, Y. K., 2010: HPLC-MS/MS shotgun proteomic research of deer antlers with multiparallel protein extraction methods. *J. Chromatogr. B.*, **878(32)**, 3370–3374.
- Gehlen, M., Beck, L., Calas, G., Flank, A. M., Bennekom, A. J. V., and Beusekom, J. E. E. V.,

- 2002: Unraveling the atomic structure of biogenic silica: evidence of the structural association of Al and Si in diatom frustules. *Geochim. Cosmochim. Ac.*, **66(9)**, 1601 – 1609.
- Gelado-Caballero, M., Torres-Padrn, M., Hernndez-Brito, J., Herrera-Melin, J., and Prez-Pea, J., 1996: Aluminium distributions in Central East Atlantic waters (Canary Islands). *Mar. Chem.*, **51(4)**, 359–372.
- Giesbrecht, T., 2007: *The distribution of aluminum in beaufort sea and the development of a sequential injection method for the determination of aluminum in natural waters*. Master's thesis, University of Victoria, Department of Chemistry.
- Ginoux, P., Chin, M., Tegen, I., Prospero, J. M., Holben, B., Dubovik, O., and Lin, S. J., 2001: Sources and distributions of dust aerosols simulated with the GOCART model. *J. Geophys. Res-Atmos.*, **106(D17)**, 20255–20273.
- Gledhill, M., and Buck, K., 2012: The organic complexation of iron in the marine environment: A review. *Front. Microbio.*, **3**, –.
- Good, N. E., Winget, G. D., Winter, W., Connolly, T. N., Izawa, S., and Singh, R. M. M., 1966: Hydrogen Ion Buffers for Biological Research*. *Biochemistry-us.*, **5(2)**, 467–477, PMID: 5942950.
- Gordon, H. R., 1997: Atmospheric correction of ocean color imagery in the Earth Observing System era. *J. Geophys. Res-Atmos.*, **102(D14)**, 17081–17106.
- Gordon, H. R., Du, T., and Zhang, T. M., 1997: Remote sensing of ocean color and aerosol properties: resolving the issue of aerosol absorption. *Appl. Optics.*, **36(33)**, 8670–8684.
- Guieu, C., Roy-Barman, M., Leblond, N., Jeandel, C., Souhaut, M., Le Cann, B., Dufour, A., and Bournot, C., 2005: Vertical particle flux in the northeast Atlantic Ocean (POMME experiment). *J. Geophys. Res-Oceans.*, **110(C7)**, C07S18.
- Hambali, C., and Haddad, P., 1980: High-performance liquid chromatography of 8-hydroxyquinoline chelates of aluminium and cobalt(III). *Chromatographia.*, **13**, 633–634, 10.1007/BF02302466.

- Han, Q., 2012: *Crustal tracers in the atmosphere and ocean: relating their concentrations, fluxes, and ages*. Doctor of philosophy in earth system science, University of California, Irvine.
- Han, Q., Moore, J. K., Zender, C., Measures, C., and Hydes, D., 2008: Constraining oceanic dust deposition using surface ocean dissolved Al. *Global. Biogeochem. Cy.*, **22(2)**, GB2003.
- Han, Q., Zender, C. S., Moore, J. K., Buck, C. S., Chen, Y., Johansen, A., and Measures, C. I., 2012: Global estimates of mineral dust aerosol iron and aluminum solubility that account for particle size using diffusion-controlled and surface-area-controlled approximations. *Global. Biogeochem. Cy.*, **26**, 0–0.
- Hand, J. L., Mahowald, N. M., Chen, Y., Siefert, R. L., Luo, C., Subramaniam, A., and Fung, I., 2004: Estimates of atmospheric-processed soluble iron from observations and a global mineral aerosol model: Biogeochemical implications. *J. Geophys. Res-Atmos.*, **109(D17)**, D17205.
- Harris, P., Heap, A., Passlow, V., Sbaffi, L., Fellows, M., Porter-Smith, R., Buchanan, C., and Daniell, J., 2005: Geomorphic features of the continental margin of Australia. Record 2003/30, 142 pp, Geoscience Australia.
- Hastings, D. A., and Emery, W. J., 1992: The Advanced Very High-resolution Radiometer (avhrr) - A Brief Reference Guide. *Photogramm. Eng. Rem. S.*, **58(8)**, 1183–1188.
- Hawas, O., Stelcer, E., Cohen, D., Button, D., and Sarbutt, A., 2003: Elemental composition of fine aerosols during the summer of 2002/03 bushfire events in eastern Australia. *Proceedings of the National Clean Air Conference*, vol. CASN03, Newcastle, Australia.
- Hedlund, T., Bilinski, H., Horvath, L., Ingri, N., and Sjoberg, S., 1988: Equilibrium and structural studies of silicon(IV) and aluminium(III) in aqueous-solution .16. Complexation and precipitation reactions in the H⁺ - Al³⁺ - Phthalate system. *Inorg. Chem.*, **27(8)**, 1370–1374.
- Helmets, E., and Vanderloeff, M. M. R., 1993: Lead and Aluminum in Atlantic surface waters (50-degrees-N to 50-degrees-S) reflecting anthropogenic and natural sources in the eolian transport. *J. Geophys. Res-Oceans.*, **98(C11)**, 20261–20273.
- Hendry, K. R., Meredith, M. R., Measures, C. I., Carson, D. S., and Rickaby, R. E. M., 2010: The

- role of sea ice formation in cycling of aluminium in northern Marguerite Bay, Antarctica. *Estuar. Coast. Shelf. S.*, **87(1)**, 103–112.
- Hernandez-Brito, J. J., Gelado-Caballero, M. D., Perez-Pena, J., and Herrera-Melian, J. A., 1994: Fast determination of aluminium reactive to 1,2-dihydroxyanthraquinone-3-sulfonic acid in seawater. *Analyst*, **119**, 1593–1597.
- Herraiz-Borreguero, L., and Rintoul, S. R., 2010: Subantarctic Mode Water variability influenced by mesoscale eddies south of Tasmania. *J. Geophys. Res-Oceans.*, **115**.
- Herraiz-Borreguero, L., and Rintoul, S. R., 2011a: Regional circulation and its impact on upper ocean variability south of Tasmania. *Deep-Sea. Res. Pt. II.*, **58(21-22)**, 2071–2081.
- Herraiz-Borreguero, L., and Rintoul, S. R., 2011b: Subantarctic mode water: distribution and circulation. *Ocean. Dynam.*, **61(1)**, 103–126.
- Hirayama, K., Sekine, T., and Unohara, N., 1994: Determination of trace aluminium in natural waters by ICP-AES after separation and preconcentration using Chromazurol S immobilized silica gel. *Bunseki Kagaku*, **43(12)**, 1065–1070.
- Hooker, S. B., and McClain, C. R., 2000: The calibration and validation of SeaWiFS data. *Prog. Oceanogr.*, **45(3-4)**, 427–465.
- Hsu, N. C., Gautam, R., Sayer, A. M., Bettenhausen, C., Li, C., Jeong, M. J., Tsay, S.-C., and Holben, B. N., 2012: Global and regional trends of aerosol optical depth over land and ocean using SeaWiFS measurements from 1997 to 2010. *Atmos. Chem. Phys.*, **12(17)**, 8037–8053.
- Hydes, D., 1983: Distribution of aluminium in waters of the North East Atlantic 25N to 35N. *Geochim. Cosmochim. Ac.*, **47(5)**, 967–973.
- Hydes, D., 1989: Seasonal variation in dissolved aluminium concentrations in coastal waters and biological limitation of the export of the riverine input of aluminium to the deep seas. *Cont. Shelf. Res.*, **9(10)**, 919 – 929.
- Hydes, D., Statham, P., and Burton, J., 1986: A vertical profile of dissolved trace metals (Al, Cd, Cu, Mn, Ni) over the median valley of the mid Atlantic ridge, 43N: Implications for Hydrothermal activity. *Sci. Total. Environ.*, **49(0)**, 133–145.

- Hydes, D. J., 1979: Aluminum in Seawater: Control by Inorganic Processes. *Science*, **205**(4412), 1260–1262.
- Hydes, D. J., de Lange, G. J., and de Baar H. J. W., 1988: Dissolved Aluminum in the Mediterranean. *Geochim. Cosmochim. Ac.*, **52**(8), 2107–2114.
- Hydes, D. J., and Kremling, K., 1993: Patchiness In Dissolved Metals (al, Cd, Co, Cu, Mn, Ni) In North-sea Surface Waters - Seasonal Differences and Influence of Suspended Sediment. *Cont. Shelf. Res.*, **13**(10), 1083–1101.
- Hydes, D. J., and Liss, P. S., 1976: Fluorimetric method for determination of low concentrations of dissolved Aluminum in natural-waters. *Analyst.*, **101**(1209), 922–931.
- Hydes, D. J., and Liss, P. S., 1977a: Behavior of Dissolved Aluminum In Estuarine and Coastal Waters. *Estuar. Coast. Mar. Sci.*, **5**(6), 755–769.
- Hydes, D. J., and Liss, P. S., 1977b: The behaviour of dissolved aluminium in estuarine and coastal waters. *Estuar. Coast. Mar. Sci.*, **5**(6), 755 – 769.
- Ito, A., 2011: Mega fire emissions in Siberia: potential supply of bioavailable iron from forests to the ocean. *Biogeosciences*, **8**(6), 1679–1697.
- Ito, A., Kok, J. F., Feng, Y., and Penner, J. E., 2012: Does a theoretical estimation of the dust size distribution at emission suggest more bioavailable iron deposition? *Geophys. Res. Lett.*, **39**, 0–0, Ito, Akinori Kok, Jasper F. Feng, Yan Penner, Joyce E.
- Jickells, T., Church, T., Veron, A., and Arimoto, R., 1994: Atmospheric inputs of Manganese and Aluminum to the Sargasso Sea and their relation to surface-water concentrations. *Mar. Chem.*, **46**(3), 283–292.
- Jickells, T. D., 1986: *Studies of trace elements in the Sargasso Sea and the mid Atlantic Bight*. Ph.D. thesis, Univ. of Southampton, Southampton, UK.
- Jickells, T. D., An, Z. S., Andersen, K. K., Baker, A. R., Bergametti, G., Brooks, N., Cao, J. J., Boyd, P. W., Duce, R. A., Hunter, K. A., Kawahata, H., Kubilay, N., laRoche, J., Liss, P. S., Mahowald,

- N., Prospero, J. M., Ridgwell, A. J., Tegen, I., and Torres, R., 2005: Global iron connections between desert dust, ocean biogeochemistry, and climate. *Science.*, **308(5718)**, 67–71.
- Johnson, K. S., Elrod, V. A., Fitzwater, S. E., Plant, J. N., Chavez, F. P., Tanner, S. J., Gordon, R. M., Westphal, D. L., Perry, K. D., Wu, J. F., and Karl, D. M., 2003: Surface ocean-lower atmosphere interactions in the Northeast Pacific Ocean Gyre: Aerosols, iron, and the ecosystem response. *Global. Biogeochem. Cy.*, **17(2)**, 1063.
- Jones, P., and Nesterenko, P. N., 2008: Use of complexing reagents as additives to the eluent for optimization of separation selectivity in high-performance chelation ion chromatography. *J. Chromatogr. A.*, **1213(1)**, 45–49.
- Joyce, R. J., Janowiak, J. E., Arkin, P. A., and Xie, P., 2004: CMORPH: A Method that Produces Global Precipitation Estimates from Passive Microwave and Infrared Data at High Spatial and Temporal Resolution. *J. Hydrometeor.*, **5(3)**, 487–503.
- Kidston, M., Matear, R., and Baird, M. E., 2011: Parameter optimisation of a marine ecosystem model at two contrasting stations in the Sub-Antarctic Zone. *Deep-Sea. Res. Pt. II.*, **58(21-22)**, 2301–2315.
- Kolesov, G. M., Anikiev, V. V., Prasad, S. K., and Sedykh, E. M., 1993: Determination of trace-elements in samples of bottom sediments, suspended matter and aerosols. *Chem. Anal-warsaw.*, **38(5)**, 625–637.
- Koshikawa, M. K., Watanabe, M., Koshikawa, H., Komatsu, K., Imai, A., Inaba, K., and Takamatsu, T., 2010: Speciation of Aluminum in Lake Kasumigaura, Japan. *Bunseki. Kagaku.*, **59(12)**, 1137–1142.
- Kremling, K., 1985: The distribution of cadmium, copper, nickel, manganese, and Aluminum in surface waters of the open Atlantic and European shelf area. *Deep-Sea. Res.*, **32(5)**, 531–555.
- Kremling, K., and Hydes, D., 1988: Summer distribution of dissolved Al, Cd, Co, Cu, Mn and Ni in surface waters around the British-Isles. *Cont. Shelf. Res.*, **8(1)**, 89–105.
- Kremling, K., and Streau, P., 1993: Saharan dust influenced trace-element fluxes in deep North-Atlantic subtropical waters. *Deep-Sea. Res. Pt. I.*, **40(6)**, 1155–1168.

- Kumar, M. D., 1999: The effect of pressure and temperature on aluminium hydrolysis: Implications to trace metal scavenging in natural waters. *Indian. J. Mar. Sci.*, **28**(1), 1–4.
- Laboratory, M. A. P., 2013: Global Precipitation Analysis: Global Monthly Merged Precipitation Analyses of GPCP (1979-present), Annual Average mm/day.
<http://precip.gsfc.nasa.gov/gifs/v2.79-06.climo.gif>
.
- Lannuzel, D., Bowie, A. R., Remenyi, T., Lam, P., Townsend, A., Ibisani, E., Butler, E., Wagener, T., and Schoemann, V., 2011a: Distributions of dissolved and particulate iron in the sub-Antarctic and Polar Frontal Southern Ocean (Australian sector). *Deep-Sea. Res. Pt. II.*, **58**(21-22), 2094–2112.
- Lannuzel, D., Bowie, A. R., van der Merwe, P. C., Townsend, A. T., and Schoemann, V., 2011b: Distribution of dissolved and particulate metals in Antarctic sea ice. *Mar. Chem.*, **124**(1-4), 134–146.
- Lannuzel, D., Schoemann, V., de Jong, J., Chou, L., Delille, B., Becquevort, S., and Tison, J.-L., 2008: Iron study during a time series in the western Weddell pack ice. *Mar. Chem.*, **108**(12), 85–95.
- Lannuzel, D., Schoemann, V., de Jong, J., Pasquer, B., van der Merwe, P., Masson, F., Tison, J. L., and Bowie, A., 2010: Distribution of dissolved iron in Antarctic sea ice: Spatial, seasonal, and inter-annual variability. *J. Geophys. Res-Biogeosci.*, **115**, G03022.
- Lannuzel, D., Schoemann, V., de Jong, J. T. M., Tison, J., and Chou, L., 2007: Distribution and biogeochemical behaviour of iron in the East Antarctic sea ice. *Mar. Chem.*, **106**, 18–32.
- Lee, B. L., Chua, L. H., Ong, H. Y., Yang, H. G., Wu, J. F., and Ong, C. N., 1996: Determination of serum and urinary aluminum by HPLC with fluorometric detection of Al-lumogallion complex. *Clin. Chem.*, **42**(9), 1405–1411.
- Lian, H., Kang, Y., Arkin, Y., Bi, S., Li, D., Mei, S., Wu, X., Tao, X., Chen, Y., Dai, L., Gan, N., and Tian, L., 2004a: Fractionation of aluminum in natural waters by fluorometry based on the competitive complexation. *Anal. Chim. Acta.*, **511**(1), 25–31.

- Lian, H., Kang, Y., Bi, S., Arkin, Y., Shao, D., Li, D., Chen, Y., Dai, L., Gan, N., and Tian, L., 2004b: Direct determination of trace aluminum with quercetin by reversed-phase high performance liquid chromatography. *Talanta*, **62**(1), 43 – 50.
- Lian, H. Z., Kang, Y. F., Bi, S. P., Yasin, A., Shao, D. L., Chen, Y. J., Dai, L. M., and Tian, L. C., 2003: Morin applied in speciation of aluminium in natural waters and biological samples by reversed-phase high-performance liquid chromatography with fluorescence detection. *Anal. Bioanal. Chem.*, **376**, 542–548, 10.1007/s00216-003-1936-8.
- Libes, S. M., 1992: *An introduction to biogeochemistry*. John Wiley and Sons, New York.
- Liu, X. J., Zheng, B. S., Wang, B. B., and Wang, M. S., 2005: The characteristics of dissolution of fluoride and aluminum from brick tea. *Chinese. J. Geochem.*, **24**, 382–385, 10.1007/BF02873802.
- Lumpkin, R., and Speer, K., 2007: Global Ocean Meridional Overturning. *J. Phys. Oceanogr.*, **37**(10), 2550–2562.
- Luo, C., Mahowald, N., Bond, T., Chuang, P. Y., Artaxo, P., Siefert, R., Chen, Y., and Schauer, J., 2008: Combustion iron distribution and deposition. *Global. Biogeochem. Cy.*, **22**(1), GB1012.
- Lydersen, E., 1990: The solubility and hydrolysis of aqueous aluminum hydroxides in dilute fresh waters at different temperatures. *Nord. Hydrol.*, **21**(3), 195–204.
- Mackenzie, F. T., Stoffyn, M., and Wollast, R., 1978: Aluminum in seawater - control by biological-activity. *Science.*, **199**(4329), 680–682.
- Mackie, D. S., Boyd, P. W., McTainsh, G. H., Tindale, N. W., Westberry, T. K., and Hunter, K. A., 2008: Biogeochemistry of iron in Australian dust: From eolian uplift to marine uptake. *Geochem. Geophys. Geosys.*, **9**, Q03Q08.
- Mackin, J. E., and Aller, R. C., 1984a: Diagenesis of Dissolved Aluminum In Organic-rich Estuarine Sediments. *Geochim. Cosmochim. Ac.*, **48**(2), 299–313.
- Mackin, J. E., and Aller, R. C., 1984b: Dissolved Al In Sediments and Waters of the East China Sea - Implications For Authigenic Mineral Formation. *Geochim. Cosmochim. Ac.*, **48**(2), 281–297.

- Mackin, J. E., and Aller, R. C., 1984c: Processes Affecting the Behavior of Dissolved Aluminum In Estuarine Waters. *Mar. Chem.*, **14(3)**, 213–232.
- Mackin, J. E., and Aller, R. C., 1986: The Effects of Clay Mineral Reactions On Dissolved Al Distributions In Sediments and Waters of the Amazon Continental-shelf. *Cont. Shelf. Res.*, **6(1-2)**, 245–262.
- Mahadevan, A., DAsaro, E., Lee, C., and Perry, M. J., 2012: Eddy-Driven Stratification Initiates North Atlantic Spring Phytoplankton Blooms. *Science*, **337(6090)**, 54–58.
- Mahowald, N. M., Ballantine, J. A., Feddema, J., and Ramankutty, N., 2007: Global trends in visibility: implications for dust sources. *Atmos. Chem. Phys.*, **7(12)**, 3309–3339.
- Mahowald, N. M., Muhs, D. R., Levis, S., Rasch, P. J., Yoshioka, M., Zender, C. S., and Luo, C., 2006: Change in atmospheric mineral aerosols in response to climate: Last glacial period, preindustrial, modern, and doubled carbon dioxide climates. *J. Geophys. Res-Atmos.*, **111(D10)**, 0–0.
- Manuel-Vez, M., Moreno, C., Gonzlez, D., and Garca-Vargas, M., 1997: Direct fluorimetric determination of dissolved aluminum in seawater at nanomolar levels. *Anal. Chim. Acta.*, **355(2-3)**, 157–161.
- Martin, J., and Fitzwater, S. E., 1988: Iron deficiency limits phytoplankton growth in the northeast Pacific subarctic. *Nature.*, **331**, 341–343.
- Martin, J. H., 1990: Glacial-interglacial CO₂ change: the iron hypothesis. *Paleoceanography.*, **vol.5, no.1**, 1–13.
- Martin, J. H., 1991: Iron, Liebig's Law, and the greenhouse. *Oceanography.*, **4(2)**, 52–55.
- Martin, J. H., Gordon, R. M., and Fitzwater, S. E., 1990: Iron in Antarctic waters. *Nature.*, **345(6271)**, 156–158.
- McGowan, H., and Clark, A., 2008: Identification of dust transport pathways from Lake Eyre, Australia using Hysplit. *Atmos. Environ.*, **42(29)**, 6915–6925.

- McMeeking, G. R., Kreidenweis, S. M., Carrico, C. M., Lee, T., Collett, J. L., and Malm, W. C., 2005: Observations of smoke-influenced aerosol during the Yosemite Aerosol Characterization Study: Size distributions and chemical composition. *J. Geophys. Res-Atmos.*, **110(D9)**, D09206.
- McTainsh, G., 1985: Dust Processes In Australia and West-Africa - A Comparison. *Search.*, **16(3-4)**, 104–106.
- McTainsh, G., and Strong, C., 2007: The role of aeolian dust in ecosystems. *Geomorphology.*, **89(1-2)**, 39–54.
- Measures, C., 2002: Antarctic Environment and Southern Ocean Process Study (AESOPS), dissolved aluminium values. Database product, United States JGOFS Data Server. Woods Hole Oceanographic Institution, USA: U.S. JGOFS Data Management Office., Accessed:18th November, 2012. http://usjgofs2.whoi.edu/jg/dir/jgofs/merged_objects/US_JGOFS/Southern_Ocean/.
- Measures, C., Edmond, J., and Jickells, T., 1986: Aluminium in the northwest Atlantic. *Geochim. Cosmochim. Ac.*, **50(7)**, 1423–1429.
- Measures, C. I., 1999: The role of entrained sediments in sea ice in the distribution of aluminium and iron in the surface waters of the Arctic Ocean. *Mar. Chem.*, **68(1-2)**, 59–70.
- Measures, C. I., and Brown, E. T., 1996: Estimating dust input to the Atlantic Ocean using surface water Al concentrations. S. Guerzoni, and R. Chester, Eds., *The Impact of African Dust Across the Mediterranean*, vol. 11, Springer, 301–311, Environmental Science and Technology Library.
- Measures, C. I., Brown, M. T., and Vink, S., 2005: Dust deposition to the surface waters of the western and central North Pacific inferred from surface water dissolved aluminum concentrations. *Geochem. Geophys. Geosys.*, **6**, 1–16.
- Measures, C. I., Cutter, G. A., Landing, W. M., and Powell, R. T., 2006: Hydrographic observations during the 2002 IOC Contaminant Baseline Survey in the western Pacific Ocean. *Geochem. Geophys. Geosys.*, **7**, Q03M06.
- Measures, C. I., and Edmond, J. M., 1989: Shipboard determination of aluminum in seawater at the nanomolar level by electron capture detection gas chromatography. *Anal. Chem.*, **61(6)**, 544–547.

- Measures, C. I., and Edmond, J. M., 1990: Aluminum in the South-Atlantic - steady-state distribution of a short residence time element. *J. Geophys. Res-Oceans.*, **95(C4)**, 5331–5340.
- Measures, C. I., Grant, B., Khadem, M., Lee, D. S., and Edmond, J. M., 1984: Distribution of Be, Al, Se and Bi In the Surface Waters of the Western North-atlantic and Caribbean. *Earth. Planet. Sc. Lett.*, **71(1)**, 1–12.
- Measures, C. I., Landing, W. M., Brown, M. T., and Buck, C. S., 2008a: A commercially available rosette system for trace metal-clean sampling. *Limnol. Oceanogr.-Meth.*, **6**, 384–394.
- Measures, C. I., Landing, W. M., Brown, M. T., and Buck, C. S., 2008b: High-resolution Al and Fe data from the Atlantic Ocean CLIVAR-CO(2) repeat hydrography A16N transect: Extensive linkages between atmospheric dust and upper ocean geochemistry. *Global. Biogeochem. Cy.*, **22(1)**, GB1005.
- Measures, C. I., Landing, W. M., Buck, C. S., Brown, M. T., Hiscock, W. T., Grand, M. M., Hatta, M., and Gosnell, K. J., 2008c: Global patterns of dust deposition deduced from dissolved Al in the surface ocean. *Geochim. Cosmochim. Ac.*, **72(12)**, A617–A617.
- Measures, C. I., Sato, T., Vink, S., Howell, S., and Li, Y. H., 2010: The fractional solubility of aluminium from mineral aerosols collected in Hawaii and implications for atmospheric deposition of biogeochemically important trace elements. *Mar. Chem.*, **120(1-4)**, 144–153.
- Measures, C. I., and Vink, S., 1999: Seasonal variations in the distribution of Fe and Al in the surface waters of the Arabian Sea. *Deep-Sea. Res. Pt. II.*, **46(8-9)**, 1597–1622.
- Measures, C. I., and Vink, S., 2000: On the use of dissolved aluminum in surface waters to estimate dust deposition to the ocean. *Global. Biogeochem. Cy.*, **14(1)**, 317–327.
- Measures, C. I., and Vink, S., 2001: Dissolved Fe in the upper waters of the Pacific sector of the Southern Ocean. *Deep-Sea. Res. Pt. II.*, **48(19-20)**, 3913–3941.
- Middag, R., 2010: *Dissolved Aluminium and Manganese in the Polar Oceans*. Doctorate of philosophy, Royal Netherlands Institute for Sea Research (NIOZ), Department of Biological Oceanography, P.O. Box 59, 1790 AB Den Burg, The Netherlands.

- Middag, R., de Baar, H., Laan, P., Cai, P., and van Ooijen, J., 2011a: Dissolved manganese in the Atlantic sector of the Southern Ocean. *Deep-Sea. Res. Pt. II.*, **58(25-26)**, 2661–2677.
- Middag, R., de Baar, H. J. W., Klunder, M. B., and Laan, P., 2013: Fluxes of dissolved aluminum and manganese to the Weddell Sea and indications for manganese co-limitation. *Limnol. Oceanogr.*, **58(1)**, 287–300.
- Middag, R., de Baar, H. J. W., Laan, P., and Bakker, K., 2009: Dissolved aluminium and the silicon cycle in the Arctic Ocean. *Mar. Chem.*, **115(3-4)**, 176 – 195.
- Middag, R., de Baar, H. J. W., Laan, P., and Huhn, O., 2012a: The effects of continental margins and water mass circulation on the distribution of dissolved aluminum and manganese in Drake Passage. *J. Geophys. Res-Oceans.*, **117**, C01019.
- Middag, R., de Baar, H. J. W., Laan, P., and Klunder, M. B., 2011b: Fluvial and hydrothermal input of manganese into the Arctic Ocean. *Geochim. Cosmochim. Ac.*, **75(9)**, 2393–2408.
- Middag, R., Van Aken, H. M., and De Baar, H. J., 2012b: Dissolved aluminium in the West-Atlantic Ocean from Greenland to the Falkland Islands / Malvinas. *Ocean Sciences Meeting, Salt Lake City*.
- Middag, R., van Slooten, C., de Baar, H., and Laan, P., 2011c: Dissolved aluminium in the Southern Ocean. *Deep-Sea. Res. Pt. II.*, **58(25-26)**, 2647–2660.
- Milne, A., Landing, W., Bizimis, M., and Morton, P., 2010: Determination of Mn, Fe, Co, Ni, Cu, Zn, Cd and Pb in seawater using high resolution magnetic sector inductively coupled mass spectrometry (HR-ICP-MS). *Anal. Chim. Acta.*, **665(2)**, 200–207.
- Mitchell, R. M., Obrien, D. M., and Forgan, B. W., 1992: Calibration of the NOAA AVHRR shortwave channels using split pass imagery: a pilot-study. *Remote. Sens. Environ.*, **40(1)**, 57–65.
- Moller, N., Christov, C., and Weare, J., Eds., 2006: *Thermodynamic models of aluminum silicate mineral solubility for application to enhanced geothermal systems*, no. SGP-TR-179 in Geochemistry, Stanford, California, Stanford University, Stanford University.

- Mongin, M., Matear, R., and Chamberlain, M., 2011a: Seasonal and spatial variability of remotely sensed chlorophyll and physical fields in the SAZ-Sense region. *Deep-Sea. Res. Pt. II.*, **58(21-22)**, 2082–2093.
- Mongin, M., Matear, R., and Chamberlain, M., 2011b: Simulation of chlorophyll and iron supplies in the Sub Antarctic Zone South of Australia. *Deep-Sea. Res. Pt. II.*, **58(21-22)**, 2126–2134.
- Mongin, M., Molina, E., and Trull, T. W., 2008: Seasonality and scale of the Kerguelen plateau phytoplankton bloom: A remote sensing and modeling analysis of the influence of natural iron fertilization in the Southern Ocean. *Deep-Sea. Res. Pt. II.*, **55(5-7)**, 880–892.
- Mongin, M. M., Abraham, E. R., and Trull, T. W., 2009: Winter advection of iron can explain the summer phytoplankton bloom that extends 1000 km downstream of the Kerguelen Plateau in the Southern Ocean. *J. Mar. Res.*, **67(2)**, 225–237.
- Moore, J. K., Doney, S. C., and Lindsay, K., 2004: Upper ocean ecosystem dynamics and iron cycling in a global three-dimensional model. *Global. Biogeochem. Cy.*, **18(4)**, GB4028.
- Moran, S., and Moore, R., 1991: The potential source of dissolved aluminum from resuspended sediments to the North-Atlantic Deep-Water. *Geochim. Cosmochim. Ac.*, **55(10)**, 2745–2751.
- Moran, S. B., and Moore, R. M., 1988: Temporal variations in dissolved and particulate aluminum during a spring bloom. *Estuar. Coast. Shelf. S.*, **27(2)**, 205 – 215.
- Moran, S. B., and Moore, R. M., 1992: Kinetics of the removal of dissolved Aluminum by diatoms in seawater - a comparison with Thorium. *Geochim. Cosmochim. Ac.*, **56(9)**, 3365–3374.
- Moran, S. B., Moore, R. M., and Westerlund, S., 1992: Dissolved Aluminum in the Weddell Sea. *Deep-Sea. Res.*, **39(3-4A)**, 537–547.
- Moulin, C., Gordon, H. R., Chomko, R. M., Banzon, V. F., and Evans, R. H., 2001: Atmospheric correction of ocean color imagery through thick layers of Saharan dust. *Geophys. Res. Lett.*, **28(1)**, 5–8.
- Moyna, A., Connolly, D., Nesterenko, E., Nesterenko, P. N., and Paull, B., 2012: Separation of selected transition metals by capillary chelation ion chromatography using acetyl-iminodiacetic acid modified capillary polymer monoliths. *J. Chromatogr. A.*, **1249**, 155–163.

- Mulhearn, P., 1983: On the climatology of East Australian Current warm-core rings. *Aust. J. Mar. Fresh. Res.*, **34**, 687–692.
- Mulon, J.-B., Destandau, È., Alain, V., and Bardez, È., 2005: How can aluminium(III) generate fluorescence? *J. Inorg. Biochem.*, **99(9)**, 1749–1755.
- Nagae, N., and Sato, M., 2005: A Fluorescence Detection / HPLC Method for the Analysis of Aluminum in Pharmaceutical Products. *Am. Lab.*, **37(11)**, 19–27.
- Narvekar, P. V., and Singbal, S. Y. S., 1993: Dissolved aluminum in the surface microlayer of the eastern arabian sea. *Mar. Chem.*, **42(2)**, 85–94.
- Nelson, D., and Treguer, P., 1992: On the role of silicon as a limiting nutrient to Antarctic diatoms: evidence from kinetic studies in the Ross Sea ice-edge zone. *Mar. Ecol. Prog. Ser.*, **80**, 255–264.
- Nelson, D. M., Anderson, R. F., Barber, R. T., Brzezinski, M. A., Buesseler, K. O., Chase, Z., Collier, R. W., Dickson, M. L., Francois, R., Hiscock, M. R., Honjo, S., Marra, J., Martin, W. R., Sambrotto, R. N., Sayles, F. L., and Sigmon, D. E., 2002: Vertical budgets for organic carbon and biogenic silica in the Pacific sector of the Southern Ocean, 1996–1998. *Deep-Sea. Res. Pt. II.*, **49(9-10)**, 1645–1674.
- Nesterenko, E. P., Nesterenko, P. N., Paull, B., Melandez, M., and Corredor, J., 2012: Fast direct determination of strontium in seawater using high-performance chelation ion chromatography. *Microchem. J.*, **na(0)**, 0–0, in press.
- Nesterenko, P., and Jones, P., 1996: The comparative investigation of several stationary phases containing iminodiacetic functional groups for the high performance chelating exchange chromatography. *J. Liq. Chromatogr. R. T.*, **19(7)**, 1033–1045.
- Nesterenko, P., and Jones, P., 1997: Single-column method of chelation ion chromatography for the analysis of trace metals in complex samples. *J. Chromatogr. A.*, **770(1-2)**, 129–135.
- Nesterenko, P., and Shpigun, O., 2002: High-performance chelation chromatography of metal ions on sorbents with grafted iminodiacetic acid. *Russ. J. Coord. Chem.*, **28(10)**, 726–735.

- Nilsson, C., and Cresswell, G., 1980: The Formation and evolution of East Australian Current warm-core eddies. *Prog. Oceanogr.*, **9**, 133–138.
- Obata, H., Alibo, D. S., and Nozaki, Y., 2007: Dissolved aluminum, indium, and cerium in the Sea of Japan and the Sea of Okhotsk: Comparison to the marginal seas of the western North Pacific. *J. Geophys. Res-Oceans.*, **112(C12)**.
- Obata, H., Karatani, H., and Nakayama, E., 1993: Automated-determination of Iron In Seawater By Chelating Resin Concentration and Chemiluminescence Detection. *Anal. Chem.*, **65(11)**, 1524–1528.
- Obata, H., Nozaki, Y., Alibo, D. S., and Yamamoto, Y., 2004: Dissolved Al, In, and Ce in the eastern Indian Ocean and the Southeast Asian Seas in comparison with the radionuclides Pb-210 and Po-210. *Geochim. Cosmochim. Ac.*, **68(5)**, 1035–1048.
- Obata, H., Shitashima, K., Isshik, K., and Nakayama, E., 2008: Iron, manganese and aluminum in upper waters of the western South Pacific ocean and its adjacent seas. *J. Oceanogr.*, **64(2)**, 233–245.
- Oberacher, H., and Huber, C. G., 2002: Capillary monoliths for the analysis of nucleic acids by high-performance liquid chromatography-electrospray ionization mass spectrometry. *TrAC-trend. Anal. Chem.*, **21(3)**, 166–174.
- Oh-yoshi, E., Sakata, T., and Kurihara, M., 1999: Complexation of aluminium with (-)-epigallocatechin gallate studied by spectrophotometry. *J. Inorg. Biochem.*, **73(1-2)**, 31–34.
- Orians, K. J., and Bruland, K. W., 1985: Dissolved Aluminum In the Central North Pacific. *Nature.*, **316(6027)**, 427–429.
- Orians, K. J., and Bruland, K. W., 1986: The biogeochemistry of Aluminum in the Pacific-Ocean. *Earth. Planet. Sc. Lett.*, **78(4)**, 397–410.
- Paces, T., 1978: Reversible Control of Aqueous Aluminum and Silica During Irreversible Evolution of Natural-waters. *Geochim. Cosmochim. Ac.*, **42(10)**, 1487–1493.

- Pachauri, R., and Reisinger, A., 2007: Climate Change 2007: Synthesis Report. Tech. Rep. 4, IPCC, Geneva, Switzerland.
- Parslow, J., Boyd, P., Rintoul, S., and Griffiths, F., 2001: A persistent subsurface chlorophyll maximum in the Interpolar Frontal Zone south of Australia: Seasonal progression and implications for phytoplankton-light-nutrient interactions. *J. Geophys. Res-Oceans.*, **106(C12)**, 31543–31557.
- Patterson, C. C., 1965: Contaminated and natural lead environments of man. *Arch. Environ. Health.*, **11(3)**, 344–360.
- Pelletier, S., and Lucy, C. A., 2006: Achieving rapid low-pressure ion chromatography separations on short silica-based monolithic columns. *J. Chromatogr. A.*, **1118(1)**, 12 – 18.
- R-Development-Core-Team, 2010: *R: A Language and Environment for Statistical Computing*.
- Radlein, N., and Heumann, K. G., 1992: Trace analysis of heavy-metals in aerosols over the Atlantic-Ocean from Antarctica to Europe. *Int. J. Environ. An. Ch.*, **48(2)**, 127–150.
- Ranau, R., Oehlenschläger, J., and Steinhart, H., 1999: Determination of aluminium in the edible part of fish by GFAAS after sample pretreatment with microwave activated oxygen plasma. *Fresen. J. Anal. Chem.*, **364**, 599–604, 10.1007/s002160051393.
- Remenyi, T. A., Nesterenko, P. N., Bowie, A. R., Butler, E. C. V., and Haddad, P. R., 2011: Fast and sensitive determination of aluminium with RP-HPLC using an ultra-short monolithic column. *Anal. Method.*, **3(11)**, 2488–2494.
- Remenyi, T. A., Nesterenko, P. N., Bowie, A. R., Butler, E. C. V., and Haddad, P. R., 2012: Reversed phase high performance liquid chromatographic determination of dissolved aluminium in open ocean seawaters. *Limnol. Oceanogr.-Meth.*, **10**, 832–839.
- Resing, J. A., and Measures, C. I., 1994: Fluorometric Determination of Al in Seawater by Flow Injection Analysis with In-Line Preconcentration. *Anal. Chem.*, **66(22)**, 4105–4111.
- Riaz, A., and Chung, D. S., 2005: Transient isotachopheresis of highly saline trace metals under strong electroosmotic flow conditions. *Electrophoresis*, **26(3)**, 668–673.

- Riaz, A., Kim, B., and Chung, D. S., 2003: Capillary electrophoresis of trace metals in highly saline physiological sample matrices. *Electrophoresis*, **24**(16), 2788–2795.
- Ridgway, K. R., 2007: Seasonal circulation around Tasmania: An interface between eastern and western boundary dynamics. *J. Geophys. Res-Oceans.*, **112**(C10), C10016.01–C10016.18.
- Ridgway, K. R., and Condie, S. A., 2004: The 5500-km-long boundary flow off western and southern Australia. *J. Geophys. Res-Oceans.*, **109**(C4), C04017.
- Ridgway, K. R., and Godfrey, J. S., 1994: Mass and heat budgets in the east australian current - a direct approach. *J. Geophys. Res-Oceans.*, **99**(C2), 3231–3248.
- Ridgway, K. R., and Godfrey, J. S., 1997: Seasonal cycle of the East Australian Current. *J. Geophys. Res-Oceans.*, **102**(C10), 22921–22936.
- Rietz, B., Heydorn, K., and Pritzl, G., 1997: Determination of aluminium in fish tissues by means of INAA and ICP-MS. *J. Radioanal. Nucl. Ch.*, **216**, 113–116, 10.1007/BF02034505.
- Rintoul, S., and Bullister, J., 1999: A late winter hydrographic section from Tasmania to Antarctica. *Deep-Sea. Res. Pt. I.*, **46**(8), 1417–1454.
- Rintoul, S., Donguy, J., and Roemmich, D., 1997: Seasonal evolution of upper ocean thermal structure between Tasmania and Antarctica. *Deep-Sea. Res. Pt. I.*, **44**(7), 1185–1202.
- Rintoul, S., and Sokolov, S., 2001: Baroclinic transport variability of the Antarctic Circumpolar Current south of Australia (WOCE repeat section SR3). *J. Geophys. Res-Oceans.*, **106**(C2), 2815–2832.
- Rintoul, S., Sokolov, S., and Church, J., 2002: A 6 year record of baroclinic transport variability of the Antarctic Circumpolar Current at 140 degrees E derived from expendable bathythermograph and altimeter measurements. *J. Geophys. Res-Oceans.*, **107**(C10).
- Rintoul, S., and Trull, T., 2001: Seasonal evolution of the mixed layer in the Subantarctic Zone south of Australia. *J. Geophys. Res-Oceans.*, **106**(C12), 31447–31462.
- Rintoul, S. R., 2007: Rapid freshening of Antarctic Bottom Water formed in the Indian and Pacific oceans. *Geophys. Res. Lett.*, **34**(6).

- Roberson, C. E., and Hem, J. D., 1969: *Solubility of aluminum in the presence of hydroxide, fluoride, and sulfate*. U.S. G.P.O., Washington, – pp.
- Roeske, T., Loeff, M., Middag, R., and Bakker, K., 2012: Deep water circulation and composition in the Arctic Ocean by dissolved barium, aluminium and silicate. *Mar. Chem.*, **132-133**, 56–67.
- Rolph, G., 2012: Real-time Environmental Applications and Display sYstem (READY). Website (<http://ready.arl.noaa.gov>). NOAA Air Resources Laboratory, Silver Spring, MD.
- Rosenberg, M., 2007: SAZ-SENSE, Marine Science Cruise AU0703 – Oceanographic Field Measurements and Analysis. unpublished report, Antarctic Climate and Ecosystems Cooperative Research Centre, Hobart, Australia.
- Rosenberg, M., 2008: CASO–SR3, Marine Science Cruise AU0806 – Oceanographic Field Measurements and Analysis. unpublished report, Antarctic Climate and Ecosystems Cooperative Research Centre, Hobart, Australia.
- Rosenberg, M., Howard, W., and Griffiths, B., 2010: ADCP data collected during the SAZ-SENSE voyage, January–February 2007. Australian Antarctic Data Centre - CAASM Metadata.
- Rutgers V.D. Loeff, M., Cai, P. H. H., Stimac, I., Bracher, A., Middag, R., Klunder, M. B., and van Heuven, S. M. A. C., 2011: (234)Th in surface waters: Distribution of particle export flux across the Antarctic Circumpolar Current and in the Weddell Sea during the GEOTRACES expedition ZERO and DRAKE. *Deep-Sea. Res. Pt. II.*, **58(25-26)**, 2749–2766.
- Saarnio, K., Aurela, M., Timonen, H., Saarikoski, S., Teinila, K., Makela, T., Sofiev, M., Koskinen, J., Aalto, P. P., Kulmala, M., Kukkonen, J., and Hillamo, R., 2010: Chemical composition of fine particles in fresh smoke plumes from boreal wild-land fires in Europe. *Sci. Total. Environ.*, **408(12)**, 2527–2542.
- Sanudo-Wilhelmy, S. A., Olsen, K. A., Scelfo, J. M., Foster, T. D., and Flegal, A. R., 2002: Trace metal distributions off the Antarctic Peninsula in the Weddell Sea. *Mar. Chem.*, **77(2-3)**, 157–170.
- Šatinský, D., Neto, I., Solich, P., Sklenářová, H., Conceição, M., Montenegro, B. S. M., and Araújo, A. N., 2004: Sequential injection chromatographic determination of paracetamol, caffeine, and acetylsalicylic acid in pharmaceutical tablets. *J. Sep. Sci.*, **27(7-8)**, 529–536.

- Šatinský, D., Solich, P., Chocholous, P., and Karlíček, R., 2003: Monolithic columns—a new concept of separation in the sequential injection technique. *Anal. Chim. Acta.*, **499(1-2)**, 205 – 214.
- Saukkoriipi, J., 2010: *Theoretical study of the hydrolysis of aluminum complexes*. Ph.D. thesis, University of Oulu, Faculty of Science, Department of Chemistry.
- Savenko, A., and Savenko, V., 2011: Aluminum hydroxides solubility and the forms of dissolved aluminums occurrence in seawaters. *Okeanologiya+*, **51(2)**, 231–234–.
- Ščančar, J., and Milačič, R., 2006: Aluminium speciation in environmental samples: a review. *Anal. Bioanal. Chem.*, **386**, 999–1012, 10.1007/s00216-006-0422-5.
- Schellinger, A. P., and Carr, P. W., 2004: Solubility of buffers in aqueous-organic eluents for reversed-phase liquid chromatography. *LC. GC. N. Am.*, **22(6)**, 544–548.
- Schlitzer, R., 2002: Interactive analysis and visualization of geoscience data with Ocean Data View. *Comput. Geosci.*, **28(10)**, 1211–1218.
- Schlitzer, R., 2012: Ocean Data View. Tech. rep., Alfred Wegener Institute for Polar and Marine Research, Bremerhaven, Germany.
- Schmitz, W. J., 1996: On the world ocean circulation. Volume I, some global features/North Atlantic circulation. Tech. rep., Woods Hole Oceanographic Institute.
- Schulz, M., Cozic, A., and Szopa, S., 2009: LMDzT-INCA Dust Forecast Model Developments and Associated Validation Efforts. J. Perez, and J. Baldasano, Eds., *WMO/GEO Expert Meeting On An International Sand And Dust Storm Warning System*, vol. 7 of *IOP Conference Series Earth and Environmental Science*, Barcelona Supercomp Ctr; World Meteorol Org; Grp Earth Observat; Agencia Estatal Meteorol; Consejo Super Investigac Cientif.
- SCOR Working Group, 2006: *GEOTRACES - An International Study of the Marine Biogeochemical Cycles of Trace Elements and Their Isotopes, Science Plan*. Scientific Committee on Oceanic Research.
- SCOR Working Group, 2007: GEOTRACES - An international study of the global marine biogeochemical cycles of trace elements and their isotopes. *Chem. Erde. Geochem.*, **67(2)**, 85–131.

- SCOR Working Group, 2012: GEOTRACES: An international study of marine biogeochemical cycles of trace elements and their isotopes. <http://www.geotraces.org/>.
- Sedwick, P., Bowie, A., and Trull, T., 2008: Dissolved iron in the Australian sector of the Southern Ocean (CLIVAR SR3 section): Meridional and seasonal trends. *Deep-Sea. Res. Pt. I.*, **55**(8), 911–925.
- Seze, W. Y. G., Letreut, H., and Desbois, M., 1991: Comparison of radiance fields observed by satellite and simulated by the LMD General-Circulation Models. *Dynam. Atmos. Oceans.*, **16**(1-2), 147–165.
- Sholkovitz, E. R., Sedwick, P. N., and Church, T. M., 2009: Influence of anthropogenic combustion emissions on the deposition of soluble aerosol iron to the ocean: Empirical estimates for island sites in the North Atlantic. *Geochim. Cosmochim. Ac.*, **73**(14), 3981–4003.
- Sholkovitz, E. R., Sedwick, P. N., Church, T. M., Baker, A. R., and Powell, C. F., 2012: Fractional solubility of aerosol iron: Synthesis of a global-scale data set. *Geochim. Cosmochim. Ac.*, **89**(0), 173–189.
- Siddall, M., Khatiwala, S., van de Flierdt, T., Jones, K., Goldstein, S. L., Hemming, S., and Anderson, R. F., 2008: Towards explaining the Nd paradox using reversible scavenging in an ocean general circulation model. *Earth. Planet. Sc. Lett.*, **274**(3-4), 448–461.
- Smirnov, A., Holben, B. N., Kaufman, Y. J., Dubovik, O., Eck, T. F., Slutsker, I., Pietras, C., and Halthore, R. N., 2002: Optical properties of atmospheric aerosol in maritime environments. *J. Atmos. Sci.*, **59**(3), 501–523.
- Sohrin, Y., Urushihara, S., Nakatsuka, S., Kono, T., Higo, E., Minami, T., Norisuye, K., and Umetani, S., 2008: Multielemental determination of GEOTRACES key trace metals in seawater by ICPMS after preconcentration using an ethylenediaminetriacetic acid chelating resin. *Anal. Chem.*, **80**(16), 6267–6273.
- Sokolov, S., and Rintoul, S., 2002: Structure of Southern Ocean fronts at 140 degrees E. *J. Mar. Syst.*, **37**(1-3), 151–184.

- Sokolov, S., and Rintoul, S. R., 2007a: Multiple jets of the Antarctic circumpolar current South of Australia. *J. Phys. Oceanogr.*, **37**(5), 1394–1412.
- Sokolov, S., and Rintoul, S. R., 2007b: On the relationship between fronts of the Antarctic Circumpolar Current and surface chlorophyll concentrations in the Southern Ocean. *J. Geophys. Res-Oceans.*, **112**(C7).
- Sokolov, S., and Rintoul, S. R., 2009a: Circumpolar structure and distribution of the Antarctic Circumpolar Current fronts: 1. Mean circumpolar paths. *J. Geophys. Res-Oceans.*, **114**.
- Sokolov, S., and Rintoul, S. R., 2009b: Circumpolar structure and distribution of the Antarctic Circumpolar Current fronts: 2. Variability and relationship to sea surface height. *J. Geophys. Res-Oceans.*, **114**.
- Stoffyn, M., 1979: Biological-control of Dissolved Aluminum In Seawater - Experimental-evidence. *Science.*, **203**(4381), 651–653.
- Stoffyn, M., and Mackenzie, F. T., 1982: Fate of dissolved Aluminum in the oceans. *Mar. Chem.*, **11**(2), 105–127.
- Strand, L., Abrahamsen, G., and Stuanes, A. O., 2002: Leaching from organic matter-rich soils by rain of different qualities: I. Concentrations. *J. Environ. Qual.*, **31**(2)(0047-2425 (Linking)), 547–556.
- Streets, D. G., Yan, F., Chin, M., Diehl, T., Mahowald, N., Schultz, M., Wild, M., Wu, Y., and Yu, C., 2009: Anthropogenic and natural contributions to regional trends in aerosol optical depth, 1980-2006. *J. Geophys. Res-Atmos.*, **114**, D00D18.
- Strong, C., Parsons, K., McTainsh, G., and Sheehan, A., 2011: Dust transporting wind systems in the lower Lake Eyre Basin, Australia: A preliminary study. *Aeol. Res.*, **2**(4), 205–214.
- Sugrue, E., Nesterenko, P., and Paull, B., 2004: Ion exchange properties of monolithic and particle type iminodiacetic acid modified silica. *J. Sep. Sci.*, **27**(10-11), 921–930.
- Sunda, W. G., and Huntsman, S. A., 1995: Iron Uptake and Growth Limitation In Oceanic and Coastal Phytoplankton. *Mar. Chem.*, **50**(1-4), 189–206.

- Sunda, W. G., Swift, D. G., and Huntsman, S. A., 1991: Low Iron Requirement For Growth In Oceanic Phytoplankton. *Nature*, **351(6321)**, 55–57.
- Tagliabue, A., Bopp, L., Dutay, J. C., Bowie, A. R., Chever, F., Jean-Baptiste, P., Bucciarelli, E., Lannuzel, D., Remenyi, T., Sarthou, G., Aumont, O., Gehlen, M., and Jeandel, C., 2010: Hydrothermal contribution to the oceanic dissolved iron inventory. *Nat. Geosci.*, **3(4)**, 252–256.
- Taylor, S. R., 1964: Abundance of chemical elements in the continental crust: a new table. *Geochim. Cosmochim. Ac.*, **28(8)**, 1273 – 1285.
- Team, J. D., 2013: *JabRef*.
- Textor, C., Schulz, M., Guibert, S., Kinne, S., Balkanski, Y., Bauer, S., Berntsen, T., Berglen, T., Boucher, O., Chin, M., Dentener, F., Diehl, T., Easter, R., Feichter, H., Fillmore, D., Ghan, S., Ginoux, P., Gong, S., Kristjansson, J. E., Krol, M., Lauer, A., Lamarque, J. F., Liu, X., Montanaro, V., Myhre, G., Penner, J., Pitari, G., Reddy, S., Seland, O., Stier, P., Takemura, T., and Tie, X., 2006: Analysis and quantification of the diversities of aerosol life cycles within AeroCom. *Atmos. Chem. Phys.*, **6**, 1777–1813.
- Tomczak, M., 1981: Bass Strait Water intrusions in the Tasman Sea and mean temperature-salinity curves. *Aust. J. Mar. Fresh. Res.*, **32(5)**, 699–708.
- Tomczak, M., 1985: The Bass Strait Water cascade during winter 1981. *Cont. Shelf. Res.*, **4(3)**, 255–278.
- Tomczak, M., 1987: The Bass Strait Water cascade during summer 1981–1982. *Cont. Shelf. Res.*, **7(6)**, 561–572.
- Tomczak, M., and Tanner, E., 1989: An estimate of Bass Strait Water-movement in the Western Tasman Sea during the Australian Coastal Experiments. *Aust. J. Mar. Fresh. Res.*, **40(5)**, 465–469.
- Tria, J., 2009: *Analytical methods to determine dissolved aluminium in natural waters*. Ph.D. thesis, Australian Centre for Research on Separation Science, School of Chemistry, University of Tasmania, Private Bag 75, Hobart TAS 7001, Australia.

- Tria, J., Butler, E. C. V., Haddad, P. R., and Bowie, A. R., 2007: Determination of aluminium in natural water samples. *Anal. Chim. Acta.*, **588**(2), 153–165.
- Tria, J., Haddad, P. R., and Nesterenko, P. N., 2008a: Determination of aluminium using high performance chelation ion chromatography. *J. Sep. Sci.*, **31**(12), 2231–2238.
- Tria, J., Haddad, P. R., and Nesterenko, P. N., 2008b: Potential applicability of a high performance chelation ion chromatographic method to the determination of Aluminium in Antarctic surface seawater. *Chem. Listy.*, **102**(15), s319–s323.
- Trull, T., Rintoul, S., Hadfield, M., and Abraham, E., 2001a: Circulation and seasonal evolution of polar waters south of Australia: Implications for iron fertilization of the Southern Ocean. *Deep-Sea. Res. Pt. II.*, **48**(11-12), 2439–2466.
- Trull, T., Sedwick, P., Griffiths, F., and Rintoul, S., 2001b: Introduction to special section: SAZ Project. *J. Geophys. Res-Oceans.*, **106**(C12), 31425–31429.
- Trull, T. W., Bray, S. G., Buesseler, K. O., Lamborg, C. H., Manganini, S., Moy, C., and Valdes, J., 2008a: In situ measurement of mesopelagic particle sinking rates and the control of carbon transfer to the ocean interior during the Vertical Flux in the Global Ocean (VERTIGO) voyages in the North Pacific. *Deep-Sea. Res. Pt. II.*, **55**(14-15), 1684–1695.
- Trull, T. W., Bray, S. G., Manganini, S. J., Honjo, S., and Francois, R., 2001c: Moored sediment trap measurements of carbon export in the Subantarctic and Polar Frontal Zones of the Southern Ocean, south of Australia. *J. Geophys. Res-Oceans.*, **106**(C12), 31489–31509.
- Trull, T. W., Davies, D., and Casciotti, K., 2008b: Insights into nutrient assimilation and export in naturally iron-fertilized waters of the Southern Ocean from nitrogen, carbon and oxygen isotopes. *Deep-Sea. Res. Pt. II.*, **55**(5-7), 820–840.
- Tsai, W., Graf, J. E., Winn, C., Huddleston, J. N., Dunbar, S., Freilich, M. H., Wentz, F. J., Long, D. G., and Jones, W. L., 1999: Postlaunch sensor verification and calibration of the NASA Scatterometer. *Ieee. T. Geosci. Remote.*, **37**(3), 1517–1542.
- Turner, D., and Hunter, K. A., Eds., 2001: *The Biogeochemistry of Iron in Seawater*, vol. 7 of

- IUPAC Series on Analytical and Physical Chemistry of Environmental Systems*. John Wiley And Sons, Ltd.
- Upadhyay, S., Liss, P. S., and Jickells, T. D., 2002: Sorption model for dissolved aluminium in freshwaters. *Aquat. Geochem.*, **8(4)**, 255–275.
- Upadhyay, S., and Sen Gupta, R., 1994: Aluminium in the Northwestern Indian-Ocean (Arabian Sea). *Mar. Chem.*, **47(3-4)**, 203–214.
- Upadhyay, S., and Sen Gupta, R., 1995: The behaviour of aluminium in waters of the Mandovi estuary, west coast of India. *Mar. Chem.*, **51(3)**, 261–276.
- Ussher, S. J., Achterberg, E. P., and Worsfold, P. J., 2004: Marine Biogeochemistry of Iron. *Environ. Chem.*, **1(2)**, 67–80.
- van den Berg, C. M., Murphy, K., and Riley, J. P., 1986: The determination of aluminium in seawater and freshwater by cathodic stripping voltammetry. *Anal. Chim. Acta.*, **188(0)**, 177 – 185.
- van der Merwe, P., Lannuzel, D., Bowie, A. R., and Meiners, K. M., 2011a: High temporal resolution observations of spring fast ice melt and seawater iron enrichment in East Antarctica. *J. Geophys. Res-Biogeosci.*, **116**, G03017.
- van der Merwe, P., Lannuzel, D., Bowie, A. R., Nichols, C. A. M., and Meiners, K. M., 2011b: Iron fractionation in pack and fast ice in East Antarctica: Temporal decoupling between the release of dissolved and particulate iron during spring melt. *Deep-Sea. Res. Pt. II.*, **58(9-10)**, 1222–1236.
- van der Merwe, P., Lannuzel, D., Nichols, C. A. M., Meiners, K., Heil, P., Norman, L., Thomas, D. N., and Bowie, A. R., 2009: Biogeochemical observations during the winter-spring transition in East Antarctic sea ice: Evidence of iron and exopolysaccharide controls. *Mar. Chem.*, **115(3-4)**, 163–175.
- van Hulst, M., Sterl, A., Tagliabue, A., Dutay, J.-C., Gehlen, M., de Baar, H., and Middag, R., 2012: Aluminium in an ocean general circulation model compared with the West Atlantic Geotraces cruises. *J. Mar. Syst.*, **xxx(0)**, xx–xx, (in press, doi: 10.1016/j.jmarsys.2012.05.005).

- Vanbennekom, A. J., Buma, A. G. J., and Nolting, R. F., 1991: Dissolved aluminum in the weddell-scotia confluence and effect of Al on the dissolution kinetics of biogenic silica. *Mar. Chem.*, **35(1-4)**, 423–434.
- VanBeusekom, J. E. E., VanBennekom, A. J., Treguer, P., and Morvan, J., 1997: Aluminium and silicic acid in water and sediments of the Enderby and Crozet Basins. *Deep-Sea. Res. Pt. II.*, **44(5)**, 987–1003.
- Victory, D., Nesterenko, P., and Paull, B., 2004: Low-pressure gradient micro-ion chromatography with ultra-short monolithic anion exchange column. *Analyst.*, **129**, 700–701.
- Vink, S., Boyle, E. A., Measures, C. I., and Yuan, J., 2000: Automated high resolution determination of the trace elements iron and aluminium in the surface ocean using a towed Fish coupled to flow injection analysis. *Deep-Sea. Res. Pt. I.*, **47(6)**, 1141–1156.
- Volpe, G., Banzon, V. F., Evans, R. H., Santoleri, R., Mariano, A. J., and Sciarra, R., 2009: Satellite observations of the impact of dust in a low-nutrient, low-chlorophyll region: Fertilization or artifact? *Global. Biogeochem. Cy.*, **23(3)**, GB3007–.
- Walker, W. J., Cronan, C. S., and Patterson, H. H., 1988: A Kinetic-study of Aluminum Adsorption By Aluminosilicate Clay-minerals. *Geochim. Cosmochim. Ac.*, **52(1)**, 55–62.
- Wedepohl, K. H., 1995: The composition of the continental-crust. *Geochim. Cosmochim. Ac.*, **59(7)**, 1217–1232.
- Westwood, K. J., Griffiths, F. B., Webb, J. P., and Wright, S. W., 2011: Primary production in the Sub-Antarctic and Polar Frontal Zones south of Tasmania, Australia; SAZ-Sense survey, 2007. *Deep-Sea. Res. Pt. II.*, **58(21-22)**, 2162–2178.
- Whitehead, P., Wilson, E., and Butterfield, D., 1998: A semi-distributed Integrated Nitrogen model for multiple source assessment in Catchments (INCA): Part I - model structure and process equations. *Sci. Total. Environ.*, **210(1-6)**, 547–558.
- Williams, T., and Barnett, N. W., 1992: 8-Quinolinol-5-sulfonic acid as a non-selective post-column reagent for fluorimetric detection of trace metals in ion chromatography. *Anal. Chim. Acta.*, **264(2)**, 297 – 301.

- Woodward, S., 2001: Modeling the atmospheric life cycle and radiative impact of mineral dust in the Hadley Centre climate model. *J. Geophys. Res-Atmos.*, **106(D16)**, 18155–18166.
- Wu, J., Zhou, C. Y., Chi, H., Wong, M. K., Lee, H. K., Ong, H. Y., and Ong, C. N., 1995: Determination of serum aluminum using an ion-pair reversed-phase high-performance liquid chromatographic-fluorimetric system with lumogallion. *J. Chromatogr. B.*, **663(2)**, 247–253.
- Xia, L., Hu, B., Jiang, Z., Wu, Y., Li, L., and Chen, R., 2005: 8-Hydroxyquinoline-chloroform single drop microextraction and electrothermal vaporization ICP-MS for the fractionation of aluminium in natural waters and drinks. *J. Anal. Atom. Spectrom.*, **20**, 441–446.
- Yaroshevsky, A. A., 2006: Abundances of chemical elements in the Earth's crust. *Geochem. Int.*, **44(1)**, 48–55.
- Zender, C. S., Bian, H. S., and Newman, D., 2003: Mineral Dust Entrainment And Deposition (DEAD) model: Description and 1990s dust climatology. *J. Geophys. Res-Atmos.*, **108(D14)**, 4416–4435.
- Zhou, C. Y., Wu, J., Chi, H., Wong, M. K., Koh, L. L., and Wee, Y. C., 1995: High-performance liquid-chromatographic determination of aluminum in natural-waters in the form of its lumogallion chelate. *Talanta.*, **42(3)**, 415–422.